Title
Integrated regulation at the levels of mRNA, translation, and protein in Saccharomyces cerevisiae

Author
Cheng, Ze

Publication Date
2019

Peer reviewed|Thesis/dissertation

Integrated regulation at the levels of mRNA, translation, and protein in *Saccharomyces cerevisiae*

by

Ze Cheng

A dissertation submitted in partial satisfaction of the

requirements for the degree of

Doctor of Philosophy

in

Molecular and Cell Biology

in the

Graduate Division

of the

University of California, Berkeley

Committee in charge:

Professor Gloria A. Brar, Chair

Professor Michael Rape

Professor Jamie H. D. Cate

Professor James A. Olzmann

Spring 2019

Abstract

Integrated regulation at the levels of mRNA, translation, and protein in *Saccharomyces cerevisiae*

by

Ze Cheng

Doctor of Philosophy in Molecular and Cell Biology

University of California, Berkeley

Professor Gloria A. Brar, Chair

Gene expression in eukaryotes is tightly controlled to determine cell identity and function, and to drive complex differentiation and developmental programs. Each step in the gene expression process can be regulated to influence the final outcome and thus, a comprehensive view of gene expression changes at multiple levels is required for full understanding of the regulation of gene expression. To investigate how the cell integrates regulatory mechanisms at multiple levels to achieve precise and coordinated regulation of gene expression, we combined genome-wide techniques and traditional methodologies to obtain key measurements of gene expression and to dissect the contribution of each step in determining gene expression levels. In chapter 2, we focus on how ribosomal deficiencies alter gene expression. We probed the changes of mRNA abundances, translation rates, and protein abundances in a panel of ribosomal protein mutants and observed changes that were both specific to individual ribosomal proteins and dose-dependent with degree of translation deficiency. We also observed strong evidence of compensatory regulation, including at the transcriptional and protein degradation levels, and distinct cellular responses to loss of small and large ribosomal subunit components. Three current models have been proposed to explain the specific phenotypes associated with loss of ribosomal proteins in diseases of ribosome deficiency, or ribosomopathies, and our data revealed evidence to support all of these models, albeit to differing extents. In chapter 3, we describe a novel regulatory mechanism in which the protein levels are determined by identity, instead of levels, of the transcripts. We collected parallel measurements of mRNA, translation, and protein through a timecourse in yeast meiosis and discovered that the toggling between canonical transcript isoforms and long undecoded transcript isoforms regulates the outcome of gene expression for 380 genes. In chapter 4, we study the regulation of ribosome biogenesis (RiBi) genes and show that global inhibition of translation de-represses RiBi mRNA transcription in a condition-dependent manner. In summary, in three different contexts, we report a surprisingly high degree of integration between different levels of gene expression, highlighting the importance of parallel measurements of different gene expression intermediates to interpret the link between gene expression and cellular outcomes.

TABLE OF CONTENTS

Abstract 1
Table of Contents i
Acknowledgements iii

Chapter 1. General introduction 1
1.1 Regulation of gene expression 1
1.2 Investigating gene regulation using next-generation sequencing based approaches 4
1.3 Using budding yeast as a model system to study the regulation of gene expression 6

Chapter 2. Small and large ribosomal subunit deficiencies lead to distinct gene expression signatures that reflect cellular growth rate 7
2.1 Abstract 8
2.2 Introduction 8
2.3 Methods 10
2.4 Results 25
2.5 Discussion 37
2.6 Acknowledgements 39
2.7 Supplemental figures 40

Chapter 3. Pervasive, coordinated protein level changes driven by transcript isoform switching during meiosis 48
3.1 Abstract 49
3.2 Introduction 49
3.3 Methods 50
3.4 Results 60
3.5 Discussion 76
3.6 Acknowledgements 80
3.7 Supplemental figures 81

Chapter 4. Global translation inhibition yields condition-dependent de-repression of ribosome biogenesis mRNAs 92
4.1 Abstract 93
4.2 Introduction 93
4.3 Methods 94
4.4 Results 99
4.5 Discussion 110
4.6 Acknowledgements 112
4.7 Supplemental figures 113

Chapter 5. Conclusions and future directions 128

5.1 Towards deep understanding of ribosomal-deficiency-induced gene expression changes 128
5.2 The implications of LUTI-based regulation 129
5.3 Uncovering artifacts in translation efficiency assays 130

References 132

Acknowledgements

I would like to thank all the people who helped me in graduate school, including my family, my mentors, and my friends. I am incredibly thankful for all of your support and contributions throughout this journey.

I want to especially thank Gloria Brar for leading me into this exciting research field and for teaching me so many valuable things that made me into a scientist. None of my goals could be achieved without your mentorship and contributions. You did everything possible to ensure my success both in and after graduate school. You are a creative and outstanding scientist as well as an extraordinary mentor, and I am extremely lucky to have you in my graduate school training.

I would like to thank Abby Dernburg, my first graduate school rotation mentor. Thank you for your help in the graduate school application process and for your support during my first rotation. Without you, I would not have the opportunity to join this great program and my transition in the beginning of graduate school would be hard. Also thank you for your help in my qualifying exam.

Thank you to my thesis committee members, Michael Rape, Jamie Cate, and James Olzmann. It was amazing to have such a strong committee in my PhD training. I am truly grateful for all your comments and suggestions on my research projects.

I would like to thank all the current and past members in the Brar lab and the Ünal lab, as well as the Weis lab people who shared lab space with us. You gave me countless support and help in my research, and made the lab to be such a lovely place to work in.

Finally, I want to thank my family. To my parents, you always give me the strongest support in every important decisions I made in my life and you always have faith in me. You may have not understood what I was doing scientifically, but none-the-less you stood by my side and did whatever you could to make me success. Special thank you to my wife, Zhan Li. You have become the most valuable person in my life since we met. Your love gave me the confidence to pursue my favorite career path and supported me to go through all the difficulties.

CHAPTER 1

General Introduction

1.1 Regulation of gene expression

In eukaryotes, genetic information is stored in DNA sequences, which are called genes, and gene expression is the process by which protein products, the primary functional units of cells, are made using the instructions encoded in these genes. The types and abundances of proteins in the cell determine its structure, function, and fate. Thus, the precise control of gene expression is critical. Gene expression consists of multiples steps, including transcription, mRNA processing, mRNA decay, translation, post-translational modification, and protein degradation. Each of these steps can be regulated to alter the final protein abundance and the cells may integrate regulations at multiple levels to control what, when, and how much protein is made in the context of complex biological processes.

1.1.1 Transcriptional and post-transcriptional regulation of mRNA

Transcription is the start of gene expression and has been deeply studied regarding its mechanism and regulation. Transcriptional regulation of gene expression typically involves the interaction between cis-acting elements on DNA and trans-acting transcription factors, as well as regulated epigenetic modifications and chromatin state changes. In budding yeast, transcriptional activators and transcriptional repressors primarily bind to upstream activation sequences and upstream repression sequences, respectively, near the core promoters and affect the mRNA synthesis of target genes through interactions with RNA Pol II or histone modifiers(Hahn and Young, 2011). In higher eukaryotes, transcription factors can also recognize various cis-regulatory elements that exist at long distances to the transcription start sites to achieve complex patterns of temporal and spatial transcription activity(Spitz and Furlong, 2012).

The primary eukaryotic transcripts are not functional and have to undergo a series of processing steps including 5’ capping, RNA splicing, and 3’ cleavage/polyadenylation. The control of mRNA splicing is an important component of gene expression regulation as a large fraction of genes in most eukaryotes produce transcript isoforms that are alternatively spliced and alternative splicing can alter the amount and sequence of the final protein product (Shin and Manley, 2004). The 3’ processing and polyadenylation of mRNA is also tightly regulated in some cases. For example, cytoplasmic polyadenylation occurs in both vertebrates and invertebrates and alters the length of poly(A) tail, which affects mRNA translation (Richter, 1999). Additionally, alternative polyadenylation sites exist in eukaryotic genes and alternative cleavage and polyadenylation (APA) generates mRNA isoforms that contains different cis-regulatory elements or even coding regions. Shifting of polyadenylation sites and shortening or lengthening of 3’ UTR have been observed in several conditions, such as in cancer cells (Mayr and Bartel, 2009) and in cell differentiation (Hoque et al., 2013).

All mRNA species are subject to turnover, which plays an important role in regulating mRNA steady state levels (Parker, 2012). The general mRNA decay initiates with shortening of the poly(A) tail, followed by either 3' to 5' exosome-mediated decay pathway or decapping and 5' to 3' exonucleolytic decay (Parker, 2012). The majority of yeast mRNA species were shown to have short half-lives, on the scale of minutes, which allows dynamic and rapid changes to the transcriptome (Chan et al., 2018). Several studies in both yeast species as well as higher eukaryotes uncovered a correlation between codon optimality, translation elongation rate, and mRNA stability (Harigaya and Parker, 2016; Presnyak et al., 2015; Radhakrishnan et al., 2016). These observations led to a model in which slowly elongating ribosomes at suboptimal codons elevate the rate of mRNA decay (Harigaya and Parker, 2016; Presnyak et al., 2015; Radhakrishnan et al., 2016). However, another model has been also proposed in which the competition between translation initiation and mRNA decay machineries determines the turnover rate of mRNA (Chan et al., 2018). Cells are also equipped with mRNA decay mechanisms that clear specific types of mRNA species. For example, nonsense-mediated mRNA decay (NMD) pathway selectively eliminates mRNAs that prematurely terminate translation and microRNAs (miRNAs) regulate translation and stability of target mRNAs through sequence-based recognition (Krol et al., 2010; Schoenberg and Maquat, 2012).

1.1.2 Translation and translational control

Eukaryotic translation consists of three phases: initiation, elongation, and termination. The ribosome, mRNA, as well as various translation factors including initiation factors (eIFs), elongation factors (eEFs), and release factors (eRFs), participate in translation(Dever and Green, 2012; Jackson et al., 2010). During 5' cap-dependent translation initiation, the 5' cap is recognized by eIF4E, which forms eIF4F complex together with eIF4G, eIF4A, and eIF4B. The initiation factors eIF3, eIF5, and eIF2-GTP-Met-tRNA ternary complex bind to small (40S) ribosome subunit and form 43S preinitiation complex. The 43S preinitiation complex is then recruited to the 5' end of mRNA and forms the 48S preinitiation complex with eIF4F. The 48S complex starts to scan along the mRNA transcript in 5' to 3' direction. Recognition of the start codon induces a series of conformational and biochemical changes on the preinitiation complex and allows the joining of 60S ribosome subunit (Jackson et al., 2010). The assembled 80S ribosome starts translation elongation, which consists of four basic steps: the positioning of tRNA and eEF1 in the ribosomal A site, the hydrolysis of GTP and the release of eEF1, the peptidyl transfer reaction that elongates the nascent polypeptide chain, and the ribosome translocation facilitated by eEF2 (Richter and Coller, 2015). Translation termination occurs upon the positioning of a stop codon into the ribosomal A site. A single termination factor, eRF1, is responsible for recognition of all three stop codons and it is delivered into the A site by eRF3 followed by GTP hydrolysis and the release of nascent peptide chain and eRF3 (Dever and Green, 2012). After the completion of translation, the 40S and 60S ribosome subunits are dissociated, which allows them to be recycled into the available ribosome pool, and this process is mediated by ribosome recycling factors such as ABCE1/Rli1, Dom34, and Hbs1 (Dever and Green, 2012).

Translation is energetically expensive and its regulation is crucial in determining the synthesis rates of proteins (Li et al., 2014). Translation is precisely regulated to control gene expression levels and to avoid production of toxic proteins(Holcik and Sonenberg, 2005; Kong and Lasko, 2012). Translational control can be mediated by 5' UTR features, the interaction between UTR regions and mRNA binding proteins, miRNAs, and pausing during elongation.

Secondary structures in 5' UTRs have been shown to affect translation efficiency and the dependency on RNA helicases. For example, yeast DEAD-box RNA helicase Ded1 is required for scanning through long, structured 5' UTRs (Sen et al., 2015). Upstream open reading frames (uORFs) also have substantial effect on the translation of the canonical open reading frames (ORF). uORFs are pervasive in 5' UTRs and it has been shown that uORFs can perform inhibitory role by competing the scanning preinitiation complex against the main ORF (Calvo et al., 2009; Johnstone et al., 2016). Together with the regulation of initiation factor activity, uORFs may have condition-dependent effects on the main ORF translation. For example, the repressive uORFs on mammalian *ATF4* and yeast *GCN4* genes become permissive under conditions where eIF2α is phosphorylated (Hinnebusch, 2005; Vattem and Wek, 2004). Internal ribosome entry sites (IRESs) are mRNA 5' UTR structures that allow cap-independent translation inhibition by directly interacting with initiation factors or ribosomal subunits (Filbin and Kieft, 2009). IRESs are initially identified in viral RNAs and are thought to enable viral RNA translation in the context of global inhibition of the canonical cap-dependent pathway(Sarnow, 2003). However, many studies have also identified functional IRES elements in cellular mRNAs and suggest important role of IRES-dependent translation in regulating the expression of cellular genes (Filbin and Kieft, 2009; Komar and Hatzoglou, 2011; Silvera et al., 2010; Xue et al., 2015).

RNA-protein interactions play an important role in gene-specific translational control. RNA binding proteins bind to specific sequences or structures on the target mRNA and affect the rate of translation initiation. For example, in iron-deficient cells, mRNA binding proteins IRP1 and IRP2 binds to the 5' UTR of ferritin mRNA, which sterically blocks the recruitment of 43S complex to ferritin mRNA (Gebauer and Hentze, 2004). Specific 3' UTR-protein interactions are even more common. For example, cytoplasmic polyadenylation element binding protein (CPEB) recognizes cytoplasmic polyadenylation element (CPE) on the 3' UTR of target mRNAs and promotes polyadenylation-induced translation in *Xenopus* oocytes (Richter, 2007). RNA-RNA interaction is another way of regulating translation. MicroRNAs (miRNAs) bind to UTRs in a sequence-based manner and have been shown to repress mRNA translation and increase the rate of mRNA decay (Djuranovic et al., 2012).

Although considered as non-rate-limiting step in translation, emerging evidence suggests that the control of polypeptide elongation can also exert profound regulatory impact (Richter and Coller, 2015). It has been show that ribosomes stall on *nanos* and *oskar* mRNAs but do not synthesize protein products in *Drosophila* early development (Andrews et al., 2011; Braat et al., 2004). In human brain, the Fragile X mental retardation protein (FMRP) binds to nearly 1,000 mRNAs and stalls ribosome translocation to prevent excess protein synthesis (Darnell et al., 2011). Additionally, tRNA abundance and codon optimality also regulate elongation rate because some codons are decoded slowly when their cognate tRNAs are limiting (Novoa and Ribas de Pouplana, 2012).

The ribosome is a highly conserved cellular machine and directly executes all phases of translation. Historically, the ribosome has been viewed as a monolithic machine, and accordingly it has been functionally explored primarily for catalytic and structural roles. However, recent studies suggest that the ribosome has regulatory function besides its known catalytic role and certain ribosomal proteins control the specificity of translation (Ferretti et al., 2017; Kondrashov et al., 2011; Landry et al., 2009; Lee et al., 2013; Simsek et al., 2017; Xue et al., 2015). Additionally, studies on ribosomal deficiency associated diseases proposed an alternative model in which cellular ribosome concentration may affect translation rates of difference mRNAs(Khajuria et al., 2018; Mills and Green, 2017).

1.2 Investigating gene regulation using next-generation sequencing based approaches

Historically, low-throughput, gene-specific techniques such as Northern blot, revere transcription quantitative PCR (RT-qPCR), and reporter-based assays have been widely used in the research of gene regulation. These studies provide valuable understanding of how gene expression is controlled and have identified various regulatory mechanisms. However, the inability to probe all genes in the genome simultaneously limit the understanding of regulatory pathways at genome-wide scale. Next-generation sequencing (NGS) techniques were developed to provide much higher throughput compared to the Sanger sequencing method and made it possible to obtain genome-wide information in a single sequencing run (Metzker, 2010). Since then, various NGS-based techniques for investigating gene regulation have been developed and in this thesis, we heavily utilize two NGS-based methods, RNA sequencing and ribosome profiling.

1.2.1 RNA sequencing

As indispensable intermediates in gene expression, the mRNA transcripts in a cell determine all possible proteins being made and, in many cases, the final protein level of a gene correlates with its mRNA abundance (Mortazavi et al., 2008). Thus, understanding the complete set of transcripts (transcriptome) and their abundances under certain conditions or developmental stages is essential for discovering gene regulation events and for investigating the mechanisms of gene expression regulation (Wang et al., 2009). Hybridization-based methods, such as expression microarrays, were developed as a first approach to measure the transcriptome. However, these approaches heavily rely on existing knowledge about the transcript sequences and may yield low dynamic range and hybridization artifacts (Mortazavi et al., 2008; Okoniewski and Miller, 2006).

RNA sequencing (RNA-seq) takes advantage of the development of next-generation sequencing and measures all transcripts in the genome simultaneously with high dynamic range and sensitivity. Either total RNA or poly(A)-selected mRNA can be starting materials for RNA-seq, and the RNA sample is fragmented and converted to a cDNA library for next-generation sequencing (Mortazavi et al., 2008). The reads are mapped to the genome and the read density provides accurate estimation of mRNA abundances in the sample. RNA-seq is also able to reveal splicing events, transcript isoforms, and unannotated transcripts (Trapnell et al., 2009, 2010).

1.2.2 Ribosome profiling

Genome-wide studies on gene expression have historically been limited to measuring mRNA levels by microarrays or RNA-seq, due to the technical challenges of precisely monitoring translation at genomic scale. However, mRNA abundances may not necessarily represent the accurate gene expression levels because of the presence of translational regulation. Ribosome profiling was developed in 2009 and for the first time enabled genome-wide detection of translation at single-codon-resolution *in vivo* (Ingolia et al., 2009). Ribosome profiling exploits the observation that a translating ribosome covers a ~28-nucleotide-long region on the mRNA and strongly protects it from nuclease digestion (Steitz, 1969). By combining the biochemical purification of ribosome protected mRNA fragments and deep-sequencing of these ribosome footprints, Ribosome profiling displays a precise snapshot picture containing all translation events in the cell, which is often referred as the translatome (Ingolia et al., 2009).

Ribosome profiling starts with immobilizing ribosomes by translation inhibitors such as cycloheximide, and harvesting biological samples (Ingolia et al., 2012). Nuclease is applied to the samples in order to produce ribosome-protected mRNA fragments and ribosomes are then isolated from other cellular components by either density gradient centrifugation or gel filtration chromatography (Ingolia et al., 2012). Ribosome footprints are converted to next-generation sequencing library, subjected to sequencing, and mapped to the genome (Ingolia et al., 2009, 2012). Ribosome profiling has been successfully performed in a variety of organisms, cell types, and conditions because of the highly conserved properties of the ribosome (Bazzini et al., 2012; Brar et al., 2012; Hirose and Horvitz, 2014; Ingolia et al., 2009, 2011; Juntawong et al., 2014; Oh et al., 2011).

Ribosome profiling provides precise positional information of translation. The codon in the ribosome P site can be predicted on a ribosome footprint based on known spatial properties of the ribosome, which allows each read to be assigned to a single nucleotide position on the mRNA, and the cumulative positional data from all the footprints reveal which regions in the genome are translated(Ingolia et al., 2009). The footprint density on translated regions shows three-nucleotide periodicity which results from the codon-based stepwise movement of ribosome during translation elongation, and the periodicity can further be utilized to distinguish real translated regions from inactive ribosome occupancies (Young et al., 2015). Analyses of ribosome profiling datasets have identified translation of both canonical open reading frames (ORF) and non-canonical sites, such as upstream open reading frames (uORF) (Brar et al., 2012; Ingolia et al., 2009, 2011).

Ribosome profiling also provides quantitative measurements of translation with high sensitivity. The average density of footprints on an ORF is proportional to the translation rate of this ORF, except for the cases where the elongation rate is regulated (Ingolia et al., 2009; Wu et al., 2019). The sensitivity of ribosome profiling is facilitated by the depth of sequencing and allows the detection of rare translation events. Translation efficiency, which is calculated by normalizing ribosome footprint density on an ORF to its RNA-seq density, indicates how frequently translation happens per transcript, and comparing translation

efficiency values at different conditions, cell types, or developmental stages reveals gene expression regulation at the translation level(Brar et al., 2012; Ingolia et al., 2009).

1.3 Using budding yeast as a model system to study the regulation of gene expression

The budding yeast *Saccharomyces cerevisiae* is a frequently used model organism due to the advantages that it is easily cultured in laboratory conditions, its genes can be manipulated with various available genetics tools, and its genome is small and has been fully sequenced (Duina et al., 2014). The fundamental mechanisms of gene expression, including transcription, mRNA processing and decay, translation, and protein degradation, are highly conserved between yeast and higher eukaryotes (Dever et al., 2016; Hahn and Young, 2011; Parker, 2012). Thus, we performed our studies in budding yeast to investigate the interconnected regulation of multiple levels of gene expression.

Gene expression in budding yeast is regulated to allow cells to adapt to different growth conditions and to drive cellular changes. Meiosis is a specialized type of cell division that produces gametes and consists of two sequential divisions; in meiosis I, DNA replication occurs and homologous chromosomes segregate, while in meiosis II, sister chromatids separate into gametes without additional round of DNA replication, generating haploid cells from diploid progenitors (Marston and Amon, 2004). Meiotic steps are strongly conserved and errors in meiosis lead to decreased fitness of progeny and diseases in humans (Nagaoka et al., 2012). To drive this complex process, gene expression is highly controlled. A study in *Saccharomyces cerevisiae* using RNA-seq and ribosome profiling revealed pervasive regulation of gene expression at multiple levels in meiosis (Brar et al., 2012). Although a small number of meiotic transcriptional pathways are well studied, the mechanisms of post-transcriptional regulation as well as how the controls at different gene expression steps are integrated to drive the changes of protein levels are largely unknown (Brar et al., 2012; Neiman, 2011). Yeast meiosis, therefore, provides an attractive system for investigating novel regulatory mechanisms in the context of cellular differentiation.

CHAPTER 2

Small and large ribosomal subunit deficiencies lead to distinct gene expression signatures that reflect cellular growth rate

Part of the work presented in this chapter has previously been published in the following manuscript: Cheng, Z., Mugler, C.F., Keskin, A., Hodapp, S., Chan, L.Y.L., Weis, K., Mertins, P., Regev, A., Jovanovic, M. and Brar, G.A., 2019. Small and large ribosomal subunit deficiencies lead to distinct gene expression signatures that reflect cellular growth rate. *Molecular cell*, *73*(1), pp.36-47.

doi.org/10.1016/j.molcel.2018.10.032

2.1 Abstract

Levels of the ribosome, the conserved molecular machine that mediates translation, are tightly linked to cellular growth rate. In humans, ribosomopathies are diseases associated with cell-type-specific pathologies and reduced ribosomal protein (RP) levels. Because gene expression defects resulting from ribosome deficiency have not yet been experimentally defined, we systematically probed mRNA, translation, and protein signatures that were either unlinked or linked to cellular growth rate in RP-deficient yeast cells. Ribosome concentration was seen to be associated with translation of gene sub-classes, and profound general secondary effects of RP loss on the spectrum of cellular mRNAs were seen. Among these effects, growth-defective 60S mutants increased synthesis of proteins involved in proteasome-mediated degradation, whereas 40S mutants accumulated mature 60S subunits and increased translation of ribosome biogenesis genes. These distinct signatures of protein synthesis suggest intriguing and currently mysterious differences in the cellular consequences of deficiency for small and large ribosomal subunits.

2.2 Introduction

The universal importance of the cytosolic ribosome—a large protein complex containing ~80 proteins and four rRNAs in eukaryotes—is clear, based on its essential role in translating coding regions of mRNAs into protein. It has also been reported that deficiency in specific ribosomal proteins (RPs) can result in mRNA-specific translation defects. Determining the cause(s) of specific translational effects resulting from RP deficiency may be informative in guiding our understanding of an array of diseases called "ribosomopathies" in humans, which have been linked to mutation in any of a large set of RP genes (reviewed in (De Keersmaecker et al., 2015; McCann and Baserga, 2013; Mills and Green, 2017)).

The observation that ribosomopathies typically result in defects in only a subset of cell types in each case has prompted a surge in research on the potential of the ribosome itself to influence translation in specific ways, beyond homogenously converting mRNA sequences into protein. Multiple molecular models have been proposed to explain the specific phenotypes observed (reviewed in (Mills and Green, 2017)). First, it has been proposed that changes in cellular ribosome concentration may be a major driver of shifts in translatability of an mRNA pool (Lodish, 1974; Mills and Green, 2017). The central idea is that a change in ribosome relative to mRNA levels may cause changes in the translatability of different classes of messages based primarily on competition for ribosomes among the cellular mRNA complement. This model has been proposed to explain at least some cases of the ribosomopathy Diamond-Blackfan anemia (DBA), as several DBA-associated lesions have been seen to lower ribosome production during hematopoiesis, resulting in translation shifts in some mRNA classes (Khajuria et al., 2018).

A distinct (but not mutually exclusive) model, argues that specialized ribosomes, containing a distinct complement of RPs, or modifications to rRNAs or RPs, may be responsible (reviewed in (Dinman, 2016; Xue and Barna, 2012)). This model is based on the idea that a ribosome with an altered structure due to specialization in a certain condition or cell-type will interact with different affinities to a subset of mRNAs than a non-specialized or

differently specialized ribosome, resulting in a shift in the population of mRNAs that are preferentially translated. A third model, which could co-exist with either of the other two but which has not been experimentally explored is that a change in ribosome quantity or functionality results in secondary compensatory effects on gene expression—for example, activation of a transcriptional response that changes the spectrum of mRNAs available for translation in the cell.

Identifying general and potentially specific effects of RP deficiency requires an approach to define the former. While a very small subset of RP genes show no general translation defect when absent, in most cases even partial RP deficiency is associated with slowed cellular growth and decreased bulk protein synthesis, which is likely to be due to defects in either ribosome assembly or stability of fully assembled ribosomes (Steffen et al., 2012). The degree of these defects varies greatly among RP gene mutants, but general defects due to RP deficiency do not preclude gene expression defects that might be directly or indirectly linked to specific to loss of a particular RP. Experimentally determining the potential relative contributions of RP-specific and -general phenotypes is challenging in complex eukaryotes. Budding yeast, however, offer a simple system in which to address this fundamental question because of the ease of modulating RP expression through mutation of paralogous RP-encoding genes in this organism. Towards this end, we measured mRNA, translation, and protein for a panel of RP mutants that showed a range of growth rate defects in rich media. In this system, cellular growth rate provides a robust proxy for total translation levels. This overall approach enabled growth rate matched comparisons between gene expression in mutants lacking different RPs, which to our knowledge has not been done before.

The resultant dataset revealed general signatures of protein synthesis that scale with total translation level, as predicted by the ribosome concentration hypothesis. Evidence for pervasive and strong secondary effects of general ribosome depletion on mRNA levels were also observed, which thus largely mirror translation changes measured by ribosome profiling. These results suggest the value of growth rate matched controls for studies investigating the effects of RP deficiency. To our surprise, these data also revealed dramatic differences in gene expression changes at the mRNA, translation, and protein levels in growth rate matched mutants depending on whether the mutation was in a gene encoding a component of the large 60S subunit (*RPL*) or the small 40S subunit (*RPS*). We report that *rpl* mutants show increased expression of a suite of genes involved in proteasome-mediated protein degradation with decreased growth rate, while *rps* mutants do not. *rps* mutants, in contrast, show a stronger upregulation in ribosome biogenesis than growth rate matched *rpl* mutants and show increased accumulation of mature 60S subunits with decreasing growth rate. These datasets provide a coherent framework to understand the interplay between specific and general, direct and indirect, and small and large subunit, in interpreting gene expression consequences of ribosome deficiency.

2.3 Methods

2.3.1 Yeast material and growth conditions

All experiments were performed using diploid *Saccharomyces cerevisiae* strains of the SK1 background. Strains were *LEU URA TRP LYS HIS* unless otherwise noted. Cells were grown in YEPD at 30°C and assayed in mid-log phase (OD_{600}0.6) for all experiments.

Strain number	Genotype
2374	*rpl26bΔ/Δ*
2435	*rpl7bΔ/RPL7B rpl7aΔ/RPL7A*
2700	*rpl40bΔ/Δ*
3654	*rpl40bΔ/RPL40B, rpl40aΔ/RPL40A*
3851	*rpl26aΔ/Δ*
3853	*rpl38Δ/Δ*
4472	*rps28aΔ/Δ*
4474	*rps28bΔ/Δ*
4480	*rps29bΔ/Δ*
4484	*WT*
4651	*rps0bΔ/Δ*
4654	*rpl26aΔ/RPL26A, rpl26bΔ/RPL26B*
4658	*rps25bΔ/Δ*
4659	*rps22aΔ/Δ*
4662	*rps22bΔ/Δ*
4665	*rps22bΔ/RPS22B, rps22aΔ/RPS22A*
5048	*rpl26bΔ/Δ, rpl26aΔ/Δ*
7461	*rpl41bΔ/Δ*
7463	*rps25bΔ/RPS25B, rps25aΔ/RPS25A*
7465	*rpl24bΔ/Δ*
7467	*rpl41aΔ/Δ*
7469	*rpl24aΔ/Δ*

7889	*rpl40bΔ/Δ*
7962	*rpl7aΔ/Δ*
13312	*rpl28bΔ/Δ HIS3 HIS4*
13316	*rps22aΔ/Δ HIS3 HIS4*
13318	*rpl24aΔ/Δ HIS3 HIS4*
13323	*rpl7aΔ/Δ HIS3 HIS4*
13390	*HIS3 HIS4*
15346	*lys2, ura3, leu2, his3 RPL26B/rpl26b::RPL26B-HA-TEV-AVI-GFP-KanMX*
15338	*lys2, ura3, leu2, his3 RPL26B/rpl26b::RPL26B-HA-TEV-AVI-GFP-KanMX, rpl40bΔ/Δ*
15340	*lys2, ura3, leu2, his3 RPL26B/rpl26b::RPL26B-HA-TEV-AVI-GFP-KanMX, rpl7aΔ/Δ*
15342	*lys2, ura3, leu2, his3 RPL26B/rpl26b::RPL26B-HA-TEV-AVI-GFP-KanMX, rps29bΔ/Δ*
15345	*lys2, ura3, leu2, his3 RPL26B/rpl26b::RPL26B-HA-TEV-AVI-GFP-KanMX, rps0bΔ/Δ*
15337	*lys2, ura3, leu2, his3 RPL29/rpl29::RPL29-HA-TEV-AVI-GFP-KanMX*
15347	*lys2, ura3, leu2, his3 RPL29/rpl29::RPL29-HA-TEV-AVI-GFP-KanMX, rpl7aΔ/Δ*
15349	*lys2, ura3, leu2, his3 RPL29/rpl29::RPL29-HA-TEV-AVI-GFP-KanMX, rpl40bΔ/Δ*
15335	*lys2, ura3, leu2, his3 RPL29/rpl29::RPL29-HA-TEV-AVI-GFP-KanMX, rps0bΔ/Δ*
15333	*lys2, ura3, leu2, his3*

	RPL29/rpl29::RPL29-HA-TEV-AVI-GFP-KanMX, *rps29bΔ/Δ*

Yeast RP gene names compared to revised systematic nomenclature from (Ban et al., 2014)

Yeast gene name (SGD)	Revised systematic name
RPL7A	uL30
RPL7B	uL30
RPL24A	eL24
RPL24B	eL24
RPL26A	uL24
RPL26B	uL24
RPL38	eL38
RPL40A	eL40
RPL40B	eL40
RPL41A	eL41
RPL41B	eL41
RPS0B	uS2
RPS22A	uS8
RPS22B	uS8
RPS25A	eS25
RPS25B	eS25
RPS28A	eS28
RPS28B	eS28
RPS29A	uS14
RPS29B	uS14

2.3.2 Sample harvesting:

Vegetative exponential samples were collected by filtration after growth of 300 ml in YEPD to OD_{600}0.6 from a dilution to OD_{600}0.05. 1.5 mL flash frozen buffer was added to ribosome profiling aliquot (also to be used for mass spectrometry) of the standard ribosome profiling composition (20mM Tris pH8, 140mM KCl, 1.5mM MgCl2, 100ug/ml cycloheximide, 1% Trition X-100) supplemented with 2ug/ml Aprotinin, 10ug/ml Leupeptin, 1mM PMSF, 1:100 PIC2, 1:100 PIC3 (both Sigma inhibitor cocktails). Samples were lysed by Retsch mixermilling (6x 3 minute rounds at 15 Hz). Resulting powder was thawed, spun once at 4C for 5 min at 3000 RCF, sup was removed and spun at 20,000 RCF at 4C for 10 minutes. Extract was aliquoted in 200ul portions and flash frozen. Identical extract was used for ribosome profiling and mass spectrometry.

2.3.3 Ribosome Profiling:

Ribosome profiling was performed as described previously in (Brar et al., 2012). In short, samples were treated with RNase I (Ambion) at 15 U per A_{260} unit of extract for 1 hour at room temperature. Samples were then loaded onto sucrose gradients (10-50%) and centrifuged for 3 hrs. at 35,000 rpm at 4^{o}C in a SW41Ti rotor (Beckman). 80S/monosome peaks were collected using a Gradient Station (BioComp). RNA was extracted using the hot acid phenol method, RNA was size selected from a polyacrylamide gel, dephosphorylated, polyA-tailed, subjected to rRNA subtraction, RT-PCR, circularization, and PCR. The enzymes used were PNK (NEB, lot 0951602), E.coli polyA polymerase (NEB, lot 0101309), Superscript III (Thermo, lot 1752971), Circ Ligase (Epicentre), Phusion polymerase (NEB). Oligos used were oCJ200-oligodT for Reverse transcription, oNTI231 and aatgatacggcgaccaccgagatcggaagagcacacgtctgaactccagtcac-barcode-cgacaggttcagagttc index primers, for PCR, all also PAGE purified from IDT, where the barcodes are six nucleotides in length. Sequencing was done for both reads with standard Illumina oligos. Results were highly reproducible, as shown in Fig. 2.S5A.

2.3.4 mRNA sequencing

The protocol followed was identical to above, except for the following: total RNA was isolated from frozen pellets, not subjected to mixermilling, by hot acid phenol extraction, total RNA was alkaline fragmented and size selected to 30-50 nt. Fragments were subjected to an identical library prep pipeline as the footprints, but no selective rRNA subtraction round was used. Results were highly reproducible, as shown in Fig. 2.S5B.

2.3.5 Sequencing

All samples were sequenced on an Illumina HiSeq 2500, 50SRR, with multiplexing, at the UC-Berkeley Vincent Coates QB3 Sequencing facility.

2.3.6 ^{35}S metabolic labeling:

Cells were inoculated into YEPD and grown overnight at 30°C with shaking. Cells were diluted to OD_{600} 0.1 in 15 mL of YEPD and grown at 30°C with shaking. The ^{35}S metabolic labeling was performed at log phase with OD_{600} of 0.5 to 0.7. The time to reach the proper cell density varied between strains due to difference in growth rate. 30 minutes before the labeling, 11 mL of cells were spun down at 3,000 rcf for 1.5 minutes, resuspended in 11 mL of pre-warmed fresh YEPD, and put back to 30°C with shaking. At the start of labeling, 1 mL of cells was transferred into a cuvette and 5 μL of EasyTag™ EXPRESS ^{35}S protein labeling mix (PerkinElmer, Cat#NEG772002MC) were added into the rest of the cells. Cells were incubated with shaking at 30°C for 10 minutes. During the incubation, OD_{600} measurements were taken from the cells saved in the cuvette. When the incubation was complete, 900 μL of cells were immediately mixed with 100 μL of 100% trichloroacetic acid (TCA), incubated at 95°C for 15 minutes with 500 rpm shaking, and chilled on ice for 15 minutes. Samples were spun down at 20,000 rcf for 2 minutes at 4°C and the pellets were washed with 1 mL of ice-cold 10% TCA. Samples were pelleted again under the same condition and washed with 1 mL ice-cold 100% ethanol. Samples were pelleted again and resuspended in 5 mL of Econo-Safe™ scintillation fluid (RPI, Cat#111175). Scintillation was counted for 2 minutes and the ^{35}S incorporation rates were derived from counts per minute (CPM) normalized to cell number. To ensure accurate and robust comparison, all ^{35}S labeling experiments were performed using two ribosomal protein mutants in parallel with one wild-type control.

2.3.7 Growth rate assay

Cells were inoculated into YEPD and grown overnight at 30°C with shaking. Cells were diluted in YEPD to OD_{600} 0.2 and grown at 30°C with shaking to log phase with OD_{600} around 0.6. Cells were diluted again to OD_{600} 0.2 and transferred into 96-well plates. Absorbance measurements were taken with a Tecan microplate reader at 15-minute interval for 8 hours. Each strain was measured in triplicate and a two-fold serial dilution of WT cells was included in each plate to generate the standard curve. Absorbance measurements of each strain were first transformed to relative cell concentrations using the standard curve, then plotted on a time-concentration graph with log-scale y axis. The slope of the linear region in this graph was used to calculate the doubling time.

2.3.8 Temperature sensitivity assay

Cells were inoculated into YEPD and grown overnight at 30°C with shaking. Five-fold serial dilutions starting at OD_{600} 0.25 were prepared from the overnight cell cultures and 3 μL of each dilution were transferred to two YEPD plates. One of the plates was incubated at 30°C and the other plate was incubated at 37°C. Images were taken after one day and two days.

2.3.9 DNA content analysis using flow cytometry

Cells were inoculated into YEPD and grown overnight at 30°C with shaking. Cells were diluted to OD_{600} 0.1 in YEPD and grown at at 30°C with shaking. At log phase with OD_{600} 0.55 to 0.6, 1 mL of cells from each strain were pelleted by spinning at 6,000 rcf for 2 minutes. The cell pellets were resuspended in 1 mL of 70% ethanol and incubated overnight at 4°C. Cells were spun down at 12,000 rcf for 3 minutes and washed in 800 μL of 50 mM sodium citrate (pH 7.2). Cells were washed again and sonicated with ten 0.4-second pulses. The sonicated cells were pelleted at 12,000 rcf for 3 minutes, resuspended in 500 μL of 50 mM sodium citrate (pH 7.2) with 0.25 mg/mL RNase A (QIAGEN, Cat#19101) and 0.05% Triton X-100, and incubated overnight at 37°C with shaking at 500 rpm. After the incubation, 5 μL of 20 mg/mL proteinase K (Thermo Scientific, Cat#EO0491) were added and the samples were incubated at 50°C for 2 hours with shaking at 500 rpm. The samples were mixed with 500 μL of 1 nM SYTOX™ Green Nucleic Acid Stain (Invitrogen, Cat#S7020) solution in 50 mM sodium citrate (pH 7.2) and incubated for 5 minutes at room temperature. Single-cell green fluoresce measurements were taken on a Guava easyCyte flow cytometer. 20,000 cells were countered for each strain and the flow cytometry data were analyzed using FlowJo.

2.3.10 Measuring cellular localization of ribosomal proteins using microscopy

Cells were inoculated into YEPD and grown overnight at 30°C with shaking. Cells were diluted to OD_{600} 0.1 and grown at 30°C with shaking for 4.5 hours. Fixation was done by mixing 900 μL of cells with 100 μL of 37% formaldehyde and incubating at room temperature for 15 minutes. Cells were pelleted at 6,000 rcf for 2 minutes and washed in 100 μL of potassium phosphate/sorbitol buffer (1.2M sorbitol, 0.1M potassium phosphate pH 7.5). Cells were spun down again and resuspended in 100 μL of potassium phosphate/sorbitol buffer. After adhering cells to a polylysine-treated glass slide, permeabilization was performed by submerging the slide into 100% ethanol, taking it out after 1 second, and air-drying for 5 minutes. VECTASHIELD Mounting Medium with DAPI (Vector, Cat#H-1200) was added to the slide and fluorescent microscopy was done on a DeltaVision microscope with a 100X objective. The nuclear region was determined by the DAPI signal and the average green fluoresce intensity in the nucleus and in the whole cell was measured with ImageJ (Schneider et al., 2012).

2.3.11 ThioU labeling

mRNA synthesis was determined using non-invasive metabolic labeling of RNA exactly as described in (Chan et al., 2018). In short, cells were grown in synthetic dextrose media with half the standard concentration of uracil to exponential phase, treated with 1 mM 4-thiouracil (4TU) and then collected over a time series by filtration. total RNA was extracted, biotinylated, and mRNA was enriched. Labeled and unlabeled mRNAs were separated using strepavidin beads and the two pools were measured either using qPCR for transcript-specific measurements or by RNASeq for whole transcriptome stability profiling.

2.3.12 Polysome gradient analysis

Extract from mixermilling flash-frozen cells (as harvested per "Sample Harvesting" method above) was subjected to polysome gradient analysis as described in (Ingolia et al., 2009). In short, 200 ul extract was loaded on 10-50% sucrose gradients with or without prior RNAse I treatment, depending on if sample would be used for ribosome profiling or simple polysome analysis, respectively. Samples were centrifuged in a Beckman XL-70 Ultracentrigue, using a Sw-Ti41 rotor for 3 hours at 35,000 rpm at 4oC. Tube was loaded on a Bio-Comp Gradient Station and analyzed for absorbance at 260 nm. For mass spectrometry of 60S or monosome fractions, sucrose fraction was collected and flash frozen prior to precipitation and mass spectrometry.

2.3.13 Northern blotting for rRNA intermediates

Northern blotting was performed as in (Babiano and de la Cruz, 2010), except that the 5' A0 and C1/C2 regions were detected by a mixture of three probes to increase signal strength. In short, 6ug of total RNA was loaded on 1.1% glyoxal agarose gel, and ran at 100V for 3 hours. The gel was transferred onto a nylon membrane (Hybond, GE), UV-crosslinked, and stained with methylene blue. The blot was preincubated for 2 hours at 42˚C in ULTRAhyb™ Ultrasensitive Hybridization Buffer (Invitrogen, AM8670) with 5X Denhardt's solution and 0.1mg/ml salmon sperm DNA. Oligonucleotide probes was end-labelled using [γ- 32 P]-ATP (PerkinElmer, NEG502A250UC) and T4 Polynucleotide Kinase (NEB, M0201S). Hybridization was performed at 37˚C overnight. The blot was washed twice with 2X SSC and twice with 2X SSC, 0.1% SDS, andvisualized using Typhoon phosphor-imaging.

Probes are listed below:

probe 5' A0 (1)	GGTCTCTCTGCTGCCGG
probe 5' A0 (2)	GCTTTTACACTCTTGACCAGC
probe 5' A0 (3)	CCATAGCACTCTTTGAGTTTCC
probe D/A2	GACTCTCCATCTCTTGTCTTCTTG
probe A2/A3	TGTTACCTCTGGGCCC
probe 5.8S	TTTCGCTGCGTTCTTCATC
probe C1/C2 (1)	GAACATTGTTCGCCTAGA
probe C1/C2 (2)	TCTTCTTATCGATAACGTTCC
probe C1/C2 (3)	AGATTAGCCGCAGTTGGTAA

2.3.14 Mass spectrometry

Mass spectrometry based protein quantification of total cell extracts by TMT-labeling

Proteins were precipitated by adding -20°C cold acetone to the lysate (acetone to eluate ratio 10:1) and overnight incubation at -20°C. The proteins were pelleted by centrifugation at 20,000 g for 15 min at 4°C. The supernatant was discarded and the pellet was left to dry by evaporation. The protein pellet was reconstituted in 200 µl urea buffer (8 M Urea, 75 mM NaCl, 50 mM Tris/HCl pH 8.0, 1 mM EDTA). As we had more than 20 samples (not all are shown), which had to be distributed to three different TMT-10plex mixes for relative quantification, we also generated a Master-sample, that was an equal volume mix of all samples. This Master-sample was included as a single reference sample in each of the 3 TMT-10plex mixes in order to allow relative normalization that would improve comparison between the three different TMT-10plex, as it should correct for systematic biases in each TMT-10plex mix. Protein concentrations of all samples plus the Master-sample were determined by BCA assay (Pierce). 20 µg of total protein per sample were processed further. Disulfide bonds were reduced with 5 mM dithiothreitol and cysteines were subsequently alkylated with 10 mM iodoacetamide. Samples were diluted 1:4 with 50 mM Tris/HCl (pH 8.0) and sequencing grade modified trypsin (Promega) was added in an enzyme-to-substrate ratio of 1:50. After 16 h of digestion, samples were acidified with 1% formic acid (final concentration). Tryptic peptides were desalted on C18 StageTips according to (Rappsilber et al., 2007) and evaporated to dryness in a vacuum concentrator. Desalted peptides were labeled with the TMT10plex mass tag labeling reagent according to the manufacturer's instructions (Thermo Scientific) with small modifications. Briefly, 0.5 units of TMT10plex reagent was used per 20 µg of sample. Peptides were dissolved in 50 µl of 50 mM Hepes pH 8.5 solution and the TMT10plex reagent was added in 20.5 µl of MeCN. After 1h incubation the reaction was stopped with 4 µl 5% Hydroxylamine for 15 min at 25°C. Differentially labeled peptides were mixed for each replicate (see mixing scheme below) and subsequently desalted on C18 StageTips (Rappsilber et al., 2007), evaporated to dryness in a vacuum concentrator and reconstituted in 200 µl of 3% acetonitrile and 0.1% formic acid.

TMT mix	**knocked out gene(s)**	**strain**	**TMT label**
1	*RPS25A* and *RPS25B*	7463	127N
1	*RPL41B*	7461	128N
1	*RPL40B*	2700	128C
1	*Rpl41A*	7467	129N
1	*RPL24A*	7469	129C
1	*RPL26A* and *RPL26B*	5048	130N
1	Master-mix (mix of all 27 samples)	N/A	131N
2	*RPL26A*	3851	126C
2	*RPS22A*	4659	127N

2	*RPS28B*	4474	127C
2	*RPS0B*	4651	128N
2	*RPL26B*	2374	128C
2	*RPS25B*	4658	129N
2	*RPS28A*	4472	130N
2	Master-mix (mix of all 27 samples)	N/A	131N
3	*RPL38*	3853	126C
3	*RPS29B*	4480	127C
3	*RPS22B*	4662	128N
3	*RPL40A*	7889	129N
3	*RPL7A*	7962	130N
3	*WT-2*	4484	130C
3	Master-mix (mix of all 27 samples)	N/A	131N
TMT mix	**knocked out gene(s)**	**strain**	**TMT label**
1	*RPS25A* and *RPS25B*	7463	127N
1	*RPL41B*	7461	128N
1	*RPL40B*	2700	128C
1	*Rpl41A*	7467	129N
1	*RPL24A*	7469	129C
1	*RPL26A* and *RPL26B*	5048	130N
1	Master-mix (mix of all 27 samples)	N/A	131N

LC-MS/MS analysis on a Q-Exactive HF was performed as previously described (Cheng et al., 2018; Keshishian et al., 2015). Briefly, around 1 µg of total peptides were analyzed on an EASY-nLC 1000 UHPLC system (Thermo Fisher Scientific) coupled via a 20 cm C18 column ID picofrit column (New Objective, Woburn, MA) packed in house with Reprosil-Pur C18 AQ 1.9 µm beads (Dr. Maisch, GmbH, Entringen, Germany) to a benchtop Orbitrap Q Exactive HF mass spectrometer (Thermo Fisher Scientific). Peptides were separated at a flow rate of 200 nL/min with a linear 206 min gradient from 2% to 25% solvent B (100% acetonitrile, 0.1% formic acid), followed by a linear 5 min gradient from 25 to 85% solvent B. Each sample was run for 270 min, including sample loading and column equilibration times. Data was

acquired in data dependent mode using Xcalibur 2.8 software. MS1 Spectra were measured with a resolution of 60,000, an AGC target of 3e6 and a mass range from 375 to 2000 m/z. Up to 15 MS2 spectra per duty cycle were triggered at a resolution of 60,000, an AGC target of 2e5, an isolation window of 1.6 m/z and a normalized collision energy of 36. Results were highly reproducible, as shown in Fig. 2.S5C.

Mass spectrometry based protein quantification of the 60S and the monosome (80S) peaks by TMT-labeling

Proteins were precipitated by adding -20°C cold acetone to the lysate (acetone to eluate ratio 10:1) and overnight incubation at -20°C. The proteins were pelleted by centrifugation at 20,000 g for 15 min at 4°C. The supernatant was discarded and the pellet was left to dry by evaporation. The protein pellet was reconstituted in 100 µl urea buffer (8 M Urea, 75 mM NaCl, 50 mM Tris/HCl pH 8.0, 1 mM EDTA) and protein concentrations were determined by BCA assay (Pierce). 10 µg of total protein per sample were processed further. Disulfide bonds were reduced with 5 mM dithiothreitol and cysteines were subsequently alkylated with 10 mM iodoacetamide. Samples were diluted 1:4 with 50 mM Tris/HCl (pH 8.0) and sequencing grade modified trypsin (Promega) was added in an enzyme-to-substrate ratio of 1:50. After 16 h of digestion, samples were acidified with 1% formic acid (final concentration). Tryptic peptides were desalted on C18 StageTips according to (Rappsilber et al., 2007) and evaporated to dryness in a vacuum concentrator. Desalted peptides were labeled with the TMT-11plex mass tag labeling reagent according to the manufacturer's instructions (Thermo Scientific) with small modifications. Briefly, 0.2 units of TMT-11plex reagent was used per 10 µg of sample. Peptides were dissolved in 30 µl of 50 mM Hepes pH 8.5 solution and the TMT-11plex reagent was added in 12.3 µl of MeCN. After 1 h incubation the reaction was stopped with 2.5 µl 5% Hydroxylamine for 15 min at 25°C. Differentially labeled peptides were mixed for each replicate (see mixing scheme below) and subsequently desalted on C18 StageTips (Rappsilber et al., 2007) , evaporated to dryness in a vacuum concentrator and reconstituted in 50 µl of 3% acetonitrile and 0.1% formic acid.

TMT mix	**knocked out gene(s)**	**strain**	**TMT label**
80S-1	*Wild-type*	4484	126C
80S-1	*RPL41B*	7461	127N
80S-1	*RPL26A*	3851	128N
80S-1	*RPL26B*	2374	128C
80S-1	*RPL26A* and *RPL26B*	5048	129N
80S-1	*RPL40B*	2700	130N
80S-1	*RPL40A*	7889	130C
80S-1	*RPL24A*	7469	131N
80S-1	*RPL7A*	7962	131C

80S-2	*wild-type*	4484	126C
80S-2	*RPL41A*	7467	127N
80S-2	*wild-type*	4484	127C
80S-2	*RPS22B*	4662	128N
80S-2	*RPS28A*	4472	128C
80S-2	*RPS25B*	4658	129N
80S-2	*RPS25A* and *RPS25B*	7463	129C
80S-2	*RPS22A* het and *RPS22B* het	4665	130N
80S-2	*RPS29B*	4480	130C
80S-2	*RPS22A*	4659	131N
80S-2	*RPS28B*	4474	131C
60S	*RPL26A* and *RPL26B* (60S full region)	5048	127N
60S	*RPL40B* (60S full region)	2700	127C
60S	*RPL7A* (60S full region)	7962	128N
60S	*WT* (60S full region)	4484	129N
60S	*RPS28A* (60S full region)	4472	129C
60S	*RPS29B* (60S full region)	4480	131N
60S	*RPS22A* (60S full region)	4659	131C
TMT mix	**knocked out gene(s)**	**strain**	**TMT label**
80S-1	*Wild-type*	4484	126C
80S-1	*RPL41B*	7461	127N
80S-1	*Wild-type 2*	1362	127C
80S-1	*RPL26A*	3851	128N
80S-1	*RPL26B*	2374	128C
80S-1	*RPL26A* and *RPL26B*	5048	129N
80S-1	*RPL24B*	7465	129C
80S-1	*RPL40B*	2700	130N
80S-1	*RPL40A*	7889	130C

80S-1	*RPL24A*	7469	131N
80S-1	*RPL7A*	7962	131C
80S-2	*wild-type*	4484	126C
80S-2	*RPL41A*	7467	127N
80S-2	*wild-type*	4484	127C
80S-2	*RPS22B*	4662	128N
80S-2	*RPL28A*	4472	128C
80S-2	*RPS25B*	4658	129N
80S-2	*RPS25A* and *RPS25B*	7463	129C
80S-2	*RPS22A* het and *RPS22B* het	4665	130N
80S-2	*RPS29B*	4480	130C
80S-2	*RPS22A*	4659	131N
80S-2	*RPS28B*	4474	131C
60S	*RPL26A* (60S full region)	3851	126C
60S	*RPL26A* and *RPL26B* (60S full region)	5048	127N
60S	*RPL40B* (60S full region)	2700	127C
60S	*RPL7A* (60S full region)	7962	128N
60S	empty	empty	128C
60S	*WT* (60S full region)	4484	129N
60S	*RPS28A* (60S full region)	4472	129C
60S	*RPS29A* (60S full region)	4479	130N
60S	*RPS29B* (extra 60S alone)	4480	130C
60S	*RPS29B* (60S full region)	4480	131N
60S	*RPS22A* (60S full region)	4659	131C

The samples were afterwards analyzed by LC-MS/MS on a Q-Exactive HF was performed as previously described (Cheng et al., 2018; Keshishian et al., 2015). Around 1 µg of total peptides were analyzed on an Eksigent nanoLC-415 HPLC system (Sciex) coupled via a 25 cm C18 column (inner diameter of 100 µm, packed in-house with 2.4 µm ReproSil-Pur C18-

AQ medium, Dr. Maisch GmbH) to a benchtop Orbitrap Q Exactive HF mass spectrometer (Thermo Fisher Scientific). Peptides were separated at a flow rate of 200 nL/min with a linear 106 min gradient from 2% to 25% solvent B (100% acetonitrile, 0.1% formic acid), followed by a linear 5 min gradient from 25 to 85% solvent B. Each sample was run for 170 min, including sample loading and column equilibration times. Data was acquired in data dependent mode using Xcalibur 2.8 software. MS1 Spectra were measured with a resolution of 60,000, an AGC target of 3e6 and a mass range from 375 to 2000 m/z. Up to 15 MS2 spectra per duty cycle were triggered at a resolution of 60,000, an AGC target of 2e5, an isolation window of 1.6 m/z and a normalized collision energy of 36.

2.3.15 Quantification and Statistical Analyses

Mass spectrometry based protein quantification of total cell extracts by TMT-labeling

All raw data were analyzed with MaxQuant software version 1.6.0.16 (Cox and Mann, 2008) using a UniProt yeast database (release 2014_09, strain ATCC 204508/ S288c), and MS/MS searches were performed with the following parameters: TMT-10plex labeling on the MS2 level, oxidation of methionine and protein N-terminal acetylation as variable modifications; carbamidomethylation as fixed modification; Trypsin/P as the digestion enzyme; precursor ion mass tolerances of 20 p.p.m. for the first search (used for nonlinear mass re-calibration) and 4.5 p.p.m. for the main search, and a fragment ion mass tolerance of 20 p.p.m. For identification, we applied a maximum FDR of 1% separately on protein and peptide level. We required 1 or more unique/razor peptides for protein identification and at least two MS/MS spectra ratio counts for quantification for each TMT channel in each of the three TMT mixes. This gave us a total of 2132 quantified protein groups.

Next, we normalized the corrected TMT MS2 intensity such that at each condition (sample) these intensity values added up to exactly 1,000,000, therefore each protein group value can be regarded as a normalized microshare (we did this separately for each TMT channel for all proteins that made our filter cutoff in all the TMT channels). Finally, in order to correct for systematic biases in each TMT-10plex mix, we did relative normalization for each protein group in each sample by calculating the relative ratio of the microshare intensity values relative to the microshare intensity values of the "Master-sample" in its corresponding TMT 10plex mix. This step of relative normalization improves comparison between the three different TMT-10plex.

Mass spectrometry based protein quantification of the 60S and the monosome (80S) peaks by TMT-labeling

All raw data were analyzed with MaxQuant software version 1.6.0.16 (Cox and Mann, 2008) using a UniProt yeast database (release 2014_09, strain ATCC 204508/ S288c), and MS/MS searches were performed with the following parameters: TMT11plex labeling on the MS2 level, the "precursor ion fraction" (PIF) was set to 0.75 (as we were here mainly interested in quantifying the ribosomal proteins and that at best accurarcy), oxidation of methionine and protein N-terminal acetylation as variable modifications; carbamidomethylation as fixed modification; Trypsin/P as the digestion enzyme; precursor ion mass tolerances of 20 p.p.m. for the first search (used for nonlinear mass re-calibration) and 4.5 p.p.m. for the main search,

and a fragment ion mass tolerance of 20 p.p.m. For identification, we applied a maximum FDR of 1% separately on protein and peptide level. We required 1 or more unique peptides for protein identification and a ratio count for each of the 11 TMT channels of the corresponding TMT-11plex mix. This gave us a total of 1384 quantified protein groups and among these 93 ribosomal proteins for the 60S peak samples. This gave us a total of 1238 quantified protein groups and among these 96 ribosomal proteins for the 80S-1 peak samples. This gave us a total of 1138 quantified protein groups and among these 96 ribosomal proteins for the 80S-1 peak samples. The combined number (union) of protein groups that passed the cut-off in either the 80S-1 and/or 80S-2 peak samples is 1526.

Finally, each protein group of a TMT labeled sample got its proportional fraction of the MS1 based iBAQ intensities based on its labeling channel specific TMT MS2 intensity relative to the sum of TMT MS2 intensities of all labeled channels for the corresponding protein group. Afterwards we normalized these fractional MS1 iBAQ intensities such that at each condition/time point these intensity values added up to exactly 1,000,000, therefore each protein group value can be regarded as a normalized microshare (we did this separately for each TMT channel for all proteins that made our filter cutoff in all the TMT channels of the corresponding TMT-11plex mix).

Ribosome footprint and mRNA-seq analyses

Sequencing data were analyzed as in (Ingolia et al., 2009). In short, bowtie2-based alignment (Langmead and Salzberg, 2012) was used and only unique sequences were mapped. Gene expression quantification involved summing unique reads over annotated ORFs and adjustment for RPKM (reads per kilobase million) values.

Data Clustering and Visualization

We used Cluster 3.0 (de Hoon et al., 2004) for our hierarchical clustering, using uncentered correlation clustering with the centered setting. We visualized the results using Java Treeview (Saldanha, 2004).

Statistics and correlations

All correlation measurements used throughout this manuscript are Pearson correlations. Enrichment in clusters was determined using H-B analyses to generate p-values within YeastMine (yeastmine.yeastgenome.org). Two-tailed Mann-Whitney tests were used for Figures 2.3E and 2.3F.

2.3.16 Data and Software Availability

Sequencing and mass spectrometry data included in this manuscript are publically available through NCBI GEO (accession number GSE121189) and MassIVE (accession number MSV000083033).

2.4 Results

2.4.1 Growth-defective Rpl-deficient cells show specific signatures of protein synthesis

Based on the ribosome concentration hypothesis, one would expect to see a protein synthesis signature resulting from decreasing ribosome abundances. We reasoned that measuring translation globally in *rp* mutants with a range of different ribosome levels should provide the type of data necessary to define such an effect. To this end, ribosome profiling was performed for a panel of 14 *rpl* mutants that were constructed anew alongside two wild-type (WT) controls (Fig. 2.1A, left and right sides). Because, following the whole genome duplication in budding yeast, many RP genes have remained encoded by two paralagous loci, controlled depletion of total levels for a given RP was possible without resulting in cellular death, which is the outcome of full loss of the vast majority of RP genes (Steffen et al., 2012). De novo strain construction was necessary, as others have reported and we also observed that RP mutants have a tendency to become aneuploid (Steffen et al., 2012). Specifically, deletion of several individual RP genes resulted in cells gaining an extra copy of the chromosome carrying the paralog for that RP gene with high efficiency. For this reason, all experiments were performed using freshly thawed cell stocks, no more cell divisions than was necessary for the experiment were used, and every set of sequencing data were checked for evidence of increased dosage from any chromosome(s). In the case of non-sequencing experiments, tetrad dissection of the diploid strains was performed under the experimental conditions used to ensure that aneuploidy did not result. We did not continue to analyze data from any experiment that showed evidence of aneuploidy. All experiments were performed in diploid cells, as this also allowed inclusion of some heterozygous mutations, which was helpful in assembling a panel of mutants with a broad range of growth defects.

It has been reported that in rich growth conditions, cellular doubling time is inversely proportional to growth rate and total translation rate, which is roughly proportional to ribosome number per cell (Marr, 1991; Vind et al., 1993; Warner, 1999). The panel of *rpl* mutants included doubling times varying from 97% to 149% of WT controls (Fig. 2.1A right, S1A, S1B). Recent studies have reported that under certain nutrient conditions, translation rate may not necessarily be reflective of ribosome number (Kafri et al., 2016; Metzl-Raz et al., 2017). This possibility was investigated in our conditions by performing ^{35}S-Methionine incorporation experiments using all strains that were subjected to ribosome profiling. Cellular doubling time for this panel of mutants was strongly inversely proportional to the total level of translation, as expected if translation is limiting for cell growth in our experimental conditions (Fig. 2.1B, 2.S1C). Growth rate is therefore used as a proxy for total translation levels for subsequent analyses.

WT replicates showed highly correlated patterns of translation and ordering translation data according to growth rate revealed that the mutants with the slowest growth rates also showed highly correlated translation patterns to each other (Fig. 2.1A, left). Analyses of specific clusters of similarly regulated genes revealed that several *rpl* mutants with no to mild growth defects exhibited translation increases in a group of genes that was strongly enriched for roles in amino acid biosynthesis (Fig. 2.1A, middle; 2.1C, 2.1D). Additionally, a

group of *rpl* mutants with severe growth defects showed increases in translation of genes involved in protein catabolism and the proteasome (Fig. 2.1A, middle; 2.1E, 2.1F).

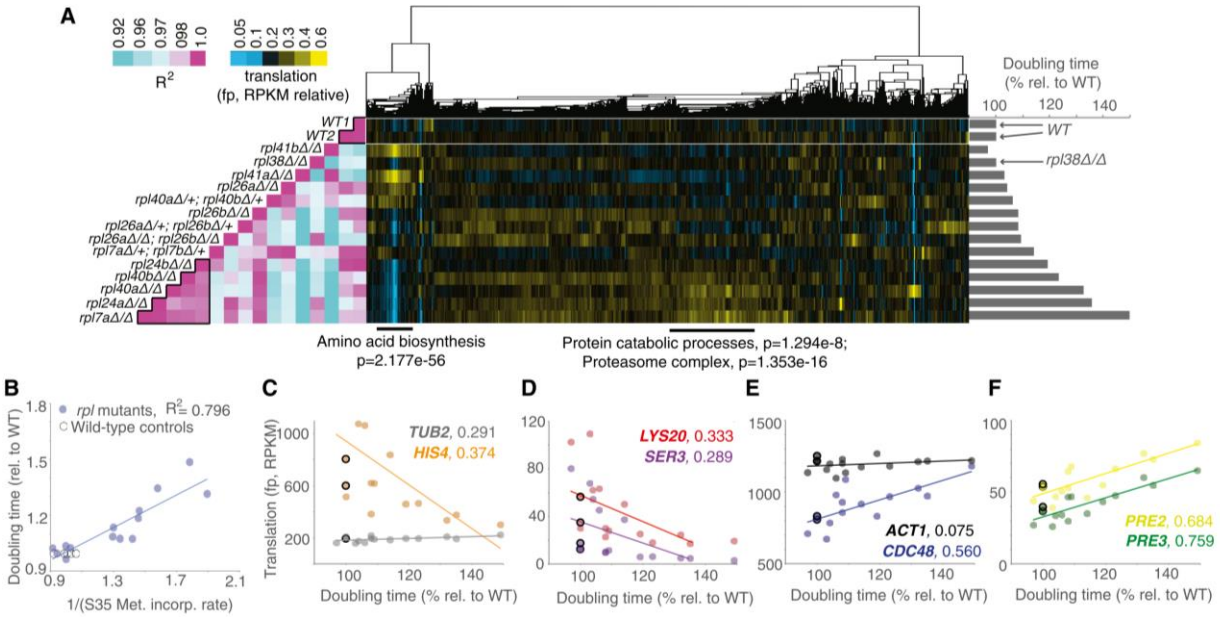

Figure 2.1: Growth rate-linked translation patterns can be seen among *rpl* mutant strains. See also Fig. 2.S1, 2.S2, 2.S4, 2.S5. A) A panel of mutants lacking genes encoding subunits of the large ribosomal subunit (60S) were subjected to growth rate analysis (bar graphs at right) and ribosome profiling (middle). Ribosome profiling data were clustered by similar expression patterns for genes (columns) across all mutants (rows). Columns are normalized to allow comparison. This analysis was highly reproducible (Fig. 2.S5A), as two wild-type controls show a near perfect correlation (Pearson, left). Note that the *rpl* mutant strains that are most defective for growth showed the most highly correlated patterns of translation (Pearson, left, boxed in pink region at bottom). Below are GO Enrichment categories with Holm-Bonferroni (H-B) p-values for two discrete gene clusters. B) Growth rates for panel of *rpl* mutants shows that doubling time is inversely proportional to bulk translation rate, as determined by ^{35}S-Methionine incorporation. C-F) Plots of protein synthesis rates versus translation levels, as assessed by ribosome footprints (RPKM). WT are represented by open black circles. C) and D) Amino acid biosynthesis genes *HIS4*, *LYS20,* and *SER3* show rates of protein synthesis that are negatively correlated with the degree of *rpl* growth rate defect. *TUB2*, a control gene, does not. *TUB2* WT values are extremely similar and thus overlapping in panel C. E) and F) Genes involved in protein catabolism, *CDC48*, *PRE2,* and *PRE3* show rates of protein synthesis that are positively correlated with the degree of *rpl* growth rate defect. *ACT1,* a control gene, does not. R^2 -values are next to gene names, based on Pearson correlation.

2.4.2 Growth-matched 40S and 60S mutants show distinct signatures of translation

If general translation defects in *rpl* mutants were due to overall translation rate, similar trends should exist in a panel of *rps* mutants with a similar spectrum of growth rates that were harvested, prepared, and sequenced in parallel to the *rpl* mutants. To address this, ribosome profiling data for 9 *rps* mutants was integrated together with the set of *rpl* mutants. Surprisingly, there were few clear trends in translation shared by *rps* and *rpl* mutants with matched growth rates (Fig. 2.S1D, 2.S1E). Clustering data after sequentially ordering *rpl* and *rps* mutants according to growth rate, however, revealed general trends that were shared among growth-defective large and small subunit mutants (Fig. 2.2A). For example, both growth defective *rps* and *rpl* mutants showed a mild upregulation in genes involved in transcription and regulation of metabolism and both showed decreases in translation of genes involved in amino acid biosynthesis compared to RP gene mutants without growth defects (Fig. 2.2A). The strongest trends observed in these data, however, differed based on whether the mutated RP gene encoded a member of the large or small ribosomal subunit. For example, the tendency for *rp* mutants with severe growth defects to upregulate proteasome-mediated protein catabolism was unique to *rpl* mutants (Fig. 2.2A, 2.2D, 2.2E). Genes involved in cytoplasmic translation were increased in translation only among *rps* mutants (Fig. 2.2A, 2.2B, 2.2C). Translation of genes involved in ribosome biogenesis was increased to some degree in both growth-defective *rpl* and *rps* mutants, but this effect was much stronger among growth-defective *rps* mutants (Fig. 2.2A).

Isolation of *rps* from *rpl* mutant data also revealed a protein synthesis signature for cells lacking Rps25 (*rps25aΔrps25bΔ*) that was distinct from other *rps* or *rpl* mutants with a similar growth defect as these cells (Fig. 2.2A). Translation patterns in *rps25aΔrps25bΔ* cells showed a generally poor correlation with all other *RP* deletes, suggesting a cellular effect due to loss of this specific RP that is distinct from lower overall ribosome number. In *rps25aΔrps25bΔ* cells, upregulation of a group of genes that are heavily enriched for mitochondrial roles, and ATP metabolism, in particular, was observed (Fig. 2.2A). Analyses of several of these genes reveal levels of expression in the *rps25aΔrps25bΔ* background that differs substantially from the trend for *rps* mutants, which instead show a slight downregulation of translation of such genes with increasing growth defect (Fig. 2.2A, 2.3A, 2.3B).

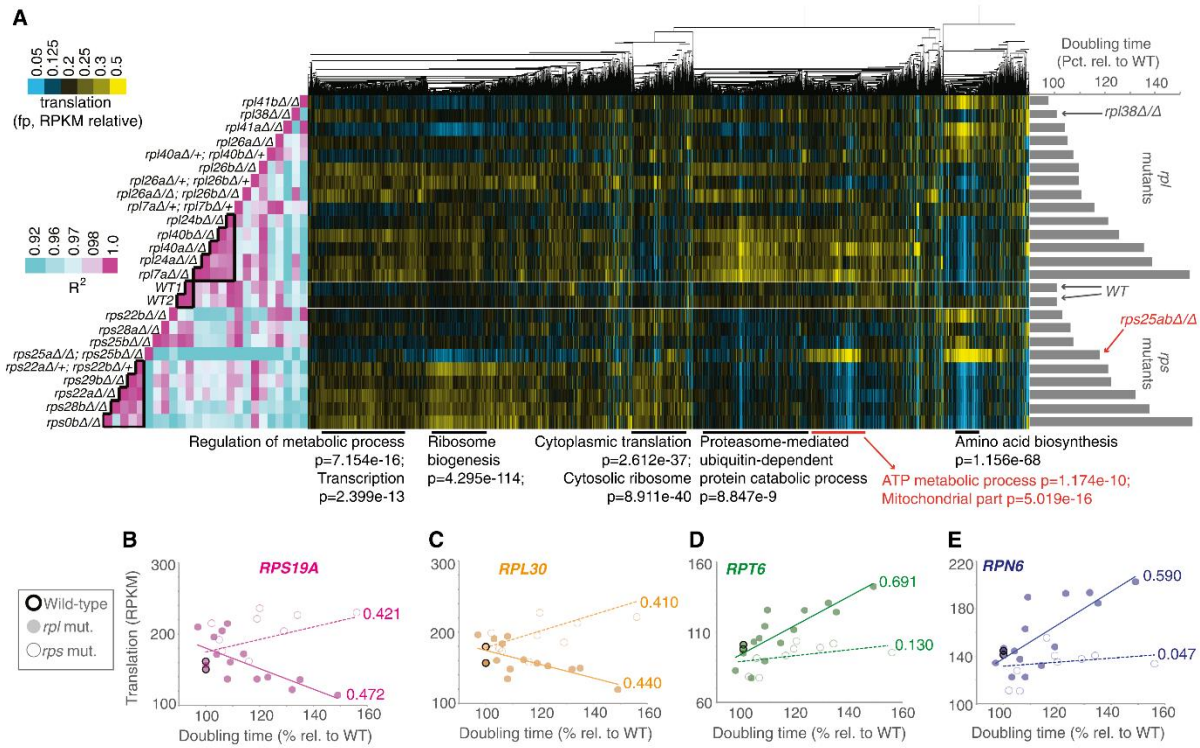

Figure 2.2: Growth rate-linked translation patterns differ between *rps* and *rpl* mutant strains. See also Fig. 2.S1, 2.S2, 2.S4, 2.S5. A panel of mutants lacking genes encoding components of the large ribosomal subunit (60S; *rpl*) or small ribosomal subunit (40S, *rps*) were subjected to growth rate analysis (bar graphs at right) and ribosome profiling (middle). Ribosome profiling data were clustered by similar expression patterns for genes across all mutants. Columns are normalized to allow comparison. Note that the *rpl* or *rps* mutant strains that are most defective for growth showed the most highly correlated patterns of translation to within each group but not between the two (Pearson correlation, left, two boxed in pink region in middle and at bottom). Note that the *rpl* data in this figure is the same as represented in Figure 2.1, analyzed in parallel with growth-matched *rps* mutants here. Below are GO enrichment categories and H-B p-values, with *rps25*-specific cluster information in red. B-E) Data for *rpl* (solid dot) and *rps* (open dot) mutants are plotted for representative RP genes B) *RPS19A,* C) *RPL30* and representative proteasome genes D) *RPT6* and E) *RPN6.* R^2 -values based on Pearson correlation are included next to lines of best fit.

2.4.3 Evidence of secondary and specific translational effects of ribosome deficiency

mRNA-seq was performed on parallel samples from all strains analyzed and, surprisingly, the general patterns observed for translation largely reflected changes in mRNA abundance, suggesting homeostatic mechanisms in constitutive *rp* mutants cells that change the cell's mRNA complement (Fig. 2.3C). When ribosome footprints were normalized to mRNA abundances to calculate translation efficiency (TE), however, one cluster of genes showed a modest decrease in TE in *rpl* mutants with a severe growth defect (Fig. 2.3C, 2.3D). This group was enriched for genes involved in cytoplasmic translation, as well as organonitrogen compound metabolic processes. A set of shared mRNA features was not apparent in this grouping. The observation that strong TE changes were rarely observed, either for growth-defective *rp* mutants or for *rps25aΔrps25bΔ* mutants, led us to consider the possibility that secondary effects from altered translation efficiency might ultimately result in lowered steady-state mRNA abundances for affected transcripts. Such secondary effects have been observed following microRNA induction, for example. In vertebrate embryos and cell culture, decreased translation efficiencies for a set of transcripts targeted by microRNAs were shown to result in subsequent degradation of affected mRNAs (Bazzini et al., 2012; Djuranovic et al., 2012). The existence of such secondary effects is likely to make steady-state interpretation of TE values in constitutive translation-associated mutants challenging.

In support of specific TE changes among growth-defective *rp* mutants that may be masked by resultant mRNA abundance changes, among the genes that show a similar trend in ribosome footprint changes with growth rate in both *rps* and *rpl* mutants (Fig. 2.2A, 2.3C), a strong association with their WT TE emerged. Namely, the set of metabolic and transcription-enriched genes that increase in translation (as judged by ribosome footprints) in growth defective *rps* and *rpl* mutants have significantly lower TE values in WT cells (Fig. 2.3E) than the overall TE spectrum for genes in WT cells; and the set of genes that are heavily enriched for roles in amino acid biosynthesis (and that are seen to decrease in translation in growth-defective *rpl* and *rps* mutants) show a significantly higher TE in WT cells than the overall WT TE spectrum (Fig. 2.3E). This observation suggests, as the ribosome concentration hypothesis proposes, that shifts in the ribosome to mRNA concentration ratio within cells may result in shifts in translation of mRNAs that are associated with their TE. These results are consistent with a study that used human models of DBA, and observed translational downregulation of genes that were normally efficiently translated and shorter in ORF length than unaffected genes (Khajuria et al., 2018). Similarly, the genes for which translation was consistently lower in RP-deficient yeast cells were moderately but not significantly shorter than the overall spectrum of ORF lengths and the genes for which translation was consistently up in RP-deficient cells were dramatically and significantly longer than the overall spectrum of ORF lengths (Fig. 2.3F).

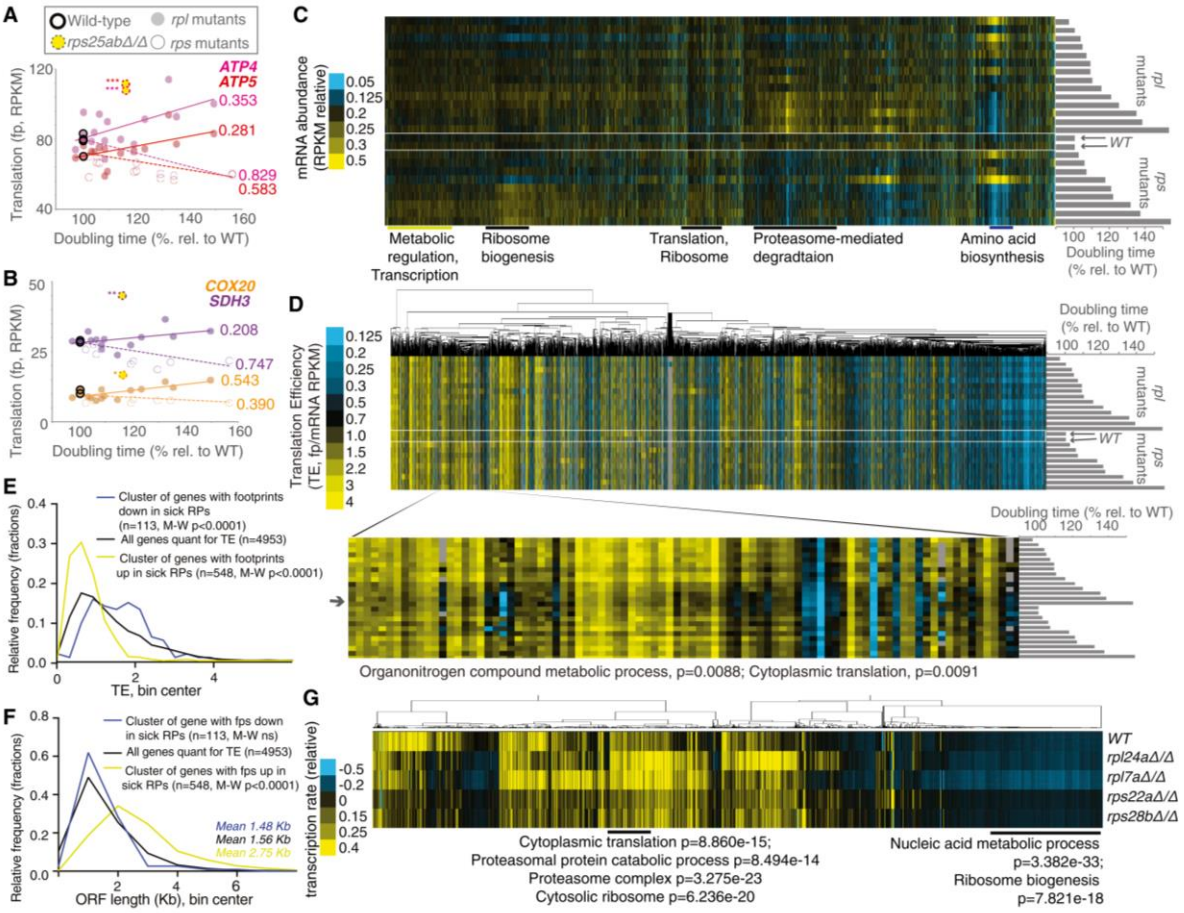

Figure 2.3: Analyses of genome-wide gene expression data suggest effects of ribosome concentration on translation and secondary effects of cellular growth rate on transcription. See also Fig. 2.S1, 2.S2, 2.S4, 2.S5. A) and B) Data for *rpl* (solid dot) and *rps* (open dot) mutants are plotted for genes involved in ATP metabolism, *ATP4*, *ATP5*, *COX20,* and *SDH3.* Yellow dash-encircled dots represent *rps25aΔrps25bΔ* cells, which show a divergent trend from growth matched *rps* mutants. R^2-values are included next to lines of best fit and are based on Pearson correlations, *values represent divergence from line of best fit for *rps* mutants, with *representing >2 standard deviations (SD) from expectation, **>4 SD, ***>7 SD. C) mRNA-seq data, resulting from total-RNA-seq (no polyA-selection) from matched samples collected in parallel for all *rps* and *rpl* mutants shown in Fig 2A are shown. Genes (columns) are ordered as in Fig 2A (top: *rpl41bΔ/Δ, rpl38Δ/Δ, rpl41aΔ/Δ, rpl26aΔ/Δ, rpl40aΔ/+ rpl40bΔ/+, rpl26bΔ/Δ, rpl26aΔ/+ rpl26bΔ/+, rpl26aΔ/Δ rpl26bΔ/Δ, rpl7aΔ/+ rpl7bΔ/+, rpl24bΔ/Δ, rpl40bΔ/Δ, rpl40aΔ/Δ, rpl24aΔ/Δ, rpl7aΔ/Δ, WT1, WT2, rps22bΔ/Δ, rps28aΔ/Δ, rps25bΔ/Δ, rps25aΔ/Δ rps25bΔ/Δ, rps22aΔ/+ rps22bΔ/+, rps29bΔ/Δ, rps22aΔ/Δ, rps28bΔ/Δ, rps0bΔ/Δ*: bottom). Columns are normalized to allow comparison. Note overall similarity to translation data (Fig. 2.2, 2.S5D). D) TE (translation efficiency, footprint/mRNA) values are shown for all genes quantified for mRNA abundance in C) and translation in Fig. 2.2A. Order of genes is matched to C). Genes (columns) are clustered according to similar patterns over all mutants (rows). Inset shows a discrete cluster of genes that show modestly lower TE values in *rpl* mutants with severe growth defects. Enrichment by H-B p-value analysis is shown below. E) The average wild-type TE values for the cluster of genes that show decreased translation in both growth-defective *rpl* and *rps* mutants in Fig. 2.2A (n=113) and the cluster with increased translation in both growth-defective *rpl* and *rps* mutants in Fig. 2.2A (n=548) are plotted and compared to the average wild-type TE values for all genes quantified (n=4953). Two-tailed Mann-Whitney (M-W) tests show that the genes with decreased ribosome footprints in growth-defective *rp* mutants have WT TE values that are significantly higher than the overall TE distribution and genes with increased ribosome footprints in growth-defective *rp* mutants have WT TE values that are significantly lower than the overall TE distribution. F) The ORF length distributions for the cluster of

genes that show decreased ribosome footprints in both growth-defective *rpl* and *rps* mutants in Fig. 2.2A (n=113) and the cluster with increased ribosome footprints in both growth-defective *rpl* and *rps* mutants in Fig. 2.2A (n=548) are plotted and compared to the average wild-type ORF lengths for all genes quantified (n=4953). Two-tailed M-W tests show that the genes with increased ribosome footprints in growth-defective *rp* mutants have ORF lengths that are significantly higher than the overall ORF length distribution. G) Metabolic labeling was used to assay new mRNA synthesis (Chan et al., 2018), with quantification of labeled mRNAs by mRNA-seq analysis. Total signal per row was normalized, as was total signal per gene. GO terms and H-B-based p-values enriched in discrete clusters are labeled below. Metabolic labeling experiments were performed by Christopher Mugler and Leon Chan and are included with their permission.

2.4.4 The mRNA complement in ribosome-deficient cells reflects homeostatic effects

When looking at the overall TE spectrum for WT controls compared to highly growth-defective *rp* mutants, a significant change in distribution was not seen (Fig. 2.S1F). This fits with the mRNA measurements, and likely reflects the effects of homeostatic mechanisms on gene expression in constitutive mutants with strong cellular effects. To determine if evidence of such mechanisms could be detected, metabolic thio-Uracil-based labeling was performed to measure relative rates of transcription in WT cells compared to two growth-defective *rpl* mutants (*rpl24aΔ* and *rpl7aΔ)* and two growth-defective rps mutants (*rps22aΔ* and *rps28bΔ*; Fig. 2.3G, ;(Chan et al., 2018)). This analysis revealed that the share of transcription devoted to RP and proteasome genes was increased in *rpl* mutants specifically (Fig. 2.3G). This was interesting because it suggested that the increase in translation (as judged by ribosome profiling) seen for proteasome-related genes in sick *rpl* mutants could be explained by an increase in transcription. This also suggested that the mild decrease in TE seen for RP genes in *rpl* mutants relative to WT cells (Fig. 2.3D) is partially counterbalanced by an increase in their transcript production. These metabolic labeling data also revealed an increase in the share of ribosome biogenesis transcription in sick *rps* mutants, specifically (Fig. 2.3G). This was consistent with the increase in ribosome footprints seen for this class of genes in these mutants. Together, these data suggest that the shifts in which mRNAs are translated in *rp* mutants is multifactorial. Evidence is observed for effects from total ribosome concentration, for *rpl*-specific gene expression effects, and for secondary effects on which transcripts are synthesized in growth-defective mutants. Together, these changes dramatically alter the spectrum of translation in a growth-defect-dependent and *rpl/rps*-dependent manner for distinct sets of genes.

2.4.5 Ribosome composition of diverse rp mutant cells is comparable

While our data were consistent with a model in which large versus small subunit mutation status and total translation levels drive gene expression changes, we wondered if different *rp* mutations or reduced translation might also result in major shifts in RP composition of ribosomes that could contribute to observed gene expression effects. To test this, matched fractions were isolated from sucrose gradients corresponding to 80S ribosomes and monosomes from two WT controls, 8 *rps* strains, and 9 *rpl* strains. Quantitative mass spectrometry was performed on these fractions, revealing that RP proteins were greatly enriched, as expected [making up an average 87.2% of mass spec signal)]. When the relative RP abundance in 80S/monosomes from *rp* mutants compared to WT was investigated, few

differences among the diverse set of mutants were observed (Fig. 2.S2). Gratifyingly, the expected lack of the protein encoded by the deleted genes was seen, but even in cases in which this removed all genes encoding a given RP (*rpl26abΔ* and *rps25abΔ*), the lack of these proteins did not generally affect the ability of other RPs to associate with the ribosome similarly as they did in WT cells (Fig. 2.S2). These data suggested that gross ribosomal heterogeneity did not generally cause the gene expression changes observed in ribosome-deficient cells.

2.4.6 Rpl versus Rps deficiency result in distinct shifts in cellular protein content

For gene expression changes to result in cellular consequences, one would expect to observe effects on protein levels. This possibility was investigated by quantitative mass spectrometry analysis of matched extract from 18 of the 23 *RP* mutants that were analyzed for translation and mRNA (Fig. 2.4A). Clustering of these data revealed the expected effects based on other gene expression measurements. For example, a cluster of genes that were heavily enriched for roles in cytoplasmic translation were seen to be increased at the protein level specifically in growth-defective *rps* mutants, consistent with the increased ribosome footprint levels (Fig. 2.2A) seen for ribosome biogenesis genes. This is also consistent with the increased ribosome footprint levels seen for RP genes in growth-defective *rps* mutants, relative to WT and growth-defective *rpl* mutants (Fig. 2.4A). Similarly, upregulation of protein levels for a cluster of genes enriched for proteasome function was seen specifically in growth-defective *rpl* mutants (Fig. 2.4A), and mirrors the ribosome footprint trends that were observed for proteasome-related genes. A decrease in proteins involved in amino acid biosynthesis in both growth-defective *rps* and *rpl* mutants, that was expected based on ribosome footprint data, was also observed (Fig. 2.4A, 2.2A). The protein level measurements thus confirmed our expectations for the effects based on measurements of prior stages of gene expression (Fig. 2.S5D) and show that significant proteome-composition changes can be seen that are dependent on the level of translation in these mutants, and whether this results from Rpl or Rps deficiency.

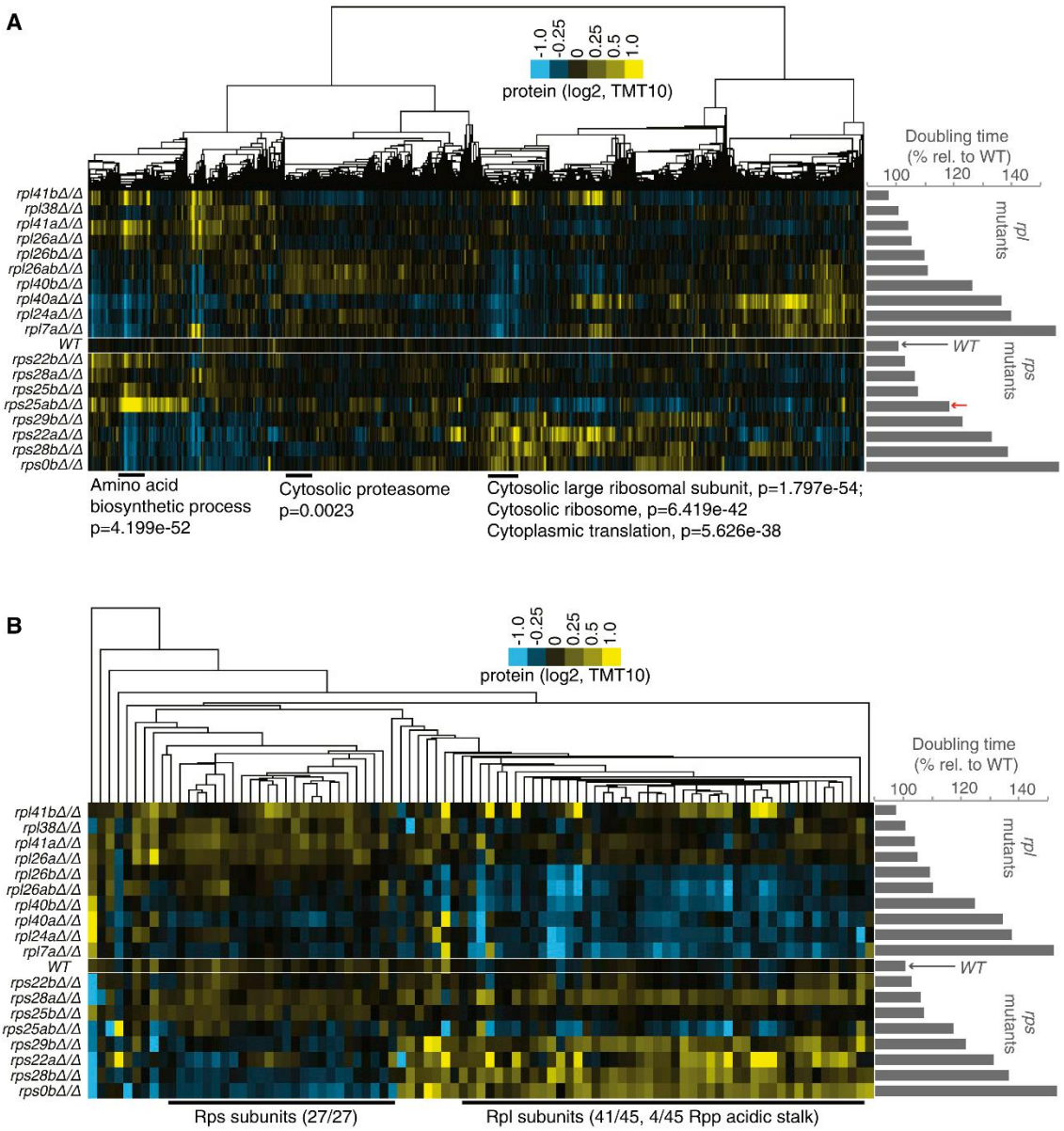

Figure 2.4: Protein levels in *rpl* and *rps* mutants generally match expectations based on translation patterns, but *rpl* mutants degrade all other RPs, while *rps* mutants only degrade other Rps subunits. See also Fig. 2.S2, 2.S4, 2.S5. A) TMT-based mass spectrometry was performed on matched extract from experiment shown in Fig. 2.2A. Genes (columns) are clustered according to similar protein abundance patterns across all mutants. Red arrow indicates the position of *rps25aΔrps25bΔ*. GO terms and H-B-based p-values enriched in discrete clusters are labeled blow plot. Columns are normalized to allow comparison. Note similarity to translation data (Fig. 2.2, 2.S5D). B) Data for RP-encoding genes only was isolated from dataset presented in A). Note that large cluster at the left contains only Rps subunits, the large cluster at right contains only Rpl and Rpp (60S acidic stalk) subunits.

2.4.7 60S mutants demonstrate general RP loss, 40S mutants retain 60S subunits

The proteomic data also offered an opportunity to directly test the degree to which loss of one RP affects the protein levels of all other RPs. It has been shown that reduced expression of even a single RP can result in degradation of others, but whether this is generally true and whether all other RPs are affected has been difficult to determine (Abovich et al., 1985). To investigate this, the mass spectrometry data for RPs only was isolated and clustered (Fig. 2.4B). A striking pattern emerged from this analysis, consisting of two major discrete clusters. The first contained 27 of the 37 Rps proteins that were measured by mass spectrometry and no other ribosomal proteins. This set was downregulated at the protein level in a manner dependent on degree of growth defect, but not dependent on whether the defect was due to loss of an Rps or Rpl (Fig. 2.4B). A larger cluster of 45 proteins contained 41 of the 47 Rpl proteins that were measured and 4 of the 6 Rpp proteins, which form the acidic stalk that is associated with the large 60S subunit (Fig. 2.4B). These proteins were downregulated at the protein level strongly and in a manner dependent on growth rate defect, but only in *rpl* mutants. All of these results were specific to protein level measurements and not observed in ribosome profiling data, suggesting that stability of the 40S subunit is dependent on individual 40S components *and* 60S components, while stability of individual 60S components appears to only depend on the presence of other 60S components.

An accumulation of 60S subunit components in growth-defective *rps* mutants suggests that an imbalance between 40S and 60S subunits is common to cells lacking Rps subunits, as previously suggested by analysis of individual *rps* cases in yeast and mammalian cells (Abovich et al., 1985; Fumagalli et al., 2009; O'Donohue et al., 2010; Volarevic et al., 2000). Polysome profiles for four *rps* and *rpl* strains were analyzed, with *rps* strains specifically showing a prominent peak at the point in the gradient corresponding to 60S subunits, proportional to their degree of growth defect. In the case of *rps0bΔ*, this peak was so prominent that it exceeded the usually dominant monosome/80S peak (Fig. 2.5A). This was not observed in *rpl* mutants, as expected (Fig. 2.5B). Notably, in growth-defective *rpl* mutants, lower polysomes than WT were not observed (see *rpl7aΔ*, in particular), despite strong evidence from ^{35}S-Methionine incorporation data suggesting significantly lower translation in these mutants (Fig. 2.5B). This could be due to either slowed translation elongation in this case or it could simply reflect limitations in making quantitative conclusions from polysome gradient analysis. The build-up of 60S subunit components relative to 40S subunits in *rps* mutants could also be confirmed by quantification of peptides originating from Rps and Rpl mutants in whole cell extract (Fig. 2.5C). Similar ratios of the two in *rpl* mutants and WT cells were seen, but growth-defective *rps* mutants showed highly elevated Rpl peptide content. This was further reflected in measurements of the ratio of a 60S rRNA (25S) to the 40S rRNA (18S) content (Fig. 2.5D) in whole cell extract.

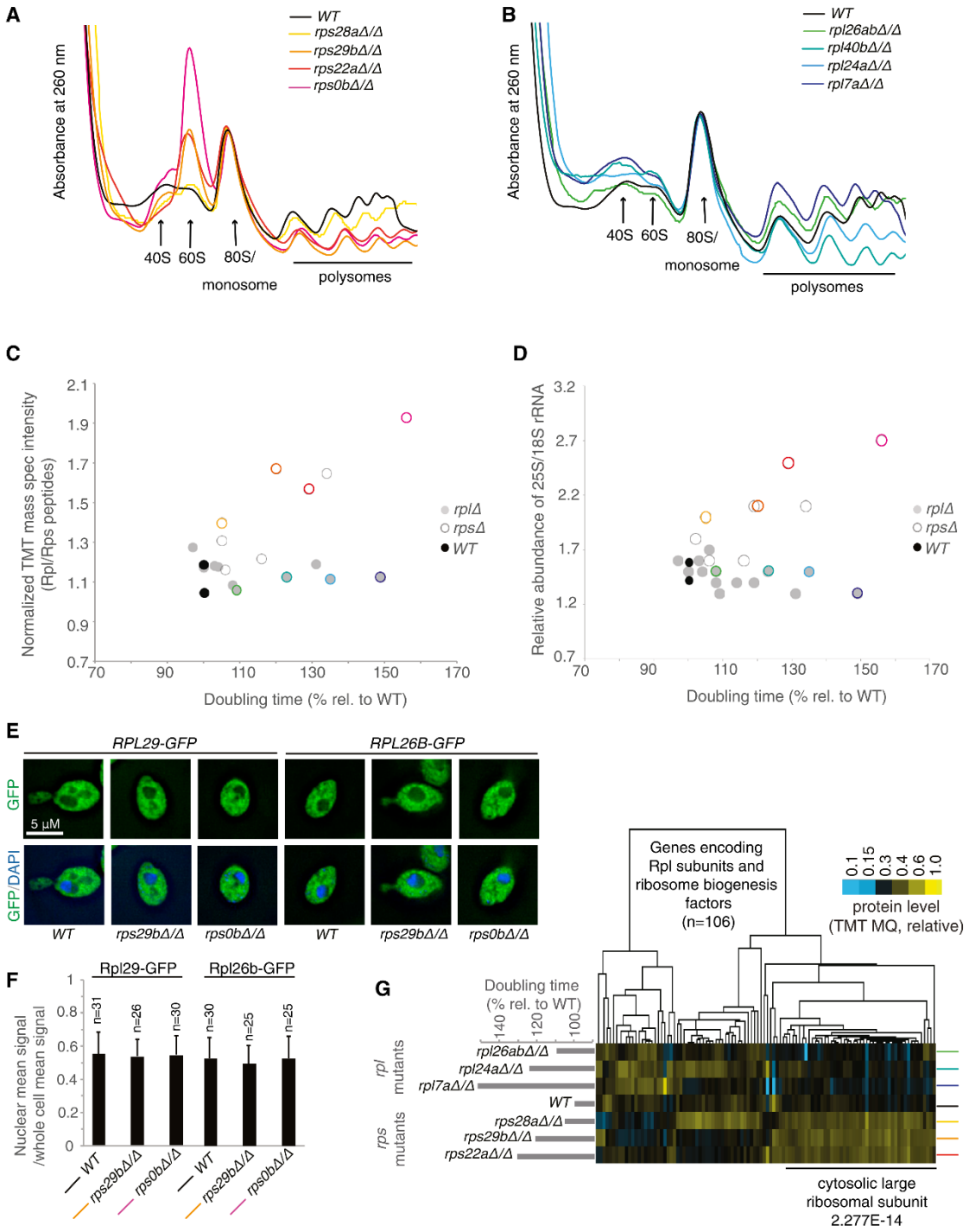

Figure 2.5: *rps* mutants accumulate mature 60S subunits. See also Fig. 2.S3. A) and B) Polysome profiling by sucrose gradient-based centrifugation to assess composition of 40S, 60S, and 80S ribosomes. A wild-type control is compared to the four growth-defective *rps* mutants in A) and four growth defective *rpl* mutants in B). The positions of these mutants on the growth spectrum are noted by colored circles in C). C) The relative ratio of peptides from Rpl and Rps subunits yielded by our mass spectrometry approach is plotted on the y-axis compared for to *rpl* and *rps* mutants of varying growth rate as noted on the x-axis. The ratios are presented as relative to a WT control. D) The ratio of 25S and 18S rRNA populations by TapeStation analysis is shown, with this ratio plotted on the y-axis and compared to *rpl* and *rps* mutants of varying growth rate as noted on the x-

axis. E). Either *RPL29* or *RPL26B* was C-terminally tagged with GFP and its localization assessed by microscopy in wild-type and two growth-defective *rps* mutant strains, compared to DAPI signal. A representative image is shown in each case. F) Quantification of GFP intensity density in the nucleus compared to the whole cell is shown for the experiment represented in Figure 2.5E. Quantification was performed using ImageJ and z-section images. Error bars represent standard deviation. G) 60S fractions were collected from sucrose gradients for wild-type cells and *rps* and *rpl* mutants. Proteins from genes (columns) encoding *RPL* or ribosome biogenesis factors are shown and clustered according to similar pattern across mutants analyzed (rows). Enrichment as determined by H-B p-value analysis is below.

2.4.8 Accumulated 60S subunits in rps mutants are not RiBi intermediates

Accumulated 60S subunits in *rps* mutants might either result from a block in maturation of such subunits, or cellular tolerance for super-stoichiometric mature large versus small ribosomal subunits. To investigate which was the case, the localization of GFP-Rpl fusion proteins was determined. In WT cells during exponential growth, any nuclear GFP signal density represents ribosomes in the process of assembly and is approximately half of that in the cell as a whole (Fig. 2.5E, 2.5F). If *rps* mutants were blocked in maturation of 60S subunits, we should observe additional GFP-Rpl signal in the nucleus in these cells. This was not the case, and rather the distribution of Rpl protein between the nucleus and cytosol in these mutants was indistinguishable from WT cells (Fig. 2.5E, 2.5F). To investigate this further, a more sensitive approach to distinguish mature from maturing 60S subunits was employed. Quantitative mass spectrometry was performed on the fractions from WT, *rpl,* and *rps* polysome gradients that corresponded to the position of 60S subunits. This fraction contained a large peak in growth-defective *rps* cells and a much smaller peak in WT and *rpl* cells. Analysis of the relative abundance of proteins present in each case, as expected, showed an overall increase of Rpl proteins, specifically, in *rps* mutants (65.1% of total signal in average *rps*, 50.3% in average *rpl*, 51.2% in WT (Fig. 2.5G, Fig. 2.S3A)). To determine the likelihood that these Rpl proteins were in mature 60S subunits, rather than maturing intermediates, data were isolated for Rpl proteins and proteins known to be involved in ribosome biogenesis (RiBi). We reasoned that if accumulated Rpl proteins represented maturing 60S subunits, we should observe a high level of specific RiBi proteins in the 60S fraction of *rps* mutants. This was not the case. A lower relative amount of RiBi proteins in this fraction was actually observed than in the equivalent fraction in WT or *rpl* mutants, suggesting that most of the excess 60S subunits in this peak in *rps* mutants were mature (Fig. 2.5G). Even proteins associated with ribosomes during late cytosolic 60S processing steps, such as Rei1, Reh1, Alb1 and Nmd3, were not seen to be enriched in the 60S fraction of growth-defective *rps* mutants (Fig. 2.5G;(Greber, 2016)). Consistently, we did not observe a build-up of large subunit-associated rRNA processing intermediates in these mutants (Fig. 2.S3B-H). We concluded that in the absence of 40S subunits, mature 60S subunits remain stable and accumulate to high levels.

2.5 Discussion

Ribosome deficiency results in strong and sometimes specific cellular effects. In humans, many such cases are thought to be responsible for diseases called ribosomopathies, which are characterized by tissue specific defects (reviewed in (McCann and Baserga, 2013)). We report here a systematic study of the link between RP deficiency and gene expression as a first step towards defining general signatures of ribosome depletion, and ultimately gaining a better understanding of the molecular underpinnings of ribosomopathies. Budding yeast offered several advantages for this study, including the ease of generating a panel of *RP* mutants with varying global levels of cellular translation, the presence of paralogs, which allow controlled depletion, and the lack of a p53-like checkpoint that responds to RP deficiency and introduces additional secondary gene expression effects (reviewed in (Bursac et al., 2014)). Our study uncovers robust gene expression signatures from RP loss that may result from primary translation defects due to a lack of ribosomes or from secondary effects of RP loss. Surprisingly, some of the strongest of these general signatures differ depending on whether ribosome deficiency results from loss of a 60S or 40S subunit component.

The reasons for the large differences in gene expression profiles in growth-matched *rpl* and *rps* mutants are unclear (Fig. 2.2, 2.3, 2.4). There have been cases in which 40S and 60S mutations have been seen to result in differing cellular phenotypes- for example, in a systematic screen for RP mutants that increase longevity, only a subset of Rpl-encoding genes, but no Rps-encoding genes, were found to show any effect when deleted (Steffen et al., 2008). In our datasets, we observe a dramatic and rpl-specific upregulation in proteasome-mediated degradation factors in a growth rate dependent manner. At least two models are attractive to explain this result. First, because *rpl* mutant cells degrade both super-stoichiometric Rpl and Rps subunits, it may be that cells require additional proteasome activity for this function (Abovich et al., 1985; Sung et al., 2016; Warner et al., 1985). Consistently, it has recently been shown that a proteasome-dependent process is indeed responsible for degradation of excess RP subunits (Sung et al., 2016). Alternatively, it is possible that mutant 60S subunits are more likely than mutant 40S subunits to result in production of poor quality nascent proteins, which subsequently increases the cellular demand for proteasome-mediated degradation. The major class of genes upregulated specifically in growth-defective *rps* mutants are involved in ribosome biogenesis. This, combined with the increased accumulation of mature 60S subunits seen in *rps* mutants of increasing growth defect was unexpected.

We cannot yet explain why *rps* mutants would continue to degrade 40S components, keep 60S components, and activate synthesis of more of both, although this is consistent with other studies of individual *rps* mutants in yeast and mammals (Abovich et al., 1985; Fumagalli et al., 2009; O'Donohue et al., 2010; Volarevic et al., 2000). Interestingly, deletion of some genes required for 60S biogenesis, *NOP53* for example, results not only in deficiency in 60S maturation but also dramatic accumulation of 40S subunits (Sydorskyy et al., 2005). In contrast to this and the reciprocal situation in *rps* mutants, a loss of 40S proteins is seen in *rpl* mutants (Fig. 2.4B, 2.5C, 2.5D), which may suggest the existence of homeostatic mechanisms that prevent a high mature 40S to 60S ratio in the cytosol. It is notable that the late cytosolic maturation steps for 40S subunits require a non-productive "test drive" translation cycle through association with 60S subunits (Strunk et al., 2012). Thus perhaps

the stockpiling of mature 60S subunits in Rps-deficient cells is a cellular adaptation to allow rapid maturation of the 40S subunits that remain. Alternatively, since translation initiation is limited by availability of 40S subunits and the small ribosomal subunit alone is the key hub for association of translation initiation factors, mRNAs, and the large subunit (Strunk et al., 2012), it may simply be that the presence of super-stoichiometric 60S subunits are tolerated by cells because they do not result in significant cellular cost, relative to excess 40S accumulation.

In addition to subunit-specific effects, we observe effects consistent with the concentration hypothesis (Fig. 2.3E;(Khajuria et al., 2018; Lodish, 1974; Mills and Green, 2017)). When considering growth rate-dependent gene expression effects that are shared by *rps* and *rpl* mutants, we find that the group of mRNAs that show upregulation of protein synthesis have a lower TE distribution than most genes in WT cells and those that show downregulation of protein synthesis have a higher TE distribution. These effects are difficult to discern by TE comparison in WT versus mutant cells, likely because the RP mutations are constitutive and translational and transcriptional changes result in secondary effects on the mRNA complement in these mutants relative to WT cells.

The ribosome concentration hypothesis consists of two parts. First, it was posited that ribosome levels could cause transcript-specific translation shifts. Second, and more specifically, it was hypothesized that mRNAs that are well translated in WT conditions should be able to outcompete poorly translated mRNAs when ribosomes are limiting (Lodish, 1974). Both parts of this model fit the observed patterns of translation in reticulocyte lysate for the two globin mRNAs originally studied. The idea that ribosome concentration alone can cause specific translation effects is also consistent with our data and with a recent human DBA study, the two studies thus far providing a direct experimental test of this hypothesis by manipulation of RP levels (Khajuria et al., 2018). In these two cases, the direction of the trend agrees with each other, but differs from the original globin–based prediction. The specific mechanisms underlying the selective translational shifts in RP-deficient cells may be based on mRNA features that are more complex than TE alone- for example, both our study and the DBA study also found an association with ORF length, which is complex to disentangle due to the known global association between ORF length with TE (Ingolia et al., 2009).

Ribosomal proteins were defined based on robust biochemical co-isolation. Subsequent structural studies have defined physical roles in the ribosome for most RPs, supporting a model in which ~80 small proteins and four RNA molecules work together as a machine to build self and other proteins from the information encoded in mRNAs (Warner, 1999). It has been proposed that the use of many small proteins in constructing a ribosome is important because it enables rapid autocatalytic production (Reuveni et al., 2017). RPs are among the most abundant proteins in cells and ribosome construction from many small pieces should be faster than if fewer, longer proteins were used. This structure provides a challenge to cells, however, which must keep many independent RPs in similar stoichiometry within cells. This seems to be largely achieved by cotranscriptonal regulation (Warner, 1999), as well as robust degradation of excess RP subunits, which appears to be highly effective for most RPs that we examined here.

We observe evidence of additional or distinct function for Rps25 in our system, beyond its general role as a core component of the ribosome, which is a valuable proof-of principle example suggesting that the approach used here should be useful in detecting cases in which specific RPs may serve additional or specialized roles. A specialized role of Rps25 has been shown in translation of viral and human mRNAs, with structural data supporting direct binding of Rps25 to IRES regions of mRNA (Hertz et al., 2013; Landry et al., 2009; Muhs et al., 2011; Nishiyama et al., 2007). Our data are consistent with a specialized role for this subunit in yeast, as well, but are also consistent with a non-ribosomal role for this protein that may produce a secondary effect on gene expression. Further work will be needed to clarify the molecular basis for this dramatic change in gene expression profile associated with yeast cells lacking Rps25. More generally, the question of whether to consider all RPs as cogs in a machine or if some of them serve distinct regulatory roles is a complex one. The fact that a handful of RPs do not result in a growth defect when deleted might be itself indicative of a specialized or condition-specific role (Fig. 2.1A; (Steffen et al., 2012)). This may, for example, be a temperature-specific role in the case of Rpl38 in yeast (Fig. 2.S4A).

Overall, however, at least for the subset of RP mutants studied here and under the conditions used here, robust and specific gene expression changes were primarily the result of decreased overall cellular translation levels and whether the mutated RP gene encodes a member of the large or small ribosomal subunit. Our study argues that orthogonal growth-matched RP mutant controls are important in disentangling specific and general gene expression effects from mutations. The high degree of secondary gene expression changes that result from mutants that strongly affect cell growth—even with no evidence of secondary mutation—is an especially notable concern for RP mutant studies, based on its prevalence in our datasets. In severely growth-defective RP mutants, we find that the mRNA complement in cells differs dramatically from that in WT cells, making analysis of translation defects, specifically, difficult. While some of these secondary effects could be due to changes in the distribution of cell cycle stages (Fig. 2.S4B, C; (Brauer et al., 2008)), the difference in effects that we observed between *rpl* and *rps* mutants with similar growth defects points to additional, yet-to-be-determined factors.

2.6 Acknowledgements

We thank Nick Ingolia and Nick Guydosh for critical reading of this manuscript and helpful suggestions. We thank Basil Greber, Jamie Cate, and Ray Deshaies for feedback on conceptual aspects of this project. This work has been funded by NIH grants (DP2-GM-119138; P50-GM-31535), investigator awards from the Alfred P. Sloan Foundation (FG-2016-6229) and Pew Charitable Trusts (00029624), and UC-Berkeley start-up funding, including from the Bowes Foundation, to GAB. KW and CFM are supported by a grant from the Swiss National Science Foundation (SNF 159731). AR is supported by NIHGRI CEGS (P50 HG006193), the Klarman Cell Observatory, and HHMI. MJ is supported by a Maximizing Investigators' Research Award for Early Stage Investigators (R35GM128802). AK is supported as a Dean's Fellow by Columbia University Graduate School of Arts and Sciences. LYC is funded by the Shurl and Kay Curci Foundation.

2.7 Supplemental figures

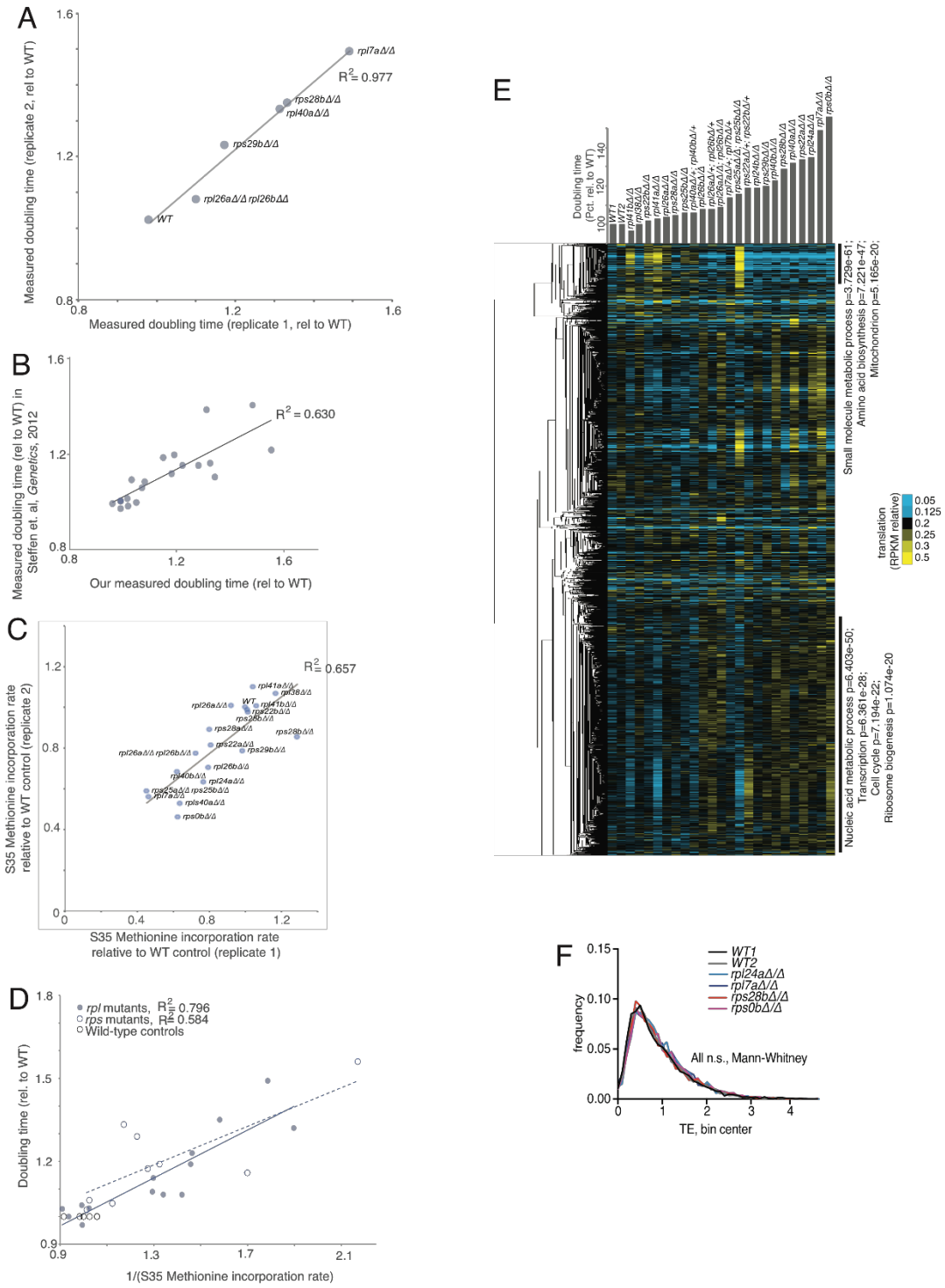

Figure 2.S1: Growth rate and bulk translation measurements are reproducible, show that *rp* mutants with lower growth rates have less translation, modest strictly growth-linked translation signatures, Related to Figures 2.1, 2.2, and 2.3. A) Reproducibility of growth rate measurements (as determined by OD600 measurements) was tested for a subset of *rp*

mutants (full biological replicates) and found to be extremely highly reproducible by Pearson correlation. B) Our growth rate measurements for *rp* mutants in diploids in the SK1 strain background were highly correlated (Pearson) with measurements from another group (Steffen et al., 2012) in haploids of the S288C strain background. C) Our ^{35}S-methionine incorporation measurements were reproducible, based on Pearson correlation. Full biological replicates were tested for ^{35}S-methionine incorporation as a proxy for bulk translation rate, compared to WT controls. D) Both *rpl* and *rps* mutants show lower bulk translation associated with lower growth rate. *rpl* data is also shown in Figure 2.1B. Pearson correlation analysis was used. E) Ribosome profiling from a panel of wild-type, *rpl* and *rps* mutants was performed. Mutants were sorted according to growth rate and subjected to hierarchical clustering. Note that trends in gene expression are less apparent than in Figure 2.2A, which plots the same data, but divided by *rpl* or *rps* status. Note that columns (genes) are normalized to enable visual comparison among them. Enrichment based on H-B analysis of GO categories is shown below. F) Steady-state TE distributions do not change in RP-defective cells. The TE value distributions for two wild-type, two growth-defective *rpl*, and two growth-defective *rps* mutants are shown. Note no significant difference in these constitutive nulls based on two-tailed Mann-Whitney analysis.

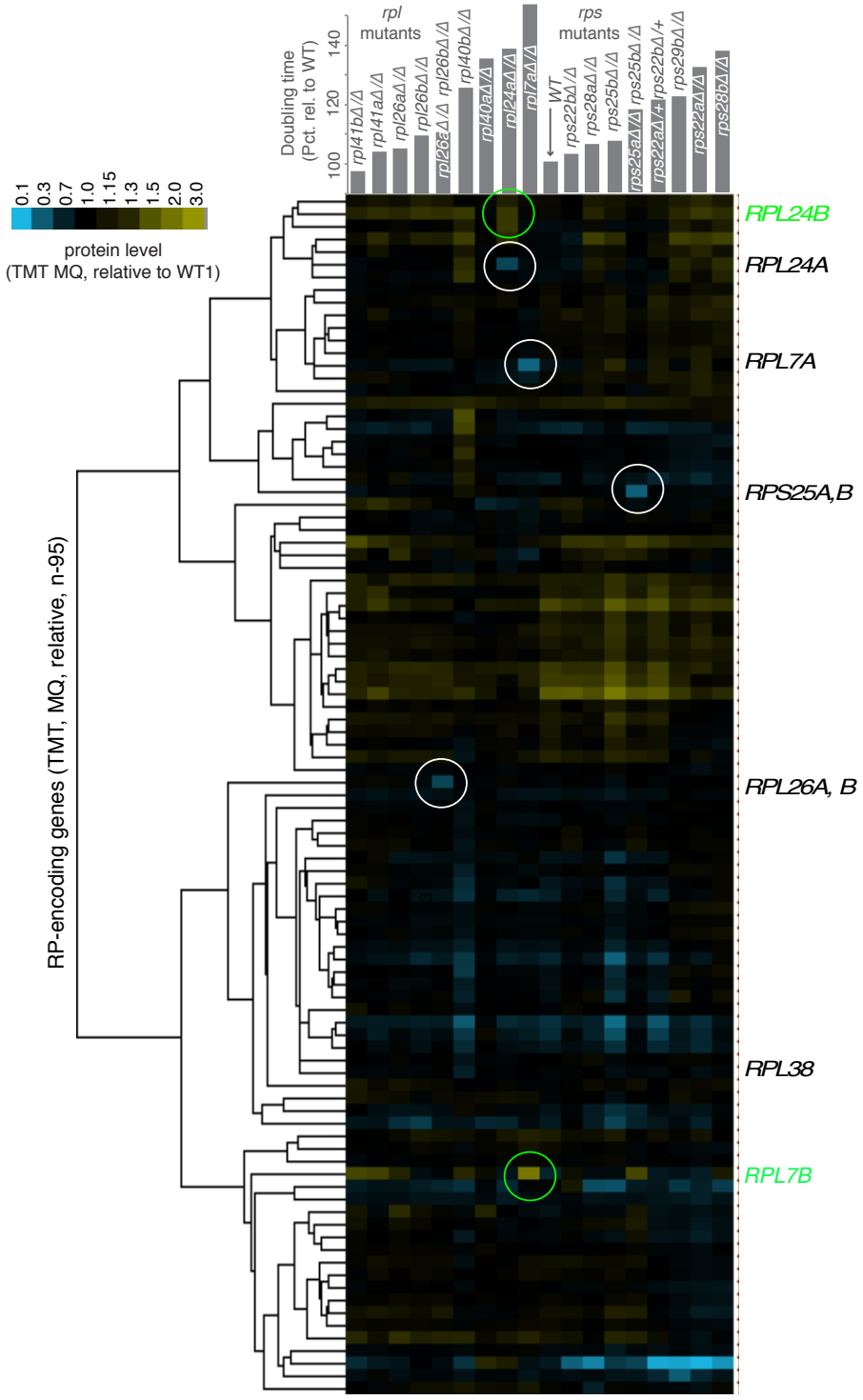

Figure 2.S2: Mass spectrometry of 80S/monosome fractions reveals similar RP composition for assembled ribosomes among *rp* mutants, Related to Figures 2.1-2.4. TMT mass spectrometry was performed on fractions corresponding to position of 80S/monosomes during polysome analysis by sucrose gradient. Rows (proteins/genes) were clustered

hierarchically for each mutant relative to the same WT sample in each case, matched to the appropriate TMT mix. Circled boxes represent changes in levels of either the protein encoded by the deleted gene or its paralog in cases in which these RPs were quantified by mass spectrometry. Note the case of Rpl7, for which we measured each paralogous gene encoding this RP and note that in cells deleted for *RPL7A,* an increase in ribosome incorporation of Rpl7B could be seen.

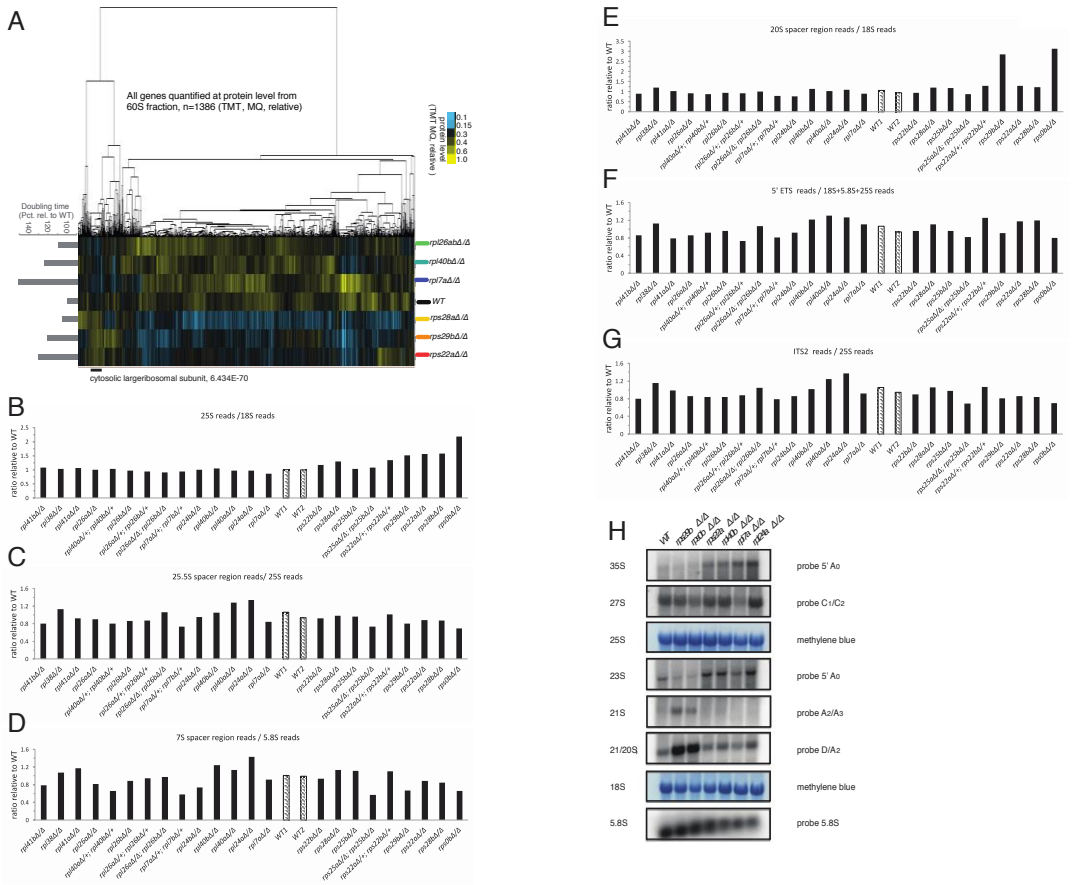

Figure 2.S3: Mass spectrometry of 60S polysome gradient fractions and rRNA analyses reveal specific enrichment for Rpl proteins in *rps* mutants, Related to Figure 2.5. A) TMT mass spectrometry was performed on fractions corresponding to position of 60S ribosomal subunits during polysome analysis by sucrose gradient. Columns (proteins/genes) were clustered hierarchically and each column was normalized to enable visual comparison among them. Note that *rps* mutants are enriched for a cluster of genes that are extremely highly enriched for large subunit RPs, based on H-B p-value analysis of GO enrichment. B-G) For all RNA species analyzed, total RNA sequencing results were aligned and quantified, order of strains is identical to Figure 2.2 and ratios are relative to WT. B) The ratio of total 25S versus 18S are shown. C) The ratio of reads from the 25.5S spacer region to 25S are shown. Note no enrichment in *rps* mutants, despite an overall high level of large subunit rRNA. D) The ratio of reads from the 7S spacer region to 5.8S are shown. E) The ratio of reads from the 20S spacer region to 18S are shown. Note that *rps29bΔ* and *rps0bΔ* cells show evidence of small subunit processing defects, consistent with published reports (Ferreira-Cerca et al., 2005; Ford et al., 1999; O'Donohue et al., 2010). F) The ratio of reads from the 5' ETS region to 18S, 5.8S, and 25S are shown. G) The ratio of reads from ITS2 to 25S are shown. H) Northern blotting for rRNA intermediates [as in (Babiano and de la Cruz, 2010)] is shown, reflecting similar trends as sequencing analyses in A-F. Note that 21S and 23S intermediates are described in (Martin-Marcos et al., 2007; Tabb-Massey, 2003).

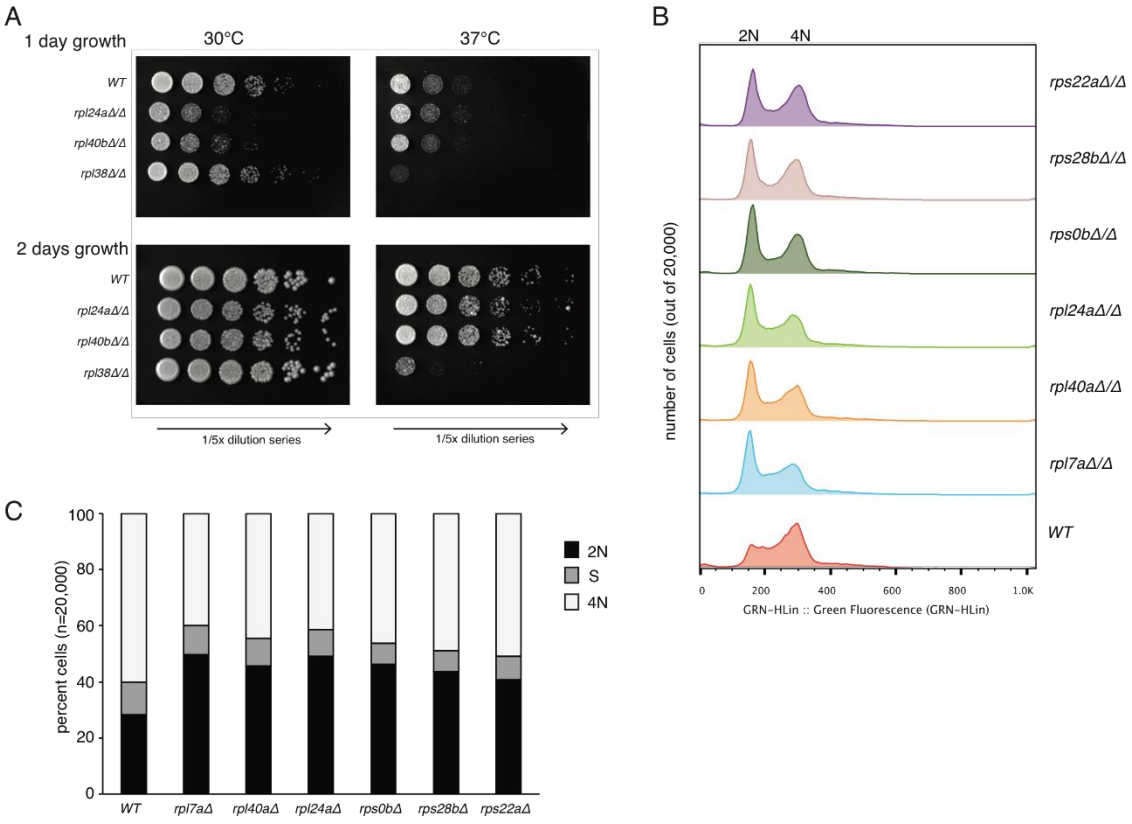

Figure 2.S4: Temperature-sensitivity and cell cycle defects in select *rp* mutants, Related to Figures 2.1-2.4. A) *rpl38Δ* cells show no growth defect at 30°C, but a profound growth defect at 37°C that is not shared by other *rpl* mutants. Cells were grown to exponential phase and plated in dilutions decreasing by 5-fold per spot from left to right. Identical cells were plated in parallel on two sets of plates and grown for either one or two days at either 30°C or 37°C. B) The results of flow cytometry on Sytox Green-treated wild-type and *rp* mutant cells show that growth defective *rpl* and *rps* mutants show G1 accumulation relative to WT controls. C) The results shown in B) were quantified according to DNA content.

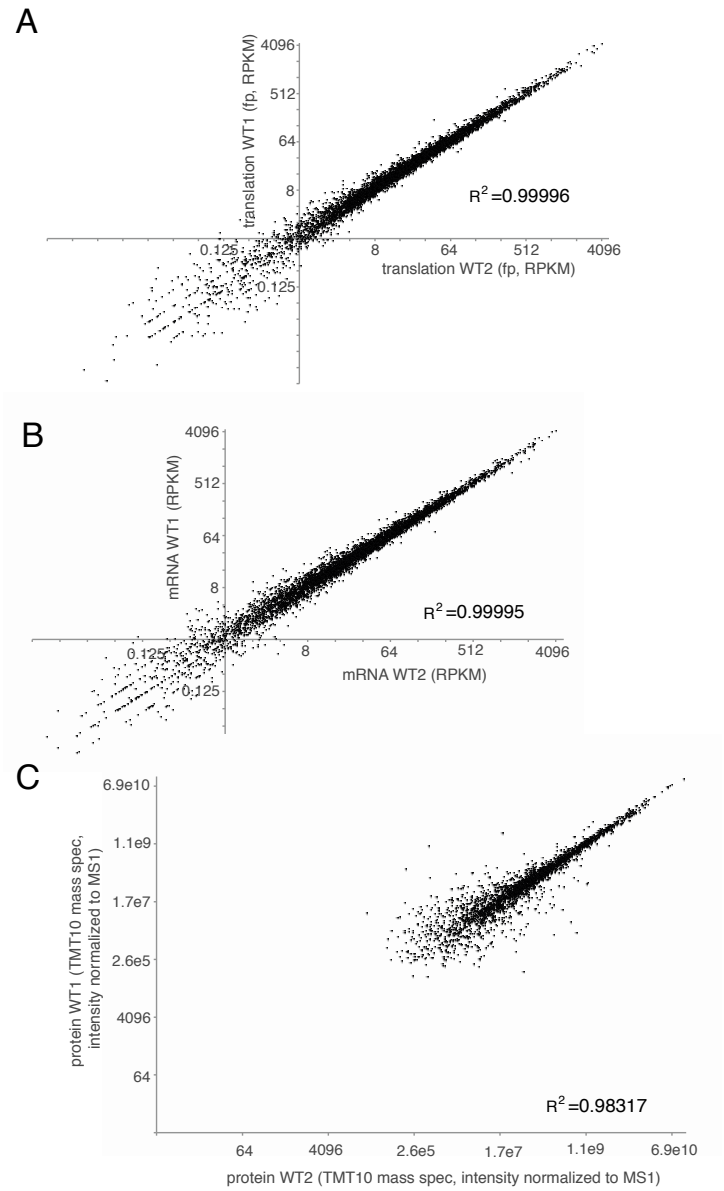

D

	*rpl41b*Δ	*rpl38*Δ	*rpl41a*Δ	*rpl26a*Δ	*rpl26b*Δ	*rpl26a*Δ *rpl26b*Δ	*rpl40b*Δ	*rpl40a*Δ	*rpl24a*Δ	*rpl7a*Δ	*WT*	*rps22b*Δ	*rps28a*Δ	*rps25b*Δ	*rps25a*Δ *rps26b*Δ	*rps29b*Δ	*rps22a*Δ	*rps28b*Δ	*rps0b*Δ
FP:RNA	0.843	0.871	0.861	0.875	0.864	0.884	0.853	0.842	0.861	0.849	0.865	0.833	0.865	0.859	0.833	0.854	0.835	0.838	0.817
FP:Prot	0.573	0.530	0.586	0.505	0.485	0.494	0.504	0.487	0.502	0.507	0.526	0.563	0.520	0.530	0.572	0.516	0.477	0.503	0.437
RNA:Prot	0.329	0.337	0.356	0.322	0.326	0.338	0.321	0.305	0.346	0.324	0.328	0.298	0.324	0.328	0.303	0.293	0.277	0.287	0.223

Key 0.20 0.30 0.40 0.50 0.60 0.70 0.80 0.90 Correlation coefficient (Pearson)

Figure 2.S5: mRNA-seq, ribosome profiling, and mass spectrometry measurements were reproducible and showed expected correlations, Related to Figures 2.1-2.4 A-C) The results of gene expression measurements for full biological replicates for wild-type cells grown in parallel with *rp* mutants analyzed in Figures 2.1, 2.2, 2.3, and 2.4 are shown and compared using Pearson correlation-based analysis. A) ribosome profiling measurements of

translation are highly reproducible in our experiments. B) mRNA-seq measurements are highly reproducible in our experiments. C) TMT-based mass spectrometry measurements of protein levels are highly reproducible in our experiments. D) Correlations among mRNA, ribosome profiling and mass spectrometry measurements. Pearson correlation coefficients are shown between each type of gene expression measurement for each strain for which we measured mRNA, translation (by ribosome footprints, abbreviated "FP"). To allow comparison to mass spectrometry data, values were first multiplied by average iBAQ value for each sample mixture.

CHAPTER 3

Pervasive, coordinated protein level changes driven by transcript isoform switching during meiosis

Part of the work presented in this chapter has previously been published in the following manuscript: Cheng, Z., Otto, G.M., Powers, E.N., Keskin, A., Mertins, P., Carr, S.A., Jovanovic, M. and Brar, G.A., 2018. Pervasive, coordinated protein-level changes driven by transcript isoform switching during meiosis. *Cell*, *172*(5), pp.910-923.

doi.org/10.1016/j.cell.2018.01.035

3.1 Abstract

To better understand the gene regulatory mechanisms that program developmental processes, we carried out simultaneous, genome-wide measurements of mRNA, translation and protein through meiotic differentiation in budding yeast. Surprisingly, we observed that the levels of several hundred mRNAs are anti-correlated with their corresponding protein products. We show that rather than arising from canonical forms of gene regulatory control, the regulation of at least 380 such cases—or over 8% of all measured genes—involves temporally regulated switching between production of a canonical, translatable transcript and a 5' extended isoform that is not efficiently translated into protein. By this pervasive mechanism for the modulation of protein levels through a natural developmental program, a single transcription factor can coordinately activate *and* repress protein synthesis for distinct sets of genes. The distinction is not based on whether an mRNA is induced or not, but rather based on the type of transcript produced.

3.2 Introduction

The decoding of cellular information from DNA to protein determines cellular identity. Despite a strong body of knowledge of how transcription and translation are controlled, our understanding of how their regulation drives fluid changes in cell structure and function over a developmental program is rudimentary. Global studies have revealed complex patterns of gene expression regulation in contexts of cellular change, especially during developmental programs, with evidence accumulating for much more regulation than we can currently explain mechanistically [for examples, see (Blank et al., 2017; Brar et al., 2012; Duncan and Mata, 2014; Jovanovic et al., 2015; Kronja et al., 2014; Peshkin et al., 2015; Tanenbaum et al., 2015); for review, see (Liu et al., 2016)]. Developmental programs include embryogenesis, as well as cellular differentiation, and are characterized by rapid and unidirectional transitions in cellular state. These changes are largely thought to be driven by transcriptional activators, which turn up mRNA production to promote protein synthesis, and repressors, which turn down mRNA production and allow gene expression to be reduced. By such classical models, gene expression patterns are thus set by transcriptional regulation, which may be subsequently enhanced or dampened by post-transcriptional regulation.

Meiosis is one such conserved process of differentiation, during which chromosome and organelle segregation are coupled to gamete formation (sporulation in budding yeast). The large body of knowledge about meiotic progression in the budding yeast *Saccharomyces cerevisiae* and the tractability of isolating large numbers of synchronous cells makes this system a valuable model for studying gene regulation in cellular differentiation. Our previous study (Brar et al., 2012), revealed extensive formerly unrecognized transcriptional and translational regulation in meiotic cells, but the mechanisms responsible for this regulation and their impact on protein levels were unclear. We therefore performed a deeper global study here, aimed at determining the impact of transcriptional and translational regulation on the meiotic proteome. To our knowledge, the resultant dataset represents the most complete gene expression atlas to date for any developmental process.

We were surprised to identify a large subset of genes for which mRNA abundance patterns were not predictive of protein patterns despite high quality and reproducibility of measurements. Our deep dataset, enabling robust detection of both qualitative and quantitative features of gene expression, allowed us to discover that many such cases show hallmarks of a non-canonical mode of regulation that involves transcriptional toggling between two transcript isoforms encoding identical Open Reading Frames (ORFs), one of which is a traditional mRNA that is zwell translated and results in protein accumulation, and one of which is an often abundant transcript that cannot be efficiently translated and results in decreased protein production (Chen et al., 2017; Chia et al., 2017). We find that this is a global regulatory mechanism that sets protein levels for over 8% of all measured genes over meiotic differentiation. By this mechanism, a transcription factor can drive synthesis of mRNA for a set of genes in concert, but this transcriptional activation results in gene expression activation in some cases and repression in others, depending on the type of transcript produced. Here, transcriptional and translational control are integrated in their regulation rather than sequential, such that the translatability of an mRNA isoform—rather than its quantity per se—is fundamental in setting protein levels through a natural and conserved developmental process.

3.3 Methods

3.3.1 Yeast material and growth conditions

All experiments were performed using diploid *Saccharomyces cerevisiae* strains of the SK1 background. All are *MAT*a/alpha except Br-Ün5805, an SK1 strain that is wild-type except for two copies of the *MATa* locus and no *MATalpha* locus (van Werven et al., 2012). This latter strain will not undergo meiosis, even when stimulated with conditions that should induce it.

For major meiotic timecourse, Br-Ün strain 1362 [equivalent to gb15 in (Brar et al., 2012)] was inoculated into YEPD overnight, then diluted to OD_{600}0.2 into buffered YTA and grown for 12 hours. Cells were washed in water and resuspended in 250 ml sporulation media supplemented with 0.02% raffinose. Cells were incubated, with shaking at 30^{o}C. For vegetative growth, strains were incubated with shaking at 30^{o}C.

3.3.2 Sample collection

Meiotic samples for main experiment were collected at the timepoints presented in Figure 3.1, as in (Brar et al., 2012), using 1 minute cyclohexamide treatment, filtration and flash freezing in liquid Nitrogen in two portions, 90% for ribosome profiling, 10% for total RNA isolation. Vegetative exponential samples were collected after growth of 750 ml in YEPD to OD_{600}0.6 from a dilution to OD_{600}0.05. *MAT*a/a samples were treated as the meiotic, but only one sample was collected, at 4.5 hours.

3 mL flash frozen buffer was added to ribosome profiling aliquot (also to be used for mass spectrometry) of the standard ribosome profiling composition (20mM Tris pH8, 140mM KCl, 1.5mM MgCl2, 100ug/ml cycloheximide, 1% Trition X-100) supplemented with 2ug/ml

Aprotinin, 10ug/ml Leupeptin, 1mM PMSF, 1:100 PIC2, 1:100 PIC3 (both Sigma inhibitor cocktails). Samples were lysed by Retsch mixermilling (6x 3 minute rounds at 15 Hz). Resulting powder was thawed, spun once at 4C for 5 min at 3000 RCF, sup was removed and spun at 20,000 RCF at 4C for 10 minutes. Extract was aliquoted in 200ul portions and flash frozen. Identical extract was used for ribosome profiling and mass spectrometry.

3.3.3 Ribosome profiling

Ribosome profiling was performed as described previously in (Brar et al., 2012). The detailed protocol is identical to (Ingolia et al., 2012) except that no linker ligation was used and instead ribosome footprints were polyA-tailed to mark the 3'ends rather than using linker ligation. In short, samples were treated with RNase I (Ambion) at 15 U per A260 unit of extract for 1 hour at room temperature. Samples were then loaded onto sucrose gradients (10-50%) and centrifuged for 3 hrs. at 35,000 rpm at 4^{o}C in a SW41Ti rotor (Beckman). 80S/monosome peaks were collected using a Gradient Station (BioComp). RNA was extracted using the hot acid phenol method, RNA was size selected from a polyacrylamide gel, dephosphorylated, polyA-tailed, subjected to rRNA subtraction, RT-PCR, circularization, and PCR. The enzymes used were PNK (NEB, lot 0951602), E.coli polyA polymerase (NEB, lot 0101309), Superscript III (Thermo, lot 1752971), Circ Ligase (Epicentre), Phusion polymerase (NEB). Oligos used were oCJ200-oligodT for Reverse transcription, oNTI231 and aatgatacggcgaccaccgagatcggaagagcacacgtctgaactccagtcac-barcode-cgacaggttcagagttc index primers, for PCR, all also PAGE purified from IDT, where the barcodes are six nucleotides in length. Sequencing was done for both reads with standard Illumina oligos.

3.3.4 mRNA sequencing

The protocol followed was identical to above, except for the following: single round polyA-selected RNA was alkaline fragmented and size selected to 30-50 nt. Fragments were subjected to an identical library prep pipeline as the footprints, but no selective rRNA subtraction round was used. A parallel set of RNA was sequenced that excluded the polyA-selection step, but sequencing depth of mRNA was much lower, as expected, and agreement with the polyA-selected data was high (Fig. 3.S2B). We thus use the polyA-selected mRNA data for all analyses presented.

3.3.5 Sequencing

All samples were sequenced on an Illumina HiSeq 2500, 50SRR, with multiplexing, at the UC-Berkeley Vincent Coates QB3 Sequencing facility.

3.3.6 Meiotic staging

Progression of cells through meiosis in each timecourse included here was determined by quantification of nuclear morphology by DAPI staining (Vectashield, Vector) of ethanol-

permeabilized cells adhered to a polylysine-treated glass slide. Prior to anaphase I, cells show mononucleate morphology, at and after anaphase I and before anaphase II, cells show binucleate morphology, during and following anaphase II, cells show tetranucleate morphology. All timecourses were also assessed at 24 hours after transfer to sporulation media by brightfield microscopy to ensure high efficiency of spore formation, which we typically observe at ~90%. The Ndt80 induction experiment (Fig. 3.5C-I, S5) was also staged using indirect immunofluorescence of alpha-tubulin, using a rat anti-tubulin antibody (Serotec) at a dilution of 1:200 and anti-rat FITC antibody (Jackson ImmunoResearch Laboratories) at 1:100. Fluorescent microscopy was done on a DeltaVision microscope with a 100X objective.

3.3.7 Ndt80 induction

Cells carrying *GAL-NDT80* and *pGPD1-GAL4(848).ER* constructs [as described in (Carlile and Amon, 2008)] were introduced to sporulation medium and incubated with shaking at 30^{O}C for 5.5 hours. At that time, β-estradiol was added to half of the culture at a concentration of 1μM. The Northern blotting of the Ndt80 release experiment in Fig. 3.5A, 5B was done using mRNA extracted for this manuscript from frozen pellets archived from the experiment published in (Brar et al., 2012). Data in Figure 3.5B is based on analysis of matched translation and mRNA-seq data from (Brar et al., 2012).

3.3.8 Strain construction

Reporter strains used for Western blotting pictured in Figure 3.4 were constructed by amplification of promoter regions, including >200 nt upstream of 5' most mRNA-seq read observed at any timepoint in our dataset. These regions were cloned upstream of a plasmid encoding eGFP to create (*pPOP4-eGFP*), pUB1288 (*pRAD16-eGFP*), and pUB1290 (*pSHS1-eGFP*). pUB1288 was mutated to remove the 50 nt region containing the proximal promoter to create pUB1324 (*pSHS1Δprox-eGFP*), using the Q5 Site-directed mutagenesis kit (New England Biolabs). All constructs were integrated into the genome by amplification *TRP1* on both sides and integration into this locus in a strain carrying a trp1::hisG allele.

3.3.9 Western blotting

Western blotting was performed using a standard trichloroacetic acid (TCA) protocol, exactly as described in (Chen et al., 2017), except using a mouse anti-GFP JL8 antibody (Clontech). In short, 5ml of meiotic cells in culture (or 2ml vegetative) were collected and incubated with 5% TCA for at least 10 minutes at 4^{o}C. Cells were centrifuged for 2 min. at 20,000 rcf and supernatant was aspirated. Cells were washed with acetone and pellets dried for at least 2 hours. Cell extract was made by addition of TE, supplemented with 3 mM DTT and protease inhibitors (Roche), and 1 volume of acid-washed glass beads. Tubes were agitated for 5 minutes, after which 3X SDS sample buffer was added, samples were boiled for 5 minutes, centrifuged for 5 min at 20,000 rcf. 8 μl supernatant was loaded onto Bis-Tris

acrylamide gels. Gels were transferred using a Turboblot system (BioRad). Primary anti-GFP antibody dilution was 1:2000, anti-hexokinase was 1:12,000, secondary (Li-Cor) was 1:20,000. Primary antibody incubation was overnight, secondary for 1-2 hours. Blots were visualized using a Li-Cor system.

3.3.10 Northern blotting

8ug of total RNA from timecourse (Fig. 3.1A) was loaded onto either 1% or 1.5% Formaldehyde agarose gels, and run at 170V for 2.5 hours. A DNA ladder was also loaded to assess rough sizing. The gel was transferred onto a nylon membrane (Hybond, GE), crosslinked, and methylene blue stained for loading. The blot was blocked with Northern Max Ultrahyb buffer (Ambion) at 68C for 30 minutes. The probe was generated by PCR of wild-type genomic yeast DNA and in vitro transcription (MaxiScript T7 kit, Thermo) using alpha-UTP and all other nucleotides cold. The blot was incubated with the probe overnight at 65C, washed as recommended by NorthernMax kit (Ambion), and visualized using Typhoon phosphor-imaging.

3.3.11 Mass spectrometry

Deep coverage meiotic time course proteomics data set generated by TMT-labeling and sample fractionation

Proteins were precipitated by adding -20°C cold acetone to the lysate (acetone to eluate ratio 10:1) and overnight incubation at -20°C. The proteins were pelleted by centrifugation at 20000xg for 15min at 4°C. The supernatant was discarded and the pellet was left to dry by evaporation. The protein pellet was reconstituted in 200µl urea buffer (8M Urea, 75mM NaCl, 50mM Tris/HCl pH 8.0, 1mM EDTA) and protein concentrations were determined by BCA assay (Pierce). 40µg of total protein per sample were processed further. Disulfide bonds were reduced with 5mM dithiothreitol and cysteines were subsequently alkylated with 10mM iodoacetamide. Samples were diluted 1:4 with 50mM Tris/HCl (pH 8.0) and sequencing grade modified trypsin (Promega) was added in an enzyme-to-substrate ratio of 1:50. After 16h of digestion, samples were acidified with 1% formic acid (final concentration). Tryptic peptides were desalted on C18 StageTips according to (Rappsilber et al., 2007) and evaporated to dryness in a vacuum concentrator. Desalted peptides were labeled with the TMT10plex mass tag labeling reagent according to the manufacturer's instructions (Thermo Scientific) with small modifications. Briefly, 0.5 units of TMT10plex reagent was used per 40µg of sample. Peptides were dissolved in 50µl of 50mM Hepes pH 8.5 solution and the TMT10plex reagent was added in 20.5µl of MeCN. After 1h incubation the reaction was stopped with 4µl 5% Hydroxylamine for 15min at 25°C. Differentially labeled peptides were mixed for each replicate and subsequently desalted on C18 StageTips (Rappsilber et al., 2007) and evaporated to dryness in a vacuum concentrator.

To reduce peptide complexity and achieve deeper proteome coverage, samples were then separated by basic reversed-phase chromatography as described in (Mertins et al., 2013). Briefly, desalted peptides were reconstituted in 20mM ammonium formate, pH 10, (900µl)

and centrifuged at 10,000*g* to clarify the mixture before it was transferred into autosampler tubes. Basic reversed-phase chromatography was conducted on a Zorbax 300Å Extend-C18 column, using an Agilent 1100 Series HPLC instrument. The separations were performed on a 2.1mm. 150mm column (Agilent, 3.5µm bead size). Prior to each separation, columns were monitored for efficient separation with standard mixtures containing 6 peptides. Solvent A (2% acetonitrile, 5mM ammonium formate, pH 10), and a nonlinear increasing concentration of solvent B (90% acetonitrile, 5mM ammonium formate, pH 10) were used to separate peptides by their hydrophobicity at a high pH. We used a flow rate of 0.2ml/min and increased the percentage of solvent B in a nonlinear gradient with 4 different slopes (0% for 1min; 0% to 9% in 6min; 9% to 13% in 8min; 13% to 28.5% in 46.5min; 28.5% to 34% in 5.5min; 34% to 60% in 23min; 60% for 26min). Eluted peptides were collected in 96 well plates with 1min (= 0.2 ml) fractions. Early eluting peptides were collected in fraction "A", which is a combined sample of all fractions collected before any major UV-214 signals were detected. The peptide samples were combined into 12 to be used for proteome analysis. Subfractions were achieved in a serpentine, concatenated pattern, combining eluted fractions from the beginning, middle, end of the run to generate subfractions of similar complexities that contain hydrophilic as well as hydrophobic peptides. For high-scale proteome analysis every 12th fraction was combined (1,13,25,37,49,61; 2,14,26,38,50,62; …). Subfractions were acidified to a final concentration of 1% formic acid and desalted on C18 StageTips according to (Rappsilber et al., 2007). LC-MS/MS analysis on a Q-Exactive HF was performed as previously described (Keshishian et al., 2015).

All mass spectra were analyzed with the Spectrum Mill software package v4.0 beta (Agilent Technologies) according to (Mertins et al., 2013) using the yeast Uniprot database (UniProt.Yeast.completeIsoforms.UP000002311.20151220; strain ATCC 204508 / S288c). For identification, we applied a maximum FDR of 1% separately on the protein and peptide level and proteins were grouped in subgroup specific manner. We required at least 1 spectral count from a unique peptide for protein identification and for protein quantification per replicate measurement. 72 proteins were identified and quantified by one spectral count in each replicate, 231 proteins by one count in one replicate and >1 in the other replicate and 4161 proteins by >1 spectral count in both replicates. Note that the S288C UniProt dataset was used because we are not aware of an equivalently complete protein dataset for SK1, and due to poorer sequencing depth and annotation of this genome relative to the reference, our attempt to create one excluded many proteins. This presumably caused us to miss capture of some proteins for which the quantifiable peptides are not identical in the two strains, but should not cause artifacts in our correlation measurements, because all measurements are relative among timepoints. Finally, we normalized the Spectrum Mill generated intensities.

Note: In order to compare protein group specific intensity values between the TMT quantified meiotic time courses and our control label free quantified (LFQ) meiotic time course (replicate 2 only, missing the "25h spores" time point only), we analyzed the above generated data also with MaxQuant (version 1.6.0.16), as that was the program of choice for our LFQ measurements. The same parameters were applied as for the LFQ data analysis (see below). Each protein group of a TMT labeled sample got its proportional fraction of the MS1 based LFQ intensities based on its labeling channel specific TMT MS2 intensity relative to the sum of TMT MS2 intensities of all labeled channels for the corresponding protein group.

Afterwards we normalized these fractional MS1 LFQ intensities such that at each condition/time point these intensity values added up to exactly 1,000,000, therefore each protein group value can be regarded as a normalized microshare. These microshare values were then compared to the normalized microshare LFQ based intensities from our label free meiotic time course samples (Figure 3.S1D, see below).

Control meiotic time course proteomics data generated by Label Free Quantification (LFQ)

In order to validate the TMT-based quantification results, we performed proteomics based LFQ, which does the quantification on the MS1 level, instead of the MS2 level and does not allow multiplexing as is the case for TMT labeling. Therefore, different systematic biases are introduced by LFQ based proteomics than by TMT based proteomics and it serves as a quite stringent test to our deep proteome quantification results obtained by our TMT based approach. We quantified 9 matched samples, all coming from the second replicate of the meiotic time course. The only sample missing was the "25 hours spore" sample.

Proteins were precipitated by adding -20°C cold acetone to the lysate (acetone to eluate ratio 10:1) and overnight incubation at -20°C. The proteins were pelleted by centrifugation at 20000xg for 15min at 4°C. The supernatant was discarded and the pellet was left to dry by evaporation. The protein pellet was reconstituted in 100µl urea buffer (8M Urea, 75mM NaCl, 50mM Tris/HCl pH 8.0, 1mM EDTA) and protein concentrations were determined by BCA assay (Pierce). 20µg of total protein per sample were processed further. Disulfide bonds were reduced with 5mM dithiothreitol and cysteines were subsequently alkylated with 10mM iodoacetamide. Samples were diluted 1:4 with 50mM Tris/HCl (pH 8.0) and sequencing grade modified trypsin (Promega) was added in an enzyme-to-substrate ratio of 1:50. After 16h of digestion, samples were acidified with 1% formic acid (final concentration). Tryptic peptides were desalted on C18 StageTips according to (Rappsilber et al., 2007) and evaporated to dryness in a vacuum concentrator. Desalted peptides were reconstituted in Buffer A (0.2% Formic acid).

LC-MS/MS analysis was performed on a Q-Exactive HF. Each sample was measured twice (a total of 18 mass spec runs). Around 1µg of total peptides were analyzed on an Eksigent nanoLC-415 HPLC system (Sciex) coupled via a 25cm C18 column (inner diameter 100µm packed in-house with 2.4µm ReproSil-Pur C18-AQ medium, Dr. Maisch GmbH) to a benchtop Orbitrap Q Exactive HF mass spectrometer (Thermo Fisher Scientific). Peptides were separated at a flow rate of 200nL/min with a linear 106min gradient from 2% to 25% solvent B (100% acetonitrile, 0.1% formic acid), followed by a linear 5min gradient from 25 to 85% solvent B. Each sample was run for 170min, including sample loading and column equilibration times. Data was acquired in data dependent mode using Xcalibur 2.8 software. MS1 Spectra were measured with a resolution of 60,000, an AGC target of 3e6 and a mass range from 375 to 2000m/z. Up to 15 MS2 spectra per duty cycle were triggered at a resolution of 15,000, an AGC target of 2e5, an isolation window of 1.6 m/z and a normalized collision energy of 27.

All raw data were analyzed with MaxQuant software version 1.6.0.16 (Cox and Mann, 2008) using a UniProt yeast database (release 2014_09, strain ATCC 204508 / S288c), and MS/MS searches were performed with the following parameters: The two replicate runs per sample were grouped together. Oxidation of methionine and protein N-terminal acetylation as

variable modifications; carbamidomethylation as fixed modification; Trypsin/P as the digestion enzyme; precursor ion mass tolerances of 20 p.p.m. for the first search (used for nonlinear mass re- calibration) and 4.5 p.p.m. for the main search, and a fragment ion mass tolerance of 20 p.p.m. For identification, we applied a maximum FDR of 1% separately on protein and peptide level. "Match between the runs" was activated, as well as the "LFQ" (at least two ratio counts were necessary to get an LFQ value). We required 1 or more unique/razor peptides for protein identification and a ratio count of 2 or more for label free protein quantification in each of the 9 samples. This gave us LFQ values for a total of 1568 protein groups.

Finally, we normalized the MaxQuant generated LFQ intensities such that at each condition/time point the LFQ intensity values added up to exactly 1,000,000, therefore each protein group value can be regarded as a normalized microshare (we did this separately for each sample for all proteins that were present in that sample).

Ndt80 release proteomics measurements

Proteins were precipitated by adding -20°C cold acetone to the lysate (acetone to eluate ratio 10:1) and overnight incubation at -20°C. The proteins were pelleted by centrifugation at 20000xg for 15min at 4°C. The supernatant was discarded and the pellet was left to dry by evaporation. The protein pellet was reconstituted in 100µl urea buffer (8M Urea, 75mM NaCl, 50mM Tris/HCl pH 8.0, 1mM EDTA) and protein concentrations were determined by BCA assay (Pierce). 15µg of total protein per sample were processed further. Disulfide bonds were reduced with 5mM dithiothreitol and cysteines were subsequently alkylated with 10mM iodoacetamide. Samples were diluted 1:4 with 50mM Tris/HCl (pH 8.0) and sequencing grade modified trypsin (Promega) was added in an enzyme-to-substrate ratio of 1:50. After 16h of digestion, samples were acidified with 1% formic acid (final concentration). Tryptic peptides were desalted on C18 StageTips according to (Rappsilber et al., 2007) and evaporated to dryness in a vacuum concentrator. Desalted peptides were labeled with the TMT10plex mass tag labeling reagent according to the manufacturer's instructions (Thermo Scientific) with small modifications. Briefly, 0.2units of TMT10plex reagent was used per 15µg of sample. Peptides were dissolved in 30µl of 50mM Hepes pH 8.5 solution and the TMT10plex reagent was added in 12.3µl of MeCN. After 1h incubation the reaction was stopped with 2.5µl 5% Hydroxylamine for 15min at 25°C. Differentially labeled peptides were mixed for each replicate and subsequently desalted on C18 StageTips (Rappsilber et al., 2007) and evaporated to dryness in a vacuum concentrator.

The peptide mixtures were fractionated by Strong Cation Exchange (SCX) using StageTips as previously described (Rappsilber et al., 2007) with slight modifications. Briefly, one StageTip was prepared per sample by 3 SCX discs (3M, #2251) topped with 2 C18 discs (3M, #2215). The packed StageTips were first washed with 100µl methanol and then with 100µl 80% acetonitrile and 0.2% formic acid. Afterwards they were equilibrated by 100µl 0.2% formic acid and the sample was loaded onto the discs. The sample was transeluted from the C18 discs to the SCX discs by applying 100µl 80% acetonitrile; 0.2% formic acid, which was followed by 3 stepwise elutions and collections of the peptide mix from the SCX discs. The first fraction was eluted with 50µl 50mM NH_4AcO; 20% MeCN (pH ~7.2), the second with 50µl 50mM NH_4HCO_3; 20% MeCN (pH ~8.5) and the sixth with 50µl 0.1% NH_4OH; 20%

MeCN (pH ~9.5). 200µl of 0.2% acetic acid was added to each of the 3 fractions and they were subsequently desalted on C18 StageTips as previously described (Rappsilber et al., 2007) and evaporated to dryness in a vacuum concentrator. Peptides were reconstituted in 10µl 0.2% formic acid. Both the unfractionated samples plus the fractionated, less complex samples were afterwards analyzed by LC-MS/MS on a Q-Exactive HF was performed as previously described (Keshishian et al., 2015).

Around 1µg of total peptides were analyzed on an Eksigent nanoLC-415 HPLC system (Sciex) coupled via a 25cm C18 column (inner diameter of 100 µ m, packed in-house with 2.4 µ m ReproSil-Pur C18-AQ medium, Dr. Maisch GmbH) to a benchtop Orbitrap Q Exactive HF mass spectrometer (Thermo Fisher Scientific). Peptides were separated at a flow rate of 200nL/min with a linear 106min gradient from 2% to 25% solvent B (100% acetonitrile, 0.1% formic acid), followed by a linear 5min gradient from 25 to 85% solvent B. Each sample was run for 170min, including sample loading and column equilibration times. Data was acquired in data dependent mode using Xcalibur 2.8 software. MS1 Spectra were measured with a resolution of 60,000, an AGC target of 3e6 and a mass range from 375 to 2000m/z. Up to 15 MS2 spectra per duty cycle were triggered at a resolution of 60,000, an AGC target of 2e5, an isolation window of 1.6 m/z and a normalized collision energy of 36.

All raw data were analyzed with MaxQuant software version 1.6.0.16 (Cox and Mann, 2008) using a UniProt yeast database (release 2014_09, strain ATCC 204508 / S288c), and MS/MS searches were performed with the following parameters: The five mass spec runs were grouped together. TMT11plex labeling on the MS2 level, oxidation of methionine and protein N-terminal acetylation as variable modifications; carbamidomethylation as fixed modification; Trypsin/P as the digestion enzyme; precursor ion mass tolerances of 20 p.p.m. for the first search (used for nonlinear mass re-calibration) and 4.5 p.p.m. for the main search, and a fragment ion mass tolerance of 20 p.p.m. For identification, we applied a maximum FDR of 1% separately on protein and peptide level. We required 1 or more unique/razor peptides for protein identification and a ratio count for each of the 10 TMT channels. This gave us a total of 2908 quantified protein groups.

Finally, we normalized the MaxQuant generated corrected TMT intensities such that at each condition/time point the corrected TMT intensity values added up to exactly 1,000,000, therefore each protein group value can be regarded as a normalized microshare (we did this separately for each TMT channel for all proteins that were made our filter cutoff in all the TMT channels).

3.3.12 Quantification and statistical analysis

Sequence alignments, data analysis

Sequencing data were analyzed exactly as in (Brar et al., 2012; Ingolia et al., 2012). In short, bowtie2-based alignment (Langmead and Salzberg, 2012) was used and only unique sequences were mapped. Bowtie2-based mapping and subsequent quantification for ribosome profiling data were executed using quality control metrics and scripts written by Nick Ingolia. These quality control metrics include analysis of ribosome footprint length

distributions in ribosome profiling samples to confirm periodicity and optimal RNAse I digestion. Gene expression quantification involved summing unique reads over annotated ORFs and adjustment for RPKM (reads per kilobase million) values. Only genes and timepoints with at least 10 raw ribosome footprint or mRNA reads were used for analyses. Mochiview was used for genome browsing and motif analysis, Cluster 3.0 and Treeview were used for cluster analyses and visualization. All correlation measurements used throughout this manuscript are Pearson correlations.

As is true of most genome-wide studies, our measurements are relative, representing the proportional levels of either mRNA, ribosome footprints, or protein in the population. For meiotic timepoints, including and between 1.5 and 8 hours, these values are expected to be quantitatively comparable, as our previous measurements determined no major shifts in bulk mRNA, translation, or protein levels over this timespan. In contrast, major metabolic shifts are expected as cells enter meiosis (from 0 hr to 1.5 hr) and as they complete spore formation, and major metabolic differences are likely to exist between cells in sporulation medium and rich medium. We chose, however, to analyze relative measurements among all timepoints for two reasons. First, our previous attempts to normalize our measurements relative to doped oligos or exogenous mRNAs introduced an additional source of noise to the data that obscured real biological regulation (Brar et al., 2012). Second, we determined based on examination of the patterns of mRNA, translation, and protein for well studied genes, that our measurements mirrored those from our own and others' published studies and thus seemed reliable despite some expected metabolic shifts. Nonetheless, we generally refrain from making quantitative comparisons between measurements made in rich media and cells in sporulation media, as these comparisons are the most likely to include complicating large bulk effects.

Note that, although full biological replicates were collected and matched extremely well in most instances, the mRNA for the vegetative exponential replicate 2 appeared contaminated. Attempts were made to re-prepare this sample once this was determined, but the issue was not identified and this sample, in particular, looks unlike vegetative exponential samples that our lab has previously prepared. Because the assignment of replicate 1 and 2 for this sample was arbitrary and because the footprint samples collected from the same culture flasks agreed very well, we used the replicate 1 data for the vegetative exponential mRNA. This was the only instance in which the samples were not completely matched from identical cells and we believe that it does not affect the results based on comparisons with our previous timecourse and thorough replicate analyses of the ribosome footprints and protein for this sample.

Genome browsing/motif analysis

We used Mochiview (Homann and Johnson, 2010) for all of our genome browser analyses and motif analyses.

Data clustering and visualization

We used Cluster 3.0 (de Hoon et al., 2004) for our hierarchical clustering, using uncentered correlation clustering with the centered setting. We visualized the results using Java Treeview (Saldanha, 2004).

Translation Efficiency measurements

Translation efficiency measurements were calculated for each gene and timepoint from the formula $FP_{RPKM}/mRNA_{RPKM}$, in both cases only using values that resulted from 10 raw reads or more and in each case, summing only over the annotated open reading frame (ORF).

LUTI annotation

We isolated the pool of genes for which we quantified protein in this dataset and had previously identified evidence for meiotic translation of an AUG-initiated uORF. This pool included 914 genes. We then filtered on the mRNA to protein Pearson correlation over all timepoints, choosing a cutoff at 0.4 to represent "poor" correlation, narrowing the pool to 624 genes. We then assayed mRNA-seq data by genome browser, comparing all timepoints and taking forward only genes that showed evidence for an alternate 5' extended transcript at some point. We also required that these genes show AUG-initiated uORF translation in this dataset by genome browser analysis of ribosome profiling data and that this translation did not mirror translation of the downstream ORF (or was broadly consistent with an inverse relationship between uORF and ORF translation). In cases in which reads for ribosome profiling reads over uORFs were low or noisy, occasionally observed due to the short nature of many of these regions, we alternatively allowed a case to be scored as positive if the TE at the timepoint when the transcript appeared long by genome browser analysis was lower than the TE when the transcript appeared short by genome browser analysis. This determination did not require any fold change cutoff so that the quantitative confirmation in part Fig. 3.6A would be independent. The results of this approach are summarized in the pie chart. In 59 cases, we could not analyze the locus for evidence of an alternate transcript due to overlap with a neighboring transcript. In 5 cases, we observed regulation that appeared similar to that observed for the *SER3/SRG1* locus [see Fig. 3.S7G for example and discussion; (Martens et al., 2004)], with regulated appearance of an alternate overlapping transcript that does not contain the full canonical ORF; in 3 cases the regulation was difficult to categorize for other reasons; and in 177 cases, there was no clear evidence for an alternate transcript. In the remaining 380 cases, there is moderate to strong evidence for LUTI-based regulation. This includes 78 of the 156 cases that we had annotated as showing alternate 5' leaders in our original mRNA-seq dataset (Brar et al., 2012).

3.3.13 Data and software availability

All raw sequencing and mass spectrometry data for use in this manuscript are available through NCBI GEO (https://www.ncbi.nlm.nih.gov/geo/; GSE108778) and the MassIVE platform (http://massive.ucsd.edu; MSV000081874).

3.4 Results

3.4.1 A deep dataset reveals meiotic gene regulation in detail from transcript to protein

To assay the degree of change in gene regulation as cells progress through meiosis, we measured matched samples for protein levels by quantitative mass spectrometry (isobaric TMT10-plex labeling), mRNA levels by mRNA-seq, and translation by ribosome profiling—on 8 stages of natural meiotic differentiation, one vegetative exponential control in rich media, and one sporulation media-matched non-meiotic (*MAT*a/a) control (Fig. 3.1A, 3.S1A, 3.S1E). Our protein measurements were highly reproducible, both when comparing to biological replicates and to label free quantification (LFQ;Fig. 3.S1C-D). Our mRNA-seq and ribosome profiling measurements also showed high reproducibility (Fig. 3.S1C).

We were able to quantify 4,464 annotated proteins at every timepoint, with an average coverage of 10.7 peptides/protein. We efficiently captured proteins from most cellular compartments, with few exceptions. Our mass spectrometry measurements reveal extensive protein level regulation when looking broadly at all quantified genes and suggest that most proteins are subject to active degradation in the meiotic program, with decreases in abundance observed for nearly every protein despite no dilution due to cell division, as would be seen during mitosis (Fig. 3.1B, 3.S1E). Patterns of protein abundance for well studied genes confirmed known regulation, and was remarkably consistent with known function [Fig. 3.S1F-K;(Zaslaver et al., 2004)].

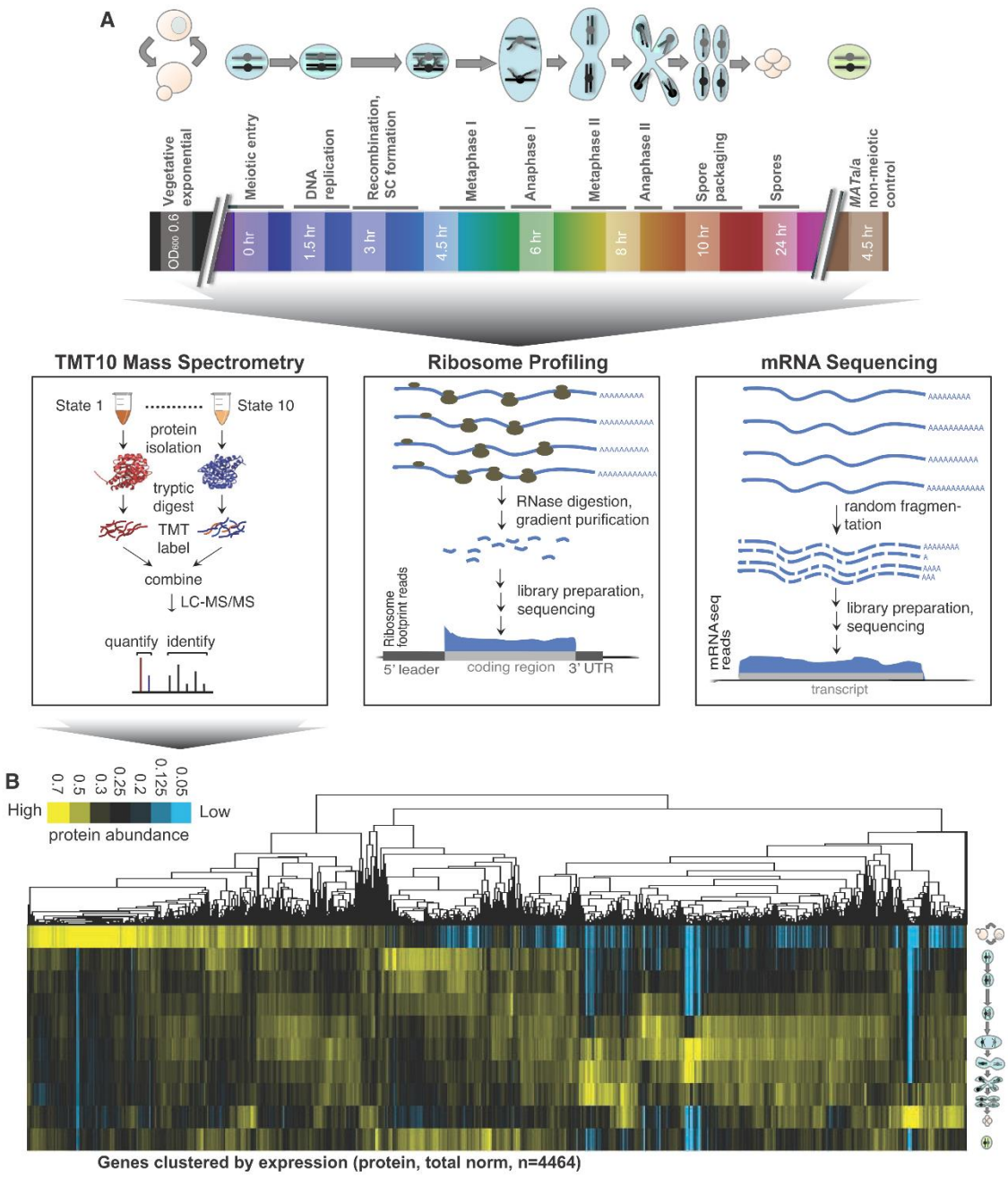

Figure 3.1: Gene expression through meiotic differentiation, from mRNA to protein. A) Matched extract was used for mRNA-seq, ribosome profiling, and quantitative mass spectrometry. B) Hierarchical clustering of protein measurements for all quantified annotated genes (n=4464, columns) over all timepoints (rows) is shown. Total signal is normalized per column to allow comparison of patterns.

3.4.2 Discordant mRNA and protein levels are common and reflect biological regulation

The degree to which regulation at the level of transcription, translation, and protein degradation drive protein levels has been a topic of extensive debate (Liu et al., 2016). We first investigated this issue in our dataset by examining the degree to which mRNA patterns predicted protein patterns. A plot of the correlation coefficients between mRNA and protein abundances revealed a positive trend, as expected based on canonical models of gene regulation (Fig. 3.2A). We were surprised to see, however, a subset of genes that showed poor, even negative, mRNA:protein correlations (Fig. 3.2A, 3.S2A). Given the large number of genes in this group, we tested whether they were lowly expressed, and thus the poor correlation could be driven by measurement noise. However, analyses of mean mRNA and protein abundance measurements indicated no association with mRNA to protein agreement over time (Fig. 3.2B). We determined that a parallel set of mRNA-seq without polyA-selection was similar to our original mRNA-seq data, and thus that the discrepancy between mRNA and protein patterns was not an artifact of polyA tail length changes, which have been observed during developmental processes [Fig. 3.S1B-D; for example (Subtelny et al., 2014)]. We concluded that the poor mRNA to protein correlation that we detect for a large subset of genes is likely to result from biological regulation.

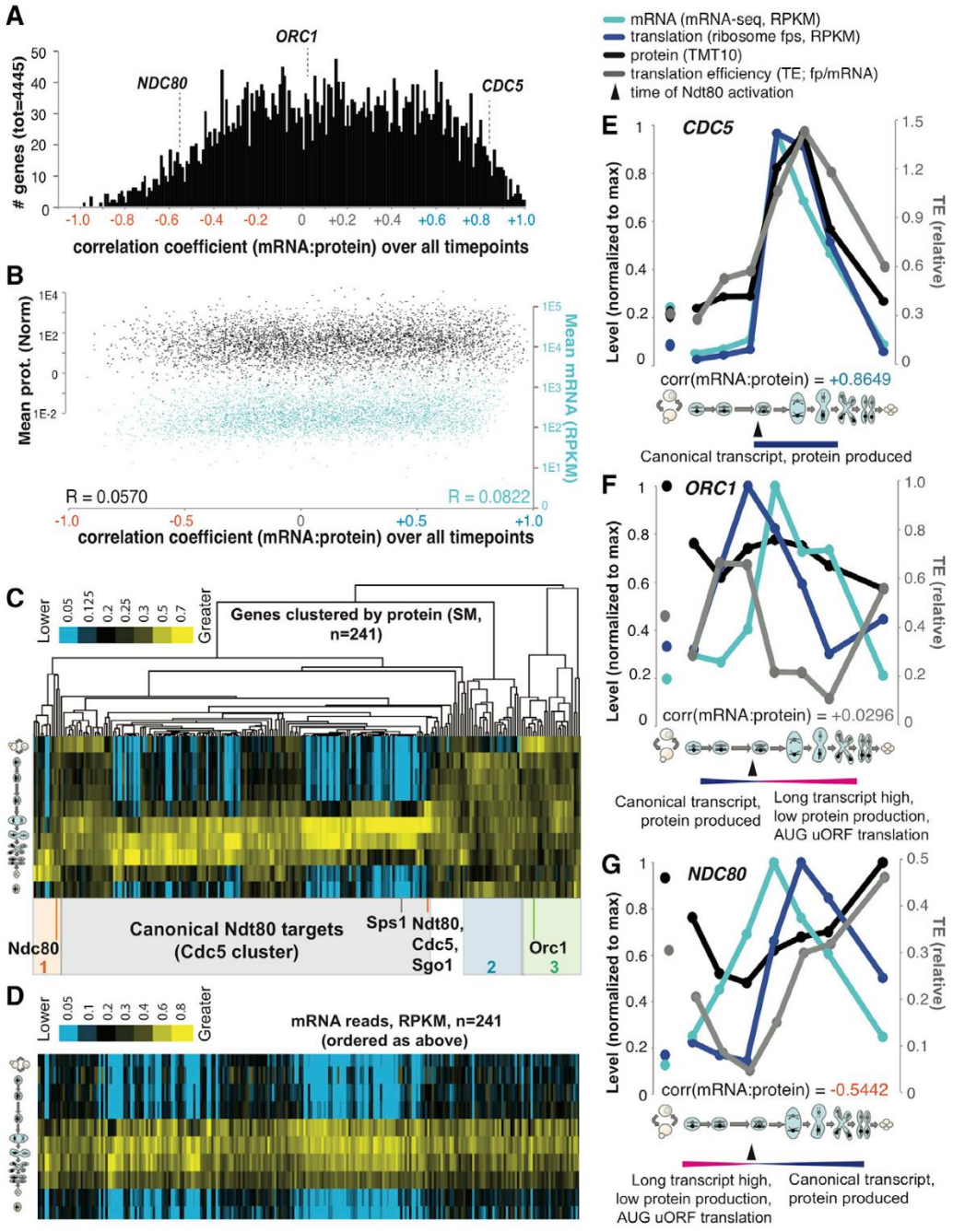

Figure 3.2: Many genes show a poor correlation between mRNA and protein in meiotic differentiation that is associated with alternate transcripts. A) A histogram of the Pearson correlation coefficients between mRNA and protein abundance measurements over all timepoints for all genes is shown. Note the general skew towards a positive correlation and a subdistribution (centered at ~-0.2) with a poor correlation. B) Mean levels of mRNA (blue) and protein (black) for each of the genes shown in the distribution above is shown. C) Protein abundances for Ndt80 targets. Columns are genes, rows are timepoints. Shaded boxes below denote discrete clusters representing patterns of protein abundance. The gray box denotes the set of genes that show protein abundance patterns that fit well with mRNA abundances in D. D) mRNA abundances matched to the columns in C. For E), F) and G), pink bars denote the timing of production of long transcripts and blue bars denote the

timing of production of short, canonical transcripts. mRNA, ribosome footprints, protein, and TE are plotted for E) canonical Ndt80 target *CDC5*, F) *ORC1* and G) *NDC80*. See also Fig. 3.S2.

3.4.3 A subset of transcriptionally co-regulated genes show discordant protein patterns

We hypothesized that we might be able to identify regulatory mechanisms that lead to specific cases of poor mRNA:protein concordance by focusing on a set of genes that are transcriptionally co-activated, and thus allow straightforward parallel comparison of their post-transcriptional regulation. Towards this end, we clustered mRNA-seq data and observed, as previously seen, that a large group of transcripts are sharply induced in concert in late meiotic prophase (Fig. 3.S2E). Several features suggest that these genes are targets of the transcription factor Ndt80 (Xu et al., 1995): they include known Ndt80 target genes [Fig. 3.2C, 3.S2E;(Chu and Herskowitz, 1998)]; they show a high expression correlation and a pattern matching expectations for Ndt80 induction (Fig. 3.S2E); and the consensus Ndt80 binding motif, termed the Middle Sporulation Element (MSE) was strongly enriched in their promoters [Fig. 3.S2F-G;(Chu and Herskowitz, 1998)].

We isolated data for the 241 of these genes quantified for protein and determined that, as expected, the most well characterized Ndt80 targets (including *NDT80* itself and the Polo kinase-encoding *CDC5*) showed a sharp uptick in protein abundance that mirrors patterns of mRNA abundance. Protein levels decrease with timing similar to mRNA decreases, suggesting a short protein half-life (Fig. 3.2C, 3.2D). Such high mRNA:protein agreement is seen for 150 (62%) of targets (Fig. 3.2C, 3.2D). However, the protein levels for the other Ndt80 targets were not well predicted by the patterns of mRNA levels, showing, for example, markedly delayed protein accumulation (orange box in Fig. 3.2C, 3.2D) or protein patterns that appeared to have little relationship to transcript patterns (blue and green boxes in Fig. 3.2C, 3.2D). These cases showed the type of paradoxical poor mRNA:protein correlation seen to be prevalent in the full dataset (Fig. 3.2A, 3.2C, 3.S2A, 3.S2H-I) and we proceeded to investigate their regulation in detail.

3.4.4 Decoupled mRNA and protein levels are associated with transcript isoform toggling

We noted that two members of this aberrant class of Ndt80 targets were *ORC1* and *NDC80* (Fig. 3.2C, 3.S2I), encoding conserved proteins that are required for DNA replication and kinetochore function, respectively. Both genes have recently been shown to be associated with regulation involving mutually exclusive alternate transcript isoforms, so we investigated the possibility that this could account for their poor mRNA:protein agreement. A recent study showed that the 5' extended *ORC1* transcript isoform results from Ndt80 activation of an upstream Transcription Start Site (TSS), producing a transcript that is poorly translated for the *ORC1* ORF and instead shows translation of several upstream Open Reading Frames [uORFs;(Brar et al., 2012; Xie et al., 2016)]. Comparison to a canonical Ndt80 target, *CDC5* (Fig. 3.2E, 3.2F), revealed that both show a robust boost in overall mRNA levels consistent with Ndt80 activation. However, in the case of *ORC1*, the translation of the ORF on

the longer, Ndt80-induced transcript is poor and thus results in a peak in translation that *precedes* the peak in total mRNA accumulation [Fig. 3.2F; (Brar et al., 2012)]. In contrast, induction of higher transcript levels of *CDC5* by Ndt80 results in increased translation and protein accumulation, as expected from canonical models of gene regulation (Fig. 3.2E).

Regulation of the kinetochore component *NDC80* shows the opposite pattern as *ORC1* with respect to transcript induction by Ndt80. In the case of *NDC80,* a long, translationally silent transcript is present early in meiosis (Chen et al., 2017; Chia et al., 2017). The poor translation of Ndc80 protein from the long transcript led to it being named a "LUTI" or "Long Undecoded Transcript Isoform", and depends on the translation of AUG-initiated uORFs. The short, translatable version of the *NDC80* transcript is induced later by Ndt80 [Fig. 3.2G;(Chen et al., 2017; Chia et al., 2017)]. In our dataset, *NDC80* showed a translation peak after the mRNA peak, and the gap was more prominent than we see for known cases of translational repression (Fig. 3.2G, Fig. 3.S2J). We interpret this delay to reflect the switch between the abundant LUTI transcript and activation of the previously silenced proximal TSS to produce the shorter transcript. This results in mRNA and protein bursts that are out of phase by hours, which is not typical of canonically regulated genes in meiosis. Strikingly, this regulation results not just in a poor correlation between mRNA and protein abundance, but an *anti-correlation* (Fig. 3.2G, 3.S2I).

Differences in translatability of alternate transcripts produced at *ORC1* and *NDC80* are apparently more important in setting protein output than the differences in overall mRNA abundance for these genes, explaining the discordance between mRNA and protein level patterns in these cases (Fig. 3.2C, 3.2F, 3.2G). Thus, the single transcription factor, Ndt80, is capable of activating transcription of three types of target genes (Fig. 3.3A, 3.3C). First, *CDC5* is a canonical target that promotes meiotic progression and its translation and protein levels increase in a manner that mirrors its sole, canonical transcript (Fig. 3.2E, 3.3A, 3.3C). Second, *ORC1*, whose protein levels decrease late in meiosis when DNA replication is complete, is silenced by Ndt80 induction through production of a longer transcript that does not efficiently produce protein and is associated with shutdown of the short, translatable transcript [Fig. 3.2F, 3.3A, 3.3C,(Xie et al., 2016)]. Translation efficiency [TE; (ribosome footprint)/(mRNA)] of the early, short *ORC1* transcript is high, but TE of the abundant longer, Ndt80-induced *ORC1* transcript is low (Fig. 3.2F, 3.3A). Thus, counter-intuitively, due to the scale of these differences in TE for the *ORC1* isoforms, Ndt80-mediated transcriptional activation is actually associated with *repressed* translation for this target (Fig. 3.3A, 3.3C). Third, *NDC80*, whose protein levels are kept low early to enable normal assembly of the meiosis I kinetochore, is required for chromosome segregation. Ndt80 drives the necessary late burst in protein levels and overcomes the silencing mediated by previous longer transcript production [Fig. 3.2G, 3.3A, 3.3C, (Chen et al., 2017; Chia et al., 2017)]. Taken together, Ndt80 is capable of functioning via transcriptional activation as both an inducer (*CDC5* and *NDC80*) and as a repressor (*ORC1*) of protein expression, depending on the position of its binding site relative to the positions of other features of the genomic locus, including uORF sequences and the ORF start codon (Fig. 3.3A, 3.3C).

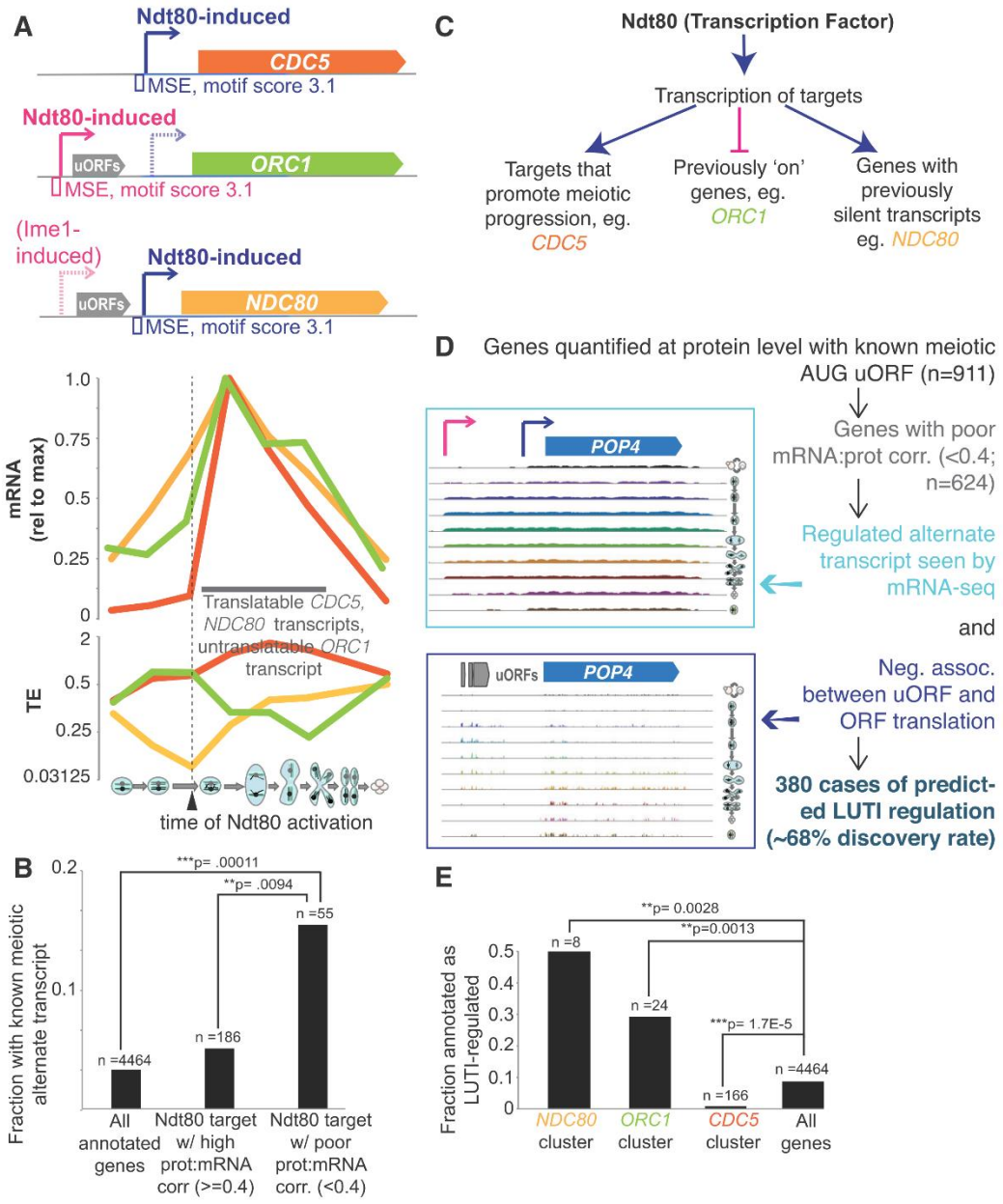

Figure 3.3: Annotation of genes regulated by transcript toggling. A) Top, transcript models are shown, along with the position of the MSE. Middle, mRNA reads (top) are plotted for *CDC5, NDC80,* and *ORC1.* Bottom, TE is plotted for these same genes. The timing of Ndt80 action corresponds with an increase in translation and TE for *NDC80* and a decrease for *ORC1*. B) Enrichment is shown for predicted alternate meiotic transcripts [as defined in (Brar et al., 2012)] for genes in the Ndt80 regulon with poor mRNA:protein correlation (<0.4, Pearson) in Fig. 3.S2A. ** p<0.01 by Fisher's exact test. C) A model for Ndt80 action on three different types of targets for which it induces an abundant transcript. Canonical targets like *CDC5* promote meiotic progression past pachytene. At these loci, a translatable transcript is made, resulting in rapid protein accumulation. Ndt80 induction induces an abundant and longer, untranslatable transcript isoform (LUTI) of *ORC1*, which results in decreased in protein levels. *NDC80* is a target that was previously kept silent by a LUTI transcript. Ndt80 induces a short transcript that overcomes the silent transcript in the population and is well translated and allows protein accumulation, albeit at a slower rate than most canonical Ndt80 targets. D) The description of our pipeline for LUTI-type identification is shown and expanded in Fig. 3.S3A. E) Enrichment of the newly

annotated LUTIs is seen in the *ORC1, CDC5* and *NDC80* clusters in Fig. 3.2C. Fisher's exact test was used for statistical significance.

3.4.5 Transcript toggling is common and reshapes the meiotic proteome

We noted that *ORC1* and *NDC80* were both members of a group of genes that we previously predicted to have alternate transcripts in meiosis, based solely on mRNA-seq data (Brar et al., 2012). Analysis of the 55 genes in the Ndt80 regulon that showed the poorest mRNA to protein correlation (<0.4, Fig. 3.S2H) revealed that this set was greatly enriched for genes with observed alternate transcripts (Fig. 3.3B), suggesting that a similar transcript toggling mechanism might be responsible for other cases of discordant mRNA to protein patterns in meiosis. We sought to define simple rules that could be used to detect such regulation in an unbiased manner. We noted that an essential feature of LUTI regulation for the one mechanistically well-defined case, *NDC80,* was a translated AUG-initiated uORF, specifically on the long transcript isoform, which prevented ribosomes from translating the ORF (Chen et al., 2017). Down-regulated ORF translation as a result of conditional uORF translation is a known mechanism, although in most reported examples, temporal control results from a change in trans-factor activity [for example, (Hinnebusch, 1993; Palam et al., 2011)], while in this case, uORF translation is enabled and ORF translation disabled simply by timed production of a longer transcript that encodes uORF sequences. We previously annotated genes with meiotically translated AUG-initiated uORFs, of which 911 were quantified at the protein level here [Fig. 3.3D; (Brar et al., 2012)]. We filtered the set of genes that show poorly correlated mRNA and protein profiles (Fig. 3.2A) for meiotic translation of an AUG uORF and examined each of these loci for evidence of a clear alternate 5' extended transcript at some point in meiosis and uORF translation that was negatively associated with ORF translation (Fig. 3.3D). In 380 cases, or 68% of genes for which these analyses were possible, we indeed observed evidence for regulation based on transcript toggling of differentially translated isoforms (Fig. 3.3D, Fig. 3.3A). This value changed little if discovery was conducted using mRNA-seq without single round polyA-selection. We noted that the clusters representing aberrant protein accumulation patterns in the Ndt80 regulon were strongly enriched for these newly annotated cases of LUTI-like regulation (Fig. 3.2C, 3.3E).

We expected, based on the parameters of their discovery, that the 380 proposed LUTI cases would be regulated by an *NDC80/ORC1*-like mechanism involving modulation of the level of two transcripts, one of which has a long 5' leader containing at least one translated AUG uORF that results in little protein production from the canonical ORF, and one of which has a shorter 5' leader and a highly translated ORF that results in robust protein production. If this is true, we should be able to detect two transcripts that both encode the ORF, and the longer transcript should be associated with poor translation efficiency. mRNA-seq data is useful for predicting the possibility of alternate transcripts, but cannot distinguish between alternate transcripts and discontinuous, overlapping transcripts. We therefore performed Northern blotting for ORFs that we predicted to show LUTI-based regulation (Fig. 3.4, 3.S4A-O). RNA pol II mediator complex gene *MED7,* for example, shows two mRNA isoforms that are differentially translated for the *MED7* ORF (Fig. 3.4A, 3.4B, 3.S4A). Timepoints with the highest total *MED7* mRNA levels also showed the lowest TE and preceded a drop in protein

levels, consistent with poor translation of the long transcript that was present at these times (Fig. 3.4A, 3.4B).

Examination of the full set of newly proposed LUTI cases showed a variety of patterns of mRNA and protein accumulation over our timecourse, suggesting that several transcription factors were likely to be involved in inducing long and short isoforms at these loci (Fig. 3.4C, top). In all cases, as expected, protein patterns did not resemble mRNA patterns (Fig. 3.4C). We confirmed the presence of two transcript isoforms and the expected relationship with respect to TE for ten additional cases (Fig. 3.4C-J, 3.S4A-O). Regulation of *RRD2*, the gene encoding a peptidyl-prolyl-isomerase, is evident if one compares the 3 hour and 4.5 hour timepoints. Both show a similar amount of $RRD2^{ORF}$, but the TE is higher at 4.5 hours, when we observe less $RRD2^{LUTI}$ isoform (Fig. 3.4D, 3.S4B). Northern blots for *POP7,* an RNase complex component-encoding gene, and *POP4,* a gene encoding a fellow member of some of these complexes, showed meiotic appearance of long and poorly translated transcript isoforms at 4.5 and 1.5 hours, respectively, corresponding to low points in translation (Fig. 3.4E, 4F, S4C, S4F). DNA damage factor *RAD16* primarily has a long transcript isoform through most of meiosis, corresponding with poor translation compared to vegetative cells (Fig. 3.4H, 3.S4D). A long isoform of septin-encoding *SHS1* was seen to peak at 6 hours into meiosis and was correlated in timing with a drop in *SHS1* TE (Fig. 3.4J, 3.S4E).

We noted that gene expression measurements for the 380 newly annotated LUTI cases were highly reproducible and that the unexpected relationship between protein levels was not due to our mass spectrometry approach (Fig. 3.S3B-D). To further confirm our measurements, we assayed protein production from reporter constructs for three of our LUTI-regulated candidates—Rad16, Shs1, and Pop4—with Green Fluorescent Protein (GFP) driven by their extended promoter regions. We observed patterns that matched expectations based on LUTI-based regulation (Fig. 3.4F-K, 3.S4P-V). We further showed that Shs1 protein production was markedly decreased by inactivation of the predicted canonical (proximal) promoter in the reporter. Cells carrying this construct still show accumulation of the long transcript isoform, actually earlier and to a higher level than the wild-type construct, but show low levels of canonical transcript. Even at timepoints with high levels of the long transcript isoform present, protein levels are ~30-fold lower than in cells carrying the wild-type construct (Fig. 3.4K-L). We conclude that, consistent with our model, the long isoform of *SHS1* is not capable of efficiently supporting protein production. Based on our stringent annotation and validation approaches (Fig. 3.3D, Fig. 3.4, 3.S4), we conclude that the newly annotated cases of discordant mRNA to protein levels are indeed likely to reflect LUTI regulation of the type outlined in Figure 3.7 below.

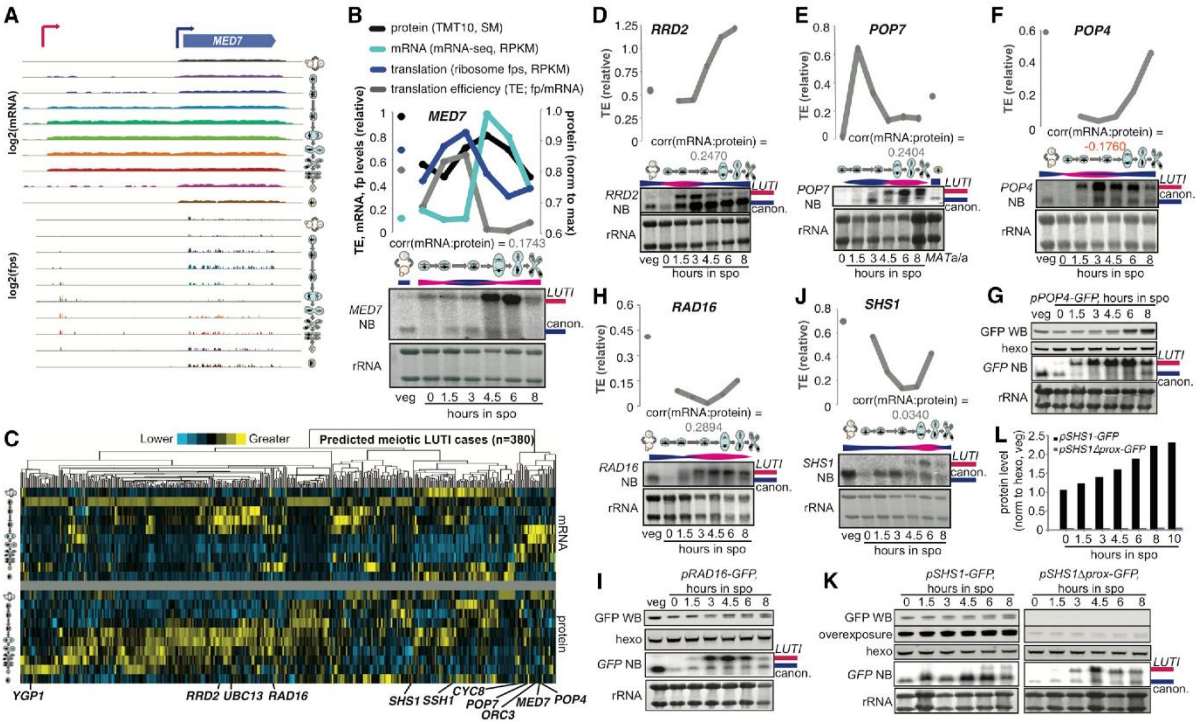

Figure 3.4: Validation of LUTI cases predicted by systematic annotation. A) mRNA-seq and ribosome profiling data is shown over all timepoints for the *MED7* locus. Existence of a long transcript that has translated uORFs and is poorly translated for *MED7* is clear at mid-meiotic timepoints. B) Comparison of levels and timing between Northern blots for the *MED7* ORF and the mRNA-seq, translation, protein, and TE measured from matched samples shows evidence for a poorly translated long transcript isoform. C) Z-score clustering to compare mRNA (top) and protein (bottom) patterns for each of the 380 predicted LUTIs discovered by the approach outlined in Fig. 3.3D. Below, the positions of the genes that are investigated in more detail in Fig. 3.4 and 3.S4 are shown. D-J) Comparison of levels and timing between Northern blots and the TE in matched samples shows evidence for a poorly translated long transcript for D) *RRD2,* E) *POP7*, F) *POP4*, H) *RAD16,* J) *SHS1*. Pink bars represent the presence of the long transcript and blue bars represent the presence of the short transcript. G) W. blotting of a GFP reporter driven by *pPOP4*, I) *pRAD16*, and K) *pSHS1*. In a paired reporter deleted for the canonical *SHS1* promoter, long transcript remains high and is increased relative to wild-type but protein production is low. Blots were run, transferred, and blotted together. L) Quantification of the Western blots in K. See also Fig. 3.S4. Northern and Western blotting experiments were performed by George Otto and Emily Powers and are included with their permission.

3.4.6 New LUTI cases show strong apparent shifts in translation efficiency

LUTI-based regulation would be expected to result in shifts in TE over time, because TE is determined by normalizing ribosome footprint counts to mRNA counts over the ORF. Indeed, the newly proposed set of 380 LUTI-regulated genes show strong relative TE shifts compared to other genes (Fig. 3.6A). It is important to note that without information about the presence of alternate transcript isoforms present at these loci, we would assume that these measurements represented temporally regulated changes in translatability for a single transcript type. In the case of genes in the *NDC80* or *ORC1* clusters in the Ndt80 regulon, there is evidence that transcript toggling (and TE shifts) are driven by Ndt80, either towards a translatable isoform in the *NDC80* cluster or towards a translationally silent isoform in the

ORC1 cluster. This conclusion is based on positioning of Ndt80 binding sites and strong similarity of our measurement patterns for these genes to others in the same clusters (Fig. 3.2C, 3.2D, 3.3A, 3.3E).

3.4.7 A transcription factor can coordinately activate and repress protein synthesis of distinct targets

If, as our data suggest, a single transcription factor can mediate both up- and down-regulation of expression from distinct sets of target genes, this would represent a powerful mechanism for coordination in differentiation and potentially cellular transitions, more generally. To determine whether this is the case, we performed Northern blotting on samples from a timecourse for which we had measured mRNA abundances and translation rates following timed induction of the transcription factor Ndt80 in a strain carrying *GAL4* under β-estradiol (βE) control and *pGAL-NDT80* (Brar et al., 2012; Carlile and Amon, 2008). We noted that three of the transcripts for which we validated transcript toggling by Northern blotting, *POP7, ORC3* (another origin recognition complex component) and *MED7*, showed similar timing for long isoform appearance following βE addition and were present in the aberrant protein level clusters among likely Ndt80 targets (Fig. 3.2C, 3.2D, 3.4C, 3.4B, 3.S4F, 3.S4H, 3.S4O). A fourth gene that we had validated by Northern blotting to have two transcript isoforms, *CYC8*, encoding a general transcriptional co-repressor, was also present in the aberrant Ndt80 target clusters but showed the opposite pattern as the other three, with a shorter transcript isoform induced in mid-meiosis (Fig. 3.2C, 3.S4N). We hypothesized that *POP7, ORC3,* and *MED7* LUTI isoforms were driven by Ndt80, and that the *CYC8* canonical isoform was driven by Ndt80, overcoming the pre-existing LUTI isoform. All four genes showed strong predicted Ndt80 binding sites adjacent to the TSS predicted to be activated (Fig. 3.S5I-L). Within one hour of βE addition, Northern blotting revealed a sharp increase in abundance of the canonical transcript for validated Ndt80 target, *CDC5*, a short transcript isoform of *CYC8*, and long isoforms of *POP7, ORC3,* and *MED7* (Fig. 3.5A). The timing of this induction was similar in all cases and corresponded with a decrease in TE of *POP7, ORC3,* and *MED7*, and an increase for canonical Ndt80 target *CDC5* and *CYC8* (Fig. 3.5B, 3.S5E), supporting our hypothesis.

To prove that Ndt80 expression and not simply time in sporulation medium was responsible for these patterns, we arrested meiotic cells in late prophase and collected subsequent timepoints with or without induction of Ndt80 (Fig. 3.5E, 3.S5A-D). We observed patterns of transcript appearance that matched those seen in our previous timecourse (Fig. 3.5A, 3.5C). Moreover, matched timepoints at 0.5 and 1.75 hours after βE addition showed distinct patterns from those without Ndt80 induction. In the cases of *POP7, MED7,* and *ORC3*, low levels of canonical transcript remained at 1.75 hours without Ndt80 induction and long transcript was not observed (Fig. 3.5C). In the case of *CYC8*, canonical transcript was strongly induced in an Ndt80-dependent manner (Fig. 3.5C). In all cases, analysis of our mRNA-seq data showed accumulation of overall mRNA levels to be strongly dependent on Ndt80 induction in a manner similar to that seen for canonical targets like *CDC5* (Fig. 3.5C, 3.5D, 3.S5E-L). Further, we observed a sharp increase in *NDT80* mRNA within 15 minutes of βE addition, and subsequent increases in other target transcripts, canonical (*CDC5, HRR25*, *CYC8*)

or LUTI (*POP7, MED7, ORC3*), with differing degrees of induction but within a shared timespan of ~45 minutes after βE addition, supporting a model in which both of these disparate target sets are simultaneous direct targets of Ndt80 (Fig. 3.5C, 3.5D).

Comparison of mass spectrometry and mRNA-seq data showed that, as expected, Ndt80 induction resulted in accumulation of first mRNA, then protein for canonical Ndt80 targets, including Cdc5 and Hrr25 (Fig. 3.5F, 3.5G). We were also able to detect Ndt80-dependent protein accumulation for Cyc8, which showed a similar pattern to these targets (Fig. 3.5H). Most interestingly, we detected protein for Pop7 (Fig. 3.4E, 3.5A, 3.5C), and observed that although overall *POP7* mRNA levels were drastically increased following and dependent on Ndt80, this condition resulted in slight decreases in protein levels with Ndt80 induction (Fig. 3.5I). In contrast, without Ndt80 induction, Pop7 protein levels were seen to increase in this same timeframe, suggesting that induction of the long *POP7* isoform by Ndt80 "turns off" pre-existing default protein production from this gene (Fig. 3.5I). This result shows that Ndt80 induction results in coordinate up-regulation and down-regulation of protein production of distinct sets of genes despite increased mRNA abundance for both types of targets (Fig. 3.5E).

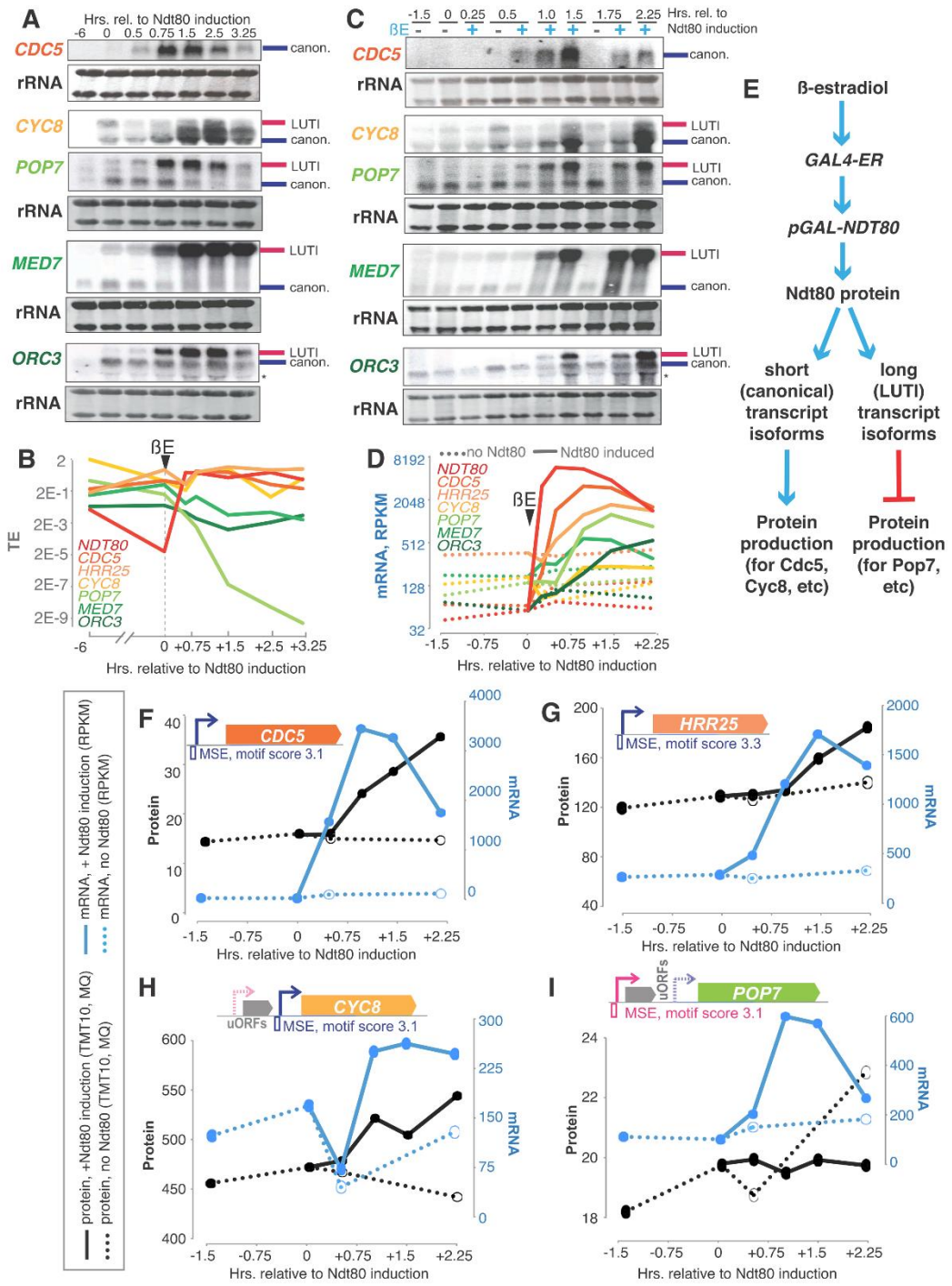

Figure 3.5: A single transcription factor coordinately induces long, translationally silent transcript isoforms and canonical transcripts, with opposing effects on protein production. A) Northern blotting reveals rapid increases in mRNA following Ndt80 induction for canonical Ndt80 target, *CDC5*, the canonical isoform of *CYC8*, and long isoforms of *POP7*, *MED7*, and *ORC3*. Pink and blue bars at the right of blots indicate canonical and LUTI isoforms. B) These increases in mRNA result in decreased TE for *POP7*, *MED7*, and *ORC3*, while *CDC5* and the short *CYC8* isoform are better translated after Ndt80 induction. C) Northern blotting reveals Ndt80-dependence to induction of *CDC5*, the canonical isoform of *CYC8*, and long isoforms of *POP7*, *MED7*, and *ORC3*, *denotes a background band. D) mRNA abundance increases for traditional and long, poorly translated Ndt80 transcript

isoform targets occur with similar timing and are dependent on Ndt80. Dotted lines show mRNA abundances without addition of β-estradiol. Solid lines show measurements with. E) Outline of experiments in A) and C) and expected effects on gene expression. F-I) mRNA (blue) and protein (black) are shown with (solid line) and without (dotted line) Ndt80 induction for F) canonical targets *CDC5* and G) *HRR25,* H) the canonical isoform of *CYC8,* and I) *POP7*^{LUTI}. Note that induction of canonical mRNAs results in an Ndt80-dependent increase in mRNA and protein, while induction of the *POP7* LUTI results in an Ndt80-dependent increase in mRNA but decrease in protein, relative to no Ndt80 induction. Northern blotting experiments were performed by George Otto and Emily Powers and are included with their permission.

3.4.8 New LUTI-type cases show evidence of spatio-temporal co-regulation

For most of the 380 LUTI cases, as is true of most canonically regulated genes that are expressed during meiotic differentiation, we do not know the transcription factor(s) responsible for their induction. We identified a signature in our new annotations, however, that supports the involvement of regulated differential transcriptional control in many cases. Among the 380 proposed LUTI-regulated genes, 42 of them— far more than would be expected by chance —were in adjacent genomic locations and in a divergent orientation such that the 5' ends were close (Fig. 3.6B).

We wondered if this enrichment for genomically neighboring positions suggested coordinated transcriptional regulation. To investigate this possibility in greater depth, we examined mRNA read patterns over time and space in the genomic vicinity of each of our 380 predicted LUTI cases for evidence of their co-regulation with any stable neighboring transcripts. In approximately half of the cases, we observed clear evidence for co-regulation in time and genomic space (Fig. 3.6C). One of these was *RRD2*, which we had annotated as showing LUTI-based regulation, and which appeared to be spatio-temporally co-regulated with production of a long version of the *RAD53* mRNA (encoding a DNA damage kinase, CHK2 in humans) that we had not identified as a candidate for LUTI-based regulation (Fig. 3.4D, 3.6D, 3.3D). We noted that both *RRD2* and *RAD53* showed short transcripts at similar times and 5' extended transcripts at similar times, and the positions of 5' ends of the longer transcripts were in close proximity (within 50 nt), suggesting transcriptional co-regulation. We confirmed the presence of the predicted longer version of the *RAD53* transcript, and noted that the ORF appeared to be poorly translated when two AUG-initiated uORFs were translated (Fig. 3.6D, 3.6E, 3.S4G), although we had not previously annotated translated AUG-initiated uORFs for this gene. 94 of our set of 380 LUTI-based regulation candidates showed evidence for spatio-temporally coordinated co-regulation of long transcript isoforms like that seen for *RAD53/RRD2* (Fig. 3.6C, Fig. 3.S6B). We further observed several other patterns that suggested neighboring transcript co-regulation (Fig. 3.S6), including cases in which LUTI transcription was correlated in time and genomic position with transcription of a canonical transcript for a gene with no evidence for LUTI-type regulation [Fig. 3.S6G-I (Xie et al., 2016)]. We noted that in all such cases, the 5' transcript ends were either overlapping or close (within 100 nt), suggesting that co-regulation of two long transcript isoforms, or a LUTI and another transcript, may be driven by a change in chromatin structure and/or a shared transcription factor at a bi-directional promoter (Xie et al., 2016). The majority of canonical Ndt80 transcriptional targets (Fig. 3.2C) also show divergent and spatiotemporally-regulated transcription, consistent with this feature as a

hallmark of transcriptional activation [data not shown; examples in Fig. 3.S6C, 3.S6G-I; (Bussemaker et al., 2001)].

The discovery that *RAD53* showed LUTI-like regulation but was missed by our annotation approach led us to investigate if our requirement for previously annotated uORFs (Fig. 3.3D) might result in other false negative cases. To investigate this possibility, we searched for genes that showed a poor mRNA:protein correlation that did not have annotated uORFs and determined whether there was evidence for translational regulation associated with an alternate transcript at the locus. We identified several cases that did appear to be associated with AUG-initiated uORF translation (Fig. 3.S7A-D). In the cases of *ADH1* (encoding alcohol dehydrogenase) and *CTT1* (encoding Catalase T), like *RAD53* above (Fig. 3.6D, 3.6E), the uORF in question was one that we had annotated as translated but not previously annotated within the leader of a canonical gene (Brar et al., 2012). It seems likely that there will be cases in which extended 5' leaders suppress translation independent of AUG-initiated uORF translation, but we have yet to confirm such an example. Nonetheless, cases like *RAD53, ADH1,* and *CTT1*, which our systematic approach (Fig. 3.6D, 3.6E, Fig. 3.S7A-D) failed to identify as LUTI-regulated, suggests that a regulatory mechanism in which transcript toggling drives protein levels is likely to be an even greater contributor to the dynamic content of the meiotic proteome than predicted by the evidence for 380 cases presented here (Fig. 3.3D).

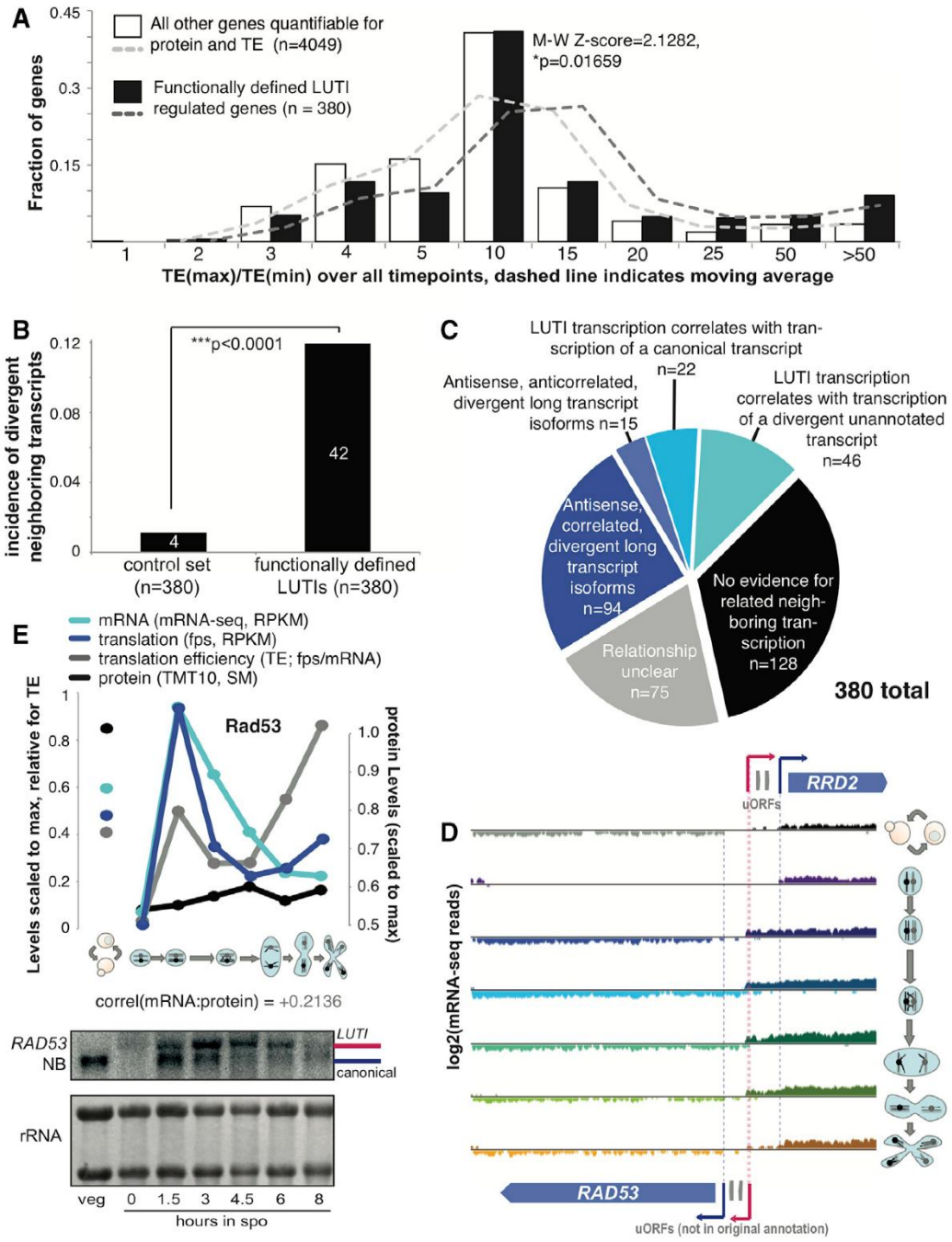

Figure 3.6: Newly identified LUTIs result in strong apparent translational control and show unusual spatio-temporal transcriptional coordination. A) A histogram of the ratio between the highest and lowest TE measured is shown for the genes that we predicted (Fig. 3.3D), revealing a higher difference for these genes compared to others. B) The incidence of directly adjacent and divergently oriented genes with their 5' ends close is shown for our newly defined prospective LUTIs and a control set, chosen to include the 380 genes with the lowest protein:translation Pearson correlation in our dataset. C) We examined the full set of 380 predicted LUTI cases for evidence of neighboring, correlated transcripts, with 94 of these cases oriented divergently and with apparently co-regulated long transcript isoform cases (Fig. 3.3D). D) mRNA seq data for the *RAD53/RRD2* locus is shown, demonstrating their divergent, neighboring orientation. *RAD53* shows a regulated longer transcript of the predicted size that is poorly translated. *RAD53* regulation looks similar to the regulation for *RRD2* (Fig.

3.4D, 3.6D-E) but we had not previously annotated translated AUG-initiated uORFs for *RAD53*. E) Translation levels, mRNA, and TE for *RAD53* are shown above Northern blotting of matched samples. See also Fig. 3.S6, 3.S7. Northern and blotting experiments were performed by George Otto and Emily Powers and are included with their permission.

3.5 Discussion

We find that gene regulation based on transcript toggling, a mechanism recently dissected in detail for a single gene (Chen et al., 2017; Chia et al., 2017), is a general mode of gene regulation during meiotic differentiation in yeast, determining the protein levels for at least 8% of measured genes (Fig. 3.7A). This regulatory mechanism, in which transcript isoform identity rather than transcript quantity drives protein accumulation, dramatically remodels the meiotic proteome relative to what would be expected from traditional models of gene regulation. Our results suggest that a substantial subset of the meiotic transcriptome contains protein coding regions that are not decoded by the ribosome into protein, and that this subset can change over time as part of this developmental program. As a result, total mRNA levels may have no relationship to protein levels for many genes in a changing cell.

We base our general model of this non-canonical regulation (Fig. 3.7) on observations from our dataset and on recent studies of *NDC80* (Chen et al., 2017; Chia et al., 2017). In short, the relative levels of two transcription factors may determine the relative levels of two transcripts for these loci. The longer transcript does not result in efficient protein synthesis due to translation of interfering uORFs, while the short transcript does (Fig. 3.7A). In the case of *NDC80,* transcription from the distal TSS promotes *cis*-silencing by epigenetic modification at the proximal TSS, a key aspect of the toggling observed between the two isoforms. This may be true for many genes in our new set, as well, based on the inverse pattern generally seen for the two isoforms (in particular, Fig. 3.4B, 3.4E, 3.4F, 3.4H, 3.S4O, 3.S7C]. LUTI-based regulation is analogous in many ways to transcriptional repressor-based regulation (Fig. 3.7B), in that in general in both cases, two *trans*-factors control the capacity for protein synthesis of a gene. In the latter case, however, mRNA levels would be predictive of protein levels, while in the LUTI case, this may not be true.

Several factors lead us to believe that our annotations are underestimating the total incidence of LUTI-based regulation. First, we identified the set of 380 cases reported here by limiting our search pool to the set of genes that we measured to show a poor mRNA:protein correlation (Fig. 3.2A, Fig. 3.3D). This requires that we searched for and captured the protein by mass spectrometry, which excludes ~2200 canonical genes and thousands of noncanonical, shorter genes (Brar et al., 2012; Ingolia et al., 2014). Second, our follow-up analysis of the mRNA-seq data and ribosome profiling data for evidence of alternate isoforms and uORF translation require high enough expression levels for such effects to be clear. Third, the 5' extension must be long enough that a shift in transcript boundary is apparent in the mRNA-seq data. Fourth, our ability to see transient isoforms is limited by population synchrony. The case of *CTT1* is informative, as the 8 hour timepoint shows a mixture of the two isoforms which is visible by Northern blotting but was not immediately evident from the mRNA-seq data alone (orange, Fig. 3.S7C-D). Finally, our LUTI prediction pipeline required previous annotation of a translated AUG-initiated uORF, but we are aware that our uORF

annotations are incomplete (demonstrated for *RAD53, ADH1,* and *CTT1*; Fig. 3.6E, Fig. 3.S7A-D) and also because there may be alternate mechanisms by which a longer 5' leader could repress translation relative to a shorter one.

Why is this mode of regulation so common in meiotic cells? It seems effective at driving up- and down- regulation of protein levels without the need for a dedicated trans-factor for transcriptional repression. This process instead allows repurposing of existing transcription factors for a new function, dependent only on cis-sequence evolution. It also appears to be readily reversible and tunable, resulting in ramping up and down of protein levels that may be important to the timing in developmental processes, which involve a series of switches in cell state (Fig. 3.2C, Fig. 3.7C-E;Chen et al., 2017; Chia et al., 2017). Further, the use of a common set of transcription factors to traditional transcriptional up-regulation provides an efficient solution for coordinated of up- and down-regulation of sets of protein targets (Fig. 3.2C, 3.3C, 3.7C-E). This feature is ideal for executing coordinated cell state changes, over biological and evolutionary time.

With the recent ability to quantify gene expression globally at multiple levels, there has been intense interest in ascertaining the relative importance of different stages of gene regulation (Liu et al., 2016). Our work suggests that a focus on relative quantitative contributions may cause us to miss important qualitative changes. A single transcription factor can activate protein expression or repress protein production, a distinction based not on whether an mRNA is induced or not, but based on the position of the TSS relative to the ORF start codon and the resultant translatability of the specific isoform induced (Fig. 3.2C, 3.3A, 3.3C, 3.7). A significant implication is that inferring protein production based on mRNA abundances may not just give an incomplete picture; rather such measurements may lead to completely false conclusions about protein levels. Similarly, our data shows that identification of alternate transcript isoforms alone is not enough to infer translational regulation. We identify cases in which regulated 5' transcript extensions are seen, even accompanied by uORF translation, but for which we cannot detect an effect on translation or protein production (example in Fig. 3.S7E-F). The basis for the difference between these cases and LUTI-based regulation remains unclear and suggests that there are important features of this regulation that are yet to be uncovered.

Our ability to systematically identify many cases of a new mode of gene regulation was enabled by the depth, time-resolved, and parallel nature of our measurements. A dataset with few timepoints or without matched measurements of mRNA and protein may not have allowed sensitive identification of the anti-correlations between mRNA and protein levels. Without matched TE measurements, we would not have been able to determine the basis for these poor correlations. Our analyses were also enabled by the apparently relatively short protein half-lives in meiotic cells relative to our timepoint spacing (Fig. 3.1B). A short protein half-life is a feature that one would expect to generally see during processes involving rapid unidirectional change in cellular state and this feature was important in revealing both the low mRNA:protein correlation among LUTI-regulated genes and the high mRNA:protein correlation for traditionally regulated genes (Fig. 3.2A, 3.2E, 3.7B). Given recent evidence of widespread alternate TSSes in mammalian cells and for variant translation efficiencies of alternate mammalian transcripts [examples in (Floor and Doudna, 2016; Wang et al., 2016)], along with the high degree of conservation of some of the genes for which we observe LUTI-

based regulation, it seems likely that this mode of integrated regulation may be used outside of yeast. A recent study that compared mRNA and protein levels over embryonic development in frogs determined that a large set of genes showed a poor mRNA:protein correlation over time (Peshkin et al., 2015). Some of those cases were deemed a result of measurement noise, but it is possible that a LUTI-based mechanism might explain a remaining subset of such cases.

We suggest that thinking of transcription and translation as independent levels of regulation in eukaryotes may obscure important principles in gene regulation. Widespread use of alternate TSSes has been seen by genome-wide approaches [for example, (Aanes et al., 2013; Pelechano et al., 2013)]. Similarly, it is clear that 5' leader identity is key in setting translation efficiency [examples in (Floor and Doudna, 2016; Hinnebusch et al., 2016; Law et al., 2005; Rojas-Duran and Gilbert, 2012; Wang et al., 2016)]. The connection between these two concepts—that a regulated toggle in TSS usage driven by the relative activity of two transcription factors can determine whether a protein-decodable or non-decodable transcript is made, and that this mechanism is employed pervasively in setting protein levels during cell fate determination, however, has not been previously apparent. By this mechanism, timed changes in the transcript pool composition for a large set of genes, rather than their levels, are key in driving the changing composition of the proteome through cellular differentiation. Further, the concept of simultaneous up- and down- regulation of distinct sets of genes by a single transcription factor provides a previously unrecognized and elegant solution to the problem of precisely coordinating increases and decreases in protein expression during a developmental program.

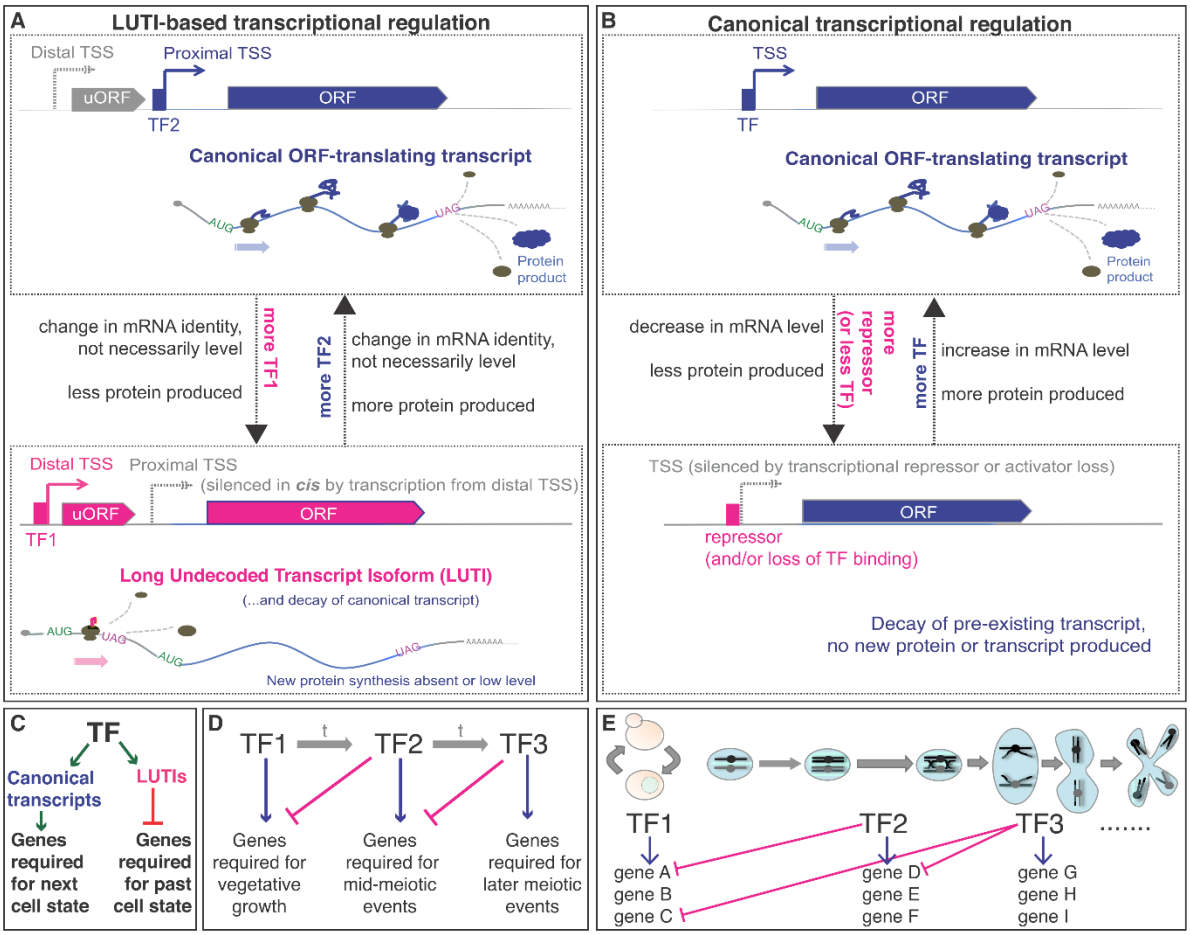

Figure 3.7: A model for the control of protein levels by transcript isoform toggling in meiosis. A) A subset of genes is encoded by two isoforms, differing in their 5' end. These isoforms result from two transcription start sites (TSSes) and the choice between these two TSSes may be controlled by the relative levels of the two transcription factors (TF2 and TF1) that can bind the proximal and distal TSS, respectively. If TF2 binds the proximal TSS, a canonical transcript is produced with a short 5' leader that is well translated and results in protein accumulation. If TF1 accumulates, it binds the distal TSS and produces a longer transcript at this locus. This transcript includes the sequence for the encoded gene, but ribosomes do not decode this region into protein due to uORFs in the extended leader region. Analysis of one case shows that transcription of the LUTI can silence the proximal TSS in cis (Chia et al., 2017). The difference in translatability of the two transcripts is more important than the abundance of transcript at these loci. Further, by this model, TF2 ultimately activates gene expression and TF1 ultimately represses gene expression. B) In contrast, canonical transcriptional repression involves either loss of binding of an activating transcription factor or the additional presence of a repressor molecule. C) In a developmental process, the LUTI mechanism can enable coordinated activation of genes required for the next cellular state and repression of genes involved in the past cellular state. D) This mode of regulation allows a relay of sequential activation and repression to time protein levels to a window of action. E) The modular nature of LUTI regulation allows genes to be turned on an off in a coordinated manner for windows of different lengths of time. For example, gene A protein production would be turned on by TF1 and turned off by production of a LUTI by TF2. Gene C, would also be turned on by TF1, but would stay on longer, until shut down by TF3.

3.6 Acknowledgements

We thank A. Regev for generous support. We thank M. Rape, N. Ingolia, A. Amon, M. Eisen, E. Ünal, L. Chan, and C. Mugler for critical reading of this manuscript and members of the Brar and Ünal labs for helpful suggestions. We thank the Ünal and Van Werven labs for sharing data prior to publication and the Vincent Coates GSL for their help in sequencing. This work was supported by NIH funding to GAB (DP2-GM-119138), investigator awards from the Alfred P. Sloan Foundation and Pew Charitable Trusts and UC-Berkeley start-up funding to GAB. GMO is supported by an NIH training grant (GM0007232) to UCB. ENP is supported by an NSF predoctoral fellowship. MJ was supported by the Marie Sklodowska-Curie IOF and he and AK are supported by Columbia start-up funding. Additionally, work at the Broad Institute was supported by NIHGRI CEGS P50 HG006193, the Klarman Cell Observatory, and HHMI (to A. Regev). We apologize for limited citations due to space constraints.

3.7 Supplemental figures

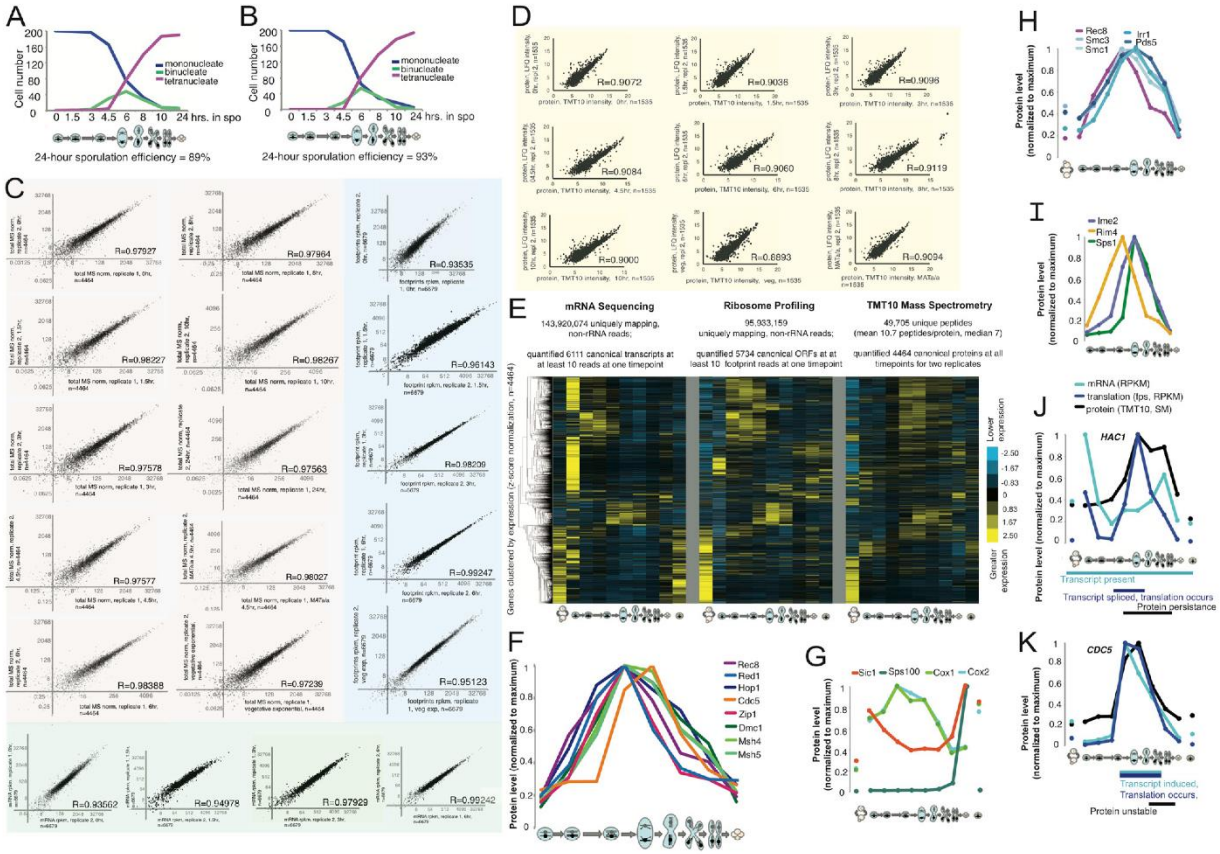

Figure 3.S1: Meiotic timecourse data were reproducible and showed expected patterns for well- studied genes, Related to Figure 3.1. A) and B) show counts of DAPI-based DNA morphology for timecourse replicate 1 and 2, respectively. 200 cells were counted per strain per timepoint for presence of a single DNA mass (mononucleate), two separated DNA masses (binucleate), or four separated DNA masses (tetranucleate). C) Full biological replicate measurements agree well for protein, mRNA, and ribosome footprints. In gray, a comparison of TMT10-based protein measurements for timecourse 1 and 2 are shown for each timepoint. In blue are similar plots for ribosome profiling samples, and in green, for mRNA-seq. R-values are to the bottom right of each graph. Each dot represents a single gene, genes are not filtered for any expression threshold. D) Mass spectrometry measurements made by independent label free quantification show high agreement with our original TMT10 measurements. All timepoints (except spores, for which sufficient material was unavailable) were subjected to mass spectrometry and label free quantification. The values for these measurements compared to TMT10 measurements for all genes that were quantified by both (n=1535) are shown in scatter plots. The TMT10 values represented in these plots are TMT based fractions of the total MS1 signal. E) An overview of the timecourse, with z-score normalization for the mRNA-seq (left), ribosome profiling (middle), and mass spectrometry (right). Plot includes all samples that were quantified by all three methods (n=4464 annotated genes). 523 proteins change by at least two-fold between 1.5 hours and 8 hours in sporulation media, a timeframe that contains no broad shift in cellular metabolism. When

including all timepoints, including transitions between rich and sporulation media, more regulation is observed, with 2087 proteins that show relative changes of at least two-fold. F) Protein abundance trends for factors involved in homologous recombination and assembly of the synaptonemal complex (SC) confirmed known regulation for proteins that have well characterized regulation (Cahoon and Hawley, 2016; Lynn et al., 2007). SC assembly begins with chromosome axis formation on each new pair of replicated sister chromatids, mediated by Rec8 (as part of the meiotic cohesin complex), Hop1, and Red1. Zip1 next assembles between the axes to stabilize homolog interactions. These assembly steps occur with timing that overlaps the progression of recombination and influences its outcome, with Dmc1 as an important mediator of strand invasion of resected double-strand breaks to allow repair, and MutS proteins, Msh4 and Msh5, forming a heterodimer that is involved in resolving crossovers. The pattern of accumulation of all of these proteins fits well with the relative timing of these known functions, as does their disappearance. Polo kinase, Cdc5, is induced in late prophase, which results in phosphorylation and degradation of Red1 and Zip1 (Prugar et al., 2017; Sourirajan and Lichten, 2008). The rapid loss of Red1 and Zip1 seen in these data, relative to other factors, like Dmc1, is consistent with single-gene studies. G) Sps100, a component of the spore wall, is low at all timepoints except the one representing mature spores (Law and Segall, 1988). Sic1 degradation is required for meiotic DNA replication (Sedgwick et al., 2006). Its timing of protein decline matches the timing of meiotic DNA replication. Sporulation media (Spo) does not contain a fermentable carbon source and thus the oxidative phosphorylation machinery is upregulated. Consistently, mitochondrial proteins, including Cox1 and Cox2 of the electron transport chain, are seen to be high early in meiosis. H) The meiotic cohesin complex consists of Rec8, the heterodimer Smc1/Smc3, and Irr1. It loads onto the chromosomes during meiotic S-phase, and is stabilized by Pds5. We measure all components to have similar patterns of protein accumulation, but Rec8 disappears first, an expected result of protein degradation through the N-end rule pathway and separase-mediated cleavage, to trigger anaphase (Buonomo et al., 2000). I) Sps1 is known to be translated only after MI, despite high prior levels of mRNA, through a mechanism that involves silencing of *SPS1* mRNA by its presence in aggregates of Rim4, which are disassembled as a result of phosphorylation by the meiotic CDK, Ime2 (Berchowitz et al., 2013, 2015). The protein *level* measurements for these factors match this known regulation remarkably well. J) We can identify known instances of translational control by comparison of mRNA and translation levels. In the case of *HAC1*, whose mRNA is high and constitutive but contains a cytoplasmically retained intron that prevents productive translation in the absence of Unfolded Protein Response activation, we observe translation during late MI and early MII, as we previously reported (Brar et al., 2012; Cox and Walter, 1996). K) Cdc5, or polo kinase, serves as a control, as it is not thought to be regulated translationally, but its transcription is driven by Ndt80 in late prophase. Consistently, we observe overlapping plots for mRNA and translation measurements, suggesting no or minimal translational control and, as also expected, protein measurements come up with similar timing as the other two. Cdc5 protein is known to be actively degraded by Ama1, and consistently, we see the levels decline rapidly after translation ceases (Okaz et al., 2012).

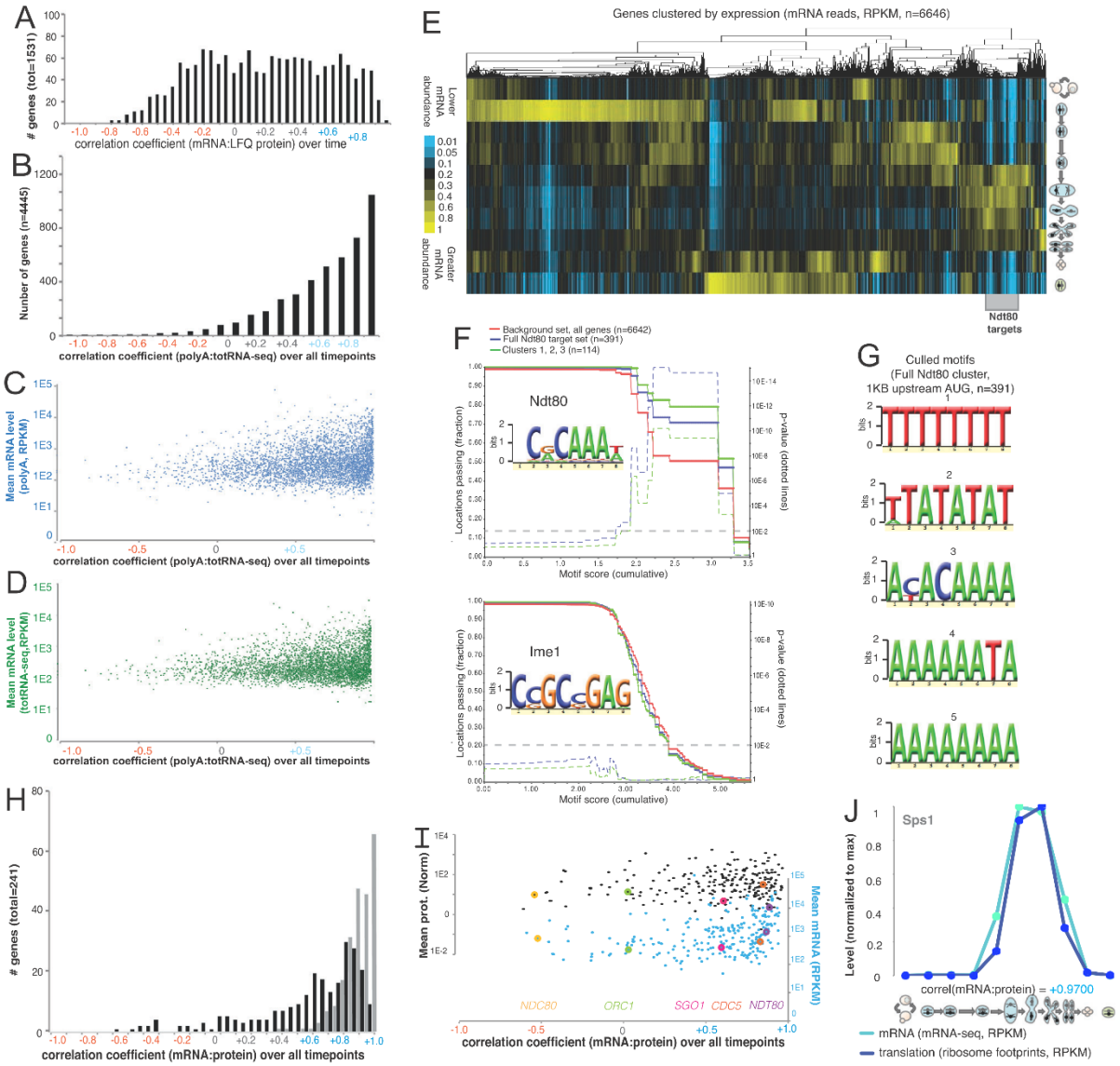

Figure 3.S2: Many genes show a poor mRNA to protein correlation, both generally and among the large set of targets of the transcription factor Ndt80, Related to Figure 3.2. A) Comparison of label-free protein quantification and mRNA-seq reveals a similar large subpopulation of genes showing anti-correlated trends between mRNA and protein over meiosis as seen when TMT10 data are used instead (compare to Fig. 3.2A). B) A histogram of the Pearson correlations between mRNA-seq for each timepoint from single round polyA selection and total RNA-seq. Note that the distribution is positive and does not show subpopulations. C) Average expression of mRNA from single round polyA selection versus correlation values from B). D) Average expression of mRNA from total RNA seq versus correlation values from B). E) A global view of transcript abundance in meiotic differentiation. Shown is the result of centroid hierarchical clustering of the ribosome profiling data for all genes (rows) quantified for mRNA abundance at all timepoints (columns). The total signal in each row is normalized to allow comparisons. The discrete cluster of genes that are thought to be Ndt80 targets are highlighted by a gray box at right. F, G) Promoters of genes identified as being Ndt80 targets

based on mRNA abundance patterns are enriched for the Ndt80 binding site, or Middle Sporulation Element (MSE), regardless of protein concordance. F) Mochiview quantification of Ndt80 binding site cumulative enrichment upstream of Ndt80 targets identified from mRNA abundance patterns, genes in the aberrant clusters (noted in Fig. 3.2A), all Ndt80 targets, and a background set is shown. Note no enrichment in the aberrant Clusters for an unrelated meiotic transcription factor, Ime1. In both plots, p-values for difference of each query set from the background set are shown as dotted lines that depend on the motif score cutoff chosen. G) An unbiased motif search using Mochiview motif finder for upstream regions of Ndt80 targets (Fig. 3.S2E; Fig. 3.2C) identified from mRNA abundance patterns revealed degenerate AT rich motifs, characteristic of intergenic regions, but only one other, specific motif, which closely matched the MSE. H) A histogram of Pearson correlation coefficients are plotted over all timepoints for the set of genes shown in Fig. 3.2C and 3.2D. Black bars represent the correlation coefficients for protein and mRNA for a given gene. Gray bars represent the correlation coefficients for mRNA of a given gene compared to mRNA for *NDT80.* I) The mean protein and mRNA levels over all timepoints are plotted for each gene, versus correlation coefficients (mRNA:protein) as shown in H. Colored dots represent known, well characterized targets of Ndt80. J) Known, robust translational regulation of *SPS1* is subtle with the resolution of our timepoints. mRNA and ribosome profiling measurements are plotted relative to max values to allow comparison. *SPS1* message is known to be translationally repressed for at least 1 hour after accumulation and a delay in the translation peak relative to the mRNA peak can be seen, but because timepoints are 1.5 hr-2hr apart, this effect appears more subtle than in previous studies with higher resolution timepoints.

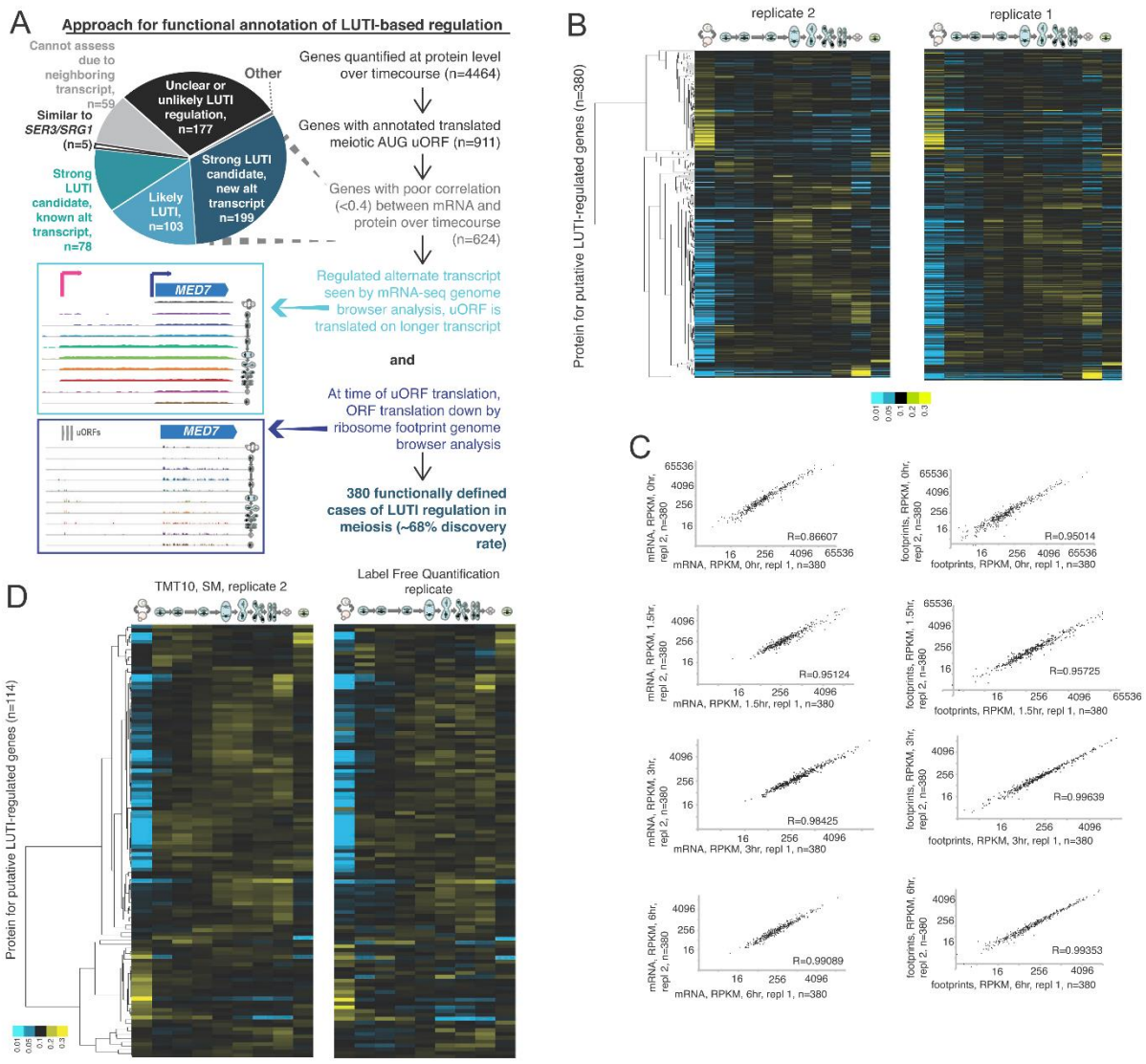

Figure 3.S3: Pipeline for identification of LUTI-based regulation reveals 380 robust cases, Related to Figure 3.3. A) A more detailed outline of approach in Fig. 3.3D. See STAR Methods for detailed description. B) TMT10 protein measurements for the 380 genes identified in the approach outlined in Fig. 3.3D as showing protein levels that are regulated by transcript toggling are shown, with hierarchical clustering performed on timecourse replicate 2 (left) and values from timecourse replicate 1 shown with rows matched at right. C) mRNA seq and ribosome profiling from the two timecourse replicates for four meiotic timepoints each were performed and comparison of these values in scatter plots is shown for each case for the 380 LUTI candidates. D) LUTI candidates show protein measurements with similar trends whether measurements are done by TMT10 or label free quantification. At left, the TMT10 values for timecourse replicate 2 are shown following hierarchical clustering of the 114/380 LUTI candidates that were quantified by both TMT10 and label free quantification over timecourse. At the right are values as measured by label free quantification.

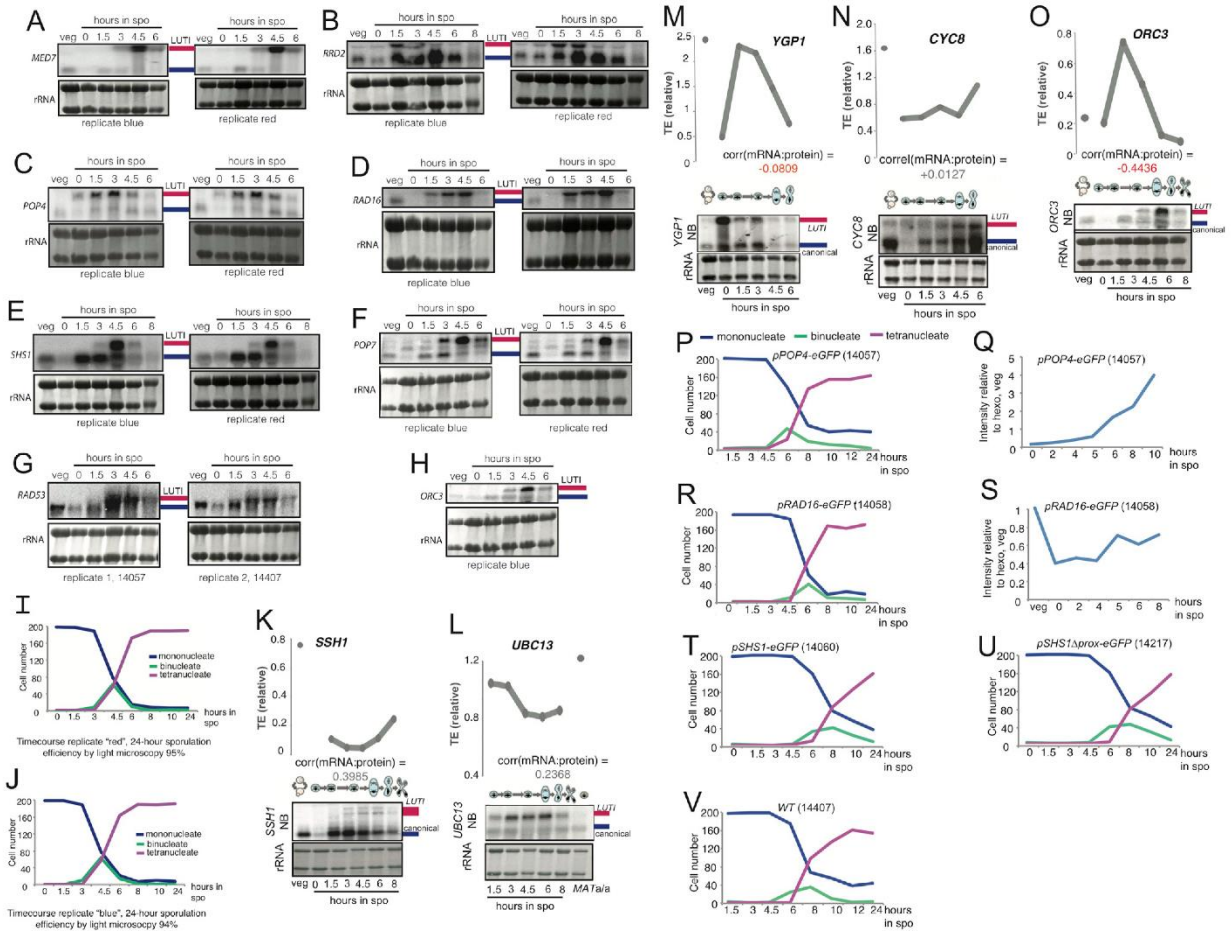

Figure 3.S4: New LUTI cases can be confirmed by robust alternate approaches, Related to Figures 3.4 and 3.6. A-H) Shown are independent meiotic timcourse replicates showing similar patterns for short and long transcripts detected in main Figs. 4 and 6. ORFs probed are: A) *MED7* B) *RRD2* C) *POP4* D) *RAD16* E) *SHS1* F) *POP7* G) *RAD53* H) *ORC3.* Only one replicate is shown for *ORC3,* as the other is in Fig. 3.S4O. *ORC3* and *POP7* replicates were run on the same gel and therefore methylene blue stain image is identical. Note that *RAD53* replicate blots are from a different set of timecourses, using strains 14057 and 14407 and RNA from the experiment staged in Fig. 3.S2P and V. I, J) Staging of additional replicate timecourses for Northern blotting. Categorization of DAPI morphology into either mononucleate, binucleate, or tetranucleate was performed for 200 cells at each timepoint. I) DAPI counting reflecting synchronous meiotic progression is shown for timecourse "red" and J) "blue", used for blotting in Figure 3.S2A-F, H. K-O) Northern blot confirmation of additional LUTI candidates highlighted in Fig. 3.4C. K) Comparison of levels and timing between Northern blots for the translocon component-encoding *SSH1* ORF and the TE in matched samples shows evidence for a poorly translated long transcript as predicted by the mechanism in Figure 3.7. A similar analysis for L) *UBC13*, encoding an E2 ubiquitin-conjugating enzyme, M) *YGP1*, encoding a cell wall glycoprotein, N) *CYC8*, a general transcriptional repressor. O) *ORC3*, a component of the origin recognition complex. Note that due to limiting extract from the original timecourse, the *ORC3* Northern blot was performed on extract from replicate "timecourse red", staged in Fig. 3.S2I. Meiotic progression, as

judged by DAPI mass morphology, is shown for experiments presented in Fig. 3.4G, 4I, 4K, 4L, S2G. P) *pPOP4-eGFP* cells (14057) R) *pRAD16-eGFP* (14058) T) *pSHS1-eGFP* (14060) U) *pSHS1Δprox-eGFP* (14217) V) WT (14407) Q) Quantification of *pPOP4-eGFP* Western blot in Fig. 3.4G. S) Quantification of *pRAD16-eGFP* Western blot in Fig. 3.4I. The experiments shown in this figure were performed by George Otto and Emily Powers and are included with their permission.

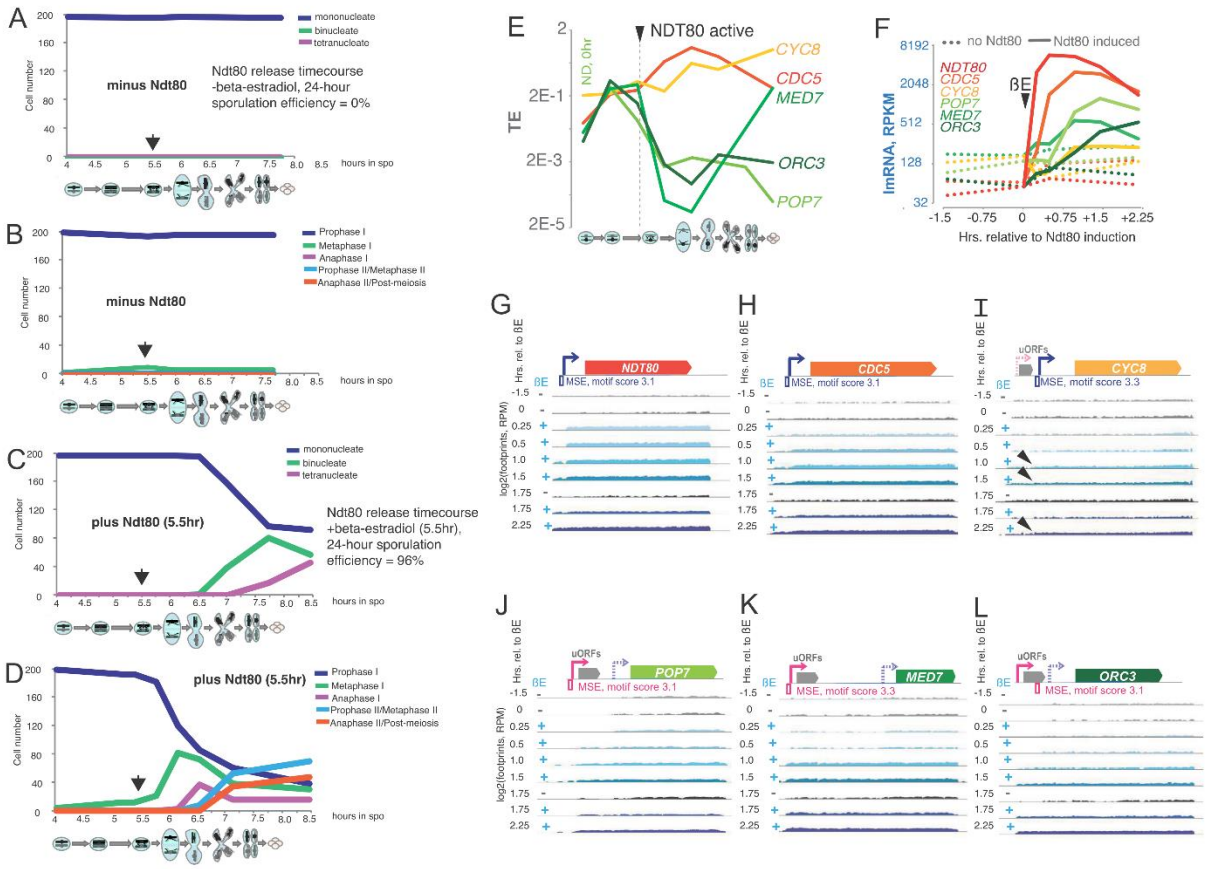

Figure 3.S5: Ndt80 induces long, translationally inactive isoforms of *POP7*, *MED7,* and *ORC3* and canonical transcript isoforms of *CDC5, HRR25,* and *CYC8*, Related to Figure 3.5. Staging for experiment shown in Fig. 3.5C-I by DAPI morphology without and with Ndt80 induction in A) and C), respectively and for spindle morphology by tubulin immunofluorescence in B) and D), respectively. Arrow indicates time of Ndt80 induction by addition of β-estradiol. E) Plots of log2(TE) for transcripts induced by Ndt80 in original timecourse data. Approximate time of Ndt80 activation is indicated by arrow. F) This figure is the same as Fig. 3.5D, but with only the genes shown in G-L to allow direct comparison. Induction of Ndt80 results in increased mRNA abundance for canonical and non- canonical targets. Arrow indicates time of Ndt80 induction by addition of β-estradiol. Note that, although levels of transcript accumulation vary, both positive (canonical) and negative (LUTI- like) targets are induced with similar timing. Note that accumulation is dependent on Ndt80. G) Rapid induction of *NDT80* mRNA can be seen within 15 minutes of addition of β-estradiol. H) *CDC5*, a canonical target is induced in an Ndt80-dependent manner within 30 minutes of addition of β-estradiol. I) A short (canonical) version of *CYC8* is induced in an Ndt80-dependent manner. Note Ndt80-dependent TSS is at arrowhead and masked somewhat by longer transcript. Compare to Northern blot in Figs. 5A and 5C. J-L) Long uORF containing transcripts defined as LUTI-regulated by approach in Fig. 3.3D are induced between 30 minutes and 1 hour after addition of β-estradiol in an Ndt80 dependent manner. Compare to Northern blots in Figs. 5A and 5C. The experiments shown in this figure were performed by George Otto and Emily Powers and are included with their permission.

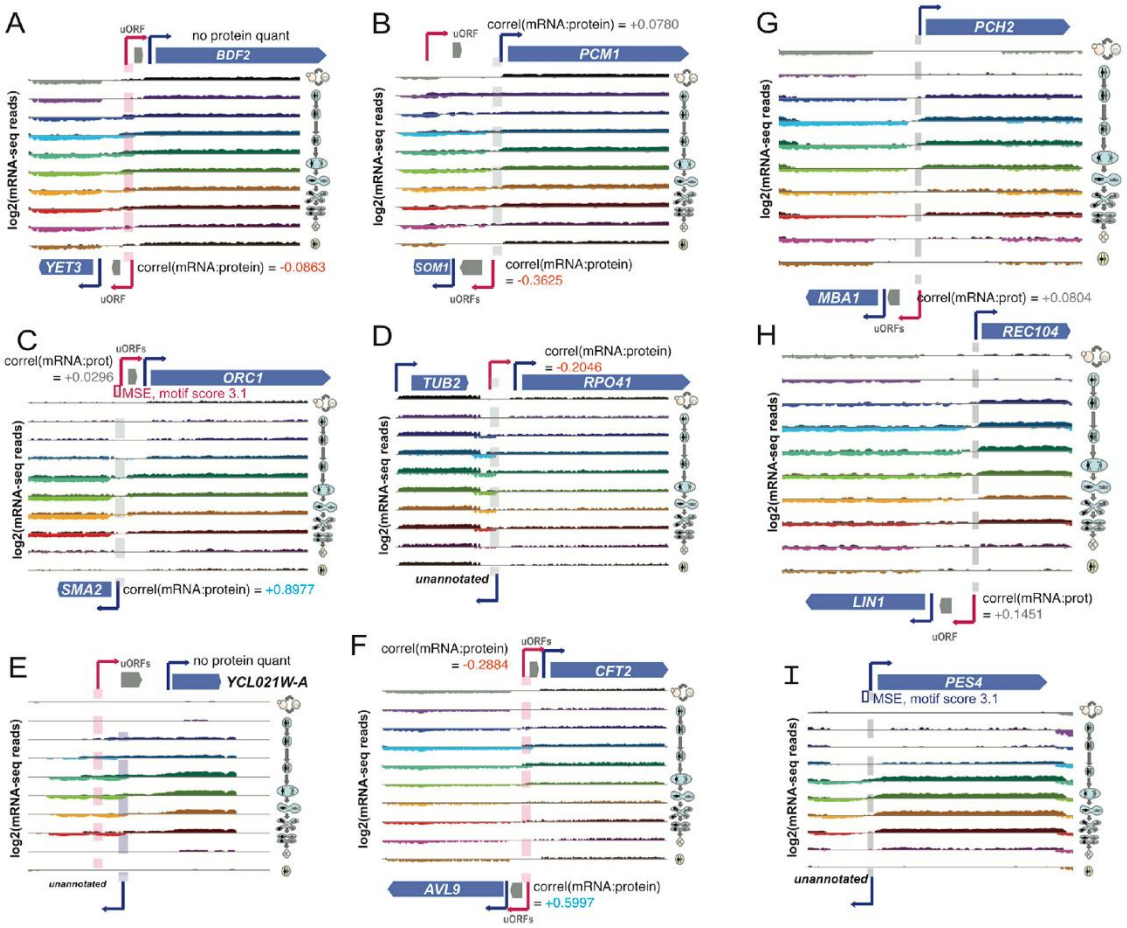

Figure 3.S6: A variety of neighboring transcript associations with LUTIs can be seen, Related to Figure 3.6. A) mRNA-seq data is shown for the *BDF2/YET3* locus, revealing apparently coordinated divergent adjacent LUTIs. B) mRNA-seq data is shown for the *PCM1/SOM1* locus, revealing apparently divergent adjacent LUTIs that show mutually exclusive LUTI transcription timing. C) mRNA-seq data is shown for the *ORC1/SMA2* locus, highlighting LUTI regulation that is coordinated with transcription of a neighboring canonical transcript. D) mRNA-seq data is shown for the *RPO41* locus, revealing apparently coordinated transcription of a divergent unannotated transcript. E) mRNA-seq data is shown for the *YCL021W-A* locus, revealing apparently coordinated transcription of a divergent unannotated transcript. F) mRNA-seq data is shown for the *CFT2/AVL9* locus, revealing apparently coordinated divergent adjacent long transcripts. *CFT2* shows hallmarks of LUTI-based regulation, including a poor correlation between protein and mRNA, while *AVL9* shows an alternate transcript but no clear evidence that this affects translation of the *AVL9* ORF. G-I) Trancription of meiosis-specific genes with spatio- temporal association with neighbors. G) Associated transcription between the *MBA1* LUTI and canonical *PCH2* transcript can be seen by mRNA-seq analysis. H) Associated transcription between the *LIN1* LUTI and canonical *REC104* transcript can be seen by mRNA-seq analysis. I) The Ndt80-induced *PES4* transcript increases with timing and TSS position closely mirroring an unannotated transcript on the minus strand. An MSE is positioned at the point at which the two transcript 5' ends meet.

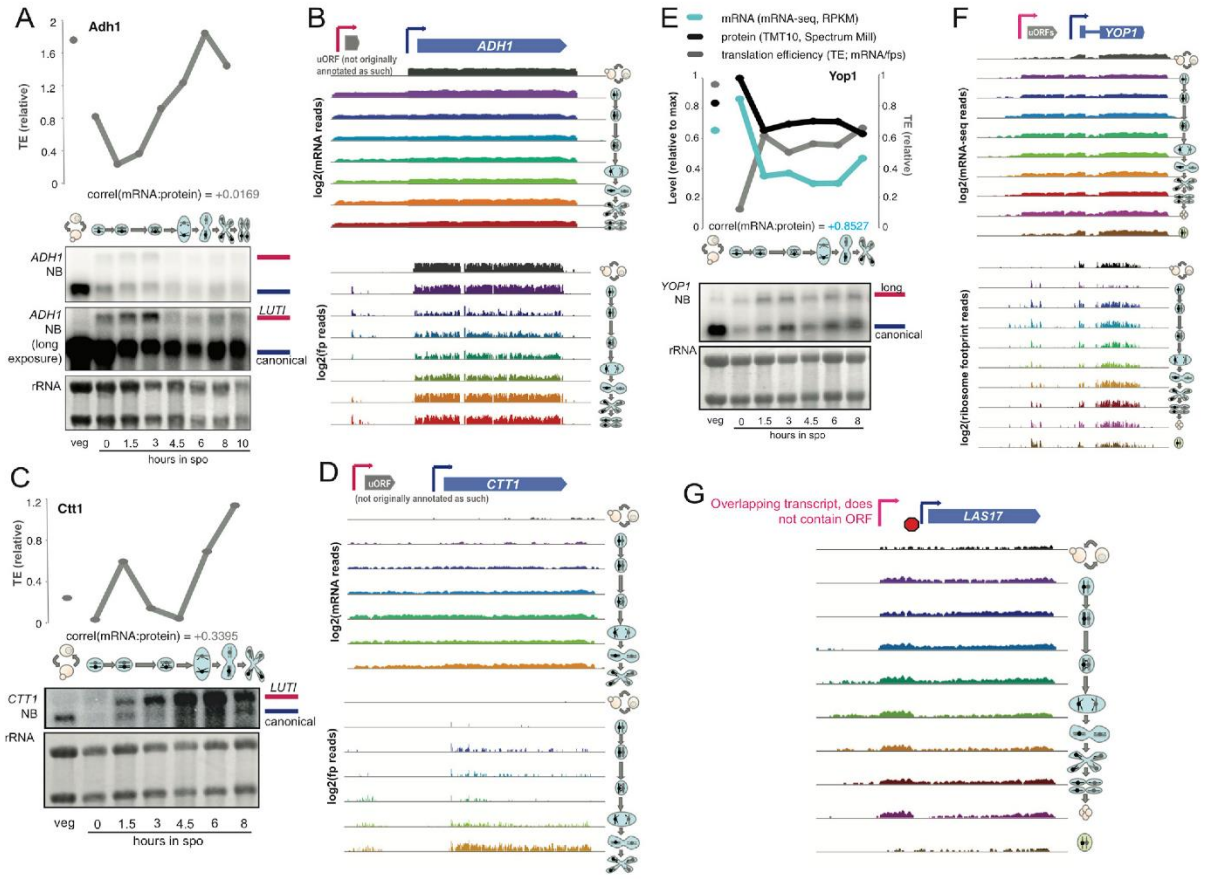

Figure 3.S7: Additional LUTIs are likely to exist that were missed in our annotations due to poorly annotated AUG-initiated uORFs, Related to Figures 3.3 and 3.6. A) *ADH1* shows a poor protein:mRNA correlation and Northern blotting reveals two transcripts, the longer of which is associated with a lower TE. B) An inverse correlation between upstream translation of a misannotated AUG-initiated uORF and *ADH1* ORF translation can be seen from ribosome footprint data at this locus. Matching mRNA-seq data are above C) *CTT1* shows a poor protein:mRNA correlation and Northern blotting reveals two transcripts, the longer of which is associated with a lower TE. D) mRNA seq data at the *CTT1* locus is ambiguous due to low expression levels. It would be difficult from mRNA-seq alone to have predicted the short vegetative transcript or the mixed transcript pool at 8 hours. Matching ribosome profiling data are below. E) *YOP1* shows a long alternate transcript with translated AUG uORFs, but it is not a LUTI. Northern blotting of *YOP1* confirms a longer alternate transcript at this locus of the size predicted from mRNA-seq data, but we do not find a clear association between the relative ratios of the two *YOP1* transcripts and the TE at this locus (above). Consistently, the correlation between mRNA and protein for *YOP1* is strongly positive (below graph). F) mRNA-seq and ribosome footprint data at this locus suggest no negative association between translation of the AUG uORFs on the log transcript and the translation of the *YOP1* ORF. G) Putative new cases of the type of regulation reported for *SER3/SRG1.* Positive strand mRNA-seq data for the *LAS17* locus are shown. Here it appears that the transcript that is initiated distally terminates and therefore does not contain the *LAS17* ORF. This type of regulation has been shown to result in decreased transcription from the one canonical TSS (Martens et

al., 2004), but would not produce a LUTI transcript. Northern blotting experiments were performed by George Otto and Emily Powers and are included with their permission.

CHAPTER 4

Global translation inhibition yields condition-dependent de-repression of ribosome biogenesis mRNAs

Part of the work presented in this chapter has been previously published in the following manuscript: Cheng, Z. and Brar, G.A., 2019. Global translation inhibition yields condition-dependent de-repression of ribosome biogenesis mRNAs. Nucleic acids research.

doi: 10.1093/nar/gkz231

4.1 Abstract

Ribosome biogenesis (RiBi) is an extremely energy intensive process that is critical for gene expression. It is thus highly regulated, including through the tightly coordinated expression of over 200 RiBi genes by positive and negative transcriptional regulators. We investigated RiBi regulation as cells initiated meiosis in budding yeast and noted early transcriptional activation of RiBi genes, followed by their apparent translational repression 1 hour after stimulation to enter meiosis. Surprisingly, in the representative genes examined, measured translational repression depended on their promoters rather than mRNA regions. Further investigation revealed that the signature of this regulation in our data depended on pre-treating cells with the translation inhibitor, cycloheximide (CHX). This treatment, at 1 hour in meiosis, but not earlier, rapidly resulted in accumulation of RiBi mRNAs that were not translated. This effect was also seen in with CHX pre-treatment of cells grown in media lacking amino acids. For *NSR1,* this effect depended on the -150 to -101 region of the promoter, as well as the RiBi transcriptional repressors Dot6 and Tod6. Condition-specific RiBi mRNA accumulation was also seen with translation inhibitor drugs that are dissimilar from CHX, suggesting that this phenomenon might represent a feedback response to global translation inhibition.

4.2 Introduction

The synthesis of ribosomes, the ribonucleoprotein machines that mediate translation of proteins from mRNA templates, is a tightly regulated process that has been well studied in the budding yeast Saccharomyces cerevisiae. 80 ribosomal proteins (RPs) and 4 ribosomal RNAs make up the ribosome, and their processing and assembly requires an additional suite of more than 200 proteins that mediate ribosome biogenesis (RiBi; (Wade et al., 2006); reviewed in (Klinge and Woolford, 2018)). RiBi genes are tightly coordinated in their transcription, which typically involves at least one general factor (Abf1, Reb1, Rap1, and Tbf1) in concert with other positive transcriptional activators (reviewed in (Bosio et al., 2017)), which are typically recruited to RiBi gene promoters by the nutrient-activated kinases Tor and PKA ((Berger et al., 2007; Hall et al., 2006; Jorgensen et al., 2004; Martin et al., 2004; Rudra et al., 2005; Schawalder et al., 2004; Wade et al., 2004; Xiao and Grove, 2009; Zhao et al., 2006); reviewed in (Bosio et al., 2017; Broach, 2012)). Therefore, under conditions in which amino acids and glucose are plentiful, RiBi gene transcription is activated, which increases the synthesis and assembly of ribosomes. Negative transcriptional regulators—including Stb3, Dot6, and Tod6—also participate in regulation of the RiBi genes by binding their promoters and recruiting the histone deacetylase Rpd3L ((Huber et al., 2011; Liko et al., 2007; Lippman and Broach, 2009), reviewed in (Broach, 2012)). Tor and/or PKA activity is known to relieve this repression via phosphorylation of these negative regulators, resulting in their removal from RiBi promoters and subsequent nuclear export (Huber et al., 2011; Lippman and Broach, 2009). Robust expression of RiBi genes thus requires coordinated de-repression as well as active induction. Transcriptional repression of RiBi genes under non-inducing conditions appears to be important, as it has been shown that cells lacking Dot6/Tod6-based repression are unable to properly adapt to nutrient-limiting

conditions (Lippman and Broach, 2009). This is presumably due to leaky RiBi gene production that depletes cellular energy reserves required for cellular adaptation.

Much of what we currently know about RiBi regulation comes from studies of yeast in either rich laboratory growth conditions or under conditions of acute amino acid starvation. It is also known that RiBi and RP genes are modulated during other cellular conditions in yeast, including during the meiotic program, the conserved process by which gametes (spores in yeast) are created (Brar et al., 2012a; Chu et al., 1998; Eisenberg et al., 2018). RP and RiBi genes are known to be transcriptionally downregulated prior to meiotic entry relative to vegetative exponentially growing cells (Chu et al., 1998), and upregulated following the meiotic divisions (Brar et al., 2012a). We previously found that translation levels and apparent ribosome number increase shortly after cells enter the meiotic program, and also that RPs are actively degraded following the meiotic divisions, concomitant with transcriptional upregulation of RP and RiBi genes (Eisenberg et al., 2018). Given these interesting patterns of regulation and the central importance of the ribosome to gene expression, we investigated the regulation of RiBi genes in meiosis in greater depth. Here, we report our observation of apparent translational repression of RiBi genes 1 hour after cells were stimulated to enter meiosis. We find that this apparent repression is limited to a narrow time window between 45 and 75 minutes after transfer of cells into sporulation medium (SPO). Surprisingly, this is not a natural part of the meiotic program, but rather a response to the drug-based inhibition of translation that we employed to collect samples. We report that global translation inhibition by CHX resulted in transcriptional upregulation of RiBi genes that is partially dependent on Tod6 and Dot6. We find that a similar effect can be seen following CHX treatment during conditions of amino acid starvation, another context in which RiBi genes are not normally transcriptionally induced and de-repression is thus unmasked. We propose that this transcriptional de-repression of RiBi genes may represent a feedback response to global translational inhibition, as it is seen in response to several distinct drug-based mechanisms of general translational inhibition.

4.3 Methods

4.3.1 Yeast strains

All experiments were performed using *Saccharomyces cerevisiae* strains of the SK1 background. Strains were fully prototrophic (*LEU URA TRP LYS HIS*). All strains are diploid (*MAT*a*/alpha*) except for 4401, which is haploid (*MATa*). All the reporters are integrated at *TRP1* locus with functional *TRP1* gene as selection marker.

Strain number	Genotype
4401	*WT*
4484	*WT*
11324	*pNSR1-NSR1-3V5*

11582	*pSAR1-NSR1-3V5*
11584	*pSAR1-NSR1-3V5 (TSS2)*
11326	*pNIP7-NIP7-3V5*
11586	*pSAR1-NIP7-3V5*
13064	*tod6::NatMX tod6::NatMX*
13070	*dot6::NatMX dot6::NatMX*
13074	*tod6::NatMX tod6::NatMX dot6::NatMX dot6::NatMX*
14203	*stb3::NatMX stb3::NatMX*
15325	*pSAR1-SAR1-3V5*
15328	*pNSR1(-100 to -51 swapped to pSAR1 sequence)-NSR1-3V5*
15329	*pNSR1(-150 to -101 swapped to pSAR1 sequence)-NSR1-3V5*
15330	*pNSR1(-200 to -151 swapped to pSAR1 sequence)-NSR1-3V5*
15331	*pNSR1(-728 to -201 swapped to pSAR1 sequence)-NSR1-3V5*
15332	*pNSR1(-50 to -1 swapped to pSAR1 sequence)-NSR1-3V5*
16268	*pNSR1-SAR1-3V5*
16272	*pNSR1(ΔRRPE-1 ΔRRPE-2 ΔPAC)-NSR1-3V5*

4.3.2 Yeast growth conditions

Vegetative samples were collected after growth of 300 ml (sequencing and polysome fractionation experiments) or 15 ml (total RNA qPCR experiments) culture in YPD from OD_{600}0.1 to OD_{600}0.6 at 30˚C with shaking. For meiotic samples, cells were grown in YEPD for 24 hours, diluted to OD_{600}0.25 in buffered YTA, and grown for 16 hours. Cells were washed in water, resuspended at OD_{600}1.9 in 300 ml (sequencing and polysome fractionation experiments) or 15 ml (total RNA qPCR experiments) sporulation media supplemented with 0.02% raffinose, and incubated at 30˚C with shaking. For amino acid starvation experiments, cells were grown in YPD overnight, diluted to OD_{600}0.1 in fresh YPD, grown to OD_{600}0.6, resuspend in equal volume of SD media without amino acids, and incubated at 30˚C with shaking.

4.3.3 Cell extract preparation

CHX (100 µg/ml final concentration) or equal volume of vehicle solvent (ethanol) was added to the cells 1.5 minutes prior to harvesting. Cells were collected by filtration and flash freezing in liquid nitrogen. Around 10% of the cells were stored in a separate tube for mRNA-seq. 3 ml frozen buffer (20 mM Tris pH8, 140 mM KCl, 1.5 mM MgCl2, 100 µg/ml cycloheximide, 1% Trition X-100) were added to the cell pellets. Samples were lysed by

Retsch mixermilling (3 x 3-minute rounds at 15 Hz). The powder was thawed at 30˚C, spun at 4˚C for 5 minutes at 3000 rcf. The supernatant was collected and spun at 20,000 rcf at 4˚C for 10 minutes. The supernatant was aliquoted in 200 µl portions and flash frozen in liquid nitrogen. Identical extracts were used for ribosome profiling and polysome gradients.

4.3.4 Ribosome Profiling and mRNA-seq data

Ribosome profiling and mRNA-seq data were analyzed from (Brar et al., 2012a) and are deposited at NCBI GEO with accession number GSE34082. Cluster 3.0 and Treeview were used for cluster analyses and visualization (de Hoon et al., 2004; Saldanha, 2004). Mochiview was used for genome browsing visualization (Homann and Johnson, 2010).

4.3.5 LTM profiling

Cells were harvested by filtration following treatment at a final concentration of 50uM LTM in DMSO and 5 minutes incubation with shaking. Extract was prepared following mixermilling and 200 µl of cell extract were incubated with 15U RNase I (Ambion) per A_{260} unit of extract for 1 hour at room temperature. Samples were loaded onto 10-50% sucrose gradients and spun at 35,000 rpm for 3 hours at 4˚C in a SW41Ti rotor (Beckman). The gradients were then fractionated using a Gradient Station (BioComp) and the 80S/monosome peaks were collected. RNA was extracted with hot acid phenol, size selected from a polyacrylamide gel, dephosphorylated with PNK (NEB), polyA-tailed with E.coli polyA polymerase (NEB), subjected to rRNA subtraction by antisense oligos, reverse transcribed with Superscript III (Thermo), circularized with Circ Ligase (Epicentre), and PCR amplified with Phusion polymerase (NEB). The Oligo oCJ200-oligodT was used for reverse transcription, and oNTI231 and aatgatacggcgaccaccgagatcggaagagcacacgtctgaactccagtcac-barcode-cgacaggttcagagttc index primers was used for PCR. The barcodes are six nucleotides in length. Sequencing was done using standard Illumina oligos. All samples were sequenced on an Illumina HiSeq 2500, 50SRR, with multiplexing, at the UC-Berkeley Vincent Coates QB3 Sequencing facility.

4.3.6 LTM sequencing data analysis

LTM ribosome profiling data were analyzed by Bowtie2-based alignment exactly as standard ribosome profiling data in (Brar et al., 2012b; Ingolia et al., 2012a; Langmead and Salzberg, 2012). Mochiview was used for genome browsing visualization (Homann and Johnson, 2010).

4.3.7 Polysome analysis

The sucrose gradients were performed exactly as in (Ingolia et al., 2009a), except without RNAse I treatment. In short, 200 ul of extract was loaded on 10-50% sucrose gradients and samples were centrifuged in a Beckman XL-70 Ultracentrigue, using a Sw-Ti41 rotor for 3

hours at 35,000 rpm at 4oC. Tube was loaded on a Bio-Comp Gradient Station and analyzed for absorbance at 260 nm. Eight fractions were collected per gradient and flash frozen in liquid nitrogen. 300ul, 500ul, and 700ul of DEPC water was added to the fractions 6, 7, and 8, respectively, to bring their density below the density of phenol/chloroform mix prior to hot acid phenol extraction.

4.3.8 Cell harvesting for RT-qPCR

All YPD samples were harvested at OD_{600}0.6 in YEPD medium. All amino acid starvation samples were harvested 20 minutes after transferring from YEPD to SD medium without amino acids, except for the experiment showed in Figures 4.3E and 4.S5C, in which the cells were harvested at the indicated timepoints.

1 ml of cells was mixed with drugs or solvent in a 2 ml screw-cap tube. The samples were kept shaking for 1.5 minutes at 30˚C, spun at 20,000 rcf for 30 seconds, and flash frozen in liquid nitrogen.

The final drug concentrations were: CHX: 100 μg/ml; LTM: 10 μM; sordarin: 100 μg/ml; anisomycin: 20 μM. For controls, an equal volume of solvent was added to the cells (ethanol for CHX and sordarin, DMSO for LTM and anisomycin).

In the TOR inhibition experiment, rapamycin was added to the cells at 0.2 μg/ml final concentration, 10 minutes prior to CHX addition. An equal volume of the solvent, DMSO, was added to the control samples.

4.3.9 RT-qPCR

RNA was isolated from the gradient fraction samples or the cell pellets by hot acid phenol extraction, DNase-treated with Turbo DNase (Invitrogen), and purified with phenol extraction. The RNA samples were adjusted to similar concentration and 150-250 ng of RNA was used in reverse transcription with Superscript III (Thermo). Transcript levels were quantified on a StepOnePlus Real-Time PCR system using the SYBR green PCR mix (ThermoFisher), and normalized to the total RNA concentrations. CT values were first transformed to fold changes (according to the standard curve of the primer pair). Values were then normalized to total RNA amount in reverse transcription reaction of each fraction, and for gradient analyses, also normalized to the average of the 8 fractions for each strain.

4.3.10 RT-qPCR analysis

For figures, to enable visualization of trends between transcripts of different expression levels, the values plotted are relative to the average values for that transcript in all fractions or conditions analyzed in the plot. Values are also relative to the total RNA in that fraction.

The qPCR primers are listed below:

NSR1-forward: 5’ GTTCAATTCTCCAACATGGAGGACG 3’

NSR1-reverse: 5’ CCATCGTTGTTTGGTCTTGGAGAAG 3’

NIP7-forward: 5’ AGGCACATGTGGGTAAAATGTCTG 3’

NIP7-reverse: 5’ ACCGAACCCTAATGGCACATC 3’

SAR1-forward: 5’ TCAAGCTCGTCGTTTATGGAAGG 3’

SAR1-reverse: 5’ TCTTTCAGGGTCAGCAGCATC 3’

REC8-forward: 5’ TCTAACAGGTTCGAGCTTCATGGG 3’

REC8-reverse: 5’ CATCAACGGGAATTTCATCCAGTGG 3’

CCW14-forward: 5’ CCTCTACCAAGGCTTCTTCCAGT 3’

CCW14-reverse: 5’ GTGGAAGAAGCCTTGCTAGAAGATG 3’

NSR1-3V5-forward: 5’ CGCTTCTTTCGCTGGTTCAAAG 3’

NIP7-3V5-forward: 5’ GTGAGTATTTGAGAGATGAAGACACCTTG 3’

SAR1-3V5-forward: 5’ TAGAGGCGTTCCAATGGTTATCTC 3’

Common-*3V5*-reverse: 5’ TGGTATTGGTTTTCCATCTAGTCCC 3’

4.3.11 5’ RACE

cDNA was synthesized from phenol extracted total RNA using GeneRacer kit with SuperScript III RT (Invitrogen), following the manufacture’s protocol. cDNA was then amplified using Q5 Hot Start High-Fidelity DNA polymerase (NEB) with adapter primer in the GeneRacer kit and gene specific primers to generate 5’ end for individual genes. The 5’ ends were incubated with 1U Taq polymerase (Invitrogen) to add 3’ A-overhangs, purified using agarose gel extraction, cloned into vector using TOPO TA Cloning Kit for Sequencing (Invitrogen), and transformed into E.coli. Around twenty clones per gene were sequenced. Only clones with intact adapter sequence were analyzed.

The gene specific primers are listed below:

NSR1: 5’ GATTCGGAGGAAGAGGAAGAGAC 3’

NIP7: 5’ GCTTAGCCAATACTGTCAAAGAAGT 3’

SAR1: 5’ TGACCACCCAAATCGAAAGTTGT 3’

4.4 Results

4.4.1 RiBi mRNAs show signatures of translational repression shortly after stimulation of cells to enter meiosis

To begin investigating the regulation of RiBi genes in meiosis, we re-analyzed a previously generated dataset from our lab, which included mRNA abundance and translation measurements made by mRNA-seq and ribosome profiling, respectively, during a high-resolution timecourse of the budding yeast meiotic program (Brar et al., 2012a). We found that, as expected, most (325/395; "ribosome biogenesis" at http://amigo.geneontology.org/amigo; PolII-dependent transcripts only; includes RP genes with roles in RiBi) annotated RiBi genes were coordinately regulated over all timepoints. mRNA levels of RiBi genes were very low prior to meiotic entry, but were rapidly increased within 30 minutes in SPO, followed by their rapid decline (Figure 4.1A). Our ability to observe this brief burst of transcription depended on the high-resolution of our timepoints relative to previous studies. We collected denser timepoints early in the meiotic program and found that RiBi transcripts peak at 15 minutes and decline by 45 minutes, timepoints that were not included in our original large-scale dataset (Figure 4.S1A). Translation levels, as assayed by ribosome footprint density over ORFs, showed a roughly similar trend as mRNA levels, which fit with our expectations (Figure 4.1B). Surprisingly, however, when we calculated the translation efficiency (TE, ribosome footprint abundance normalized to mRNA abundance) for RiBi mRNAs, we noted that there was apparent translational repression at approximately 1 hr after transfer of cells to SPO, shortly after transcript levels had plummeted (Figure 4.1C, 4.1D, 4.S1A) and after expression of the early meiosis-specific gene, *REC8,* was detected, indicating commitment to the meiotic differentiation program (Figure 4.S1A). This translational repression was strong and consistent for RiBi genes (Figure 4.1D, 4.S1B, and 4.S1C).

To independently confirm the translational repression that we measured by global approaches, we analyzed the distribution of RiBi mRNAs in polysome gradients at 15 minutes and 1 hour after transfer to SPO, timepoints prior to and during the period in which translational repression was measured, respectively (Figure 4.1C, 4.1E, 4.1F). Comparison of the mRNA distribution for representative RiBi genes *NSR1* and *NIP7* to non-RiBi gene *SAR1* revealed that all were abundant in heavy polysome fractions at 15 minutes after transfer to SPO, suggesting high levels of translation, which was consistent with TE measurements from the global meiotic study (Figure 4.1C). Extract from cells 1 hr after transfer to SPO showed a specific shift to the monosome/80S fraction for *NSR1* and *NIP7*, but not *SAR1,* again consistent with our analysis of the global study (Figure 4.1C, 4.1F). To identify the regulatory regions of *NSR1* and *NIP7* responsible for this apparent translational repression, we mapped the 5' ends of these mRNAs by 5' RACE, along with that of *SAR1* (Figure 4.S2A-C). Because disruption of *NSR1*, *NIP7*, or *SAR1* would have likely resulted in secondary cellular consequences based on the critical cellular roles for these genes, we constructed strains carrying reporter constructs that did not alter the wild-type *NSR1*, *NIP7*, or *SAR1* loci. To do this, we added a reporter construct integrated at the *TRP1* locus, which expressed a 3' 3V5-tagged version of each of these proteins. We collected fractions from polysome gradients from cell extract of strains carrying these reporter constructs, and performed RT-qPCR against the 3V5 tag region in these fractions to distinguish our reporters from the

endogenous genes. We found that these reporter constructs recapitulated the regulation seen at the endogenous locus for all three genes at 1 hr after transfer to SPO (Figure 4.2A-D, left panels).

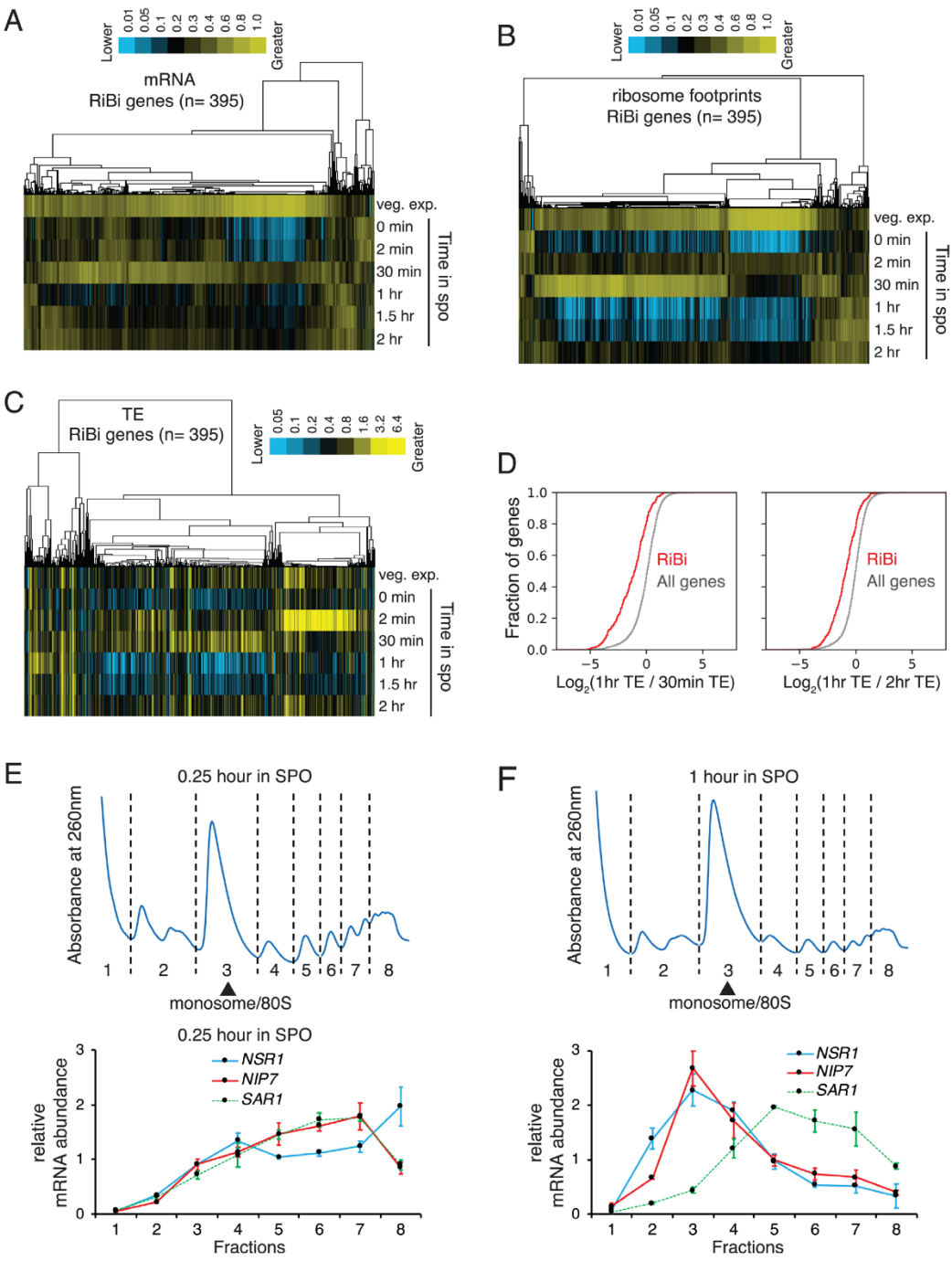

Figure 4.1: RiBi genes show translational repression at 1 hour in sporulation medium. A) – C) mRNA-seq, ribosome profiling, and TE values of RiBi genes from a high-resolution timecourse of the budding yeast meiotic program (Brar et al., 2012a). Data are clustered by similar expression patterns of genes (columns) across timepoints in sporulation medium (rows). The arrowhead in panel C indicates the timing of the translational repression. Kolmogerov-Smirnov test used to determine significance. D) Left: Cumulative histogram showing $\log_2$ values of the ratio between 1 hour and 30 min TEs. The red line represents RiBi genes and the gray line represents all genes. Kolmogerov-Smirnov (K-S) test used to determine significance. p=7.99E-54. Right: Cumulative histogram showing $\log_2$ values of the ratio between 1 hour and 2 hour TEs. The red line represents RiBi genes and the gray line represents all genes. K-S test p-value 1.75E-48. E) and F) Distributions of RiBi mRNA (*NSR1* and *NIP7*) and non-RiBi mRNA (*SAR1*) in polysome gradients as determined by RT-qPCR. Error

bars represent measurement variability as determined by three qPCR replicates. The sample shown in panel E was collected at 0.25 hour in SPO, and the sample shown in panel F was collected at 1 hour in SPO. Polysome gradients for these timepoints are shown above in each case.

4.4.2 An interval of the *NSR1* promoter is necessary and sufficient for its apparent translational repression

We next sought to identify the cis-regulatory regions responsible for this regulation. Interestingly, pilot experiments revealed that replacing the *NSR1 promoter* alone with that of *SAR1*, resulted in the retention of *NSR1*-3V5 in heavy polysome fractions at 1 hour in SPO (Figure 4.2A, 4.S2D, 4.S3A). A similar effect was seen when the *SAR1* promoter was used to drive *NIP7* with its 5' UTR intact (Figure 4.2B). These results were a surprise because most translational regulation is thought to be mediated through untranslated regions (UTRs) of mRNAs and, although it has been reported that promoter regions can affect downstream processes including mRNA translatability and decay (Bregman et al., 2011; Enssle et al., 1993; Trcek et al., 2011; Zid and O'Shea, 2014), this type of regulation had not been reported for RiBi genes, to our knowledge. We further explored this promoter-based RiBi regulation, finding that the *NSR1* promoter was not only required for the shift of the reporter mRNA to the monosome fraction at 1 hour in SPO, it was also sufficient for this shift, as a *SAR1-3V5* reporter driven by the *NSR1* promoter was seen in the monosome fraction at 1 hour (Figure 4.2C). This was not the case for another non-RiBi mRNA, *CCW14* at the same timepoint, suggesting that the effect seen was transcript-specific rather than a global perturbation of translation (Figure 4.2C). To identify the specific promoter region that was required for translational repression, we swapped out intervals of the *NSR1* promoter with the corresponding region of the *SAR1* promoter and found that one such interval replacement, for the region between -150 and -101 bp upstream of the *NSR1* transcription start site ("TSS" in Figure 4.S2A), was necessary for the shift of the *NSR1* reporter into the monosome/80S fraction at 1 hour in SPO (Figure 4.2D, 4.S3A, and 4.S3B). This region of the *NSR1* promoter contains binding sites for the three known RiBi transcriptional repressors, Dot6, Tod6, and Stb3 (Figure 4.S3C; (Zhu et al., 2009)). Deletion of any one of these proteins did not result in a loss of the observed translational repression at 1 hour in SPO (Figure 4.S3D). Because Dot6 and Tod6 are homologs and both bind the same DNA element (PAC motif;(Badis et al., 2008; Zhu et al., 2009)), we attempted to assay a *dot6Δtod6Δ* double mutant, but found that these cells showed markedly reduced ability to undergo meiosis, obscuring our ability to observe normal RiBi regulation timing.

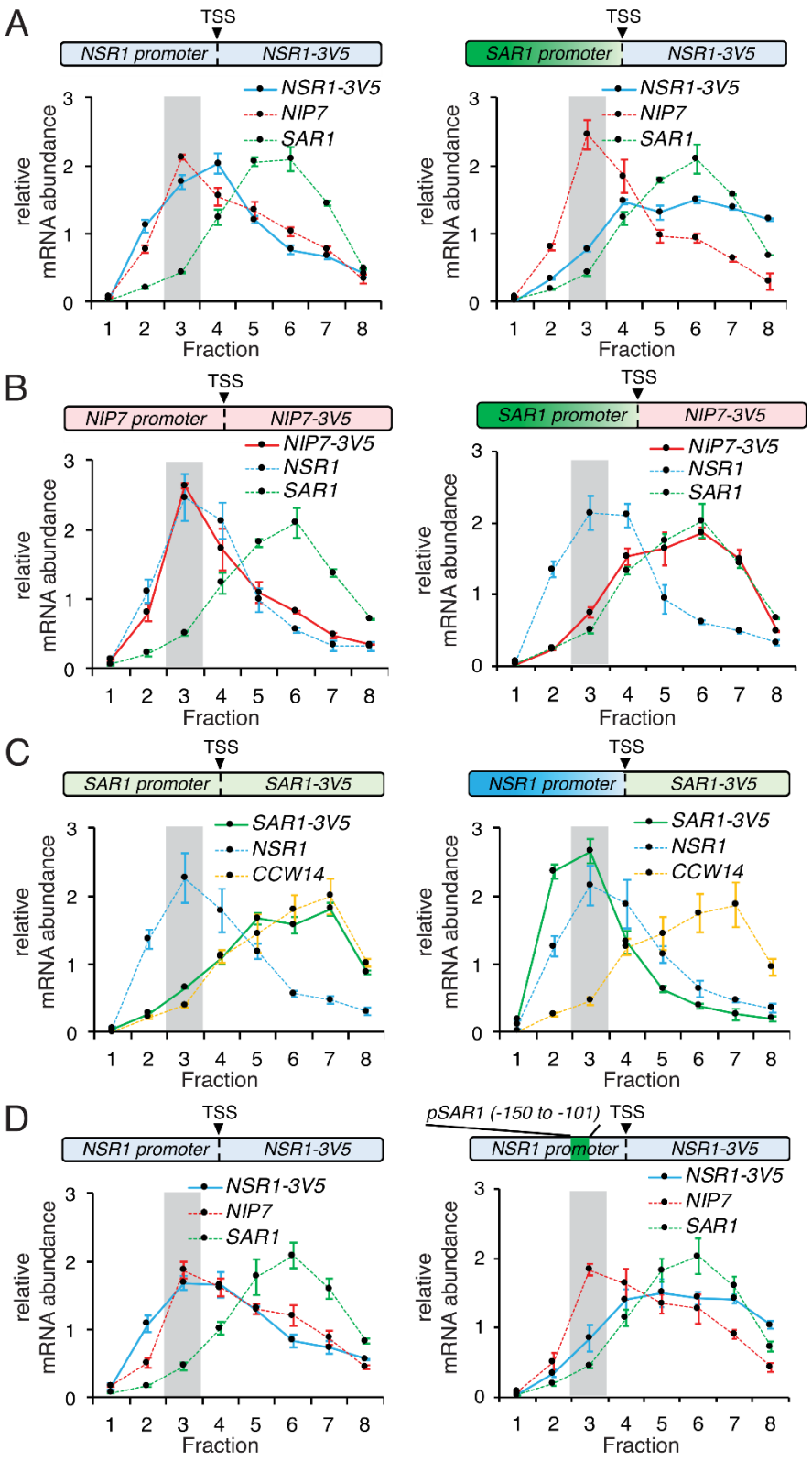

Figure 4.2: RiBi promoters are necessary and sufficient for their translational repression. A-D) RT-qPCR was used to quantify mRNAs in polysome fractions at 1 hour in SPO. Highlighted regions represent monosome/80S fractions. Error bars represent measurement variability as determined by three qPCR replicates. A)

Distribution of *WT NSR1* reporter mRNA (left) and the *NSR1* reporter under the *SAR1* promoter (right) in polysome gradients at 1 hour in SPO. B) Distribution of *WT* the *NIP7* reporter mRNA (left) and the *NIP7* reporter under the *SAR1* promoter (right) in polysome gradients at 1 hour in SPO. C) Distribution of the *WT SAR1* reporter mRNA (left) and the *SAR1* reporter under the *NSR1* promoter (right) in polysome gradients at 1 hour in SPO. D) Distribution of the *WT NSR1* reporter mRNA (left) and the *NSR1* reporter with its -150 to -101 promoter region swapped to the corresponding *SAR1* promoter sequence (right) in polysome gradients at 1 hour in SPO.

4.4.3 Cycloheximide treatment leads to context-dependent de-repression of RiBi mRNAs

The rapid decline in TE that we observed in meiotic cells was reminiscent of translational repression seen by the same ribosome profiling protocol applied to yeast cells that were transferred from rich media to media lacking amino acids (Ingolia et al., 2009a). In addition, we became aware that a similar type of time- interval-specific apparent translational repression was detected by another group during amino acid starvation and metabolic cycling in yeast, and that it appeared to be dependent on the translation inhibitor, CHX, due to a resultant increase in RiBi mRNAs (personal communication, Dan Santos; reported in accompanying study (Santos et al., 2019)). CHX is a chemical that is frequently used to pre-treat cells prior to harvesting for ribosome profiling (Ingolia et al., 2009a, 2012b). In our study, CHX pre-treatment occurs for less than 2 minutes prior to harvesting of cells by filtration and flash freezing in liquid nitrogen. CHX pre-treatment has been reported to affect the distribution of ribosome footprints within mRNAs but has been reported to have a minimal effect on gene-by-gene quantification in most contexts examined (Duncan and Mata, 2017; Duncan et al., 2018; Gerashchenko and Gladyshev, 2014; Hussmann et al., 2015; Ingolia et al., 2009b; Lareau et al., 2014; Requião et al., 2016). Because of this, and because harvesting with filtration without CHX pre-treatment results in loss of ribosomes from 5' regions of ORFs (Ingolia et al., 2009a), CHX is typically included in our protocols for harvesting cells for translation assays, including both ribosome profiling and polysome analyses. It seemed possible that this could explain the apparent translational repression that we observed.

Indeed, when we performed polysome analyses without CHX pre-treatment, we no longer observed a shift of *NSR1* and *NIP7* to the monosome/80S fraction at 1 hour in SPO (Figure 4.3A). We assayed *NSR1*, *NIP7*, and *SAR1* mRNA abundances by RT-qPCR at 15 minutes and 1 hour in SPO with and without CHX pre-treatment and found that the high level of all of these mRNAs seen at 15 minutes in SPO was unaffected by CHX (Figure 4.3B, S4A). The total level of *NSR1* and *NIP7* mRNA was much lower at 1 hour than at 15 minutes in SPO with or without CHX pre-treatment, but it was higher with CHX pre-treatment at 1 hour in SPO than without CHX pre-treatment, a result that was not seen for *SAR1* (Figure 4.3B, S4A) This change, while small in absolute terms, represented a 4- to 16-fold increase in *NIP7* and *NSR1*, respectively (Figure 4.3B, S4A). This is approximately the degree of TE shift that we measured by ribosome profiling for these genes at 1 hour in SPO (Figure 4.1C). Because TE is calculated by dividing the ribosome footprint RPKM (reads per kilobase million) by mRNA RPKM, and because CHX treatment inhibits new translation (Schneider-Poetsch et al., 2010; Siegel and Sisler, 1963), we concluded that the apparent translational effect that we

observed for RiBi genes at 1 hour in SPO (Figure 4.1E) was an artifact of the time-window-specific mRNA induction of these genes in response to translation inhibition by CHX. In support of this model, we observed a build-up of ribosome footprints at start codons of RiBi genes specifically at ~1 hour in SPO in an experiment in which CHX-pretreatment was used (Figure 4.S4B and C). This type of build-up has been previously observed more globally in ribosome profiling data collected from cells under stress conditions and has been reported to represent the fact that CHX inhibits post-initiation ribosomes (Gerashchenko and Gladyshev, 2014). CHX treatment does not prevent new translation initiation, but does prevent elongation, which results in a build-up of ribosomes at start codons. This effect can be seen to some extent under all conditions, but is most extreme in cases in which many ribosomes are free to re-initiate, which appears to be the case following acute stress conditions that results in general inhibition of new translation.

Because the TE effect that we observed early in meiosis was similar to that observed previously in amino acid-starved cells (Ingolia et al., 2009a), we next compared polysome fractions from vegetative cells grown in rich media (YPD) or shifted to media lacking amino acids (-AA), and observed a small but specific and reproducible CHX-dependent shift of *NSR1* to the monosome fraction (Figure 4.3C, 4.3D, and 4.S5A). As expected, much lower levels of ribosomes in polysome relative to monosome fractions was observed in cells shifted to media lacking amino acids (Figure 4.3C). The CHX- dependent shift to the monosome fraction of *NSR1* and *NIP7,* was modest compared to 1 hour in SPO (Figure 4.3A, D, and 4.S5A). Consistently, a much more subtle CHX-dependent mRNA increase was seen following amino acid starvation than the one that we observed at 1 hour in SPO (2.6-fold vs 17.3-fold for *NSR1*, 1.9-fold vs 4.8-fold for *NIP7*; Figure 4.3B, 4.S4A, 4.3E, and 4.S5B-D). Despite the reduced degree of the effect, the specific mechanism of this mRNA induction appeared to be similar in meiosis and under conditions of amino acid limitation, as the CHX-dependent fold-increase in mRNA seen after transfer to media lacking amino acids was substantially reduced in the *NSR1* reporter construct mutated for the -150 to -101 interval defined based on meiotic regulation (Figure 4.2D, 4.3E, and 4.S5B-D). The muted CHX-dependent fold increase in *NSR1* mRNA was because removal of this *NSR1* promoter region resulted in an increase in *NSR1* mRNA whether or not CHX pre-treatment was used for cell harvesting (Figure 4.3E and 4.S5B-D). This result suggested that the CHX-dependent mRNA increases that we observed could be a result of faulty RiBi repression at 1 hour in SPO and under amino acid deplete conditions.

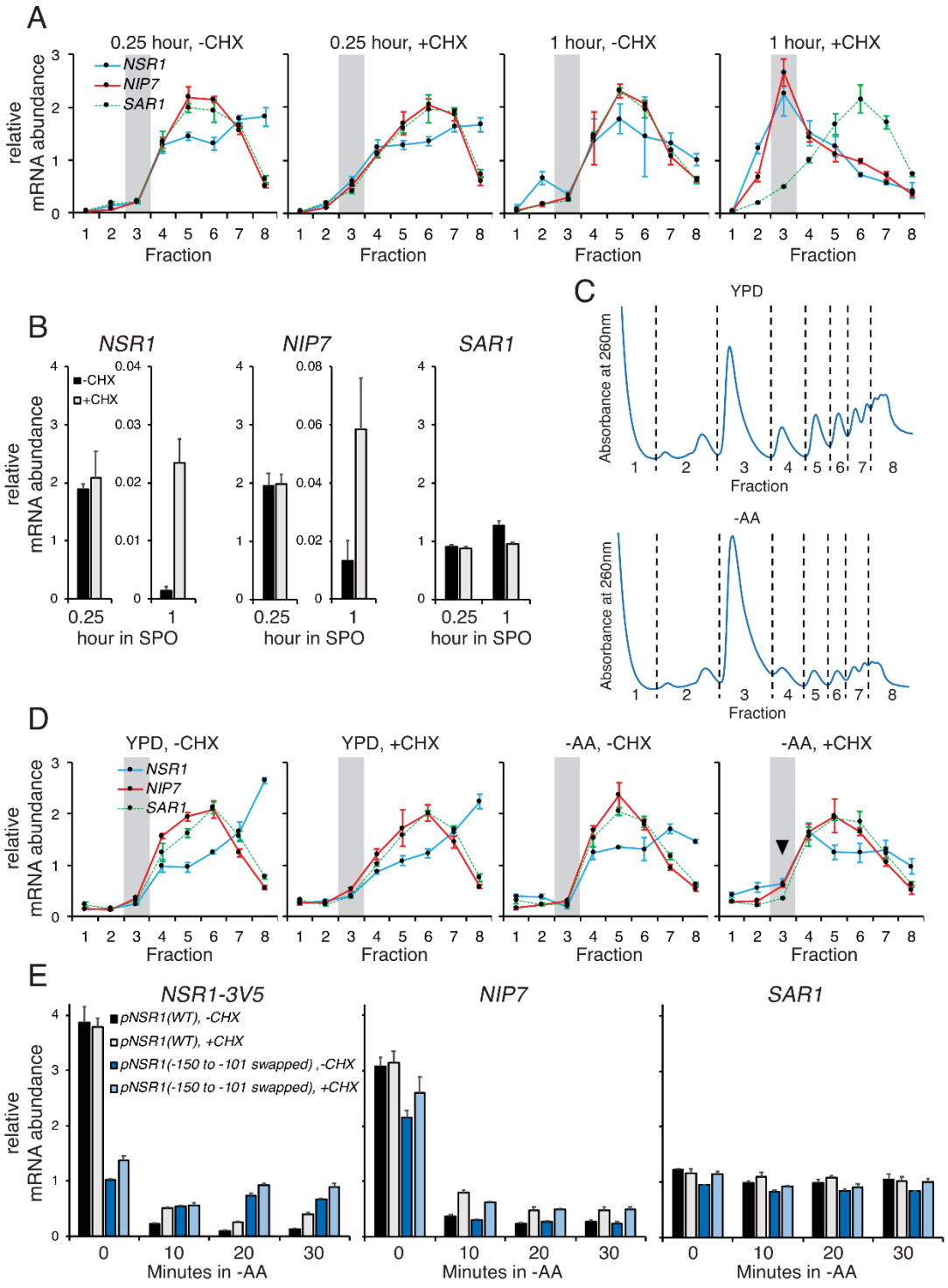

Figure 4.3: CHX treatment causes accumulation of RiBi transcripts, explaining the apparent translational repression at 1 hr in SPO. Throughout this figure, mRNA is quantified by RT-qPCR and error bars represent measurement variability as determined by three qPCR replicates. A) Distributions of RiBi mRNA (*NSR1* and *NIP7*) and non-RiBi mRNA (*SAR1*) in polysome gradients without or with CHX treatment at 0.25 hour or 1 hour in SPO. Highlighted region represents monosome/80S fraction. B) mRNA levels of *NSR1* (left), *NIP7* (middle), and *SAR1* (right) without or with 2-minute CHX treatment at 1 hour in SPO. C) Sucrose gradient absorbance

profiles of exponentially growing cells (OD_{600}0.6) in YPD (left) and after 20 minutes of amino acid starvation (right). D) Distributions of RiBi mRNAs (*NSR1* and *NIP7*) and a non-RiBi mRNA (*SAR1*) in polysome gradients without or with CHX treatment at 20 minutes in rich medium (YPD) or amino acid starvation (-AA). Highlighted region represents monosome/80S fraction and arrowhead emphasizes the reproducible difference observed in –AA conditions. E) mRNA levels of *NSR1* (left), *NIP7* (middle), and *SAR1* (right) in response to CHX treatment following amino acid starvation. The first timepoint (0 minute) was collected prior to the media switch from YPD. The CHX-dependent mRNA increase is greatly diminished in the *NSR1* reporter with its -150 to -101 promoter region swapped to the corresponding *SAR1* promoter sequence. Note that the increase in *NSR1* mRNA seen with CHX in –AA conditions is statistically significant (Student's t-test p-value 0.0014 at 20 minutes) when comparing to the biological replicate data in Figure 4.S5C. This difference is no longer significant in the -150 to -101 promoter mutant.

4.4.4 Loss of negative regulators of RiBi transcription, Dot6 and Tod6, ablates CHX-dependent RiBi de-repression

We previously noted that the -150 to -101 promoter region of *NSR1* contained binding sites for repressors Stb3, Dot6, and Tod6 (Figure 4.S3C). The lack of binding of a repressor in this region was consistent with the CHX-independent de-repression that was seen in our reporter experiments (Figure 4.3B, 4.3E, 4.S5B-D). While single deletions of *STB3, DOT6*, or *TOD6* in meiosis did not ablate the effect (Figure 4.S3D), amino acid-depleted conditions did not rely on the type of sensitive time window that was seen during meiosis and allowed us to assay double-mutants without confounding effects on meiotic entry that previously stymied our meiotic *dot6Δtod6Δ* experiment. We found that cells deleted for both *DOT6* and *TOD6* no longer showed a CHX-dependent shift away from polysomes or an increase in either *NSR1* or *NIP7* mRNA in media lacking amino acids, suggesting that the CHX-dependent mRNA increase in these RiBi genes is mediated through these two factors (Figure 4.4A, 4.S6A-D). Akin to the reporter experiment in which the -150 to -101 promoter region was deleted (Figure 4.3E), the loss of CHX-dependent mRNA increase is associated with an elevated absolute level of RiBi mRNA relative to wild-type cells without CHX-treatment, and these levels do not increase more in cells harvested with CHX (Figure 4.4A, 4.S6B-D). As in the meiotic experiments (Figure 4.S3D), mutation of *STB3* had no effect on the CHX-dependent regulation (Figure 4.4A, 4.S6B-D). Mutation of the consensus binding sites for *STB3, DOT6*, and *TOD6*, within the -150 to -101 interval, however, did not recapitulate this effect, suggesting that Dot6 and/or Tod6 may have additional cryptic binding sites in this region or they are recruited by another factor (Figure 4.S7A-D).

The known regulation of RiBi genes, which involves transcriptional activation and removal of transcriptional repression, along with the time-interval specificity of CHX-based mRNA induction during both meiotic and amino acid-starvation conditions and the low absolute levels of mRNAs for these genes seen during both of these time intervals (Figure 4.3B and E), suggested a possible mechanism for the effect that we observed. It seemed that the condition-specificity of this response might be based on whether RiBi transcriptional activation is occurring. If it is not, de-repression of transcription through Dot6 and Tod6 by a CHX-based mechanism could explain the modest absolute mRNA increases that resulted in large fold-change increases, and thus the measured TE decreases that we observed. We tested this hypothesis by treating cells in either rich media or under conditions of amino acid starvation with rapamycin, which inhibits activity of the Tor kinase (Heitman et al., 1991), a

major driver of RiBi transcriptional activation (Jorgensen et al., 2004; Powers and Walter, 1999). This treatment resulted in lower overall mRNA levels for RiBi genes *NSR1* and *NIP7* in rich (YPD) media (Figure 4.S8A), as expected. This also resulted in a robust CHX-dependent increase in mRNA levels under these conditions, which was not observed without Tor inhibition (Figure 4.S8A and B). A similar effect was not seen for non-RiBi gene *SAR1*. In the case of amino-acid-starved cells, rapamycin treatment resulted in a more modest decrease in the levels of mRNA without CHX treatment, consistent with lower Tor activity in these conditions (Cardenas et al., 1999), but a CHX-dependent mRNA level increase was still evident (Figure 4.S8A and B). We note that the CHX-dependent mRNA increase remained in the presence of rapamycin in the prototrophic strain background used for all of our experiments, but that this was not seen in the auxotrophic strain background used for the accompanying study (Santos et al., 2019). The reason for this difference is unclear, but is consistent with the finding from Santos et al. that auxotrophies can modify the CHX-dependent effect on RiBi mRNAs (Santos et al., 2019).

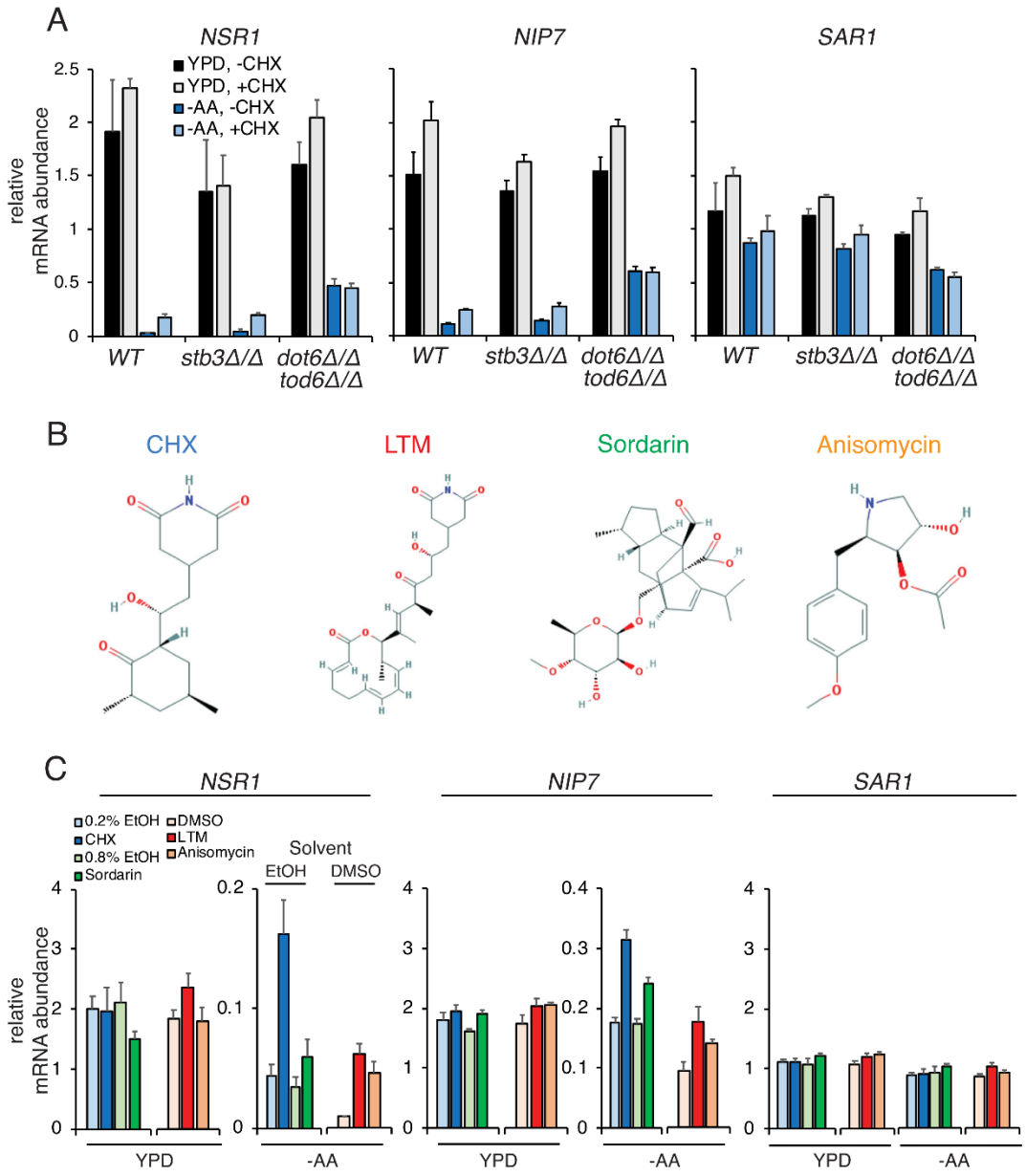

Figure 4.4: The increase of RiBi transcript levels in response to CHX is mediated by Dot6/Tod6 and is caused by translational inhibition. Throughout this figure, mRNA is quantified by RT-qPCR and error bars represent measurement variability as determined by three qPCR replicates. A) mRNA levels of *NSR1* (left), *NIP7* (middle), and *SAR1* (right) in response to CHX treatment. Deletion of *DOT6* and *TOD6* eliminates the CHX-induced accumulation of RiBi transcripts following amino acid starvation. Note that the increase in *NSR1* in –AA conditions with CHX is statistically significant (Student's t-test p-value 0.0331) when comparing to the biological replicate data in Figure 4.S6C. This difference is no longer significant in cells lacking *DOT6* and *TOD6.* B) The structures of the translation inhibitors used in panel C are shown, from NCBI PubChem. C) mRNA levels of *NSR1* (left), *NIP7* (middle), and *SAR1* (right) in response to CHX (100 µg/ml), LTM (10 µM), anisomycin (20 µM), and sordarin (100 µg/ml). Stock solutions of CHX and sordarin were prepared in ethanol (EtOH), and stock solutions of LTM and anisomycin were prepared in DMSO. Note that LTM, and anisomycin treatment together with their vehicle control (DMSO) was done in a separate experiment from sordarin and CHX treatment and their vehicle controls (EtOH). Also note that sordarin-based inhibition of cell growth is less complete than other drugs (Figure 4.S9).

4.4.5 RiBi mRNA de-repression is a response to inhibition of global translation

Our results to this point could be explained by two general models. By the first model, CHX results in de-repression of RiBi mRNA accumulation through Tod6 and Dot6 independent of its role in inhibiting translation. By the second model, it is inhibition of translation itself that causes RiBi mRNA accumulation. To distinguish between these possibilities, we treated cells grown in YPD and those starved for amino acids with three other drugs that rapidly inhibit translation: lactimidomycin (LTM), sordarin, and anisomycin ((Grollman, 1967; Justice et al., 1998; Schneider-Poetsch et al., 2010);(Figure 4.4B, 4.S9A, and 4.S9B)). CHX inhibits ribosome translocation through E-site binding (Garreau de Loubresse et al., 2014). LTM shows some structural similarity to CHX, but is larger, which causes its preferential binding to empty E-sites and thus preferential inhibition of the first ribosome translocation event on an mRNA. (Garreau de Loubresse et al., 2014) LTM is known to specifically inhibit translation initiation at 50 uM in mammalian cells, but we find that it inhibits both translation initiation and elongation at this concentration in yeast ((Lee et al., 2012); Figure 4.S10A). Sordarin inhibits translation elongation by inhibiting elongation factor 2 activity (Justice et al., 1998). Anisomycin has been reported to Anisomycin has been reported to partially inhibit translation elongation by binding at the peptidyl transfer center, but also results in a number of other cellular effects, including mitogen activated kinase pathway activation (Grollman, 1967; Barros et al., 1997; Mailliot et al., 2016). Importantly, sordarin and anisomycin have structures that are dissimilar from CHX (Figure 4.4B), and thus would be likely to have different off-target cellular effects. All drugs, however, resulted in an increase on *NSR1* mRNA abundance in conditions of amino acid starvation that were independent of their vehicle solvents (Figure 4.4C; 4.S10B-D, 4.S11A-D). Effects on *NIP7* abundance were similar to *NSR1* for CHX, LTM, and sordarin, but somewhat variable in the case of anisomycin for reasons that we do not yet understand. Nonetheless, these results suggested to us that condition-specific RiBi mRNA accumulation may represent a cellular response to poor translation rather than an artifact of treatment with CHX.

4.5 Discussion

Ribosome biogenesis is a conserved, critical, and extremely energy intensive process that is thus highly regulated (Warner, 1999). Hundreds of RiBi genes are coordinately transcriptionally controlled and constitute targets of all three RNA polymerases (Pols I, II, and III). Robust induction of protein-coding PolII RiBi target genes requires both activation of a gas pedal (Tor-activated binding of activating transcription factors) and release of a brake (Tor- or PKA-based removal of repressive RiBi promoter-bound factors Dot6, and Tod6). Our study shows that inhibition of translation results in an increase in RiBi mRNA accumulation that is modest in absolute quantity but represents a high fold change early in meiosis. The de-repression of mRNA seen with CHX and other translational inhibitors could, in principle, be due to de-repression of transcription of RiBi genes or inhibition of degradation or RiBi mRNAs. We strongly favor the former model for two reasons. First, the CHX-based RiBi gene mRNA accumulation is dependent on Dot6 and Tod6, which are known to bind to RiBi promoters and repress their transcription. Second, this mRNA accumulation requires an interval in the promoter of *NSR1* that is known to bind Tod6 and Dot6. The

accompanying paper (Santos et al., 2019) reports that CHX-dependent RiBi mRNA accumulation is also associated with nuclear to cytoplasmic shuttling of Dot6, Tod6, and Stb3, which also supports a model of transcriptional de-repression.

We were unable to assay the effects of *DOT6* and *TOD6* loss on RiBi transcript abundance at 1 hour in SPO because cells deleted for both of these genes could not efficiently complete meiosis (15% sporulation compared to 91% for WT cells). This defect suggests importance to RiBi transcriptional repression during meiosis, which is also consistent with the rapid and dramatic transcript regulation that naturally occurs as cells enter the meiotic program (Figure 4.1A, 4.S1A). Prior to transfer of budding yeast cells to SPO, cellular ribosome and translation levels are extremely low because pre-sporulation medium lacks a non-fermentable carbon source and added amino acids, and meiotic entry requires low PKA activity (Weidberg et al., 2016). SPO is at least as nutrient-poor pre-sporulation medium, yet within 30 minutes of transfer to SPO, ribosome and translation levels increase dramatically (Brar et al., 2012a), which is consistent with the rapid transcript induction of RiBi genes that we observe by 15 minutes in SPO (Figure 4.S1A) and the fact that Tor activity is required for meiotic entry (Weidberg et al., 2016). Why is this transcriptional burst so brief? Although ribosome synthesis is likely required for cells to translate the proteins needed for meiotic progression, the low nutrient conditions that are also necessary for meiosis to occur in yeast may mean that cells must carefully balance their ribosome number to retain resources to make other proteins. Consistently, the wave of early genes that are transcribed in meiosis, including *REC8*, rise concomitant with a drop in RiBi transcript levels (Figure 4.S1A). A related explanation invokes splicing regulation. Most transcripts in budding yeast are not spliced, but the spliced set is highly enriched for RP genes and meiotic genes. Because RP transcripts and meiotic transcripts compete for splicesome components (Munding et al., 2013; Venkataramanan et al., 2017), very early transcriptional induction followed repression of RiBi/RP gene transcription may be required for meiotic yeast cells to properly process many of the transcripts that drive early meiotic events. By either model, rapid RiBi gene induction in conditions that favor sporulation may have evolved to enable the increase in protein synthesis capacity that is needed for meiotic commitment, and the low RiBi transcript levels seen soon after may enable expression of transcripts required for meiotic progression and, for the purposes of our study, represent a sensitized condition in which CHX-dependent de-repression is unmasked.

An important lesson of our study is that rapid secondary cellular responses can result from inhibition of core gene expression machinery. We were alerted to investigate the RiBi-specific CHX-dependent effect by authors of the accompanying study (Santos et al., 2019). We were surprised to observe the same effect our context, due to both on the speed of our cell harvesting—within 2 minutes of CHX treatment— and the specificity of the effect in time and scale. CHX-dependent mRNA increases were only seen for a subset of genes, strongly enriched for RiBi function, and only for a period of less than 1 hour during the meiotic program, as discussed above. This effect is also observed following amino acid starvation of vegetatively growing cells. In both conditions, RiBi mRNA levels are low and this effect can be mimicked in cells grown in rich media in Tor-inhibited conditions, when RiBi mRNAs are also resultantly low. Interestingly, in meiosis, low RiBi mRNA levels do not appear sufficient

to see this response. *NSR1* mRNA levels, for example, are low during the meiotic divisions and the very low TE measurement that is the signature of this effect is not seen at this time, suggesting additional determinants that enable the effect to be observed. The rare conditions in which the CHX-dependent effect is seen and its isolation to specific gene subsets caused this artifact to appear to represent specific and temporally modulated translational control. This highlights a major challenge of measuring translation in vivo. Because translation is a dynamic process, ideal harvesting conditions should capture cells instantaneously. Unfortunately, no such conditions have been reported, to our knowledge. Flash freezing cells in the absence of CHX is one excellent alternative to CHX pretreatment, but because this requires a human to transfer cells from a filter membrane to liquid nitrogen, ribosomes would be expected to move at least several codons along mRNAs during the process, which might also result in specific artifacts, and does result in general loss of ribosome density from the 5' ends of ORFs. Confirmation of results from translation experiments using complementary harvesting conditions may be the best solution to avoid the type of prolonged data misinterpretation that was the basis for our study.

Does the unexpected artifact of our methodology offer insight into a real biological response? We argue that this is likely, based on the similarity of the response seen with treatment of cells by four different translation inhibitors. While these drugs all inhibit translation elongation, they do not share any particular structural feature and thus it does not seem likely that they would all share an off-target effect on RiBi mRNAs. Rather, these results are consistent with at least two biological models. First, it is possible that acute translational inhibition increases intracellular amino acid pools, which may mimic addition of nutrients and thus activate ribosome biogenesis through Tor activation. While this type of effect has been seen in mammalian cells treated with translation inhibitors (Beugnet et al., 2003) and consistent results exist in yeast (Urban et al., 2007), those experiments employed much longer inhibitor treatment times than ours (at least 30 minutes compared to less than 2 minutes), which may reveal downstream effects rather than the initial cellular response. Consistently, we did not find inhibition of Tor activity by rapamycin treatment to abolish CHX-dependent RiBi gene transcription in our prototrophic strain background. Alternatively, a feedback loop may exist in cells such that low or stalled translation leads to an increase in ribosome synthesis. Given the direct relationship between active ribosome number and cellular growth (Marr, 1991; Warner, 1999), it may not be surprising for such a failsafe to exist to enable synthesis of more ribosomes when a condition of reduced translation is encountered. It is possible, in fact, that one advantage of the evolution of dual RiBi gene regulation by gas pedals and brakes is that regulated brake release allows leaky ribosome production so that cells in poor nutrient conditions can maintain just enough translation to survive until conditions improve. It will be interesting to determine whether physiological conditions can be identified in which this type of regulation can be seen.

4.6 Acknowledgements

We thank Dan Santos and Jonathan Weissman for generous communication of results prior to publication. We thank Emily Powers and Tina Sing for helpful comments on this manuscript and all members of the Brar and Ünal lab for helpful project feedback.

4.7 Supplemental figures

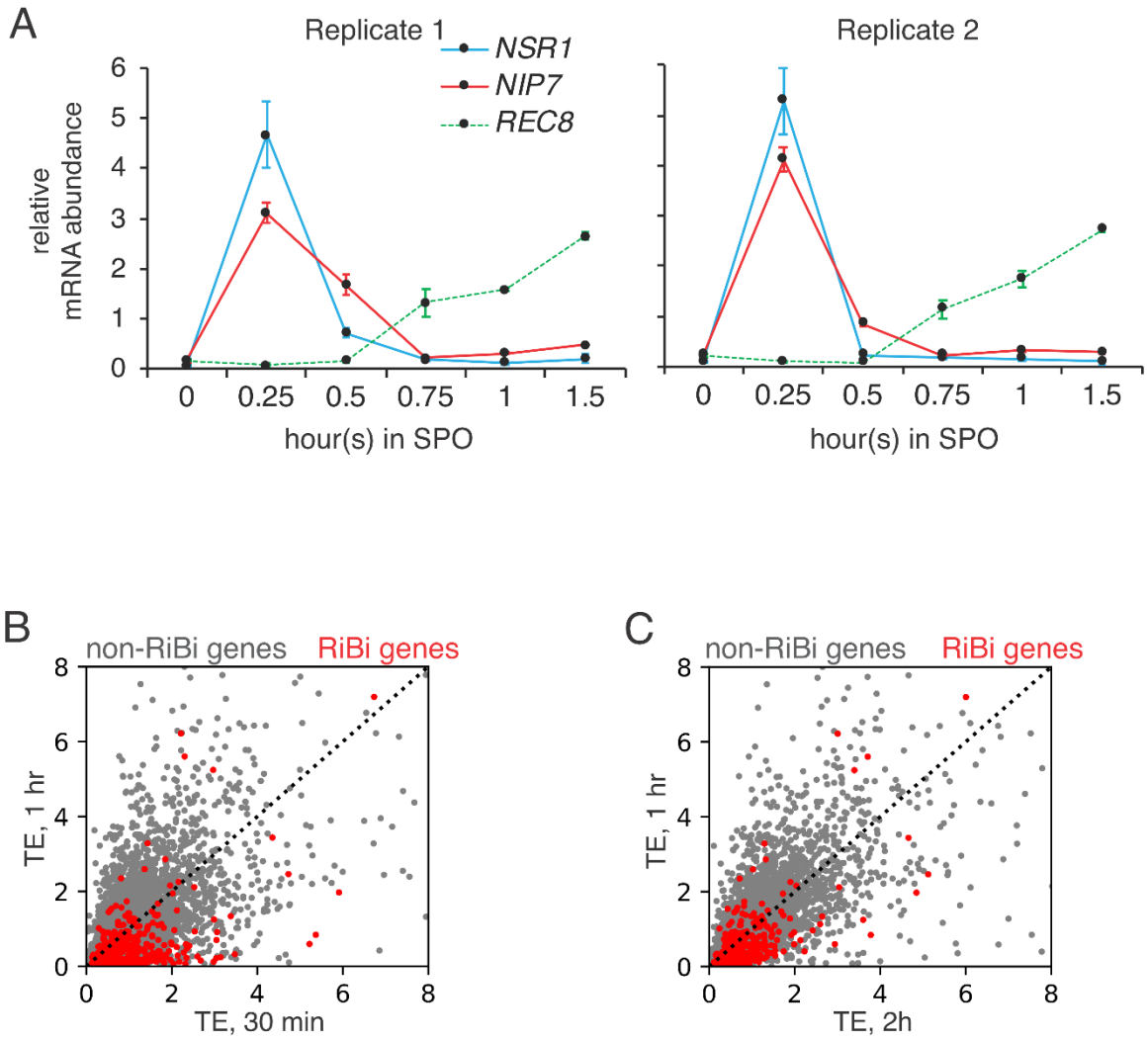

Figure 4.S1: RiBi gene expression is highly regulated early in the meiotic program. A) mRNA level changes of *NSR1* and *NIP7* in early meiosis. mRNA was quantified by RT-qPCR and error bars represent measurement variability as determined by three qPCR replicates.. *REC8* is an early meiotic gene; its expression indicates entry into meiosis. B) Scatter plot showing TE values at 30 min (x-axis) and 1 hour (y-axis) in SPO of RiBi genes (red dots) and non-RiBi genes (gray dots). C) Scatter plot showing TE values at 2 hour (x-axis) and 1 hour (y-axis) in SPO of RiBi genes (red dots) and non-RiBi genes (gray dots).

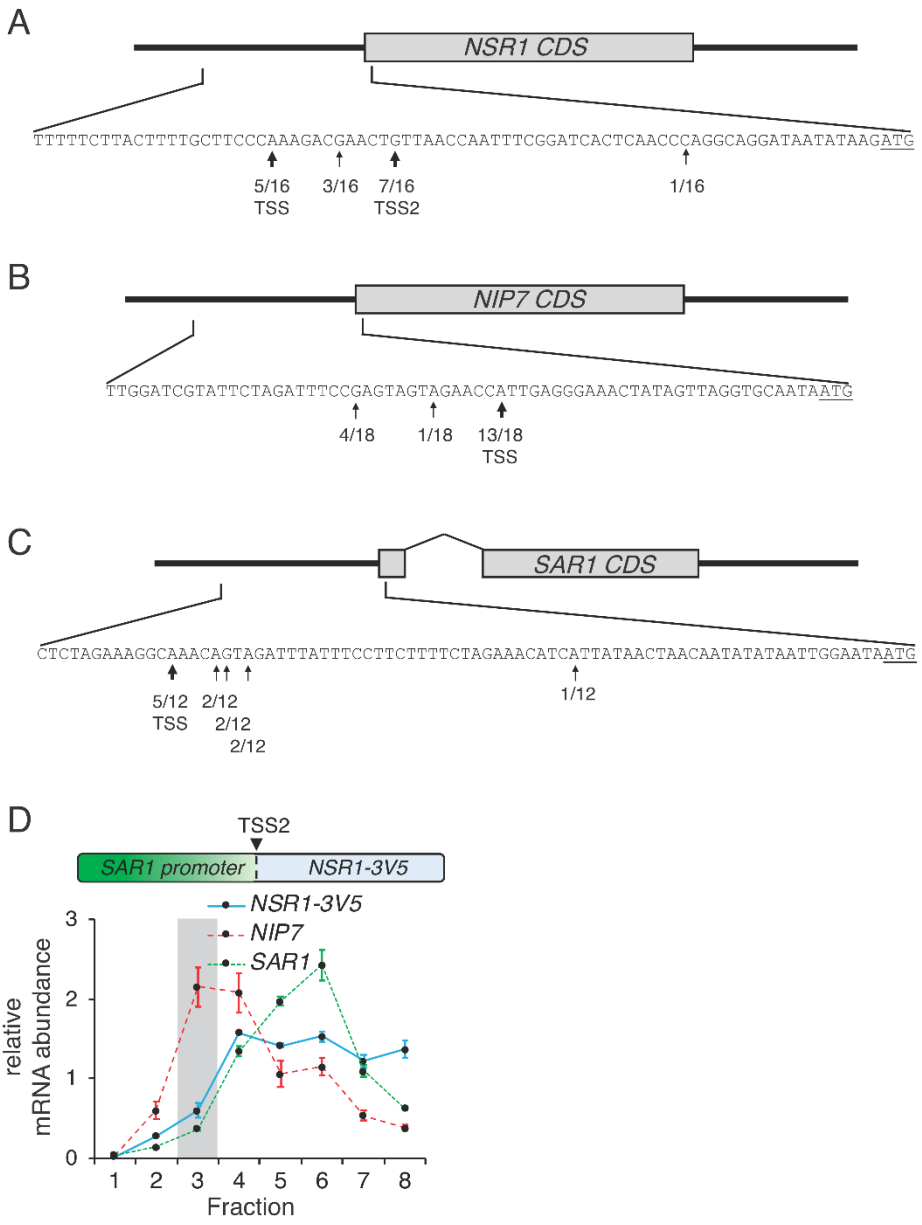

Figure 4.S2: Validation of TSSes for genes of interest by 5'RACE. Throughout this figure, mRNA was quantified by RT-qPCR and error bars represent measurement variability as determined by three qPCR replicates. A-C) Schematic diagrams of *NSR1*, *NIP7*, and *SAR1* genes. Arrows indicate ends of 5' RACE clones. X/Y means in Y total 5' RACE clones, X clones start from this position. The bigger arrows indicate the transcription start sites (TSSes) chosen for reporter analysis. D) Because two prominent TSSes were seen for *NSR1*, both were tested by reporter and yielded similar results. TSS1 was used for experiments throughout this manuscript, but we saw no difference when TSS2 was used instead. The polysome distribution of *pSAR1-NSR1* reporter using TSS2 indicated in panel A at 1 hour in SPO is shown here, compare to Figure 4.2A. Highlighted region represents monosome/80S fraction.

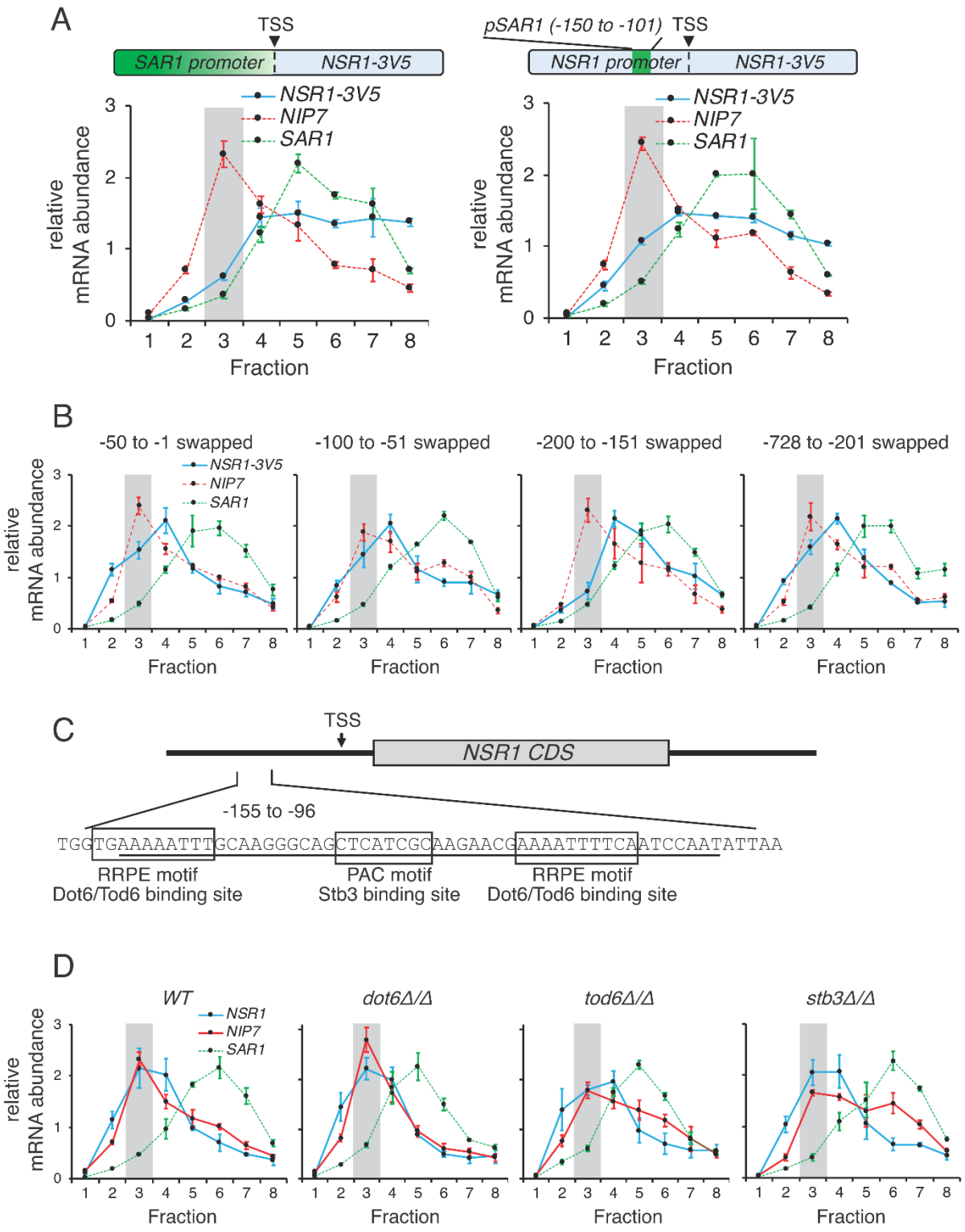

Figure 4.S3: Mapping of the *NSR1* promoter element responsible for its apparent translational repression. Throughout this figure, mRNA was quantified by RT-qPCR and error bars represent measurement variability as determined by three qPCR replicates. Highlighted regions represent monosome/80S fractions. A) Additional biological replicate

experiments of Figure 4.2A and 4.2D. B) Distribution of *NSR1* reporter with various regions swapped to *SAR1* promoter sequences in polysome gradients at 1 hour in SPO. C) Schematic diagram of the location of the Stb3 and Dot6/Tod6 binding sites in *NSR1* promoter. The sequence of the -155 to -96 upstream of transcription start site (TSS) is shown. The -150 to -101 region is underlined. The bindings sites are marked. D) Distributions of RiBi mRNA (*NSR1* and *NIP7*) and non-RiBi mRNA (*SAR1*) in *WT*, *dot6Δ/Δ, tod6Δ/Δ,* and *stb3Δ/Δ* cells in polysome gradients at 1 hour in SPO.

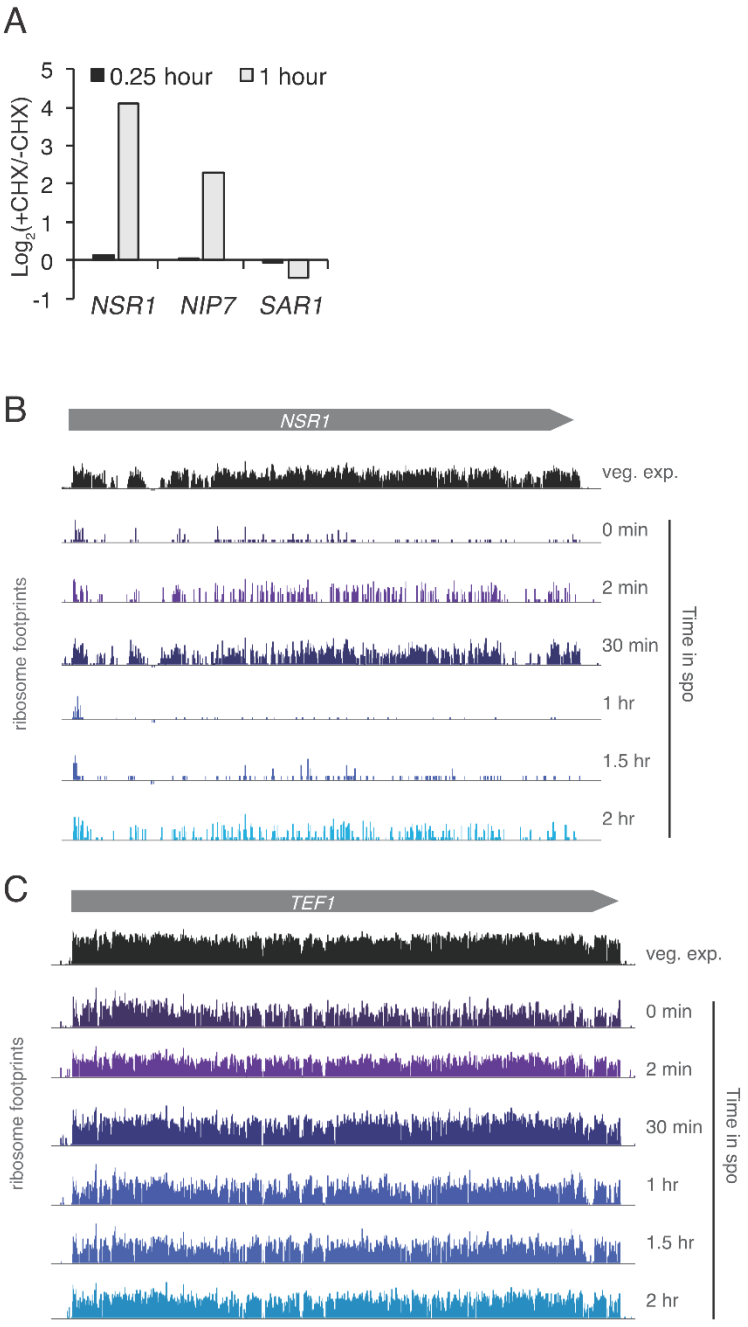

Figure 4.S4: RiBi apparent translational repression in meiosis is accompanied by a ribosome build-up at start codons. A) $\log_2$ values of mRNA of *NSR1* (left), *NIP7* (middle), and *SAR1* (right) without or with 2-minute CHX treatment at 1 hour in SPO. Data shown are matched to data in Figure 4.3B. B) Distributions of ribosome footprints on RiBi gene, *NSR1*, at timepoints following transfer to SPO. Note that the footprint build-up near the start codon at 1 hour in SPO. C) Distributions of ribosome footprints on non-RiBi gene, *TEF1*, at timepoints following transfer to SPO.

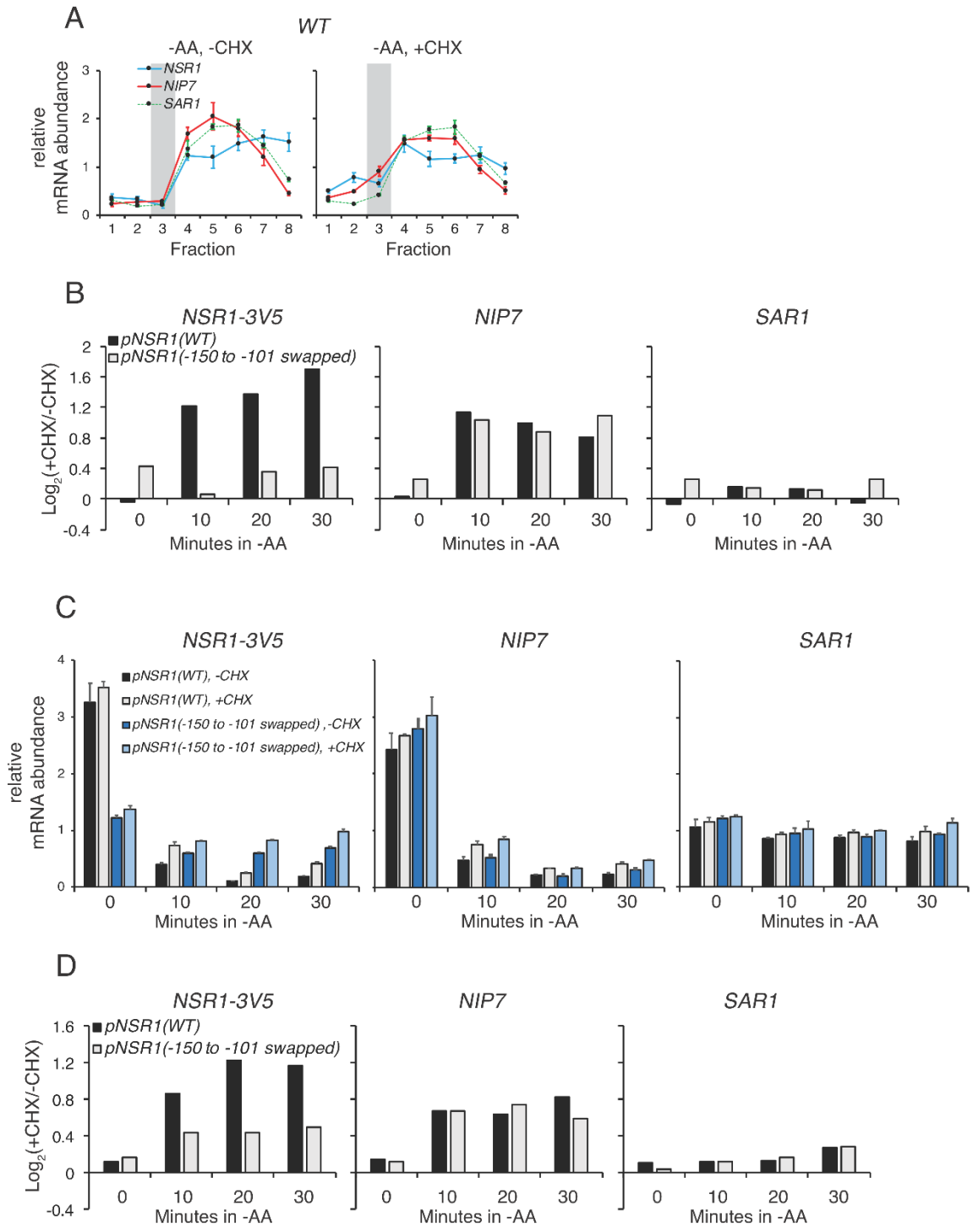

Figure 4.S5: Similar RiBi regulation is seen following amino acid starvation as at 1 hr in SPO. Throughout this figure, mRNA was quantified by RT-qPCR and the values represent the average of three qPCR replicates. Error bars represent measurement variability as determined by three qPCR replicates. A) Biological replicate experiment of Figure 4.3D. B) The same data as Figure 4.3E, but $\log_2$ values of mRNA ratios are plotted. C) and D) Biological replicate experiment of Figure 4.3E and 4.S5B.

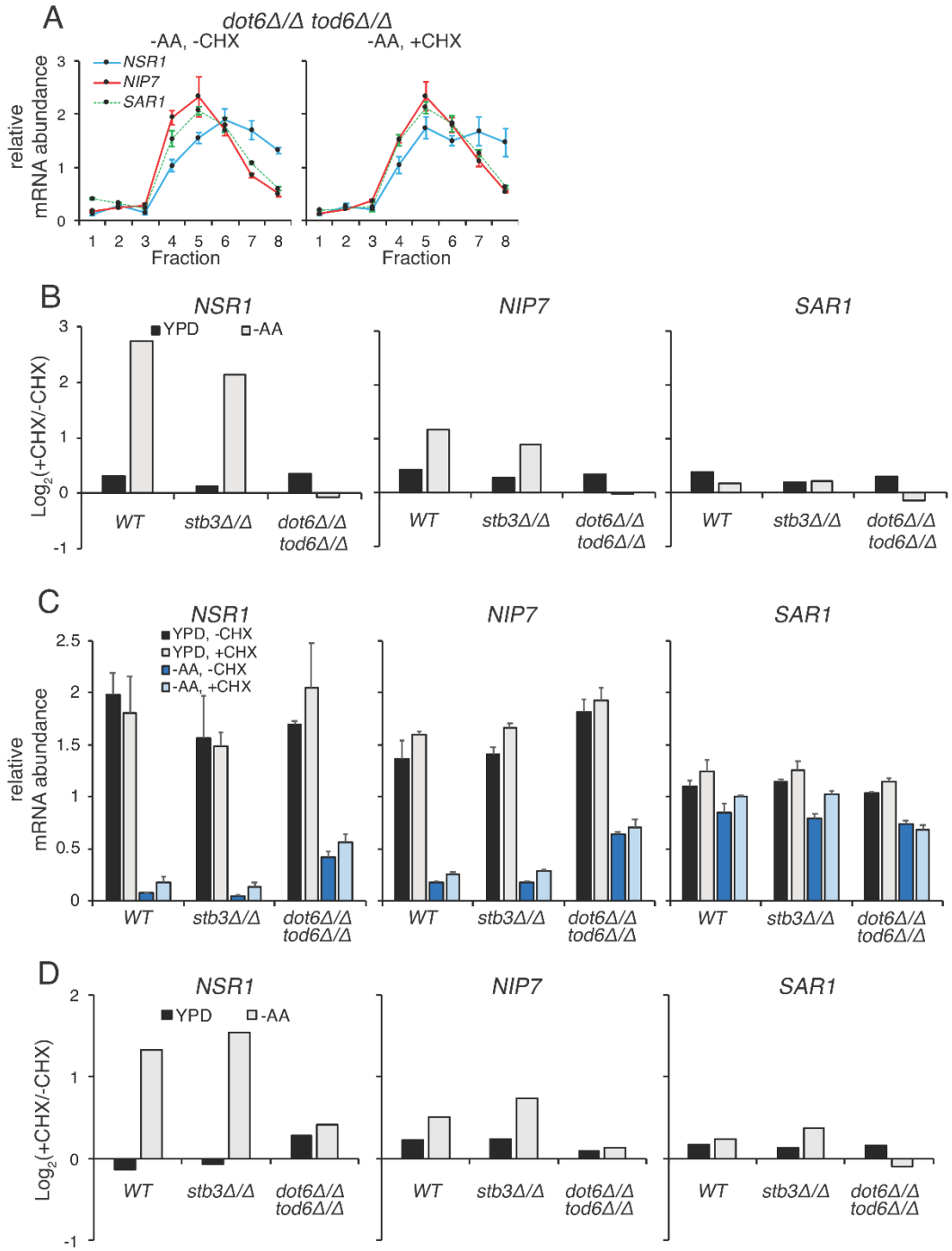

Figure 4.S6: Dot6/Tod6, but not Stb3, mediate CHX-dependent RiBi mRNA regulation. Throughout this figure, mRNA was quantified by RT-qPCR and the values represent the average of three qPCR replicates. Error bars represent measurement variability as determined by three qPCR replicates. A) Distributions of RiBi mRNA (*NSR1* and *NIP7*) and non-RiBi mRNA (*SAR1*) in *dot6Δ tod6Δ* cells in polysome gradients at 20 minutes in amino acid starvation. Highlighted region represents monosome/80S fraction. B) The same data as

Figure 4.4A, but $\log_2$ values of mRNA ratios are plotted. C) and D) Biological replicate experiment of Figure 4.4A and 4.S6B.

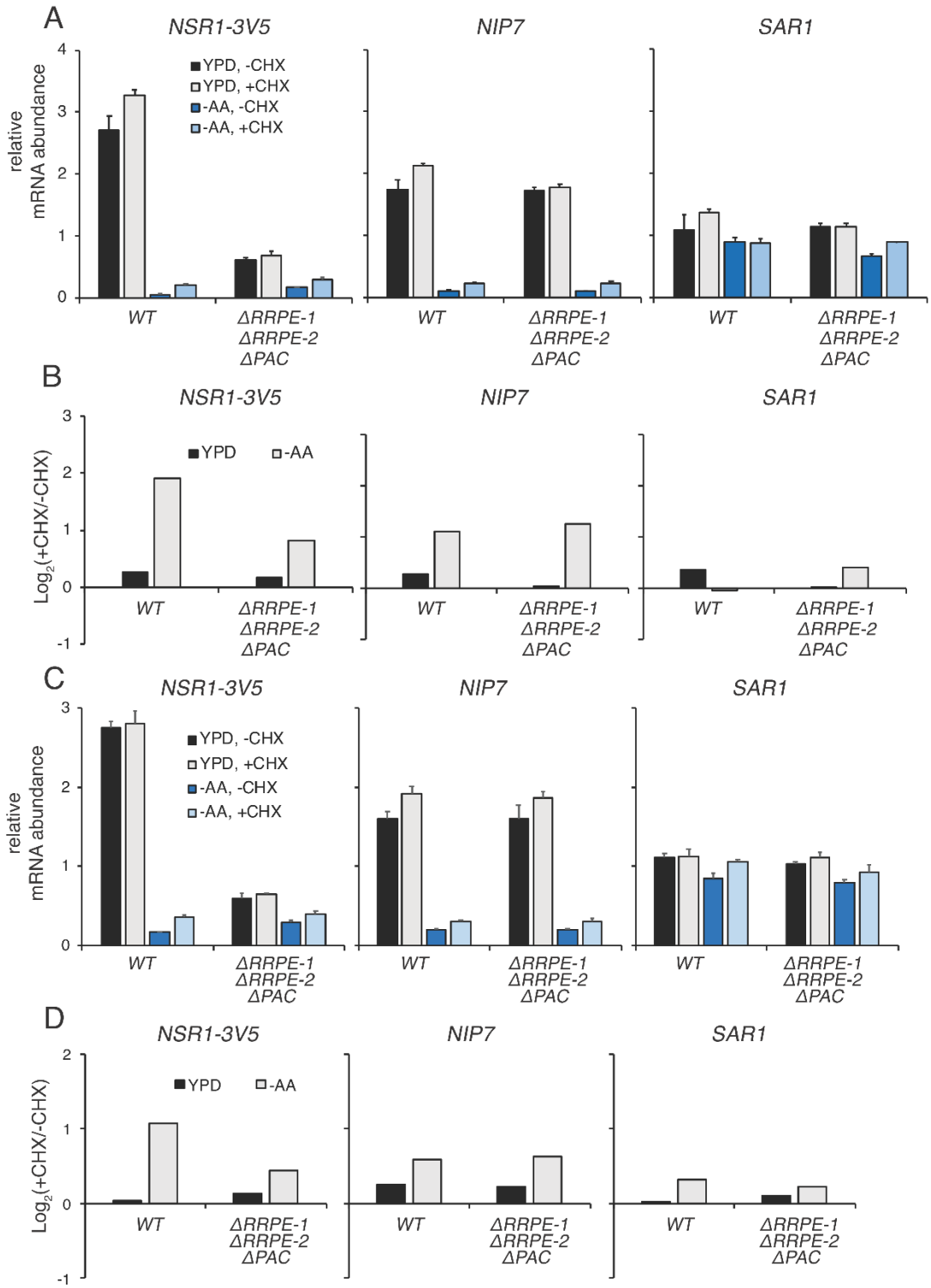

Figure 4.S7: Known Dot6/Tod6 and Stb3 binding sites cannot explain CHX-dependent RiBi mRNA increase seen upon amino acid starvation. Throughout this figure, mRNA was quantified by RT-qPCR and the values represent the average of three qPCR replicates. Error bars represent measurement variability as determined by three qPCR replicates. A) mRNA

levels of *NSR1* (left), *NIP7* (middle), and *SAR1* (right) in response to CHX treatment. Mutating all three binding sites shown in Figure 4.S3C does not eliminate this regulation. B) The same data as S7A, but $\log_2$ values of mRNA ratios are plotted. C) and D) Biological replicate experiment of Figure 4.S7A and B.

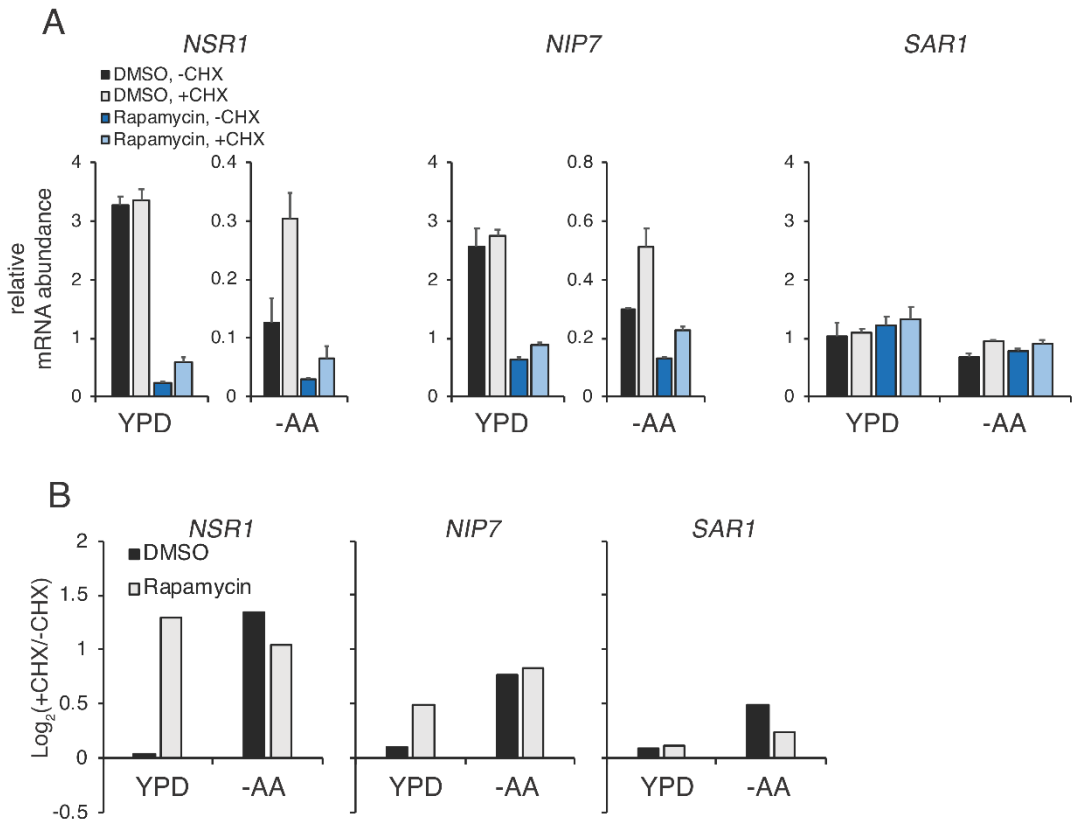

Figure 4.S8: Inhibition of Tor reveals CHX-dependent RiBi mRNA increases in rich media. A) mRNA levels of *NSR1* (left), *NIP7* (middle), and *SAR1* (right) following TOR inhibition by rapamycin addition 10 minutes prior to CHX addition. mRNA was quantified by RT-qPCR and the values represent the average of three qPCR replicates. Error bars represent measurement variability as determined by three qPCR replicates. B) The same data as S7A, but $\log_2$ values of mRNA ratios are plotted.

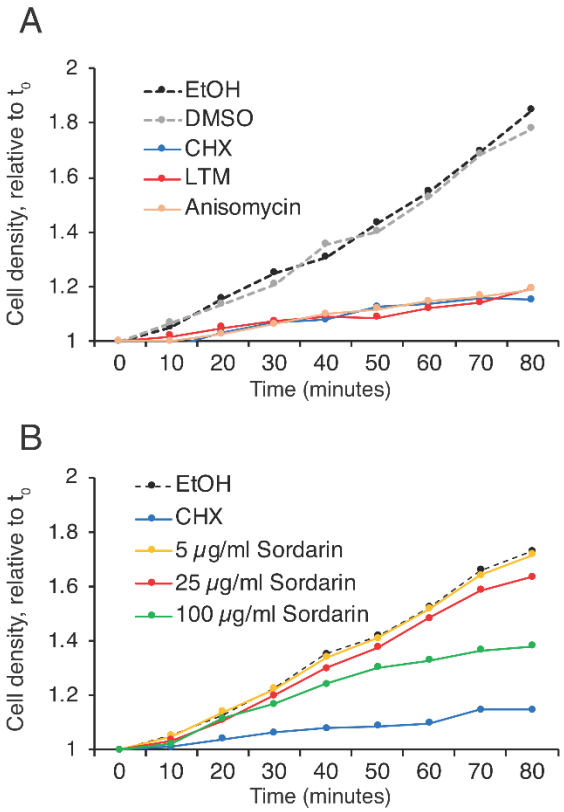

Figure 4.S9: Translation elongation inhibiters, CHX, LTM, anisomycin, and sordarin repress growth under our experimental conditions. A) Growth curve of cells treated with 0.2% EtOH, 100 µg/ml CHX, 0.25% DMSO, 10 µM LTM, and 20 µM anisomycin in YPD media. B) Growth curve of cells treated with 0.8% EtOH, 100 µg/ml CHX, 5 µg/ml sordarin, 25 µg/ml sordarin, and 100 µg/ml sordarin in YPD media. Note that we were not able to achieve inhibition of cell growth with sordarin that was equivalent to that seen with the other translation inhibitors for reasons that we cannot explain.

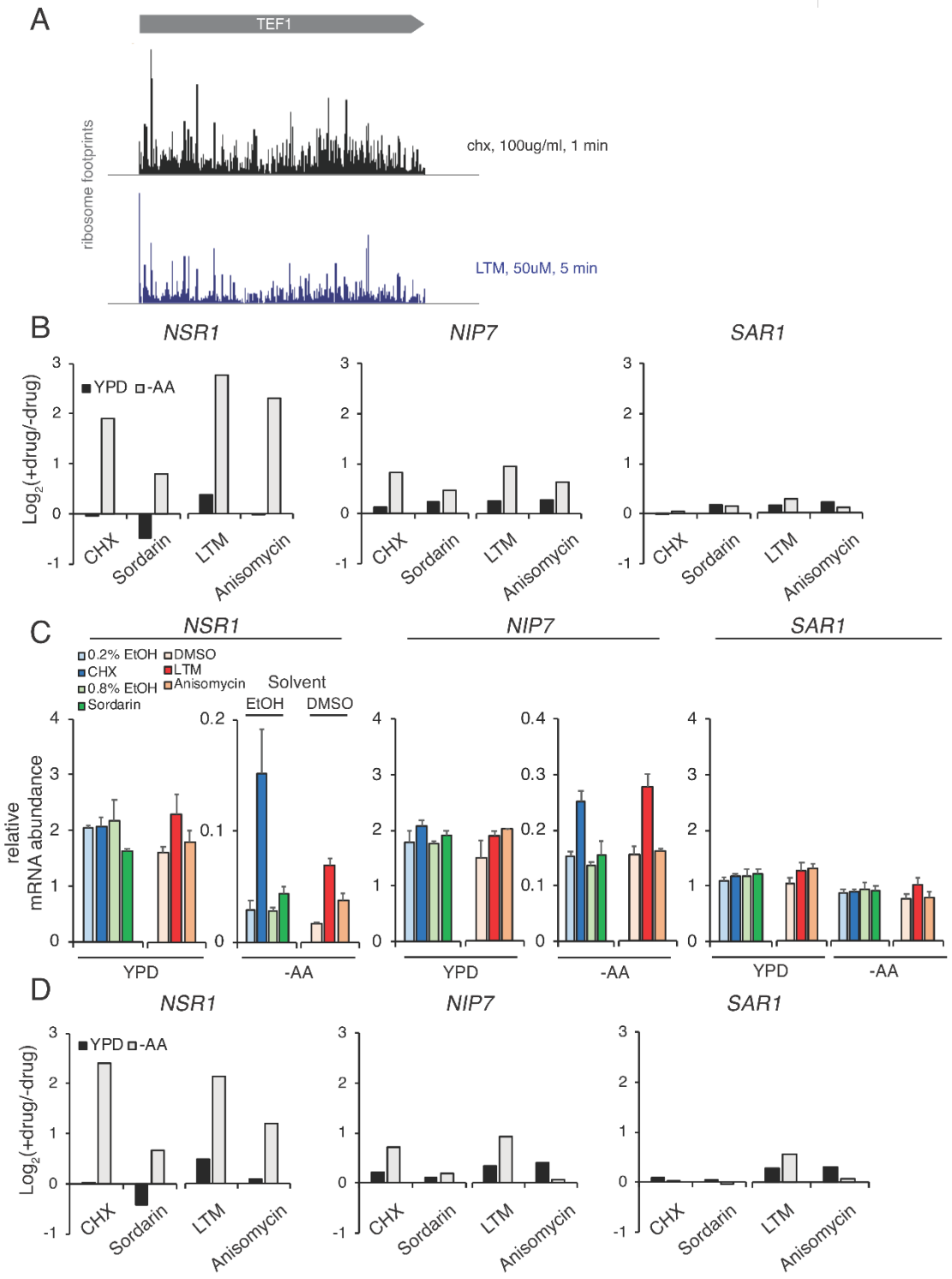

Figure 4.S10: Translation elongation inhibition by drugs other than CHX also results in condition-specific RiBi mRNA increases. Throughout this figure, mRNA is quantified by RT-qPCR and the values represent the average of three qPCR replicates. Error bars represent measurement variability as determined by three qPCR replicates. Note that LTM, and

anisomycin treatments together with their vehicle control (DMSO) was done in a separate experiment from sordarin and CHX treatment and their vehicle controls (EtOH) A) Distributions of ribosome footprints on *TEF1* in CHX-treated (top) and LTM-treated (bottom) cells. Note that there are many ribosome footprints in the body of the gene in the LTM-treated sample, indicating that LTM is al inhibiting translation elongation under these conditions. B) The same data as Figure 4.4C, but $\log_2$ values of mRNA ratios are plotted. C) and D) Additional biological replicate experiment for Figure 4.4C and Figure 4.S10B.

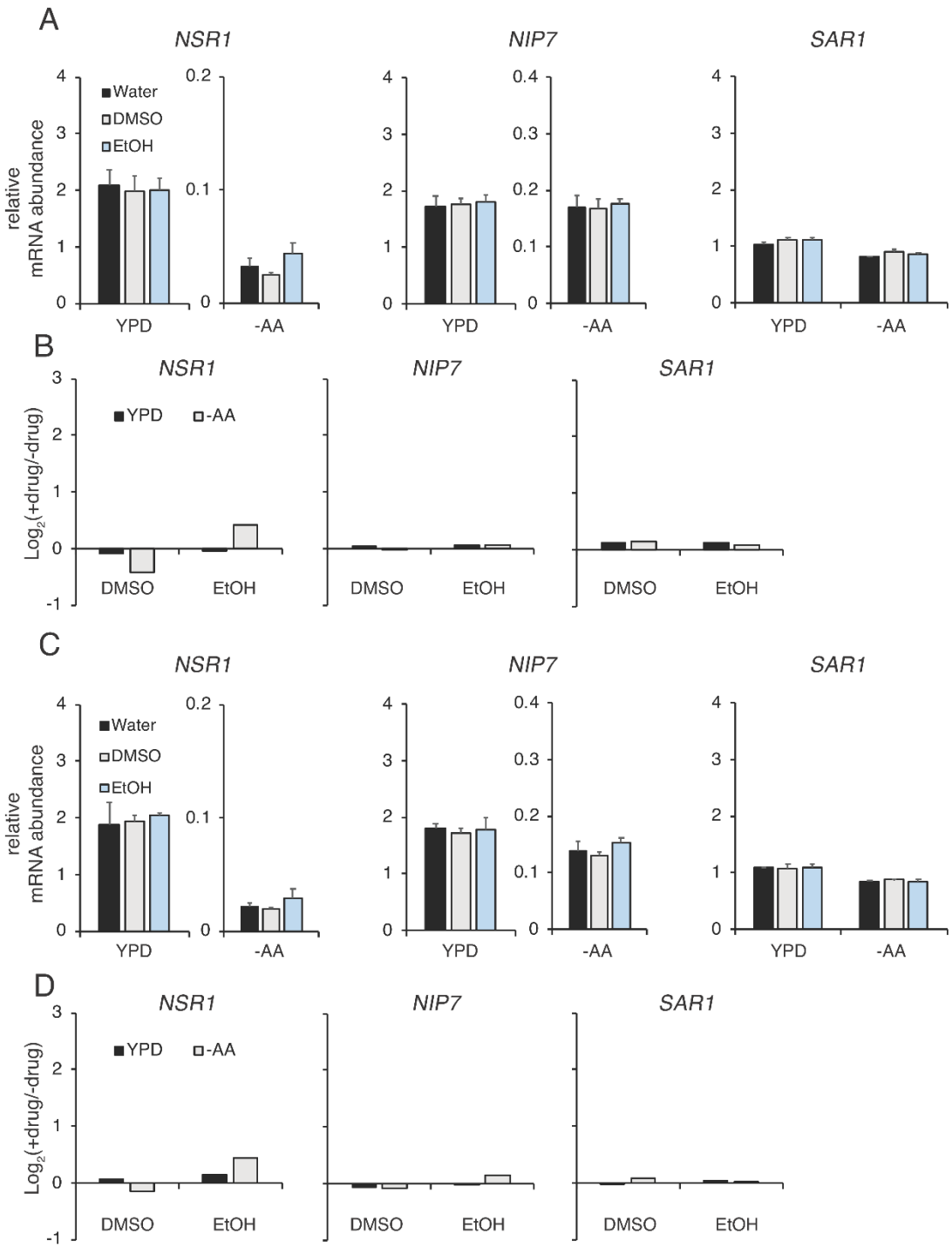

Figure 4.S11: Ethanol and DMSO do not induce condition-specific RiBi mRNA increases under our experimental conditions. A) mRNA levels of NSR1 (left), NIP7 (middle), and SAR1 (right) in response to 0.2% water, 0.2% EtOH, and 0.25% DMSO treatment. B) The same data as Figure 4.S11A, but log2 values of mRNA ratios are plotted. C) and D) Biological replicate experiment for Figure 4.S11A and B.

CHAPTER 5

Conclusions and Future Directions

The control of gene expression is critical for life, and the change in any one of the steps in the gene expression pathway may lead to changes in the final output of gene expression, which is the protein level. In some cases, living systems regulate multiple gene expression steps to achieve precise control of protein levels. Thus, it is important to obtain a comprehensive view of gene expression changes that happen on multiple levels in order to fully understand how gene expression is regulated. In our research, we use RNA-seq, ribosome profiling, and quantitative mass spectrometry to measure three key components in the gene expression process – mRNA abundance, translation, and protein abundance. The datasets generated by these techniques allow us to systematically dissect the changes in each key step, and by combining with other molecular biology tools, we present three studies that investigate the integrated regulation of gene expression in different conditions.

5.1 Towards deep understanding of ribosomal-deficiency-induced gene expression changes

In chapter 2, we probed the gene expression changes induced by ribosomal deficiencies genome-wide and found both gene-specific and ribosomal-dose-dependent gene expression changes at transcriptome, translatome, and proteasome levels. With our dataset, we were able to test three current hypotheses regarding human ribosomal deficiencies associated diseases and we found evidence for all of these models. Additionally, we report that growth-rate-matched 40S and 60S mutants show distinct gene expression patterns and ribosomal proteins are post-translationally regulated which results in the degradation of extra 40S subunits in sick 60S mutants.

In our study, the cells were grown under rich growth medium at optimal temperature and it is possible that certain specialized ribosome effects only exist under non-optimal conditions. It would thus be interesting to repeat our experiments under other growth conditions. One possible way to quickly screen for ribosomal protein candidates that may play condition-dependent role is to compare the degree of growth defect under different conditions, such as changes in temperature or cellular state. If a ribosomal protein mutant specifically shows severe growth defect under one condition but not others, it indicates specialized role of this ribosomal protein and further characterization by our systematic approach would be highly promising. Once a ribosomal protein is determined as a candidate to have a specialized role, selective ribosome profiling that specifically detects mRNAs that are translated by ribosomes containing this ribosomal protein may provide further information about the translational role of this ribosomal protein (Becker et al., 2013; Jan et al., 2014; Oh et al., 2011; Shi et al., 2017).

Our analysis was done using constitutive ribosomal protein mutants and in such mutants, secondary changes happen and may obscure the detection of direct translational effects. Conditional and rapid depletion of proteins is feasible in budding yeast using tools such as the auxin-inducible degron (AID) system (Nishimura and Kanemaki, 2014). Future studies

may use this technique to generate conditional ribosomal protein mutants and directly ask how translational pattern changes after the acute depletion of a ribosomal protein. The reversibility of AID system also allows the comparison between the translational patterns before, during, and after the conditional depletion. If a translational change is observed only during the depletion but not after the recovery of the protein level of a certain ribosomal protein, it strongly suggests a direct role of either this ribosomal protein, or the change of total functional ribosomal number caused by loss of this ribosomal protein, on this translational change.

Another general open question from our study is the degree of conservation of cellular response to ribosomal deficiency in yeast and human. We performed our analysis using buddying yeast as a model system due to the biochemical and genetic advantages of yeast, high conservation of the ribosome, as well as the previous finding that the growth rate of yeast under rich condition is proportional to the total ribosome number. We observed similar evidence supporting the ribosome concentration hypothesis as a study using human cell culture (Khajuria et al., 2018). Our analysis suggests specialized role of Rps25 in our yeast system, and Rps25 has been shown to have a specialized function in IRES translation of viral and human mRNAs (Hertz et al., 2013; Landry et al., 2009). These correlations suggest common properties of ribosomal deficiency associated gene expression regulation between yeast and human, likely due to homology of yeast and human ribosomal proteins as well as highly conserved basic translation mechanisms. Thus, our systematic analysis is likely to provide valuable information for understanding the fundamental mechanisms of ribosomal deficiency induced gene expression changes. It would still be interesting to perform a similar systematic study using human cell culture system, and including both known ribosomopathy-associated mutants as well as mutants that are not disease-associated would provide insights to the understanding of pathology of ribosomopathies.

5.2 The implications of LUTI-based regulation

In chapter 3, we focus on a novel regulatory mechanisms in meiotic yeast cells. We report that the switching between the long undecoded transcript isoform (LUTI) and the canonical transcript isoform determines the outcome of gene expression for 380 genes in budding yeast meiosis. The combination of canonical transcription and LUTI mechanism allows a single transcription activator to activate a set of target genes by inducing the synthesis of canonical transcripts, as well as to repress another set of target genes by activating the transcription of LUTIs. We propose that this regulatory mechanism enables differentiating cells to coordinate the activation of genes that are required for the current stage and the silencing of the genes that are used in the past stages.

We performed our study in buddying yeast meiosis because of the large amount of gene regulatory events in meiosis and the previous understanding of yeast meiotic transcription factors and functional genes. Another study in our lab revealed expression of LUTIs during ER stress (Dalfsen et al., 2018). Further studies may expand the analysis to other biological processes in yeast. Dynamic and coordinated regulation of gene expression is essential for any differentiation and development program, and the basic regulatory components of the LUTI mechanism, such as the presence of distal promoters, chromatin modifications, and

uORF-mediated translational repression, are not unique to yeast. Thus, there is no reason to believe that the LUTI mechanism only exists in yeast. Additionally, higher eukaryotes display more complex transcriptome due to the prevalent use of alternative splicing, which potentially may also lead to LUTI effect by altering the 5' UTR (Modrek and Lee, 2002). And a recent study from our lab identified features of LUTI regulation to be used for regulating the oncogene *MDM2* in human cells. Therefore the future investigation of LUTI-based regulation in higher eukaryotes is highly promising and may reveal regulatory events that have been ignored or misinterpreted by previous mRNA-abundance-based research.

In our systematic annotation of LUTIs, we started with genes that contain AUG-uORFs, which is a well-known translation inhibitory element, however, other repressive mRNA elements may also serve to block productive translation of the long transcript. Thus, it is likely that LUTIs using other translational repressive mechanisms exist in yeast or in other eukaryotes and investigation of them will be an important future direction. Another unexplored direction is the possibility that the long transcripts may have better translatability than the short one under certain conditions. Studies in various species have shown uORFs can become permissive for the translation of the downstream ORF when phosphorylation of eukaryotic initiation factor-2 (eIF2) occurs (Hinnebusch, 2005; Vattem and Wek, 2004). Additionally, internal ribosomal entry sites (IRESs) enable cap-independent translation inhibition, which may yield higher translation activity than the canonical cap-dependent initiation under certain circumstances (Hellen and Sarnow, 2001). If the long transcript isoform contains these elements and the short transcript isoform does not, the long isoform may be translated more efficiently and in this case, transcript switching still determines the outcome, however, the transcription activator that induces the long isoform actually activates the gene expression, instead of playing repressive role in the LUTI mechanism that we describe in chapter 3.

5.3 Uncovering artifacts in translation efficiency assays

Lastly, we investigated the regulation of RiBi genes in yeast under poor nutritional conditions. We report that RiBi genes are transcriptionally repressed at least partially through Tod6/Dot6 under amino acid starvation and in early meiosis. Upon global inhibition of translation, RiBi genes are rapidly de-repressed and RiBi mRNA levels increase. The translational repression of RiBi genes under amino acid starvation has been previously reported (Ingolia et al., 2009). We show that the apparent translational repression is due to the use of the translation inhibitor cycloheximide (CHX) in translation assays, such as ribosome profiling and polysome profiling. CHX induces de-repression of RiBi genes and the newly synthesized RiBi mRNAs cannot be efficiently translated in the presence of CHX, which leads to apparent low translation efficiency.

Since translation is a highly dynamic process, harvesting biological samples for ribosome profiling without global inhibition of translation is often infeasible and leads to loss of footprints at 5' end of ORFs. CHX is thus commonly applied to biological samples during cell harvesting step of ribosome profiling assay in order to immobilize ribosomes and keep physiological translation events unaffected by the sample preparation (Ingolia et al., 2012). To minimize variation, samples for RNA-seq are often collected together with ribosome

profiling samples, which means RNA-seq samples are also CHX-treated and any CHX-induced or global translation inhibition induced mRNA level changes will appear in the RNA-seq data. We report that RiBi genes show mRNA increase upon global inhibition of translation under amino acid starvation and at 1 hour in sporulation condition, however, it is unclear whether RiBi genes are the only group of genes responsive for global translation inhibition or additional genes are also up- or down-regulated. Comparing mRNA abundance changes by performing RNA-seq with and without CHX treatment may answer this question. CHX-induced response may exist under other conditions and, theoretically, they may lead to translation efficiency artifacts as well. Future studies using ribosome profiling and RNA-seq should consider potential CHX effect on the calculation of translation efficiency and carefully confirm the translation control events that they study are real by performing control experiments without the addition of CHX. It would also be interesting to determine whether any physiological conditions exist in which the CHX-dependent mechanism that we defined is naturally used for regulation of RiBi genes.

References

Aanes, H., Østrup, O., Andersen, I.S., Moen, L.F., Mathavan, S., Collas, P., and Alestrom, P. (2013). Differential transcript isoform usage pre- and post-zygotic genome activation in zebrafish. BMC Genomics 14, 331.

Abovich, N., Gritz, L., Tung, L., and Rosbash, M. (1985). Effect of RP51 gene dosage alterations on ribosome synthesis in Saccharomyces cerevisiae. Mol. Cell. Biol. 5, 3429–3435.

Andrews, S., Snowflack, D.R., Clark, I.E., and Gavis, E.R. (2011). Multiple mechanisms collaborate to repress nanos translation in the Drosophila ovary and embryo. RNA 17, 967–977.

Babiano, R., and de la Cruz, J. (2010). Ribosomal protein L35 is required for 27SB pre-rRNA processing in Saccharomyces cerevisiae. Nucleic Acids Research 38, 5177–5192.

Badis, G., Chan, E.T., van Bakel, H., Pena-Castillo, L., Tillo, D., Tsui, K., Carlson, C.D., Gossett, A.J., Hasinoff, M.J., Warren, C.L., et al. (2008). A library of yeast transcription factor motifs reveals a widespread function for Rsc3 in targeting nucleosome exclusion at promoters. Mol. Cell 32, 878–887.

Ban, N., Beckmann, R., Cate, J.H.D., Dinman, J.D., Dragon, F., Ellis, S.R., Lafontaine, D.L.J., Lindahl, L., Liljas, A., Lipton, J.M., et al. (2014). A new system for naming ribosomal proteins. Curr. Opin. Struct. Biol. 24, 165–169.

Barros, L.F., Young, M., Saklatvala, J., and Baldwin, S.A. (1997). Evidence of two mechanisms for the activation of the glucose transporter GLUT1 by anisomycin: p38(MAP kinase) activation and protein synthesis inhibition in mammalian cells. J. Physiol. (Lond.) 504 (Pt 3), 517–525.

Bazzini, A.A., Lee, M.T., and Giraldez, A.J. (2012). Ribosome Profiling Shows That miR-430 Reduces Translation Before Causing mRNA Decay in Zebrafish. Science 336, 233–237.

Becker, A.H., Oh, E., Weissman, J.S., Kramer, G., and Bukau, B. (2013). Selective ribosome profiling as a tool for studying the interaction of chaperones and targeting factors with nascent polypeptide chains and ribosomes. Nature Protocols 8, 2212–2239.

Berger, A.B., Decourty, L., Badis, G., Nehrbass, U., Jacquier, A., and Gadal, O. (2007). Hmo1 is required for TOR-dependent regulation of ribosomal protein gene transcription. Mol. Cell. Biol. 27, 8015–8026.

Beugnet, A., Tee, A.R., Taylor, P.M., and Proud, C.G. (2003). Regulation of targets of mTOR (mammalian target of rapamycin) signalling by intracellular amino acid availability. Biochemical Journal 372, 555–566.

Blank, H.M., Perez, R., He, C., Maitra, N., Metz, R., Hill, J., Lin, Y., Johnson, C.D., Bankaitis, V.A., Kennedy, B.K., et al. (2017). Translational control of lipogenic enzymes in the cell cycle of synchronous, growing yeast cells. EMBO J. 36, 487–502.

Bosio, M.C., Fermi, B., and Dieci, G. (2017). Transcriptional control of yeast ribosome biogenesis: A multifaceted role for general regulatory factors. Transcription 8, 254–260.

Braat, A.K., Yan, N., Arn, E., Harrison, D., and Macdonald, P.M. (2004). Localization-Dependent Oskar Protein Accumulation: Control after the Initiation of Translation. Developmental Cell 7, 125–131.

Brar, G.A., Yassour, M., Friedman, N., Regev, A., Ingolia, N.T., and Weissman, J.S. (2012). High-Resolution View of the Yeast Meiotic Program Revealed by Ribosome Profiling. Science 335, 552–557.

Brauer, M.J., Huttenhower, C., Airoldi, E.M., Rosenstein, R., Matese, J.C., Gresham, D., Boer, V.M., Troyanskaya, O.G., and Botstein, D. (2008). Coordination of growth rate, cell cycle, stress response, and metabolic activity in yeast. Mol. Biol. Cell 19, 352–367.

Bregman, A., Avraham-Kelbert, M., Barkai, O., Duek, L., Guterman, A., and Choder, M. (2011). Promoter elements regulate cytoplasmic mRNA decay. Cell 147, 1473–1483.

Broach, J.R. (2012). Nutritional control of growth and development in yeast. Genetics 192, 73–105.

Bursac, S., Brdovcak, M.C., Donati, G., and Volarevic, S. (2014). Activation of the tumor suppressor p53 upon impairment of ribosome biogenesis. Biochim. Biophys. Acta 1842, 817–830.

Bussemaker, H.J., Li, H., and Siggia, E.D. (2001). Regulatory element detection using correlation with expression. Nat. Genet. 27, 167–171.

Calvo, S.E., Pagliarini, D.J., and Mootha, V.K. (2009). Upstream open reading frames cause widespread reduction of protein expression and are polymorphic among humans. PNAS 106, 7507–7512.

Cardenas, M.E., Cutler, N.S., Lorenz, M.C., Di Como, C.J., and Heitman, J. (1999). The TOR signaling cascade regulates gene expression in response to nutrients. Genes Dev. 13, 3271–3279.

Carlile, T.M., and Amon, A. (2008). Meiosis I is established through division-specific translational control of a cyclin. Cell 133, 280–291.

Chan, L.Y., Mugler, C.F., Heinrich, S., Vallotton, P., and Weis, K. (2018). Non-invasive measurement of mRNA decay reveals translation initiation as the major determinant of mRNA stability. ELife 7, e32536.

Chen, J., Tresenrider, A., Chia, M., McSwiggen, D.T., Spedale, G., Jorgensen, V., Liao, H., van Werven, F.J., and Ünal, E. (2017). Kinetochore inactivation by expression of a repressive mRNA. Elife 6.

Cheng, Z., Otto, G.M., Powers, E.N., Keskin, A., Mertins, P., Carr, S.A., Jovanovic, M., and Brar, G.A. (2018). Pervasive, Coordinated Protein-Level Changes Driven by Transcript Isoform Switching during Meiosis. Cell 172, 910-923.e16.

Chia, M., Tresenrider, A., Chen, J., Spedale, G., Jorgensen, V., Ünal, E., and van Werven, F.J. (2017). Transcription of a 5' extended mRNA isoform directs dynamic chromatin changes and interference of a downstream promoter. Elife 6.

Chu, S., and Herskowitz, I. (1998). Gametogenesis in Yeast Is Regulated by a Transcriptional Cascade Dependent on Ndt80. Molecular Cell 1, 685–696.

Chu, S., DeRisi, J., Eisen, M., Mulholland, J., Botstein, D., Brown, P.O., and Herskowitz, I. (1998). The transcriptional program of sporulation in budding yeast. Science 282, 699–705.

Cox, J., and Mann, M. (2008). MaxQuant enables high peptide identification rates, individualized p.p.b.-range mass accuracies and proteome-wide protein quantification. Nat. Biotechnol. 26, 1367–1372.

Dalfsen, K.M.V., Hodapp, S., Keskin, A., Otto, G.M., Berdan, C.A., Higdon, A., Cheunkarndee, T., Nomura, D.K., Jovanovic, M., and Brar, G.A. (2018). Global Proteome Remodeling during ER Stress Involves Hac1-Driven Expression of Long Undecoded Transcript Isoforms. Developmental Cell 46, 219-235.e8.

Darnell, J.C., Van Driesche, S.J., Zhang, C., Hung, K.Y.S., Mele, A., Fraser, C.E., Stone, E.F., Chen, C., Fak, J.J., Chi, S.W., et al. (2011). FMRP Stalls Ribosomal Translocation on mRNAs Linked to Synaptic Function and Autism. Cell 146, 247–261.

De Keersmaecker, K., Sulima, S.O., and Dinman, J.D. (2015). Ribosomopathies and the paradox of cellular hypo- to hyperproliferation. Blood 125, 1377–1382.

Dever, T.E., and Green, R. (2012). The Elongation, Termination, and Recycling Phases of Translation in Eukaryotes. Cold Spring Harb Perspect Biol 4, a013706.

Dever, T.E., Kinzy, T.G., and Pavitt, G.D. (2016). Mechanism and Regulation of Protein Synthesis in Saccharomyces cerevisiae. Genetics 203, 65–107.

Dinman, J.D. (2016). Pathways to Specialized Ribosomes: The Brussels Lecture. J. Mol. Biol. 428, 2186–2194.

Djuranovic, S., Nahvi, A., and Green, R. (2012). miRNA-Mediated Gene Silencing by Translational Repression Followed by mRNA Deadenylation and Decay. Science 336, 237–240.

Duina, A.A., Miller, M.E., and Keeney, J.B. (2014). Budding Yeast for Budding Geneticists: A Primer on the Saccharomyces cerevisiae Model System. Genetics 197, 33–48.

Duncan, C.D.S., and Mata, J. (2014). The translational landscape of fission-yeast meiosis and sporulation. Nat. Struct. Mol. Biol. 21, 641–647.

Duncan, C.D.S., and Mata, J. (2017). Effects of cycloheximide on the interpretation of ribosome profiling experiments in Schizosaccharomyces pombe. Sci Rep 7, 10331.

Duncan, C.D.S., Rodríguez-López, M., Ruis, P., Bähler, J., and Mata, J. (2018). General amino acid control in fission yeast is regulated by a nonconserved transcription factor, with functions analogous to Gcn4/Atf4. Proc. Natl. Acad. Sci. U.S.A. 115, E1829–E1838.

Eisenberg, A.R., Higdon, A., Keskin, A., Hodapp, S., Jovanovic, M., and Brar, G.A. (2018). Precise Post-translational Tuning Occurs for Most Protein Complex Components during Meiosis. Cell Rep 25, 3603-3617.e2.

Enssle, J., Kugler, W., Hentze, M.W., and Kulozik, A.E. (1993). Determination of mRNA fate by different RNA polymerase II promoters. Proc. Natl. Acad. Sci. U.S.A. 90, 10091–10095.

Ferretti, M.B., Ghalei, H., Ward, E.A., Potts, E.L., and Karbstein, K. (2017). Rps26 directs mRNA-specific translation by recognition of Kozak sequence elements. Nature Structural & Molecular Biology 24, 700–707.

Filbin, M.E., and Kieft, J.S. (2009). Toward a structural understanding of IRES RNA function. Current Opinion in Structural Biology 19, 267–276.

Floor, S.N., and Doudna, J.A. (2016). Tunable protein synthesis by transcript isoforms in human cells. Elife 5.

Fumagalli, S., Di Cara, A., Neb-Gulati, A., Natt, F., Schwemberger, S., Hall, J., Babcock, G.F., Bernardi, R., Pandolfi, P.P., and Thomas, G. (2009). Absence of nucleolar disruption after impairment of 40S ribosome biogenesis reveals an rpL11-translation-dependent mechanism of p53 induction. Nat. Cell Biol. 11, 501–508.

Garreau de Loubresse, N., Prokhorova, I., Holtkamp, W., Rodnina, M.V., Yusupova, G., and Yusupov, M. (2014). Structural basis for the inhibition of the eukaryotic ribosome. Nature 513, 517–522.

Gebauer, F., and Hentze, M.W. (2004). Molecular mechanisms of translational control. Nature Reviews Molecular Cell Biology 5, 827–835.

Gerashchenko, M.V., and Gladyshev, V.N. (2014). Translation inhibitors cause abnormalities in ribosome profiling experiments. Nucleic Acids Res. 42, e134.

Greber, B.J. (2016). Mechanistic insight into eukaryotic 60S ribosomal subunit biogenesis by cryo-electron microscopy. RNA 22, 1643–1662.

Grollman, A.P. (1967). Inhibitors of protein biosynthesis. II. Mode of action of anisomycin. J. Biol. Chem. 242, 3226–3233.

Hahn, S., and Young, E.T. (2011). Transcriptional Regulation in Saccharomyces cerevisiae : Transcription Factor Regulation and Function, Mechanisms of Initiation, and Roles of Activators and Coactivators. Genetics 189, 705–736.

Hall, D.B., Wade, J.T., and Struhl, K. (2006). An HMG protein, Hmo1, associates with promoters of many ribosomal protein genes and throughout the rRNA gene locus in Saccharomyces cerevisiae. Mol. Cell. Biol. 26, 3672–3679.

Harigaya, Y., and Parker, R. (2016). Analysis of the association between codon optimality and mRNA stability in Schizosaccharomyces pombe. BMC Genomics 17, 895.

Heitman, J., Movva, N.R., and Hall, M.N. (1991). Targets for cell cycle arrest by the immunosuppressant rapamycin in yeast. Science 253, 905–909.

Hellen, C.U.T., and Sarnow, P. (2001). Internal ribosome entry sites in eukaryotic mRNA molecules. Genes Dev. 15, 1593–1612.

Hertz, M.I., Landry, D.M., Willis, A.E., Luo, G., and Thompson, S.R. (2013). Ribosomal Protein S25 Dependency Reveals a Common Mechanism for Diverse Internal Ribosome Entry Sites and Ribosome Shunting. Molecular and Cellular Biology 33, 1016–1026.

Hinnebusch, A.G. (1993). Gene-specific translational control of the yeast GCN4 gene by phosphorylation of eukaryotic initiation factor 2. Mol. Microbiol. 10, 215–223.

Hinnebusch, A.G. (2005). Translational Regulation of Gcn4 and the General Amino Acid Control of Yeast. Annual Review of Microbiology 59, 407–450.

Hinnebusch, A.G., Ivanov, I.P., and Sonenberg, N. (2016). Translational control by 5'-untranslated regions of eukaryotic mRNAs. Science 352, 1413–1416.

Hirose, T., and Horvitz, H.R. (2014). The Translational Regulators GCN-1 and ABCF-3 Act Together to Promote Apoptosis in C. elegans. PLOS Genetics 10, e1004512.

Holcik, M., and Sonenberg, N. (2005). Translational control in stress and apoptosis. Nature Reviews Molecular Cell Biology 6, 318–327.

Homann, O.R., and Johnson, A.D. (2010). MochiView: versatile software for genome browsing and DNA motif analysis. BMC Biol. 8, 49.

de Hoon, M.J.L., Imoto, S., Nolan, J., and Miyano, S. (2004). Open source clustering software. Bioinformatics 20, 1453–1454.

Hoque, M., Ji, Z., Zheng, D., Luo, W., Li, W., You, B., Park, J.Y., Yehia, G., and Tian, B. (2013). Analysis of alternative cleavage and polyadenylation by 3′ region extraction and deep sequencing. Nature Methods 10, 133–139.

Huber, A., French, S.L., Tekotte, H., Yerlikaya, S., Stahl, M., Perepelkina, M.P., Tyers, M., Rougemont, J., Beyer, A.L., and Loewith, R. (2011). Sch9 regulates ribosome biogenesis via Stb3, Dot6 and Tod6 and the histone deacetylase complex RPD3L. EMBO J. 30, 3052–3064.

Hussmann, J.A., Patchett, S., Johnson, A., Sawyer, S., and Press, W.H. (2015). Understanding Biases in Ribosome Profiling Experiments Reveals Signatures of Translation Dynamics in Yeast. PLoS Genet. 11, e1005732.

Ingolia, N.T., Ghaemmaghami, S., Newman, J.R.S., and Weissman, J.S. (2009). Genome-Wide Analysis in Vivo of Translation with Nucleotide Resolution Using Ribosome Profiling. Science 324, 218–223.

Ingolia, N.T., Lareau, L.F., and Weissman, J.S. (2011). Ribosome Profiling of Mouse Embryonic Stem Cells Reveals the Complexity and Dynamics of Mammalian Proteomes. Cell 147, 789–802.

Ingolia, N.T., Brar, G.A., Rouskin, S., McGeachy, A.M., and Weissman, J.S. (2012). The ribosome profiling strategy for monitoring translation in vivo by deep sequencing of ribosome-protected mRNA fragments. Nature Protocols 7, 1534–1550.

Ingolia, N.T., Brar, G.A., Stern-Ginossar, N., Harris, M.S., Talhouarne, G.J.S., Jackson, S.E., Wills, M.R., and Weissman, J.S. (2014). Ribosome profiling reveals pervasive translation outside of annotated protein-coding genes. Cell Rep 8, 1365–1379.

Jackson, R.J., Hellen, C.U.T., and Pestova, T.V. (2010). The mechanism of eukaryotic translation initiation and principles of its regulation. Nature Reviews Molecular Cell Biology 11, 113.

Jan, C.H., Williams, C.C., and Weissman, J.S. (2014). Principles of ER cotranslational translocation revealed by proximity-specific ribosome profiling. Science 346, 1257521.

Johnstone, T.G., Bazzini, A.A., and Giraldez, A.J. (2016). Upstream ORFs are prevalent translational repressors in vertebrates. The EMBO Journal 35, 706–723.

Jorgensen, P., Rupes, I., Sharom, J.R., Schneper, L., Broach, J.R., and Tyers, M. (2004). A dynamic transcriptional network communicates growth potential to ribosome synthesis and critical cell size. Genes Dev. 18, 2491–2505.

Jovanovic, M., Rooney, M.S., Mertins, P., Przybylski, D., Chevrier, N., Satija, R., Rodriguez, E.H., Fields, A.P., Schwartz, S., Raychowdhury, R., et al. (2015). Dynamic profiling of the protein life cycle in response to pathogens. Science 347, 1259038–1259038.

Juntawong, P., Girke, T., Bazin, J., and Bailey-Serres, J. (2014). Translational dynamics revealed by genome-wide profiling of ribosome footprints in Arabidopsis. PNAS 111, E203–E212.

Justice, M.C., Hsu, M.J., Tse, B., Ku, T., Balkovec, J., Schmatz, D., and Nielsen, J. (1998). Elongation factor 2 as a novel target for selective inhibition of fungal protein synthesis. J. Biol. Chem. 273, 3148–3151.

Kafri, M., Metzl-Raz, E., Jona, G., and Barkai, N. (2016). The Cost of Protein Production. Cell Rep 14, 22–31.

Keshishian, H., Burgess, M.W., Gillette, M.A., Mertins, P., Clauser, K.R., Mani, D.R., Kuhn, E.W., Farrell, L.A., Gerszten, R.E., and Carr, S.A. (2015). Multiplexed, Quantitative Workflow for Sensitive Biomarker Discovery in Plasma Yields Novel Candidates for Early Myocardial Injury. Mol. Cell Proteomics 14, 2375–2393.

Khajuria, R.K., Munschauer, M., Ulirsch, J.C., Fiorini, C., Ludwig, L.S., McFarland, S.K., Abdulhay, N.J., Specht, H., Keshishian, H., Mani, D.R., et al. (2018). Ribosome Levels Selectively Regulate Translation and Lineage Commitment in Human Hematopoiesis. Cell 173, 90-103.e19.

Klinge, S., and Woolford, J.L. (2018). Ribosome assembly coming into focus. Nat. Rev. Mol. Cell Biol.

Komar, A.A., and Hatzoglou, M. (2011). Cellular IRES-mediated translation. Cell Cycle 10, 229–240.

Kondrashov, N., Pusic, A., Stumpf, C.R., Shimizu, K., Hsieh, A.C., Xue, S., Ishijima, J., Shiroishi, T., and Barna, M. (2011). Ribosome-Mediated Specificity in Hox mRNA Translation and Vertebrate Tissue Patterning. Cell 145, 383–397.

Kong, J., and Lasko, P. (2012). Translational control in cellular and developmental processes. Nature Reviews Genetics 13, 383–394.

Krol, J., Loedige, I., and Filipowicz, W. (2010). The widespread regulation of microRNA biogenesis, function and decay. Nature Reviews Genetics 11, 597–610.

Kronja, I., Yuan, B., Eichhorn, S.W., Dzeyk, K., Krijgsveld, J., Bartel, D.P., and Orr-Weaver, T.L. (2014). Widespread Changes in the Posttranscriptional Landscape at the Drosophila Oocyte-to-Embryo Transition. Cell Rep 7, 1495–1508.

Landry, D.M., Hertz, M.I., and Thompson, S.R. (2009). RPS25 is essential for translation initiation by the Dicistroviridae and hepatitis C viral IRESs. Genes Dev. 23, 2753–2764.

Langmead, B., and Salzberg, S.L. (2012). Fast gapped-read alignment with Bowtie 2. Nat. Methods 9, 357–359.

Lareau, L.F., Hite, D.H., Hogan, G.J., and Brown, P.O. (2014). Distinct stages of the translation elongation cycle revealed by sequencing ribosome-protected mRNA fragments. Elife 3, e01257.

Law, G.L., Bickel, K.S., MacKay, V.L., and Morris, D.R. (2005). The undertranslated transcriptome reveals widespread translational silencing by alternative 5' transcript leaders. Genome Biol. 6, R111.

Lee, A.S.-Y., Burdeinick-Kerr, R., and Whelan, S.P.J. (2013). A ribosome-specialized translation initiation pathway is required for cap-dependent translation of vesicular stomatitis virus mRNAs. PNAS 110, 324–329.

Lee, S., Liu, B., Lee, S., Huang, S.-X., Shen, B., and Qian, S.-B. (2012). Global mapping of translation initiation sites in mammalian cells at single-nucleotide resolution. Proc. Natl. Acad. Sci. U.S.A. 109, E2424-2432.

Li, G.-W., Burkhardt, D., Gross, C., and Weissman, J.S. (2014). Quantifying Absolute Protein Synthesis Rates Reveals Principles Underlying Allocation of Cellular Resources. Cell 157, 624–635.

Liko, D., Slattery, M.G., and Heideman, W. (2007). Stb3 binds to ribosomal RNA processing element motifs that control transcriptional responses to growth in Saccharomyces cerevisiae. J. Biol. Chem. 282, 26623–26628.

Lippman, S.I., and Broach, J.R. (2009). Protein kinase A and TORC1 activate genes for ribosomal biogenesis by inactivating repressors encoded by Dot6 and its homolog Tod6. Proc. Natl. Acad. Sci. U.S.A. 106, 19928–19933.

Liu, Y., Beyer, A., and Aebersold, R. (2016). On the Dependency of Cellular Protein Levels on mRNA Abundance. Cell 165, 535–550.

Lodish, H.F. (1974). Model for the regulation of mRNA translation applied to haemoglobin synthesis. Nature 251, 385–388.

Mailliot, J., Garreau de Loubresse, N., Yusupova, G., Meskauskas, A., Dinman, J.D., and Yusupov, M. (2016). Crystal Structures of the uL3 Mutant Ribosome: Illustration of the Importance of Ribosomal Proteins for Translation Efficiency. Journal of Molecular Biology 428, 2195–2202.

Marr, A.G. (1991). Growth rate of Escherichia coli. Microbiol. Rev. 55, 316–333.

Marston, A.L., and Amon, A. (2004). Meiosis: cell-cycle controls shuffle and deal. Nature Reviews Molecular Cell Biology 5, 983–997.

Martens, J.A., Laprade, L., and Winston, F. (2004). Intergenic transcription is required to repress the Saccharomyces cerevisiae SER3 gene. Nature 429, 571–574.

Martin, D.E., Soulard, A., and Hall, M.N. (2004). TOR regulates ribosomal protein gene expression via PKA and the Forkhead transcription factor FHL1. Cell 119, 969–979.

Mayr, C., and Bartel, D.P. (2009). Widespread Shortening of 3′ UTRs by Alternative Cleavage and Polyadenylation Activates Oncogenes in Cancer Cells. Cell 138, 673–684.

McCann, K.L., and Baserga, S.J. (2013). Genetics. Mysterious ribosomopathies. Science 341, 849–850.

Mertins, P., Qiao, J.W., Patel, J., Udeshi, N.D., Clauser, K.R., Mani, D.R., Burgess, M.W., Gillette, M.A., Jaffe, J.D., and Carr, S.A. (2013). Integrated proteomic analysis of post-translational modifications by serial enrichment. Nat. Methods 10, 634–637.

Metzker, M.L. (2010). Sequencing technologies — the next generation. Nature Reviews Genetics 11, 31–46.

Metzl-Raz, E., Kafri, M., Yaakov, G., Soifer, I., Gurvich, Y., and Barkai, N. (2017). Principles of cellular resource allocation revealed by condition-dependent proteome profiling. Elife 6.

Mills, E.W., and Green, R. (2017). Ribosomopathies: There's strength in numbers. Science 358, eaan2755.

Modrek, B., and Lee, C. (2002). A genomic view of alternative splicing. Nature Genetics 30, 13–19.

Mortazavi, A., Williams, B.A., McCue, K., Schaeffer, L., and Wold, B. (2008). Mapping and quantifying mammalian transcriptomes by RNA-Seq. Nature Methods 5, 621–628.

Muhs, M., Yamamoto, H., Ismer, J., Takaku, H., Nashimoto, M., Uchiumi, T., Nakashima, N., Mielke, T., Hildebrand, P.W., Nierhaus, K.H., et al. (2011). Structural basis for the binding of IRES RNAs to the head of the ribosomal 40S subunit. Nucleic Acids Res. 39, 5264–5275.

Munding, E.M., Shiue, L., Katzman, S., Donohue, J.P., and Ares, M. (2013). Competition between pre-mRNAs for the splicing machinery drives global regulation of splicing. Mol. Cell 51, 338–348.

Nagaoka, S.I., Hassold, T.J., and Hunt, P.A. (2012). Human aneuploidy: mechanisms and new insights into an age-old problem. Nature Reviews Genetics 13, 493–504.

Neiman, A.M. (2011). Sporulation in the Budding Yeast Saccharomyces cerevisiae. Genetics 189, 737–765.

Nishimura, K., and Kanemaki, M.T. (2014). Rapid Depletion of Budding Yeast Proteins via the Fusion of an Auxin-Inducible Degron (AID). Current Protocols in Cell Biology 64, 20.9.1-20.9.16.

Nishiyama, T., Yamamoto, H., Uchiumi, T., and Nakashima, N. (2007). Eukaryotic ribosomal protein RPS25 interacts with the conserved loop region in a dicistroviral intergenic internal ribosome entry site. Nucleic Acids Res. 35, 1514–1521.

Novoa, E.M., and Ribas de Pouplana, L. (2012). Speeding with control: codon usage, tRNAs, and ribosomes. Trends in Genetics 28, 574–581.

O'Donohue, M.-F., Choesmel, V., Faubladier, M., Fichant, G., and Gleizes, P.-E. (2010). Functional dichotomy of ribosomal proteins during the synthesis of mammalian 40S ribosomal subunits. J. Cell Biol. 190, 853–866.

Oh, E., Becker, A.H., Sandikci, A., Huber, D., Chaba, R., Gloge, F., Nichols, R.J., Typas, A., Gross, C.A., Kramer, G., et al. (2011). Selective Ribosome Profiling Reveals the Cotranslational Chaperone Action of Trigger Factor In Vivo. Cell 147, 1295–1308.

Okoniewski, M.J., and Miller, C.J. (2006). Hybridization interactions between probesets in short oligo microarrays lead to spurious correlations. BMC Bioinformatics 7, 276.

Palam, L.R., Baird, T.D., and Wek, R.C. (2011). Phosphorylation of eIF2 facilitates ribosomal bypass of an inhibitory upstream ORF to enhance CHOP translation. J. Biol. Chem. 286, 10939–10949.

Parker, R. (2012). RNA Degradation in Saccharomyces cerevisae. Genetics 191, 671–702.

Pelechano, V., Wei, W., and Steinmetz, L.M. (2013). Extensive transcriptional heterogeneity revealed by isoform profiling. Nature 497, 127–131.

Peshkin, L., Wühr, M., Pearl, E., Haas, W., Freeman, R.M., Gerhart, J.C., Klein, A.M., Horb, M., Gygi, S.P., and Kirschner, M.W. (2015). On the Relationship of Protein and mRNA Dynamics in Vertebrate Embryonic Development. Dev. Cell 35, 383–394.

Powers, T., and Walter, P. (1999). Regulation of ribosome biogenesis by the rapamycin-sensitive TOR-signaling pathway in Saccharomyces cerevisiae. Mol. Biol. Cell 10, 987–1000.

Presnyak, V., Alhusaini, N., Chen, Y.-H., Martin, S., Morris, N., Kline, N., Olson, S., Weinberg, D., Baker, K.E., Graveley, B.R., et al. (2015). Codon Optimality Is a Major Determinant of mRNA Stability. Cell 160, 1111–1124.

Radhakrishnan, A., Chen, Y.-H., Martin, S., Alhusaini, N., Green, R., and Coller, J. (2016). The DEAD-Box Protein Dhh1p Couples mRNA Decay and Translation by Monitoring Codon Optimality. Cell 167, 122-132.e9.

Rappsilber, J., Mann, M., and Ishihama, Y. (2007). Protocol for micro-purification, enrichment, pre-fractionation and storage of peptides for proteomics using StageTips. Nat. Protocols 2, 1896–1906.

Requião, R.D., de Souza, H.J.A., Rossetto, S., Domitrovic, T., and Palhano, F.L. (2016). Increased ribosome density associated to positively charged residues is evident in ribosome profiling experiments performed in the absence of translation inhibitors. RNA Biol 13, 561–568.

Reuveni, S., Ehrenberg, M., and Paulsson, J. (2017). Ribosomes are optimized for autocatalytic production. Nature 547, 293–297.

Richter, J.D. (1999). Cytoplasmic Polyadenylation in Development and Beyond. Microbiol. Mol. Biol. Rev. 63, 446–456.

Richter, J.D. (2007). CPEB: a life in translation. Trends in Biochemical Sciences 32, 279–285.

Richter, J.D., and Coller, J. (2015). Pausing on Polyribosomes: Make Way for Elongation in Translational Control. Cell 163, 292–300.

Rojas-Duran, M.F., and Gilbert, W.V. (2012). Alternative transcription start site selection leads to large differences in translation activity in yeast. RNA 18, 2299–2305.

Rudra, D., Zhao, Y., and Warner, J.R. (2005). Central role of Ifh1p-Fhl1p interaction in the synthesis of yeast ribosomal proteins. EMBO J. 24, 533–542.

Saldanha, A.J. (2004). Java Treeview--extensible visualization of microarray data. Bioinformatics 20, 3246–3248.

Santos, D.A., Shi, L., Tu, B.P., and Weissman, J.S. (2019) Cycloheximide can distort measurements of mRNA levels and translation efficiency. Nucleic Acids Res.

Sarnow, P. (2003). Viral Internal Ribosome Entry Site Elements: Novel Ribosome-RNA Complexes and Roles in Viral Pathogenesis. Journal of Virology 77, 2801–2806.

Schawalder, S.B., Kabani, M., Howald, I., Choudhury, U., Werner, M., and Shore, D. (2004). Growth-regulated recruitment of the essential yeast ribosomal protein gene activator Ifh1. Nature 432, 1058–1061.

Schneider, C.A., Rasband, W.S., and Eliceiri, K.W. (2012). NIH Image to ImageJ: 25 years of image analysis. Nat. Methods 9, 671–675.

Schneider-Poetsch, T., Ju, J., Eyler, D.E., Dang, Y., Bhat, S., Merrick, W.C., Green, R., Shen, B., and Liu, J.O. (2010). Inhibition of eukaryotic translation elongation by cycloheximide and lactimidomycin. Nat. Chem. Biol. 6, 209–217.

Schoenberg, D.R., and Maquat, L.E. (2012). Regulation of cytoplasmic mRNA decay. Nature Reviews Genetics 13, 246–259.

Sen, N.D., Zhou, F., Ingolia, N.T., and Hinnebusch, A.G. (2015). Genome-wide analysis of translational efficiency reveals distinct but overlapping functions of yeast DEAD-box RNA helicases Ded1 and eIF4A. Genome Res. 25, 1196–1205.

Shi, Z., Fujii, K., Kovary, K.M., Genuth, N.R., Röst, H.L., Teruel, M.N., and Barna, M. (2017). Heterogeneous Ribosomes Preferentially Translate Distinct Subpools of mRNAs Genome-wide. Molecular Cell 67, 71-83.e7.

Shin, C., and Manley, J.L. (2004). Cell signalling and the control of pre-mRNA splicing. Nature Reviews Molecular Cell Biology 5, 727–738.

Siegel, M.R., and Sisler, H.D. (1963). INHIBITION OF PROTEIN SYNTHESIS IN VITRO BY CYCLOHEXIMIDE. Nature 200, 675–676.

Silvera, D., Formenti, S.C., and Schneider, R.J. (2010). Translational control in cancer. Nature Reviews Cancer 10, 254–266.

Simsek, D., Tiu, G.C., Flynn, R.A., Byeon, G.W., Leppek, K., Xu, A.F., Chang, H.Y., and Barna, M. (2017). The Mammalian Ribo-interactome Reveals Ribosome Functional Diversity and Heterogeneity. Cell 169, 1051-1065.e18.

Spitz, F., and Furlong, E.E.M. (2012). Transcription factors: from enhancer binding to developmental control. Nature Reviews Genetics 13, 613.

Steffen, K.K., MacKay, V.L., Kerr, E.O., Tsuchiya, M., Hu, D., Fox, L.A., Dang, N., Johnston, E.D., Oakes, J.A., Tchao, B.N., et al. (2008). Yeast life span extension by depletion of 60s ribosomal subunits is mediated by Gcn4. Cell 133, 292–302.

Steffen, K.K., McCormick, M.A., Pham, K.M., MacKay, V.L., Delaney, J.R., Murakami, C.J., Kaeberlein, M., and Kennedy, B.K. (2012). Ribosome deficiency protects against ER stress in Saccharomyces cerevisiae. Genetics 191, 107–118.

Steitz, J.A. (1969). Polypeptide Chain Initiation: Nucleotide Sequences of the Three Ribosomal Binding Sites in Bacteriophage R17 RNA. Nature 224, 957.

Strunk, B.S., Novak, M.N., Young, C.L., and Karbstein, K. (2012). A translation-like cycle is a quality control checkpoint for maturing 40S ribosome subunits. Cell 150, 111–121.

Subtelny, A.O., Eichhorn, S.W., Chen, G.R., Sive, H., and Bartel, D.P. (2014). Poly(A)-tail profiling reveals an embryonic switch in translational control. Nature 508, 66–71.

Sung, M.-K., Reitsma, J.M., Sweredoski, M.J., Hess, S., and Deshaies, R.J. (2016). Ribosomal proteins produced in excess are degraded by the ubiquitin-proteasome system. Mol. Biol. Cell 27, 2642–2652.

Sydorskyy, Y., Dilworth, D.J., Halloran, B., Yi, E.C., Makhnevych, T., Wozniak, R.W., and Aitchison, J.D. (2005). Nop53p is a novel nucleolar 60S ribosomal subunit biogenesis protein. Biochemical Journal 388, 819–826.

Tanenbaum, M.E., Stern-Ginossar, N., Weissman, J.S., and Vale, R.D. (2015). Regulation of mRNA translation during mitosis. Elife 4.

Trapnell, C., Pachter, L., and Salzberg, S.L. (2009). TopHat: discovering splice junctions with RNA-Seq. Bioinformatics 25, 1105–1111.

Trapnell, C., Williams, B.A., Pertea, G., Mortazavi, A., Kwan, G., van Baren, M.J., Salzberg, S.L., Wold, B.J., and Pachter, L. (2010). Transcript assembly and quantification by RNA-Seq reveals unannotated transcripts and isoform switching during cell differentiation. Nature Biotechnology 28, 511–515.

Trcek, T., Larson, D.R., Moldón, A., Query, C.C., and Singer, R.H. (2011). Single-molecule mRNA decay measurements reveal promoter- regulated mRNA stability in yeast. Cell 147, 1484–1497.

Urban, J., Soulard, A., Huber, A., Lippman, S., Mukhopadhyay, D., Deloche, O., Wanke, V., Anrather, D., Ammerer, G., Riezman, H., et al. (2007). Sch9 Is a Major Target of TORC1 in Saccharomyces cerevisiae. Molecular Cell 26, 663–674.

Vattem, K.M., and Wek, R.C. (2004). Reinitiation involving upstream ORFs regulates ATF4 mRNA translation in mammalian cells. PNAS 101, 11269–11274.

Venkataramanan, S., Douglass, S., Galivanche, A.R., and Johnson, T.L. (2017). The chromatin remodeling complex Swi/Snf regulates splicing of meiotic transcripts in Saccharomyces cerevisiae. Nucleic Acids Res. 45, 7708–7721.

Vind, J., Sørensen, M.A., Rasmussen, M.D., and Pedersen, S. (1993). Synthesis of Proteins in Escherichia coli is Limited by the Concentration of Free Ribosomes. Journal of Molecular Biology 231, 678–688.

Volarevic, S., Stewart, M.J., Ledermann, B., Zilberman, F., Terracciano, L., Montini, E., Grompe, M., Kozma, S.C., and Thomas, G. (2000). Proliferation, but not growth, blocked by conditional deletion of 40S ribosomal protein S6. Science 288, 2045–2047.

Wade, C.H., Umbarger, M.A., and McAlear, M.A. (2006). The budding yeast rRNA and ribosome biosynthesis (RRB) regulon contains over 200 genes. Yeast 23, 293–306.

Wade, J.T., Hall, D.B., and Struhl, K. (2004). The transcription factor Ifh1 is a key regulator of yeast ribosomal protein genes. Nature 432, 1054–1058.

Wang, X., Hou, J., Quedenau, C., and Chen, W. (2016). Pervasive isoform‐specific translational regulation via alternative transcription start sites in mammals. Molecular Systems Biology 12, 875.

Wang, Z., Gerstein, M., and Snyder, M. (2009). RNA-Seq: a revolutionary tool for transcriptomics. Nature Reviews Genetics 10, 57–63.

Warner, J.R. (1999). The economics of ribosome biosynthesis in yeast. Trends Biochem. Sci. 24, 437–440.

Warner, J.R., Mitra, G., Schwindinger, W.F., Studeny, M., and Fried, H.M. (1985). Saccharomyces cerevisiae coordinates accumulation of yeast ribosomal proteins by modulating mRNA splicing, translational initiation, and protein turnover. Mol. Cell. Biol. 5, 1512–1521.

Weidberg, H., Moretto, F., Spedale, G., Amon, A., and van Werven, F.J. (2016). Nutrient Control of Yeast Gametogenesis Is Mediated by TORC1, PKA and Energy Availability. PLoS Genet. 12, e1006075.

van Werven, F.J., Neuert, G., Hendrick, N., Lardenois, A., Buratowski, S., van Oudenaarden, A., Primig, M., and Amon, A. (2012). Transcription of two long noncoding RNAs mediates mating-type control of gametogenesis in budding yeast. Cell 150, 1170–1181.

Wu, C.C.-C., Zinshteyn, B., Wehner, K.A., and Green, R. (2019). High-Resolution Ribosome Profiling Defines Discrete Ribosome Elongation States and Translational Regulation during Cellular Stress. Molecular Cell 73, 959-970.e5.

Xiao, L., and Grove, A. (2009). Coordination of Ribosomal Protein and Ribosomal RNA Gene Expression in Response to TOR Signaling. Curr. Genomics 10, 198–205.

Xie, B., Horecka, J., Chu, A., Davis, R.W., Becker, E., and Primig, M. (2016). Ndt80 activates the meiotic ORC1 transcript isoform and SMA2 via a bi-directional middle sporulation element in Saccharomyces cerevisiae. RNA Biol 13, 772–782.

Xu, L., Ajimura, M., Padmore, R., Klein, C., and Kleckner, N. (1995). NDT80, a meiosis-specific gene required for exit from pachytene in Saccharomyces cerevisiae. Molecular and Cellular Biology 15, 6572–6581.

Xue, S., and Barna, M. (2012). Specialized ribosomes: a new frontier in gene regulation and organismal biology. Nat. Rev. Mol. Cell Biol. 13, 355–369.

Xue, S., Tian, S., Fujii, K., Kladwang, W., Das, R., and Barna, M. (2015). RNA regulons in Hox 5′ UTRs confer ribosome specificity to gene regulation. Nature 517, 33–38.

Young, D.J., Guydosh, N.R., Zhang, F., Hinnebusch, A.G., and Green, R. (2015). Rli1/ABCE1 Recycles Terminating Ribosomes and Controls Translation Reinitiation in 3′ UTRs In Vivo. Cell 162, 872–884.

Zaslaver, A., Mayo, A.E., Rosenberg, R., Bashkin, P., Sberro, H., Tsalyuk, M., Surette, M.G., and Alon, U. (2004). Just-in-time transcription program in metabolic pathways. Nat. Genet. 36, 486–491.

Zhao, Y., McIntosh, K.B., Rudra, D., Schawalder, S., Shore, D., and Warner, J.R. (2006). Fine-structure analysis of ribosomal protein gene transcription. Mol. Cell. Biol. 26, 4853–4862.

Zhu, C., Byers, K.J.R.P., McCord, R.P., Shi, Z., Berger, M.F., Newburger, D.E., Saulrieta, K., Smith, Z., Shah, M.V., Radhakrishnan, M., et al. (2009). High-resolution DNA-binding specificity analysis of yeast transcription factors. Genome Res. 19, 556–566.

Zid, B.M., and O'Shea, E.K. (2014). Promoter sequences direct cytoplasmic localization and translation of mRNAs during starvation in yeast. Nature 514, 117–121.